

**Kelp-urchin dynamics: Stability and thresholds for phase shifts in
Newfoundland and the Gulf of St. Lawrence**

by

© Anne Provencher St-Pierre

A thesis submitted to the School of Graduate Studies
in partial fulfillment of the requirements for the degree of
Doctor of Philosophy, Marine Biology

Department of Ocean Sciences
Memorial University of Newfoundland
St. John's, Newfoundland, Canada

July 2020

ABSTRACT

In eastern Canada, studies of kelp-urchin systems have been generally restricted to small spatial (few 100s m²) and temporal (<5 years) extents by the traditional scuba-based monitoring techniques employed. Investigation of the drivers of kelp distribution over multiple spatiotemporal scales (including broad spatial [$<km^2$] and temporal [years] extents) and in regions poorly studied is key to assessing the stability of these systems and understanding regional specificities of kelp dynamics across eastern Canada. This thesis investigates the factors controlling kelp distribution and the stability of kelp-urchin systems in southeastern Newfoundland (SEN) and the northern Gulf of St. Lawrence (nGSL) over multiple spatiotemporal scales by applying traditional and novel techniques. In a scuba-based manipulative field experiment in SEN, no significant effect of urchin density was observed on the rate of kelp bed destruction from urchin grazing, suggesting that the minimal urchin density required to maintain destructive feeding on kelp beds may be equal to the lowest density tested (88 urchins·m⁻²) or lower. The suitability of remote sensing and geographic information system (GIS) approaches for mapping kelp in the nGSL was assessed by comparing three image classification methods applied to aerial and satellite imagery. Supervised classification of satellite imagery (89% accuracy) and visual classification of aerial imagery (90% accuracy) were the best methods. Visually classified imagery from the nGSL was used to compute spatial pattern metrics quantifying kelp distribution patterns. These metrics showed that kelp distribution is not uniform, as kelp patches exhibited considerable variation in size and geometric complexity. Kelp presence was negatively correlated with depth, urchin density, and exposure to waves. Investigation of kelp distribution patterns from imagery acquired in six years between 1983 and 2016 in

the nGSL revealed an increase in kelp cover since 1999. Harsh oceanographic conditions in late winter and spring were correlated with decreased kelp cover and smaller, more numerous kelp patches. Kelp patches persisting through time were more frequent in shallow areas. Overall, this thesis increases knowledge of scale dependency in the drivers of kelp distribution in eastern Canada. It speaks to the importance of exploring multiple scales to understand, predict, and mitigate changes in kelp-urchin systems.

ACKNOWLEDGEMENTS

I thank my supervisor Dr. Patrick Gagnon for giving me the opportunity to pursue a PhD program within his lab. I am thankful for his encouragement and guidance throughout every stage of this research project. I am also grateful to the members of my supervisory committee, Dr. Yolanda Wiersma and Dr. Jonathan Fisher, for their support and constructive comments that helped improve my thesis. I am thankful for the opportunity I had to collaborate with Dr. Renae Hovey and Dr. Gary Kendrick, who helped me discover the great potential of GIS studies.

My PhD work included a fair amount of field work which could not have been completed without help. My sincere thanks go to all who have been involved in field work conducted for this thesis. Thanks to David Bélanger, Samantha Trueman, Kyle Millar, Chelsey Hounsell, and Nick Brown for the countless hours spent by my side in Flatrock. I am also grateful to the team of Dr. Ladd Johnson's lab – Carla Narvaez Diaz, Benoît Dumas, Heather Hawk, Ignacio Garrido, Paula Bruning, and Ladd himself – for their collaboration to my field campaign in the Mingan Archipelago. Special thanks to my sister Maude who volunteered her time and muscles to help me out in during this field work as well. I want to thank the summer students and volunteers who worked with me throughout my PhD, both in the field and in the lab; Kaitlyn Graham, Dana Mallowney, Katie Brenton, Magdalena Maeland, Aragorne Lomond, Sean A. Munro, and Rebecca Bowering. I am also grateful for the time that Dr. David Schneider, Dr. Yolanda Wiersma, Dr. Kristen Bøe, and Dr. Amanda Bates repeatedly took to discuss statistical issues with me.

I am grateful for the support and encouragement of my family and friends. I want to address special thanks to my sister Laurence for her wisdom about graduate student life and moral support during the rough hours of our PhDs. To David Bélanger, I must say that your help and encouragements were indispensable to the completion of my thesis. Finally, my acknowledgements could not be complete without thanking my partner, Bruno, who has been of undeniable support throughout my PhD. Bruno, our engaging discussions and your endless encouragements in my moments of doubts have been incredibly helpful.

This research was funded by Natural Sciences and Engineering Research Council of Canada (NSERC Discovery Grant), Canada Foundation for Innovation (CFI Leaders Opportunity Funds), and Research & Development Corporation of Newfoundland and Labrador (IngniteR&D) grants to Patrick Gagnon. Anne Provencher St-Pierre was supported by the NSERC Canada Graduate Scholarship – Doctorate program.

TABLE OF CONTENTS

Abstract.....	II
Acknowledgements	IV
Table of contents	VI
List of tables.....	X
List of figures.....	XIII
List of appendices.....	XIX
Co-authorship statement	XX

CHAPTER I

General introduction	1
1.1. Drivers of species distribution.....	2
1.2. Kelp-urchin systems	4
1.3. Main objectives and thesis structure	10
1.4. References	13

CHAPTER II

Quantifying the threshold urchin density for kelp bed destruction in southeastern Newfoundland in relation to temperature and flow acceleration.....	22
2.1. Abstract	23
2.2. Introduction	24
2.3. Material and methods	28
2.3.1. Study area	28
2.3.2. Experimental setup	31
2.3.3. Image acquisition and data extraction	36
2.3.4. Monitoring of environmental parameters	39
2.3.5. Statistical analyses	42
2.4. Results	44
2.4.1. Rate of kelp bed retreat.....	44
2.4.2. Urchin densities at the front.....	44

2.4.3. Urchin density in the barren	51
2.5. Discussion	54
2.6. Acknowledgements	64
2.7. References	65

CHAPTER III

Kelp-bed dynamics across scales: Enhancing mapping capability with remote sensing and GIS	71
3.1. Abstract.....	72
3.2. Introduction	73
3.3. Materials and methods	78
3.3.1. Study system.....	78
3.3.2. Image acquisition and pre-processing	84
3.3.3. Ground truthing	89
3.3.4. Image classification	93
3.3.5. Accuracy of classification	95
3.4. Results	97
3.4.1. Visual assessment of thematic maps	97
3.4.2. Spatial overlap in distribution of benthic classes	102
3.4.3. Accuracy of classifications.....	106
3.5. Discussion	108
3.6. Acknowledgements	116
3.7. References	117

CHAPTER IV

Kelp-bed dynamics across scales: Assessing distribution patterns with spatial pattern metrics and modelling.....	127
4.1. Abstract	128
4.2. Introduction	129
4.3. Material and methods	133

4.3.1. Study area	133
4.3.2. Image acquisition and field measurements.....	137
4.3.3. Data extraction from aerial imagery	141
4.3.4. Kelp coverage and spatial pattern metrics	141
4.3.5. Relationships between environmental factors and kelp distribution	144
4.4. Results	151
4.5. Discussion	160
4.6. Acknowledgements	171
4.7. References	171

CHAPTER V

Kelp-bed dynamics across scales: Stability and drivers of kelp distribution patterns over broad spatiotemporal scales

5.1. Abstract	182
5.2. Introduction	183
5.3. Material and methods	187
5.3.1. Study site	187
5.3.2. Acquisition, pre-processing, and classification of aerial imagery	190
5.3.3. Spatial pattern metrics and correlations with oceanographic and atmospheric conditions	192
5.3.4. Effects of site characteristics on the stability of kelp bed distribution	199
5.4. Results	206
5.4.1. Overview of spatial pattern metrics	206
5.4.2. Correlation between spatial pattern metrics and environmental parameters	206
5.4.3. KSI and CTVI distributions.....	212
5.4.4. Model selection.....	218
5.5. Discussion	220
5.6. Acknowledgements	230
5.7. References	230

CHAPTER VI

Summary and general conclusions239

6.1. Summary 240

 6.1.1. Urchin density and kelp bed destruction in southeastern Newfoundland .242

 6.1.2. Framework for broad-scale (km²) kelp bed detection 243

 6.1.3. Patterns of spatial distribution of kelp beds in the Mingan Archipelago ..244

 6.1.4. Temporal trends in kelp distribution in the Mingan Archipelago 244

6.2. Importance of the study 245

6.3. Future directions..... 248

6.4. References 251

APPENDICES253

LIST OF TABLES

Table 2.1. Estimates of slope obtained from the three-way ANCOVA examining the effect of Treatment (Natural, High, Medium, Low, and Very low densities, and Control corridor), Julian date (continuous variable), and Year (2015 and 2016) on the density of urchins at the front, which indicated a significant effect of the triple interaction between these factors (see Table 2.B.5 and Sections 2.3.5 and 2.4.2). Estimates with different letters are significantly different from each other based on comparison of the lower and upper 95% confidence interval (CI) around the slope estimate. See Figure 2.6 for a visual representation of each slope.	47
Table 3.1. Depth-specific proportions of the study area classified as kelp or non-kelp by the six classification methods used (unsupervised, supervised, and visual applied to both types of imagery) or classified differently by at least one classification method.	103
Table 3.2. Coincidence matrix showing the proportion (%) of overlap in seabed classified as kelp or non-kelp (kelp; non-kelp) within each pair of comparison of classification methods used. Bolded values in the bottom row indicate overall proportions of the seabed classified as kelp or non-kelp with each classification method.	105
Table 3.3. Classification methods used for mapping kelp and non-kelp benthic classes and associated measures of accuracy. Producer's, user's, and overall accuracies are in %. Numbers in parentheses are the 95% confidence intervals.	107
Table 4.1. Spatial pattern metrics examined in the present study. All metrics were calculated with FRAGSTATS (v.4, Amherst, MA; McGarigal et al., 2012).	143
Table 4.2. Hypotheses and corresponding models used in model selection to investigate the relationship between kelp distribution and a combination of four explanatory variables, i.e., depth, bottom slope, relative exposure index (REI, a measure of exposure to waves), and urchin density (see section 4.3.5). The + symbol indicates an additive effect between parameters, while the * symbol indicates an interactive effect between parameters.	148

Table 4.3. Outcome of model selection applied to determine the relative influence of four explanatory variables (Depth, Relative Exposure Index [REI], Slope, and Urchin density) on kelp presence (see Section 4.3.5 for details). AIC_i is the value of the Akaike Information Criterion (AIC) calculated for model i (where i represents any of the 11 models tested), and Δ_i is the difference between the AIC of the best fitting model and that of model i . k represents the number of parameters, $\text{Exp}(-0.5\Delta_i)$ represents the relative likelihood of model i , and w_i represents the Akaike weights. The + symbol indicates additive effects, while the * symbol indicates interactive effects among model factors. Model 10 (bold) was selected as the most informative. 161

Table 4.4. Coefficient estimate (β), p-values, and odds ratios for the explanatory variables in Model 10, which was selected as the most informative by comparison of Akaike’s Information Criterion (AIC; see Table 4.3 and Section 4.3.5). Odds ratios indicate the relative change in the odds of kelp being present at a given location, for an increase of one unit in the exploratory variable. As the explanatory variables were scaled and centered prior to analyses, the odds ratios represent the change in odd for an increase of one standard deviation of the exploratory variable. The odds ratios were back-transformed to present the change in odds for an increase of one unit of the explanatory variable (first column from the right). All changes in odds represent declines in the odds of kelp being present, since the coefficient estimates are of negative values. 162

Table 5.1 Environmental parameters assessed for their correlation with spatial pattern metrics. “C” indicates that the data was acquired concurrent to the year of imagery acquisition (i.e., 1983, 1988, 1999, 2004, 2009, 2016). “P” indicates data acquired for the year preceding image acquisition (i.e., 1982, 1987, 1998, 2003, 2008, 2015). The North Atlantic Oscillation (NAO) index used for averaging consists of monthly values calculated by the National Oceanic and Atmospheric Administration (NOAA) using a station-based definition based on pressure differences between Lisbon (Portugal) and Reykjavik (Iceland). Further details regarding the calculation of this index can be found on NOAA’s Climate Prediction Center website: <https://www.cpc.ncep.noaa.gov/data/teledoc/nao.shtml>..... 195

Table 5.2. Outcome of model selection for the Kelp Stability Index (KSI). AIC_i is the value of the Akaike Information Criterion (AIC) calculated for model i , and Δ_i is the difference between the AIC of the best fitting model and that of model i . Value of k represents the number of parameters in each model. $\text{Exp}(-0.5\Delta_i)$ represents the

relative likelihood of model i , and w_i represents the Akaike weights. The “+” symbol indicates additive effects, while the “*” symbol indicates interactive effects among model factors. Model 1 (bold) was selected as the most informative model and used for subsequent analyses, because it is the most parsimonious among models with $\Delta_i < 2$. REI refers to the relative exposure index (see Section 5.3.4).204

Table 5.3. Outcome of model selection for the Cover Type Variability Index (CTVI). AIC_i is the value of the Akaike Information Criterion (AIC) calculated for model i , and Δ_i is the difference between the AIC of the best fitting model and that of model i . Value of k represents the number of parameters in each model. $\text{Exp}(-0.5\Delta_i)$ represents the relative likelihood of model i , and w_i represents the Akaike weights. The “+” symbol indicates additive effects, while the “*” symbol indicates interactive effects among model factors. Model 1 (bold) was selected as the most informative model and used for subsequent analyses, because it is the most parsimonious among models with $\Delta_i < 2$205

Table 5.4. Outcome of the spatial pattern metrics calculated for the kelp benthic class on imagery from each of the six years studied. Mean values are presented with standard error ($\pm SE$).207

Table 5.5. Coefficient estimates for Model 01, which only contained the variable Depth (selected as the most informative by comparison of Akaike’s Information Criterion (AIC); see Table 5.3 and 5.5 and Section 5.3.4), applied to Kelp Stability Index (KSI) and to the Cover Type Variability Index (CTVI). As the data was scaled prior to analyses, both the scaled and back-transformed coefficients are presented, with 95% confidence intervals (CI).219

LIST OF FIGURES

Figure 2.1. Location of the study area in Flatrock cove (Newfoundland, Canada), highlighted in red.30

Figure 2.2. Panel A: Schematic representation of the position of fences (dashed lines) and eyebolts (circles) forming the corridors at the kelp-barren interface in the experimental sites. This example shows the configuration of the corridors at site 4 (see below) in 2015. Letters within each corridor identify the six experimental urchin density treatments at this site in 2015, where N = Natural density, H = High density, M = Medium density, L = Low density, V = Very low density, and C = Control corridor (see section 2.3.2 for details). Experimental treatments were randomly assigned to each corridor at each site following a complete-block design and re-randomized each year. **Panel B:** Picture of the corridors built at site 4 in 2015 prior to the start of the experiment (Photo: Anne P. St-Pierre). **Panel C:** Position of the four experimental sites (labeled 1 to 4) and the control site (labelled “C”) within the study area.33

Figure 2.3. Temperature (**Panel A**, in °C) and relative Flow acceleration (**Panel B**, in $\text{m}\cdot\text{s}^{-2}$) in the study area from August 2015 to November 2016. Vertical lines identify days on which data collection (i.e., acquisition of underwater imagery and measurement of urchin densities) took place (see section 2.3.2 and 2.3.3), while black dots represent temperature and flow acceleration (in panels A and B, respectively) on each day of data collection.41

Figure 2.4. Relationship between the rate of kelp bed retreat (in $\text{m}\cdot\text{mo}^{-1}$) and Julian date for observations obtained during summer within the experimental sites ($r^2=0.046$, $p=0.004$). Because de factors Treatment and Year did not have a significant effect on the rate of kelp bed retreat within the experimental sites (see Table 2.B.1), data is pooled over the two years in which the experiment took place (2015 and 2016) and over the six experimental density treatments.45

Figure 2.5. Relationship between the rate of kelp bed retreat (in $\text{m}\cdot\text{mo}^{-1}$) and temperature (°C), for observations obtained year-round (i.e., from August 2015 to October 2016, see section 2.3.2) within the control site ($r^2=0.152$, $p=0.009$). Because the factor Flow acceleration did not have a significant effect on the rate of kelp bed retreat within the control site (see Appendix 2.B, Table 2.B.4), flow acceleration is not shown. Data from both years (2015 and 2016) was pooled for analyses of environmental parameters (see section 2.3.5).46

Figure 2.6. Relationship between urchin density at the front and Julian date, for observations obtained in summer within the experimental sites. Each panel represents one level of the six experimental urchin front density treatments applied, including the natural average mid-summer front density in the study area (350 urchins·m⁻²), the high, medium, low, and very low densities representing respectively 125%, 75%, 50%, and 25% of the mid-summer average, and the control corridors (see section 2.3.2 for details). Data from 2015 is identified by white circles and dashed lines, while data from 2016 is identified by gray circles and full lines. Slopes not sharing the same letter are significantly different based on comparison of the 95% confidence interval for the slope estimates. Because the triple interaction between the factors Treatment, Julian date, and Year was significant ($p=0.003$, Appendix 2.B, Table 2.B.5), the 12 regression lines present in this figure are compared simultaneously.....50

Figure 2.7. Relationship between urchin density in the barren zone (i.e., at a distance of ~2 m from the lower kelp bed edge towards the barren) and Julian date in 2015 (white circles, dashed line) and 2016 (gray circles, full line). **Panel A** presents data obtained in summer within the experimental sites ($r^2=0.014$ in 2015 and $r^2=0.037$ in 2016). The two slopes are significantly different from each other ($p=0.048$ for the interaction between factors Julian date and Year, see Appendix 2.B Table 2.B.9). Because the factor Treatment did not have a significant effect (Table 2.B.9), data are pooled over the six experimental density treatments. **Panel B** presents data obtained year-round within control site ($r^2=0.247$ in 2015 and $r^2=0.186$ in 2016). The two slopes are significantly different from each other ($p<0.001$ for the interaction between factors Julian date and Year, see Appendix 2.B Table 2.B.10).53

Figure 2.8. 3D plot of the multiple regression of urchin density in the barren zone (in urchins·m⁻²) with the factors Temperature (°C), and Flow acceleration (m·s⁻²) as independent variables, for observations obtained year-round (i.e., from August 2015 to October 2016, see section 2.3.2) within control site. Data from both years (2015 and 2016) was pooled for analyses of environmental parameters (see section 2.3.5 and Appendix 2.B Table 2.B.12).55

Figure 3.1. Location of study areas (shaded polygons) at Île à Firmin, Île du Havre, Île aux Goélands, and Petite île au Marteau in the western sector of the Mingan Archipelago, northern Gulf of St. Laurence, eastern Canada.80

Figure 3.2. A) Kelp bed [mainly *Alaria esculenta*] at a depth of ~2 m within the Île du Havre study area (photo: Anne P. St-Pierre). B) Green sea urchin

(*Strongylocentrotus droebachiensis*) barrens with a few kelp patches at a depth of 6 m within the Île du Havre study area (photo: Anne P. St-Pierre). **C**) Sharp transition between the lower edge of a kelp bed and upper edge of an urchin barrens caused by an urchin grazing front advancing over kelp at a depth of ~2 m within the Île du Havre study area (photo: Anne P. St-Pierre). **D**) Satellite [SPOT 7] image of a portion of the Île du Havre study area. E) Aerial image of the same portion shown in D (photo: Patrick Gagnon).82

Figure 3.3. Break down of steps in each of the four methodological modules used in the present study. **(1)** Image acquisition and pre-processing: satellite imagery of the study area was used as a base map to georectify [dashed arrow within box 1] corresponding aerial imagery. Both sets of images were digitally balanced to enhance contrast between kelp and other benthic components. Bathymetric mask was applied to restrict analysis to shallow (0 to 7 m deep) seabed. **(2)** Ground truthing: bathymetric data acquired in situ with an echosounder and from the Canadian Hydrographic Service [CHS] were used to support delineation of each study area and image classification [dashed arrows from box 2 to box 1]. Benthic photo quadrats acquired within each study area were used to validate the presence and absence of kelp on satellite and aerial imagery and support image classification and accuracy assessment [dashed arrows from box 2 to boxes 3 and 4]. **(3)** Image classification: pre-processed satellite and aerial imagery and ground truth data were used to create maps of kelp distribution from three different classification methods: unsupervised, supervised, and visual. **(4)** Accuracy assessment: classification accuracy for each of the six thematic maps created was calculated based on test location ground truth data [dashed arrow from box 2 to box 4].86

Figure 3.4. Bathymetry of the study system used to map kelp from satellite and aerial imagery with locations of ground truth data acquisition (see summary of methodological details in Figure 3.3).91

Figure 3.5. Satellite (SPOT 7) imagery of the study system in the Mingan Archipelago (from west to east; île à Firmin, île du Havre, île aux Goélands, and Petite île au Marteau) (A) and associated thematic maps obtained with the three image classification methods tested: unsupervised (B), supervised (C), and visual (D).99

Figure 3.6. Aerial imagery (mosaic of aerial photographs) of the study system in the Mingan Archipelago (from west to east; île à Firmin, île du Havre, île aux Goélands, and Petite île au Marteau) (A) and associated thematic maps obtained with the three image classification methods tested: unsupervised (B), supervised (C), and visual (D).101

Figure 3.7. Location and extent of seabed consistently classified as kelp or non-kelp by the six classification methods used (unsupervised, supervised, and visual applied to both types of imagery) or classified differently by at least one classification method. ...104

Figure 4.1. Location of the study area (pale blue) and of fine-scale study units (dark blue) at Île Niapiskau, Île à Firmin, Île du Havre, Île aux Goélands, and Petite île au Marteau, in the western sector of the Mingan Archipelago, northern Gulf of St. Lawrence, eastern Canada.134

Figure 4.2. **A)** Kelp bed [mainly *Alaria esculenta*] at a depth of ~2 m at Île Niapiskau. **B)** Sharp transition between the lower edge of the kelp bed and upper edge of an urchin barrens caused by an urchin grazing front advancing over kelp at a depth of ~2 m. **C)** Green sea urchin (*Strongylocentrotus droebachiensis*) barrens with a few kelp patches at a depth of 6 m (Photos: Anne P. St-Pierre).136

Figure 4.3. Map of the specific study area on the southward-facing subtidal fringe of five islands in the Mingan Archipelago, showing the bathymetry (within the 0 to 7 m depth range, **Panel A**), bottom slope (in degrees, **Panel B**), relative exposure index (REI, **Panel C**), and urchin density (in urchins·m⁻² **Panel D**). Urchin density is shown only for the 360 locations surveyed during ground truthing.140

Figure 4.4. Map issued from the visual classification of the aerial imagery acquired around the five studied islands in the Mingan Archipelago showing the distribution of the kelp (brown) and non-kelp (green) benthic classes.152

Figure 4.5. Comparison of kelp cover (%) as measured within the study area of each island (columns), and within fine-scale units of approximately 200 x 200 m (~40,000 m²; gray circles). The number of fine-scale units at each island was determined proportionally to the size of each island's study area, for a total of 30 sites (with 4 at Île Niapiskau, 4 at Île à Firmin, 16 at Île du Havre, 3 at Île aux Goélands, and 3 at Petite île au Marteau). The bar furthest to the right represents the overall kelp cover (62.5%) calculated over the entire study area.153

Figure 4.6. Spatial pattern metrics for the kelp (white) and non-kelp (gray) benthic classes. Metrics were calculated individually for each of the five islands and for the entire study area. **Panel A** shows the largest patch index (%). **Panel B** shows patch area where bars represent the mean (in m², ± SE) and symbols represent minimum (diamond) and maximum (circles) values. **Panel C** shows patch density (number of patches per km²). **Panel D** shows shape index (unitless, mean ± SE). **Panel E** shows

Euclidian nearest neighbour distance (in m, mean \pm SE). **Panel F** shows clumpiness index (unitless). Details regarding each metric are presented in Table 4.1..... 156

Figure 4.7. Frequency distribution of patch size (surface area, in m²) for the kelp (left side panels, from A to F) and non-kelp benthic classes (right side panels, from G to L) for each island and the entire study area. Note the exponential scale of the abscissas and various scales along the ordinates. 158

Figure 5.1 General location of the western sector of the Mingan Archipelago (boxed) within the Gulf of St. Lawrence (eastern Canada) and of the Anticosti Channel oceanographic region (hatched) as defined by Galbraith et al. (2017). The enlarged area shows the location of the study area (shaded subtidal areas) at Île Niapiskau, Île à Firmin, Île du Havre, Île aux Goélands, and Petite île au Marteau. 189

Figure 5.2. Relationship between the amount of change in kelp cover (in %) for each possible pair of images and the number of years between collection date of the images.....208

Figure 5.3. Relationships between spatial pattern metrics calculated for the kelp benthic class and environmental parameters measured in the same years as the collections occurred. Only statistically significant correlations are shown ($p < 0.05$, see Appendix C, Table 5.C.1). Pearson correlation coefficient (r) is indicated for each correlation ($n = 6$). NAO index refers to the North Atlantic Oscillation Index (see Section 5.3.3). 211

Figure 5.4. Relationships between spatial pattern metrics calculated for the kelp benthic class and environmental parameters measured in the year prior to each collection occurring. Only statistically significant correlations are shown ($p < 0.05$, see Appendix 5.C, Table 5.C.2). Pearson correlation coefficient (r) is indicated for each correlation. ($n = 6$, except for panel B where $n = 5$). NAO index refers to the North Atlantic Oscillation Index (see Section 5.3.3)..... 214

Figure 5.5. Panel A: Spatial distribution of the Kelp Stability Index (KSI) values across the study area. KSI was calculated as the sum of the presence/absence values from each grid intersect on the imagery from each year, such that a value of 6 indicated the presence of a temporally stable kelp bed (i.e., kelp beds were present in all six years studied) and 0 indicated the presence of a temporally stable non-kelp area (i.e., kelp beds were absent in all six years studied). Intermediate values indicated that the cover type had changed over time at least once (see Section 5.3.4). Panel B: Spatial

distribution of the Cover Type Variability Index (CTVI) values across the study area. CTVI was calculated by counting the number of times that the cover type identified in one grid intersect changed between one year and the subsequent year studied. Thus, a CTVI of 0 indicates that no changes in cover type occurred for a given grid intersect over the studied time period, while a value of 5 indicates that the cover type changed between each pair of successive years studied (see Section 5.3.4).216

Figure 5.6. Percent cover of each value of the Kelp Stability Index (KSI) and Cover Type Variability Index (CTVI) for each island and for the study area as a whole. Note that the KSI values range from 0 to 6, while the CTVI values range from 0 to 5 (see Section 5.3.4 and Figure 5.5 for details regarding these two indices).....217

LIST OF APPENDICES

APPENDIX 2.A: Further details regarding field equipment: fences used to create urchin enclosures and modified underwater swell kinetic instrument (URSKI).....	254
APPENDIX 2.B: Outcome of statistical analyses (see Material and Methods – Statistical analysis for a detailed description of each analysis)	259
APPENDIX 3.A: Glossary of common terms in remote sensing and GIS used in the present study.	271
APPENDIX 3.B: Contingency tables for each combination of classification technique and image source.	273
APPENDIX 5.A: Assessment of the transferability of observer training in visual classification	277
APPENDIX 5.B: Spatial pattern metrics of the non-kelp benthic class and their correlation with oceanographic and atmospheric parameters.....	285
APPENDIX 5.C: Correlations between environmental parameters and spatial pattern metrics calculated for the kelp benthic cover class.....	295
APPENDIX 5.D: Maps of the distribution of kelp and non-kelp benthic classes in the Mingan Archipelago.....	297

CO-AUTHORSHIP STATEMENT

The work described in the present thesis was conducted by Anne Provencher St-Pierre with guidance from Patrick Gagnon, Yolanda Wiersma, Jonathan Fisher, and Ladd E. Johnson. Anne Provencher St-Pierre was responsible for field and laboratory data collection and analysis, with assistance from Patrick Gagnon. All chapters were written by Anne Provencher St-Pierre with intellectual and editorial input by Patrick Gagnon. Chapter III has been published in the *Journal of Experimental Marine Biology and Ecology* (see complete reference below). Any additional publication in the primary literature resulting from work presented in this thesis will be co-authored by Anne P. St-Pierre and Patrick Gagnon (Chapters II and IV) or by Anne P. St-Pierre, Patrick Gagnon, and Ladd E. Johnson (Chapter V).

St-Pierre, A.P., Gagnon, P., 2020. Kelp-bed dynamics across scales: Enhancing mapping capability with remote sensing and GIS. *Journal of Experimental Marine Biology and Ecology* 522, 151246.

CHAPTER I

General introduction

1.1. DRIVERS OF SPECIES DISTRIBUTION

In both terrestrial and marine systems, understanding the drivers of species distribution and their impact on species coexistence, diversity patterns, as well as community resilience, represents a crucial and active area of ecological research (Brown et al., 2016; Chesson, 2000; Elith and Leathwick, 2009). Based on studies from different systems, it is generally recognized that abiotic drivers define the boundaries of the fundamental niche in which a species can establish and grow, based on its physiological limits (Chase and Leibold, 2003). Within these boundaries, variations in abiotic conditions can influence the species' abundance, dispersion, and long-term resilience (Boulangeat et al., 2012; Buma and Wessman, 2012; Ehrlén and Morris, 2015; Perkol-Finkel and Airoidi, 2010). On the other hand, biotic interactions also influence species distribution in a variety of ways including by modulating resource availability (competition and facilitation) or altering consumer-resource dynamics (predation and herbivory; Louthan et al., 2015; Van Dam, 2009; Wisz et al., 2013). Indeed, the role of herbivory as a major driver of species distribution and community structure has been extensively documented in various systems (Holmes and Webster, 2011; Lodge et al., 1998; Suzuki et al., 2013; Vergés et al., 2009); in particular, the consumption of habitat forming species (e.g., macroalgae, trees) affects functionally important attributes of ecosystems by altering rates of primary production, nutrient cycling, and species interactions (Abbas et al., 2012; Filbee-Dexter and Scheibling, 2014; Pagès et al., 2012). As such, herbivory has significant consequences for biodiversity patterns, productivity, and ecosystem resilience (Burkepile, 2013; Poore et al., 2012; Thrush et al., 2008).

It is generally accepted that patterns in species distribution and the processes driving them are scale-dependant (Huston, 1999; Kendall et al., 2011; Schneider, 2001). Hence, biotic and abiotic factors modulating species distribution at one spatial and/or temporal scale may not have a dominant impact at another scale (Karlson and Cornell, 1998; Lecours et al., 2015; Turner et al., 1989). It is often proposed that abiotic (e.g., climatic) drivers play a major role in dictating broad-scale (regional, continental, or global) species distribution patterns, while biotic interactions such as herbivory are considered to prevail at smaller (local) scales (Edwards, 2004; Pearson and Dawson, 2003; Soberón, 2007). However, these notions remain under debate; studies have shown that integrating biotic interactions into continental-scale species distribution models can greatly improve modelling outcomes (Araújo and Luoto, 2007; Boulangeat et al., 2012; Meier et al., 2010), thus implying that the effect of biotic parameters is not restricted to small spatial scales. In order to better understand scale-dependency in the effects of biotic and abiotic factors, studies must specifically investigate the links between these factors and species distribution patterns at multiple spatial and temporal scales (Hobbs, 2003; Lecours et al., 2015; Levin, 1992). Yet, because multiscale experiments can be difficult to put in place, establishing single-scale studies targeting a spatial or temporal scale which has been overlooked in a particular system can be of great use in providing a new perspective (Hobbs, 2003; Lecours et al., 2015).

The field of landscape ecology offers a spatially explicit framework for the study of the causes and consequences of spatial patterning in ecosystems (Fu et al., 2011; Turner, 2005; Turner et al., 2001). Key research topics of this field are centered around identifying links between spatial patterns in species distribution (e.g., spatial arrangement, patch size,

or diversity) and ecological processes, quantifying the importance of scale on the patterns observed, and understanding the effects of changes in spatial patterns on ecosystem functioning (Fu et al., 2011; Pittman, 2017; Turner et al., 2001). Methods from landscape ecology based on remote sensing techniques (used to survey and map landscapes over broad spatial extents, e.g., $<km^2$) have been routinely applied in terrestrial systems to assess species distribution patterns and their ecological drivers over multiple spatiotemporal scales (Frohn and Lopez, 2017; Naveh and Lieberman, 2013; Turner, 2005). For example, spatial pattern metrics (also known as landscape metrics) are commonly employed to quantify the composition, configuration, and complexity of habitat patches within a landscape from remotely acquired imagery or distribution maps (Gustafson, 1998; Mcgarigal and Marks, 1995). Approaches developed in terrestrial landscape ecology are increasingly applied to marine systems to address questions relative to species distribution, patch dynamics, and fragmentation, which cannot be fully investigated without a broad-scale perspective (Boström et al., 2011; Grober-Dunsmore et al., 2007; Pittman, 2017; Qingzhong et al., 2004; Wedding et al., 2011). In marine systems, these approaches are particularly valuable for the study of habitat-forming foundation species (*sensu* Dayton, 1972) such as macroalgae and seagrasses. Because the loss of foundation species has wide-ranging consequences on diversity, productivity, and ecosystem services (Ellison et al., 2005; Filbee-Dexter and Scheibling, 2014; Thomson et al., 2015), a strong understanding of the drivers and consequences of the spatial distribution of foundation species is crucial to predict and mitigate changes to these ecosystem.

1.2. KELP-URCHIN SYSTEMS

Brown algae of the order Laminariales, called kelp, are foundation species found along ~25% of the world's coastlines (Filbee-Dexter and Scheibling, 2014; Steneck et al., 2013). These macroalgae generally develop on rocky substrate in areas of largely cold, nutrient rich water such as temperate coastal zones and upwelling zones, in depths up to 10-25 m (Bartsch et al., 2008; Steneck et al., 2002). Kelp sporophytes are perennial, with some species reaching individual longevity of up to 25 years (Smale et al., 2013; Steneck and Dethier, 1994). Kelp forests (i.e., with floating surface canopies) and beds (i.e., completely submerged) are some of the most productive habitats on earth (Mann, 1973); by forming biogenic habitats with complex three-dimensional structures, kelps provide habitat for mobile fauna and substratum for sessile fauna and algae (Dayton, 1985; Smale et al., 2013; Steneck et al., 2002). Kelp beds have been identified as important refuge and nursery ground for a variety of pelagic and benthic species (Smale and Wernberg, 2013; Steneck et al., 2002), including commercially important species of fish (Gotceitas et al., 1995; Norderhaug et al., 2005) and crustaceans (Johnson and Hart, 2001). In addition to enhancing local biodiversity and secondary productivity, kelp also provide valuable ecosystem services, including nutrient cycling and coastal protection (Beaumont et al., 2007; Smale et al., 2013).

Abiotic factors such as nutrient availability (Dayton et al., 1999; Hernandez-Carmona et al., 2001), light conditions (Henley and Dunton, 1997), ice scouring (Gagnon et al., 2004; Keats et al., 1985), wave action (Bekkby et al., 2009; Frey and Gagnon, 2015; Hepburn et al., 2007), and temperature (Buschmann et al., 2004; Fredersdorf et al., 2009) have been shown to modulate kelp presence and growth. However, herbivory by sea urchins has been identified as the main driver of kelp distribution in many systems (Gagnon et al., 2004;

Konar et al., 2014; Lauzon-Guay and Scheibling, 2007; Norderhaug and Christie, 2009), and destructive grazing by sea urchins is a major cause of kelp deforestation worldwide (Filbee-Dexter and Scheibling, 2014; Graham, 2004; Ling et al., 2015). Because of this relationship, so-called kelp-urchin systems often present a dichotomous community structure, divided between kelp communities and urchin barrens. In the latter, fleshy seaweed are scarce as they are consumed by the numerous sea urchins and encrusting coralline algae is abundant, thus presenting lower levels of biodiversity and productivity than kelp communities (Chapman and Johnson, 1990; Christie et al., 2009).

Kelp beds and urchin barrens are generally found side by side with the boundary between the two being largely determined by urchin grazing (Gagnon et al., 2004; Konar and Estes, 2003). In some systems, these communities alternate temporally, creating phase shifts in which a system transitions from a kelp-dominated state to an urchin-dominated state, or vice-versa (Filbee-Dexter and Scheibling, 2014; Simenstad et al., 1978; Steneck et al., 2013). Phase shifts are generally caused by variations in urchin density, either becoming too low for the urchins to effectively graze on kelp (causing a shift from urchin- to kelp-dominated states) or increasing so high that urchins destructively consume the kelp and prevent its recolonization in the barren (causing a shift from kelp- to urchin-dominated states; reviewed in Filbee-Dexter and Scheibling, 2014). In most kelp-urchin systems where phase shifts have been documented, the threshold urchin density required for forward (kelp- to-urchin) shift is up to an order of magnitude higher than the density required for a reverse (urchin-to-kelp) shift, indicative of a discontinuous phase shift (deYoung et al., 2008; Filbee-Dexter and Scheibling, 2014; Scheffer et al., 2001). This type of transition signals the presence of alternate stable states (also called multiple stable states), in which each state

1) can exist under the same environmental conditions, 2) persists after the driver of the transition (in this case, urchin density) is relaxed or reversed (i.e., the system presents hysteresis), and 3) is maintained through feedback mechanisms which confer resilience to small perturbations or fluctuations in urchin density (Filbee-Dexter and Scheibling, 2014; Scheffer et al., 2001).

General understanding of the drivers of phase shifts in kelp-urchin systems vary greatly among regions. In areas where phase shifts are numerous, factors controlling urchin populations have been identified as modulating phase shifts (Filbee-Dexter and Scheibling, 2014). In eastern Canada, for instance, transitions between kelp- and urchin-dominated states have been well documented in Nova Scotia where several phase shifts have occurred since the 1960s (Breen and Mann, 1976; Scheibling et al., 1999). In this region, overgrazing by the green sea urchin, *Strongylocentrotus droebachiensis*, after pulse recruitment events lead to abrupt transitions from kelp- to urchin-dominated states over several kilometres of coastline (Hart and Scheibling, 1988). Similarly, in the Gulf of Maine and the North Pacific, removal of urchin predators such as predatory fish (cod, haddock and wolffish) and sea otters, respectively, led to increases in urchin populations and facilitated shifts from kelp- to urchin-dominated states (Oshurkov et al. 1988, Steneck et al., 2004, Watson & Estes 2011). Once created, urchin barrens persist for several years through a series of stabilizing feedback mechanisms; for example, urchin grazing pressure in barrens prevents recolonization of kelp and the barren state facilitates urchin settlement (Filbee-Dexter and Scheibling, 2014). Urchin populations do not tend to crash with the exhaustion of their food source; rather, these consumers can survive for long time periods (up to several years) in kelp-depleted barren grounds by consuming biofilm while decreasing their growth rate and

gonad size (Lang and Mann, 1976). In Nova Scotia, a reverse shift from urchin- to kelp-dominated states can be triggered by disease outbreaks (caused by the pathogenic amoeba *Paramoeba invadens*; Feehan et al., 2013; Jones, 1985) which decimate urchin population and release kelp from urchin grazing pressure (Scheibling et al., 1999).

Yet, phase shifts between kelp beds and urchin barrens are not ubiquitous and several regions worldwide present either community state without exhibiting large-scale phase shifts (Filbee-Dexter and Scheibling, 2014; Johnson et al., 2019; Krumhansl et al., 2016). For example, extensive urchin barrens are found along the coast of the northern Gulf of St. Lawrence (nGSL) and southeastern Newfoundland (SEN) and, unlike the cyclical shifts observed in Nova Scotia, these barrens appear to have remained present for decades, without exhibiting large-scale shifts in community states (Gagnon et al., 2004; Himmelman, 1984, 1991; Keats et al., 1985). These regions are dominated by urchin barrens but still sustain small, shallow (generally <8 m) kelp beds (Frey and Gagnon, 2015; Gagnon et al., 2004; Himmelman and Dutil, 1991). Urchins generally form feeding fronts at the deeper edge of these kelp beds and graze through the latter during summer, pushing back the kelp bed edge at a rate up to $2.5 \text{ m}\cdot\text{mo}^{-1}$ (Frey and Gagnon, 2015; Gagnon et al., 2004). During winter when urchins are less active due to colder temperature (Frey and Gagnon, 2015; Siikavuopio et al., 2006), kelp recruitment occurs and kelp beds can recover, generally over a few metres (DFO, 2013; Gagnon et al., 2004; Scheibling et al., 1999). In both the nGSL and SEN, kelp-urchin systems appear to be locked in an urchin-barren state where urchin grazing dictates the distribution of kelp beds (Frey and Gagnon, 2015; Gagnon et al., 2004) while the lack of either urchin predators or diseases allows urchin populations to maintain high densities (Himmelman et al., 1983; Johnson et al., 2019;

Scheibling, 1997). While the threshold urchin density necessary to maintain grazing on kelp beds in summer in the nGSL region has been estimated to be $\sim 5 \text{ kg}\cdot\text{m}^{-2}$ (Gagnon et al., 2004), such information is lacking for the SEN region. In addition, an understanding of the conditions required for a large-scale phase shift from urchin- to kelp-dominated states remain largely unexplored in both regions but is necessary to identify the drivers of stability and predict change in community states in these systems.

In eastern Canada, the biology and ecology of kelp has been scrutinized over the past few decades; however, studies have generally been limited to small spatial (few 100s of m^2 at most) and temporal (3-5 years) extents due to the difficulty of monitoring completely submerged benthic systems (Filbee-Dexter et al., 2019; Frey and Gagnon, 2015; Gagnon et al., 2004; Lauzon-Guay and Scheibling, 2007). Indeed, traditional kelp monitoring generally relies on time consuming and costly SCUBA-based methods, often forcing researchers to constrain the spatiotemporal extent of their studies. Hence, drivers of kelp distribution at broad spatiotemporal scales (km^2 , years to decades) remain poorly understood, despite the recognized importance of multi-scale observations to properly document how alternative stable state systems are established and maintained in natural systems (Petraitis and Latham, 1999). Addressing this lack of knowledge requires the exploration of novel techniques to monitor submerged kelp distribution at various spatiotemporal scales. As such, approaches from landscape ecology that take advantage of recent advances in the precision and accessibility of remote sensing and geographic information system (GIS) technologies are an ideal alternative to small-scale SCUBA-based methods. For kelp-urchin systems in particular, these approaches will allow the study of kelp distribution patterns (including the abundance, shape, area, and clustering of kelp

beds) and of the boundary dynamics between kelp and urchin communities at broad spatiotemporal scales unexplored so far.

1.3. MAIN OBJECTIVES AND THESIS STRUCTURE

The present thesis investigates the factors leading to the apparent stability of kelp beds and urchin barrens observed in southeastern Newfoundland (SEN) and the northern Gulf of St. Lawrence (nGSL), Canada. It aims to assess small-scale (m^2) interactions between kelp and urchins and identify the thresholds urchin density required to maintain the destructive grazing on kelp bed in SEN by applying traditional SCUBA-based monitoring techniques (Chapter II). Another aim of this thesis is to investigate kelp distribution patterns and their drivers at broad spatiotemporal scales (km^2) which have been largely overlooked in studies of kelp-urchin systems to date due to the restrictions imposed by traditional sampling methods (i.e., SCUBA). To that effect, a combination of remote sensing techniques, landscape ecology approaches, and modelling techniques are applied in three of the core chapters (Chapters III, IV, and V) to assess broad-scale (km^2) kelp distribution patterns in the Mingan Archipelago, nGSL, and investigate the causes and consequences of the configuration, complexity, and stability of kelp aggregates over time. This GIS-based investigation of kelp dynamics was conducted in the Mingan Archipelago due to the reasonable knowledge of kelp dynamics at the metre scale in that region from previous studies (Gagnon et al., 2004; Gagnon et al., 2005; Himmelman, 1991) offering a basis for comparison of broader scale studies.

Specifically, Chapter II focuses on the effect of herbivore pressure on kelp bed destruction and recovery in southeastern Newfoundland. While the threshold urchin density

required to consume kelp beds has been the subject of investigation in other areas of eastern Canada, information regarding urchin density and feeding in SEN is still scarce. Because the threshold urchin density for kelp bed destruction and the thresholds for phase shifts between kelp- and urchin-dominated community states vary among regions (e.g., between nGSL and Nova Scotia; Gagnon et al., 2004; Lauzon-Guay and Scheibling, 2007), investigating the effect of urchin density on kelp bed destruction in Newfoundland provides insight in the kelp-urchin dynamics of this understudied region. A manipulative field experiment was designed to identify the threshold urchin density required to maintain destructive grazing upon kelp beds and to examine the effects of environmental factors (i.e., temperature and wave action as estimated by flow acceleration) on urchin activity at one site in SEN over two consecutive summers (2015 and 2016).

Chapters III, IV, and V form a trilogy which sets aside the traditional kelp monitoring techniques and explores alternative methods based on remote sensing and GIS technologies to investigate kelp-bed dynamics across various scales. Initially, the applicability and accuracy of such methods needed to be investigated in the context of completely submerged kelp systems. Therefore, Chapter III aimed to establish the foundation of a simple, accessible, and robust set of remote sensing and GIS-based methods to quantify the spatial distribution of completely submerged kelp beds over broad (km^2) spatial extents. This chapter tested the suitability of conventional image classification methods (i.e., a software-led unsupervised classification, a software-led supervised classification, and a visual classification by a trained observer) for mapping kelp from digital aerial and satellite imagery of $\sim 2.5 \text{ km}^2$ of seabed in the Mingan Archipelago (nGSL).

The findings from Chapter III were used as a basis for the work presented in Chapter IV. In the latter, the most accurate method for kelp bed detection identified in Chapter III (i.e., visual classification of aerial imagery) was applied to imagery of the shallow subtidal fringe of five islands in the Mingan Archipelago. This imagery acquired in 2016 represents a snapshot of kelp distribution and was used to quantify kelp distribution patterns by measuring spatial pattern metrics to describe and compare the patterns in kelp distribution among islands within the archipelago. In addition, this chapter examines the correlations between kelp presence and physical and biotic parameters (namely depth, slope, exposure to waves, and urchin density) to identify potential drivers of kelp distribution at a broad spatial scale (km²).

Lastly, Chapter V examines temporal variations in kelp bed distribution in the Mingan Archipelago by applying the methods described in Chapter IV to a time-series of aerial imagery covering the same extent of seabed. Aerial images were acquired in six years between 1983 and 2016. Spatial pattern metrics were used to quantify the spatial characteristics of kelp beds in each year studied, including kelp coverage, number of kelp patches, mean patch area, and largest patch index, which were then correlated with atmospheric or oceanographic conditions to identify potential drivers of temporal changes in kelp distribution patterns. The effects of depth, bottom slope, and exposure to waves on the persistence of kelp beds and variability in cover type over time were assessed to identify drivers of stability and change in this system. The analyses conducted in this chapter represent the most spatially and temporally broad investigation of the drivers of kelp bed distribution and stability in the Gulf of St. Lawrence to date and present a novel broad-scale perspective of the variability in distribution patterns of completely submerged kelp beds.

The four core chapters of this thesis (Chapters II, III, IV, and V) were written in a format compatible with publication in the primary scientific literature as stand-alone papers, which explains the repetition of some biological, ecological, or technical information among chapters. The last chapter of this thesis (Chapter VI) summarizes the main findings of the research and their contribution to advancing our understanding of kelp-urchin systems and presents future research avenues.

1.4. REFERENCES

- Abbas, F., Merlet, J., Morellet, N., Verheyden, H., Hewison, A., Cargnelutti, B., Angibault, J., Picot, D., Rames, J., Lourtet, B., 2012. Roe deer may markedly alter forest nitrogen and phosphorus budgets across Europe. *Oikos* 121, 1271-1278.
- Araújo, M.B., Luoto, M., 2007. The importance of biotic interactions for modelling species distributions under climate change. *Glob Ecol Biogeogr* 16, 743-753.
- Bartsch, I., Wiencke, C., Bischof, K., Buchholz, C.M., Buck, B.H., Eggert, A., Feuerpfeil, P., Hanelt, D., Jacobsen, S., Karez, R., 2008. The genus *Laminaria sensu lato*: recent insights and developments. *Eur J Phycol* 43, 1-86.
- Beaumont, N., Austen, M., Atkins, J., Burdon, D., Degraer, S., Dentinho, T., Deros, S., Holm, P., Horton, T., Van Ierland, E., 2007. Identification, definition and quantification of goods and services provided by marine biodiversity: implications for the ecosystem approach. *Mar Pollut Bull* 54, 253-265.
- Bekkby, T., Rinde, E., Erikstad, L., Bakkestuen, V., 2009. Spatial predictive distribution modelling of the kelp species *Laminaria hyperborea*. *ICES J Mar Sci* 66, 2106-2115.
- Boström, C., Pittman, S.J., Simenstad, C., Kneib, R.T., 2011. Seascape ecology of coastal biogenic habitats: advances, gaps, and challenges. *Mar Ecol Prog Ser* 427, 191-217.
- Boulangeat, I., Gravel, D., Thuiller, W., 2012. Accounting for dispersal and biotic interactions to disentangle the drivers of species distributions and their abundances. *Ecol Lett* 15, 584-593.
- Breen, P.A., Mann, K.H., 1976. Destructive grazing of kelp by sea urchins in eastern Canada. *J Fish Res Board of Canada* 33, 1278-1283.

- Brown, C.J., O'Connor, M.I., Poloczanska, E.S., Schoeman, D.S., Buckley, L.B., Burrows, M.T., Duarte, C.M., Halpern, B.S., Pandolfi, J.M., Parmesan, C., Richardson, A.J., 2016. Ecological and methodological drivers of species' distribution and phenology responses to climate change. *Global Change Biol* 22, 1548-1560.
- Buma, B., Wessman, C.A., 2012. Differential species responses to compounded perturbations and implications for landscape heterogeneity and resilience. *Forest Ecol Manag* 266, 25-33.
- Burkepile, D.E., 2013. Comparing aquatic and terrestrial grazing ecosystems: is the grass really greener? *Oikos* 122, 306-312.
- Buschmann, A., Vásquez, J., Osorio, P., Reyes, E., Filún, L., Hernández-González, M., Vega, A., 2004. The effect of water movement, temperature and salinity on abundance and reproductive patterns of *Macrocystis spp.* (Phaeophyta) at different latitudes in Chile. *Mar Biol* 145, 849-862.
- Chapman, A.R.O., Johnson, C.R., 1990. Disturbance and organization of macroalgal assemblages in the Northwest Atlantic. *Hydrobiologia* 192, 77-121.
- Chase, J.M., Leibold, M.A., 2003. Ecological niches: linking classical and contemporary approaches. University of Chicago Press.
- Chesson, P., 2000. Mechanisms of maintenance of species diversity. *Annu Rev Ecol Syst* 31, 343-366.
- Christie, H., Norderhaug, K.M., Fredriksen, S., 2009. Macrophytes as habitat for fauna. *Mar Ecol Prog Ser* 396, 221-233.
- Dayton, P.K., 1972. Toward an understanding of community resilience and the potential effects of enrichments to the benthos at McMurdo Sound, Antarctica, Proceedings of the colloquium on conservation problems in Antarctica. Allen Press Lawrence, KS, pp. 81-96.
- Dayton, P.K., 1985. Ecology of kelp communities. *Annu Rev Ecol Syst* 16, 215-245.
- Dayton, P.K., Tegner, M.J., Edwards, P.B., Riser, K.L., 1999. Temporal and spatial scales of kelp demography: the role of oceanographic climate. *Ecol Monogr* 69, 219-250.
- deYoung, B., Barange, M., Beaugrand, G., Harris, R., Perry, R.I., Scheffer, M., Werner, F., 2008. Regime shifts in marine ecosystems: detection, prediction and management. *Trends Ecol Evol* 23, 402-409.
- DFO, 2013. Assessment of Information on Irish Moss, Rockweed, and Kelp Harvests in Nova Scotia. Department of Fisheries and Ocean Canada. Sci Advis Sec Sci Advis Rep 2013/004.

- Edwards, M.S., 2004. Estimating scale-dependency in disturbance impacts: El Niños and giant kelp forests in the northeast Pacific. *Oecologia* 138, 436-447.
- Ehrlen, J., Morris, W.F., 2015. Predicting changes in the distribution and abundance of species under environmental change. *Ecol Lett* 18, 303-314.
- Elith, J., Leathwick, J.R., 2009. Species distribution models: ecological explanation and prediction across space and time. *Annu Rev Ecol Evol Syst* 40, 677-697.
- Ellison, A.M., Bank, M.S., Clinton, B.D., Colburn, E.A., Elliott, K., Ford, C.R., Foster, D.R., Kloeppel, B.D., Knoepp, J.D., Lovett, G.M., 2005. Loss of foundation species: consequences for the structure and dynamics of forested ecosystems. *Front Ecol Environ* 3, 479-486.
- Feehan, C.J., Johnson-Mackinnon, J., Scheibling, R.E., Lauzon-Guay, J.-S., Simpson, A.G.B., 2013. Validating the identity of *Paramoeba invadens*, the causative agent of recurrent mass mortality of sea urchins in Nova Scotia, Canada. *Dis Aquat Organ* 103, 209-227.
- Filbee-Dexter, K., Scheibling, R.E., 2014. Sea urchin barrens as alternative stable states of collapsed kelp ecosystems. *Mar Ecol Prog Ser* 495, 1-25.
- Filbee-Dexter, K., Wernberg, T., Fredriksen, S., Norderhaug, K.M., Pedersen, M.F., 2019. Arctic kelp forests: Diversity, resilience and future. *Glob Planet Change* 172, 1-14.
- Fredersdorf, J., Müller, R., Becker, S., Wiencke, C., Bischof, K., 2009. Interactive effects of radiation, temperature and salinity on different life history stages of the Arctic kelp *Alaria esculenta* (Phaeophyceae). *Oecologia* 160, 483-492.
- Frey, D.L., Gagnon, P., 2015. Thermal and hydrodynamic environments mediate individual and aggregative feeding of a functionally important omnivore in reef communities. *Plos One* 10, e0118583.
- Frohn, R.C., Lopez, R.D., 2017. Remote sensing for landscape ecology: New metric indicators: monitoring, modeling, and assessment of ecosystems. CRC Press.
- Fu, B., Liang, D., Lu, N., 2011. Landscape ecology: Coupling of pattern, process, and scale. *Chin Geogr Sci* 21, 385.
- Gagnon, P., Himmelman, J.H., Johnson, L.E., 2004. Temporal variation in community interfaces: kelp-bed boundary dynamics adjacent to persistent urchin barrens. *Mar Biol* 144, 1191-1203.
- Gagnon, P., Johnson, L.E., Himmelman, J.H., 2005. Kelp patch dynamics in the face of intense herbivory: Stability of *Agarum clathratum* (Phaeophyta) stands and associated flora on urchin barrens. *J Phycol* 41, 498-505.

- Gotceitas, V., Fraser, S., Brown, J.A., 1995. Habitat use by juvenile Atlantic cod (*Gadus morhua*) in the presence of an actively foraging and non-foraging predator. *Mar Biol* 123, 421-430.
- Graham, M.H., 2004. Effects of local deforestation on the diversity and structure of Southern California giant kelp forest food webs. *Ecosystems* 7, 341-357.
- Grober-Dunsmore, R., Frazer, T. K., Beets, J. P., Lindberg, W. J., Zwick, P., & Funicelli, N. A., 2008. Influence of landscape structure on reef fish assemblages. *Landsc Ecol*, 23(1), 37-53.
- Gustafson, E.J., 1998. Quantifying landscape spatial pattern: what is the state of the art? *Ecosystems* 1, 143-156.
- Hart, M.W., Scheibling, R.E., 1988. Heat waves, baby booms, and the destruction of kelp beds by sea urchins. *Mar Biol* 99, 167-176.
- Henley, W.J., Dunton, K.H., 1997. Effects of nitrogen supply and continuous darkness on growth and photosynthesis of the arctic kelp *Laminaria solidungula*. *Limnol Oceanogr* 42, 209-216.
- Hepburn, C.D., Holborow, J.D., Wing, S.R., Frew, R.D., Hurd, C.L., 2007. Exposure to waves enhances the growth rate and nitrogen status of the giant kelp *Macrocystis pyrifera*. *Mar Ecol Prog Ser* 339, 99-108.
- Hernandez-Carmona, G., Robledo, D., Serviere-Zaragoza, E., 2001. Effect of nutrient availability on *Macrocystis pyrifera* recruitment and survival near its southern limit off Baja California. *Bot Mar* 44, 221-229.
- Himmelman, J.H., 1984. Urchin feeding and macroalgal distribution in Newfoundland, eastern Canada. *Nat Can* 111, 337-348.
- Himmelman, J.H., 1991. Diving observations of subtidal communities in the northern Gulf of St. Lawrence. *Can Special Pub Fish Aquat Sci* 113, 319-332.
- Himmelman, J.H., Dutil, C., 1991. Distribution, population-structure and feeding of subtidal seastars in the northern Gulf of St-Lawrence. *Mar Ecol Prog Ser* 76, 61-72.
- Himmelman, J.H., Lavergne, Y., Axelsen, F., Cardinal, A., Bourget, E., 1983. Sea urchins in the Saint Lawrence Estuary: their abundance, size-structure, and suitability for commercial exploitation. *Can J Fish Aquat Sci* 40, 474-486.
- Hobbs, N.T., 2003. Challenges and opportunities in integrating ecological knowledge across scales. *Forest Ecol Manag* 181, 223-238.

- Holmes, S.A., Webster, C.R., 2011. Herbivore-induced expansion of generalist species as a driver of homogenization in post-disturbance plant communities. *Plant Ecology* 212, 753-768.
- Huston, M.A., 1999. Local processes and regional patterns: appropriate scales for understanding variation in the diversity of plants and animals. *Oikos*, 393-401.
- Johnson, L.E., MacGregor, K.A., Narvaez, C.A., Suskiewicz, T.S., 2019. Subtidal rocky shores of the north-west Atlantic Ocean: The complex ecology of a simple ecosystem, in: Williams, G.A., Bohn, K., Firth, L.B., Hawkins, S.J. (Eds.), *Interactions in the Marine Benthos: Global Patterns and Processes*. Cambridge University Press, Cambridge, pp. 90-127.
- Johnson, M., Hart, P., 2001. Preliminary report of the coastal fisheries around the coasts of the British Isles 1950–1999. Fisheries impacts on North Atlantic ecosystems: catch, effort and national/regional datasets. Fisheries Centre Research Report, University of British Columbia, Vancouver, Canada, 135-140.
- Jones, G.M., 1985. *Paramoeba invadens* n. sp. (Amoebida, Paramoebidae), a pathogenic amoeba from the sea urchin, *Strongylocentrotus droebachiensis*, in eastern Canada. *J Protozool* 32, 564-569.
- Karlson, R.H., Cornell, H.V., 1998. Scale-dependent variation in local vs. regional effects on coral species richness. *Ecol Monogr* 68, 259-274.
- Keats, D., South, G., Steele, D., 1985. Algal biomass and diversity in the upper subtidal at a pack-ice disturbed site in eastern Newfoundland. *Mar Ecol Prog Ser*, 151-158.
- Kendall, M.S., Miller, T.J., Pittman, S.J., 2011. Patterns of scale-dependency and the influence of map resolution on the seascape ecology of reef fish. *Mar Ecol Prog Ser* 427, 259-274.
- Konar, B., Edwards, M.S., Estes, J.A., 2014. Biological interactions maintain the boundaries between kelp forests and urchin barrens in the Aleutian Archipelago. *Hydrobiologia* 724, 91-107.
- Konar, B., Estes, J.A., 2003. The stability of boundary regions between kelp beds and deforested areas. *Ecology* 84, 174-185.
- Krumhansl, K.A., Okamoto, D.K., Rassweiler, A., Novak, M., Bolton, J.J., Cavanaugh, K.C., Connell, S.D., Johnson, C.R., Konar, B., Ling, S.D., Micheli, F., Norderhaug, K.M., Pérez-Matus, A., Sousa-Pinto, I., Reed, D.C., Salomon, A.K., Shears, N.T., Wernberg, T., Anderson, R.J., Barrett, N.S., Buschmann, A.H., Carr, M.H., Caselle, J.E., Derrien-Courtet, S., Edgar, G.J., Edwards, M., Estes, J.A., Goodwin, C., Kenner, M.C., Kushner, D.J., Moy, F.E., Nunn, J., Steneck, R.S., Vásquez, J., Watson, J.,

- Witman, J.D., Byrnes, J.E.K., 2016. Global patterns of kelp forest change over the past half-century. *Proc Natl Acad Sci USA* 113, 13785-13790.
- Lang, C., Mann, K.H., 1976. Changes in sea urchin populations after the destruction of kelp beds. *Mar Biol* 36, 321-326.
- Lauzon-Guay, J.S., Scheibling, R.E., 2007. Behaviour of sea urchin *Strongylocentrotus droebachiensis* grazing fronts: food-mediated aggregation and density-dependent facilitation. *Mar Ecol Prog Ser* 329, 191-204.
- Lecours, V., Devillers, R., Schneider, D.C., Lucieer, V.L., Brown, C.J., Edinger, E.N., 2015. Spatial scale and geographic context in benthic habitat mapping: review and future directions. *Mar Ecol Prog Ser* 535, 259-284.
- Levin, S.A., 1992. The problem of pattern and scale in ecology: the Robert H. MacArthur award lecture. *Ecology* 73, 1943-1967.
- Ling, S., Scheibling, R., Rassweiler, A., Johnson, C., Shears, N., Connell, S., Salomon, A., Norderhaug, K., Pérez-Matus, A., Hernández, J., 2015. Global regime shift dynamics of catastrophic sea urchin overgrazing. *Phil Trans R Soc B* 370, 20130269.
- Lodge, D.M., Cronin, G., van Donk, E., Froelich, A.J., 1998. Impact of Herbivory on Plant Standing Crop: Comparisons Among Biomes, Between Vascular and Nonvascular Plants, and Among Freshwater Herbivore Taxa, in: Jeppesen, E., Søndergaard, M., Søndergaard, M., Christoffersen, K. (Eds.), *The structuring role of submerged macrophytes in lakes*. Springer New York, New York, NY, pp. 149-174.
- Louthan, A.M., Doak, D.F., Angert, A.L., 2015. Where and when do species interactions set range limits? *Trends Ecol Evol* 30, 780-792.
- Mann, K., 1973. Seaweeds: their productivity and strategy for growth. *Science* 182, 975-981.
- Mcgarigal, K., Marks, B.J., 1995. Spatial pattern analysis program for quantifying landscape structure. Gen. Tech. Rep. PNW-GTR-351. US Department of Agriculture, Forest Service, Pacific Northwest Research Station, 1-122.
- Meier, E.S., Kienast, F., Pearman, P.B., Svenning, J.C., Thuiller, W., Araújo, M.B., Guisan, A., Zimmermann, N.E., 2010. Biotic and abiotic variables show little redundancy in explaining tree species distributions. *Ecography* 33, 1038-1048.
- Naveh, Z., Lieberman, A.S., 2013. *Landscape ecology: theory and application*. Springer Science & Business Media.

- Norderhaug, K.M., Christie, H., Fosså, J.H., Fredriksen, S., 2005. Fish–macrofauna interactions in a kelp (*Laminaria hyperborea*) forest. *J Mar Biol Assoc Uk* 85, 1279-1286.
- Norderhaug, K.M., Christie, H.C., 2009. Sea urchin grazing and kelp re-vegetation in the NE Atlantic. *Mar Biol Res* 5, 515-528.
- Oshurkov V.V., Bazhin A.G., Lukin V.I., Sevostyanov V.F., 1988. Sea otter predation and the benthic community structure of Commander Islands. *Biol Mora* 6, 50–60.
- Pagès, J.F., Farina, S., Gera, A., Arthur, R., Romero, J., Alcoverro, T., 2012. Indirect interactions in seagrasses: fish herbivores increase predation risk to sea urchins by modifying plant traits. *Funct Ecol* 26, 1015-1023.
- Pearson, R.G., Dawson, T.P., 2003. Predicting the impacts of climate change on the distribution of species: are bioclimate envelope models useful? *Glob Ecol Biogeogr* 12, 361-371.
- Perkol-Finkel, S., Airoidi, L., 2010. Loss and recovery potential of marine habitats: an experimental study of factors maintaining resilience in subtidal algal forests at the Adriatic Sea. *Plos One* 5.
- Petraitis, P.S., Latham, R.E., 1999. The importance of scale in testing the origins of alternative community states. *Ecology* 80, 429-442.
- Pittman, S.J., 2017. *Seascape ecology*. John Wiley & Sons.
- Poore, A.G., Campbell, A.H., Coleman, R.A., Edgar, G.J., Jormalainen, V., Reynolds, P.L., Sotka, E.E., Stachowicz, J.J., Taylor, R.B., Vanderklift, M.A., 2012. Global patterns in the impact of marine herbivores on benthic primary producers. *Ecol Lett* 15, 912-922.
- Qingzhong, Z., Qingyi, C., Wenliang, W., 2004. Landscape ecology: a new perspective on the researches of marine ecosystem. *Acta Ecologica Sinica*, 24(4), 819-824.
- Scheffer, M., Carpenter, S., Foley, J.A., Folke, C., Walker, B., 2001. Catastrophic shifts in ecosystems. *Nature* 413, 591-596.
- Scheibling, R., 1997. The role of predation in regulating sea urchin populations in eastern Canada. *Oceanog Lit Rev* 2, 135.
- Scheibling, R.E., Hennigar, A.W., Balch, T., 1999. Destructive grazing, epiphytism, and disease: the dynamics of sea urchin-kelp interactions in Nova Scotia. *Can J Fish Aquat Sci* 56, 2300-2314.

- Schneider, D.C., 2001. The rise of the concept of scale in ecology: The concept of scale is evolving from verbal expression to quantitative expression. *AIBS Bulletin* 51, 545-553.
- Siikavuopio, S.I., Christiansen, J.S., Dale, T., 2006. Effects of temperature and season on gonad growth and feed intake in the green sea urchin (*Strongylocentrotus droebachiensis*). *Aquaculture* 255, 389-394.
- Simenstad, C.A., Estes, J.A., Kenyon, K.W., 1978. Aleuts, sea otters, and alternate stable-state communities. *Science* 200, 403-411.
- Smale, D.A., Burrows, M.T., Moore, P., O'Connor, N., Hawkins, S.J., 2013. Threats and knowledge gaps for ecosystem services provided by kelp forests: a northeast Atlantic perspective. *Ecol Evol* 3, 4016-4038.
- Smale, D.A., Wernberg, T., 2013. Extreme climatic event drives range contraction of a habitat-forming species. *P Roy Soc B: Biol Sci* 280.
- Soberón, J., 2007. Grinnellian and Eltonian niches and geographic distributions of species. *Ecol Lett* 10, 1115-1123.
- Steneck, R.S., Dethier, M.N., 1994. A functional group approach to the structure of algal-dominated communities. *Oikos*, 476-498.
- Steneck, R.S., Graham, M.H., Bourque, B.J., Corbett, D., Erlandson, J.M., Estes, J.A., Tegner, M.J., 2002. Kelp forest ecosystems: biodiversity, stability, resilience and future. *Environ Conserv* 29, 436-459.
- Steneck, R., Vavrinec, J. & Leland, A., 2004. Accelerating Trophic-level Dysfunction in Kelp Forest Ecosystems of the Western North Atlantic. *Ecosystems* 7, 323–332.
- Steneck, R.S., Leland, A., McNaught, D.C., Vavrinec, J., 2013. Ecosystem flips, locks, and feedbacks: The lasting effects of fisheries on Maine's kelp forest ecosystem. *Bull Mar Sci* 89, 31-55.
- Suzuki, M., Miyashita, T., Kabaya, H., Ochiai, K., Asada, M., Kikvidze, Z., 2013. Deer herbivory as an important driver of divergence of ground vegetation communities in temperate forests. *Oikos* 122, 104-110.
- Thomson, J.A., Burkholder, D.A., Heithaus, M.R., Fourqurean, J.W., Fraser, M.W., Statton, J., Kendrick, G.A., 2015. Extreme temperatures, foundation species, and abrupt ecosystem change: an example from an iconic seagrass ecosystem. *Global Change Biol* 21, 1463-1474.

- Thrush, S.F., Halliday, J., Hewitt, J.E., Lohrer, A.M., 2008. The effects of habitat loss, fragmentation, and community homogenization on resilience in estuaries. *Ecol Appl* 18, 12-21.
- Turner, M.G., 2005. Landscape ecology in North America: Past, present, and future. *Ecology* 86, 1967-1974.
- Turner, M.G., Gardner, R.H., O'Neill, R.V., 2001. Landscape ecology in theory and practice: patterns and process. (Vol. 401) Springer, New York.
- Turner, M.G., O'Neill, R.V., Gardner, R.H., Milne, B.T., 1989. Effects of changing spatial scale on the analysis of landscape pattern. *Landsc Ecol* 3, 153-162.
- Van Dam, N., 2009. How plants cope with biotic interactions. *Plant Biol* 11, 1-5.
- Vergés, A., Alcoverro, T., Ballesteros, E., 2009. Role of fish herbivory in structuring the vertical distribution of canopy algae *Cystoseira spp.* in the Mediterranean Sea. *Mar Ecol Prog Ser* 375, 1-11.
- Watson J., Estes J.A., 2011. Stability, resilience, and phase shifts in rocky subtidal communities along the west coast of Vancouver Island, Canada. *Ecol Monogr* 81, 215–239.
- Wedding, L.M., Lepczyk, C.A., Pittman, S.J., Friedlander, A.M., Jorgensen, S., 2011. Quantifying seascape structure: extending terrestrial spatial pattern metrics to the marine realm. *Mar Ecol Prog Ser* 427, 219-232.
- Wisz, M.S., Pottier, J., Kissling, W.D., Pellissier, L., Lenoir, J., Damgaard, C.F., Dormann, C.F., Forchhammer, M.C., Grytnes, J.-A., Guisan, A., Heikkinen, R.K., Høye, T.T., Kühn, I., Luoto, M., Maiorano, L., Nilsson, M.-C., Normand, S., Öckinger, E., Schmidt, N.M., Termansen, M., Timmermann, A., Wardle, D.A., Aastrup, P., Svenning, J.-C., 2013. The role of biotic interactions in shaping distributions and realised assemblages of species: implications for species distribution modelling. *Biol Rev* 88, 15-30.

CHAPTER II

Quantifying the threshold urchin density for kelp bed destruction in southeastern Newfoundland in relation to temperature and flow acceleration

2.1. ABSTRACT

Green sea urchin (*Strongylocentrotus droebachiensis*) feeding aggregations (fronts) modulate community structure of shallow rocky reefs in eastern Canada through their grazing of kelp, but the minimum urchin density required to destructively graze through kelp beds varies within this region. The present study uses a manipulative field experiment to identify the threshold urchin density required to maintain destructive feeding on kelp beds in southeastern Newfoundland and examine the effects of environmental factors modulating urchin activity (temperature and flow acceleration) on urchin movement and grazing. The experimental setup consisted of enclosures secured to the seafloor (~5 m deep) at the interface between kelp bed and urchin barren. Each enclosure was stocked with urchins to create front densities representing 0%, 25%, 50%, 75%, 100%, and 125% of the natural urchin front density in the study area and monitored using underwater videography biweekly over two summers. An adjacent unmanipulated control site was monitored over 14 months. Results obtained within the experimental setup showed an increase in the rate of kelp bed retreat over time during summer. However, no effect of urchin density, temperature, or flow acceleration was detected on the rate of kelp bed retreat in the experimental setup. The combined effect of the density treatment applied, Julian date, and year influenced urchin front density in the experimental setup, with the two highest density treatments (100% and 125% of the natural front density) showing stronger decreases in front density over time compared to other treatments. In the unmanipulated control site, kelp bed retreat increased with increasing temperature, and urchin density in the barren zone (~2 m from the kelp bed) decreased with increasing temperature while it increased with increasing wave action. Overall, results suggest that the minimal urchin front density

necessary for the destructive grazing of kelp beds during summer is either equal to the lowest density treatment tested (25% of the natural urchin front density, i.e., 88 urchins·m⁻²) or may be lower. Urchin density in the barren ground several metres away from the kelp bed are higher than this estimated threshold (~150 urchins·m⁻²), supporting the idea that urchin grazing pressure maintains the area locked in an urchin-dominated state.

2.2. INTRODUCTION

The formation of feeding groups or aggregations is observed in both terrestrial and marine species, either as a strategy to facilitate the capture of prey (Clua and Grosvalet, 2001; Stander, 1992) or reduce predator attacks during feeding (Grand and Dill, 1999; Studd et al., 1983), or as a consequence of the patchy distribution of food (Fiedler and Bernard, 1987; Hoffmayer et al., 2007; Wilson and Richards, 2000). A common example of feeding aggregations is the formation of feeding fronts in which consumers form a narrow band which moves in a progressive, linear fashion along a food gradient (Breen and Mann, 1976; Lauzon-Guay et al., 2008). Feeding fronts are observed in a variety of animals such as ungulates (Gueron and Liron, 1989), insect larvae (Burrows and Balciunas, 1997), and marine invertebrates (Kayal et al., 2012; Lauzon-Guay et al., 2008; Silliman et al., 2005), and their feeding pressure can regulate the abundance and distribution of prey populations (Silliman et al., 2013). For instance, in marine benthic systems, high-density urchin fronts are created by the accumulation of urchins at the edge of macroalgal beds (e.g., as observed in *Strongylocentrotus droebachiensis*, Lauzon-Guay and Scheibling, 2007b; and *Heliocidaris erythrogramma*, Wright et al., 2005) where their concentrated grazing pressure can decimate macroalgal populations and subsequently prevent their

regeneration (Filbee-Dexter and Scheibling, 2014; Johnson and Mann, 1988; Silliman et al., 2013), thus modulating benthic community structure.

In temperate and sub-polar shallow reef systems, large brown seaweeds of the order Laminariales, called kelp, create 3-D structures which enhance habitat complexity, productivity, and biodiversity (Dayton, 1985; Estes et al., 2004; Steneck et al., 2002). In such systems, sea urchins are dominant grazers which preferentially consume kelp by forming extensive feeding fronts at the deeper edge of kelp beds, leaving behind barren grounds largely devoid of fleshy seaweed and dominated by encrusting calcified algae (Himmelman, 1984; Scheibling and Hatcher, 2007; Scheibling et al., 1999; Steneck et al., 2002). The presence of urchin fronts consuming and pushing back the edge of kelp beds creates a sharp boundary between kelp bed and urchin barren (Gagnon et al., 2004; Lauzon-Guay et al., 2008; Lauzon-Guay and Scheibling, 2007b; Scheibling et al., 1999). Large-scale shifts between kelp bed-dominated and urchin barren-dominated community states (termed phase shifts or regime shifts) have been reported worldwide following sporadic or cyclical variations in urchin densities (reviewed in Filbee-Dexter and Scheibling, 2014; Ling et al., 2015; Norderhaug and Christie, 2009). Field observations suggest that urchins must exceed a threshold density to effectively (and destructively) consume kelp beds (reviewed in Filbee-Dexter and Scheibling, 2014; Lauzon-Guay et al., 2009). Kelp-urchin systems demonstrate hysteresis as the urchin density required to maintain a system as urchin-dominated is generally an order of magnitude lower than that required to produce a shift from kelp- to urchin-dominated states (Filbee-Dexter and Scheibling, 2014; Ling et al., 2015).

In eastern Canada, the green sea urchin, *Strongylocentrotus droebachiensis*, preferentially feeds on kelp and modulates seasonal and annual variations in kelp abundance (Frey and Gagnon, 2015; Gagnon et al., 2004; Gagnon et al., 2005; Lauzon-Guay and Scheibling, 2007c; Scheibling et al., 1999). In this region, feeding fronts of *S. droebachiensis* can destructively graze through kelp beds at rates up to 4 m·mo⁻¹ in summer (Gagnon et al., 2004; Lauzon-Guay, 2007; Scheibling et al., 1999). Urchins grazing reduces the spatial distribution of kelp beds in summer (Frey and Gagnon, 2015; Gagnon et al., 2004; Keats, 1991), but kelp recruitment and growth during winter generally allow kelp beds to reform. When kelp beds become depleted, urchin populations endure in barren grounds with minimal food intake by consuming calcified encrusting algae, biofilm, and algal drift (Lang and Mann, 1976). Urchin movement and grazing vary locally based on kelp bed attributes, as increasing kelp biomass and stipe density decrease the rate of advance of urchin fronts, which can also vary depending on the algal species present (Lauzon-Guay and Scheibling, 2007b; Lauzon-Guay et al., 2009; Wright et al., 2005). Additionally, urchin behaviour is strongly modulated by environmental parameters as increasing wave action decreases urchin movement and feeding, mainly because the latter are inhibited by the sweeping motion of algal fronds in swell (Gagnon et al., 2006; Konar and Estes, 2003), while increasing temperature (up to a threshold) increases feeding activity (Feehan et al., 2012; Frey and Gagnon, 2015; Konar and Estes, 2003; Lauzon-Guay and Scheibling, 2007b, c). Therefore, density thresholds for kelp bed destruction cannot readily be extrapolated among regions and investigation of how local environmental conditions modulate kelp-urchin interactions is crucial to understand and predict community shifts.

In eastern Newfoundland (Canada), environmental conditions appear ideal for kelp bed growth with cold (-1 to 16°C) nutrient rich water, exposed and moderately-exposed shorelines, and abundant hard substratum (Bekkby et al., 2009; Catto et al., 2003; Frey and Gagnon, 2015; Kerrison et al., 2015). Yet, kelp beds in this region are limited to narrow bands near the water's edge in shallow (<6 m) areas (Himmelman, 1970; Himmelman, 1984; Keats, 1991). Extensive urchin barrens appear to have persisted through several decades (Frey and Gagnon, 2015, 2016; Himmelman, 1970; Himmelman, 1984), likely due to the lack of top-down control on urchins. Indeed, predation pressure is generally low as the cryptic behaviour of small (<15 mm test diameter) urchins protects them from predation from crabs, fish, sea stars, or conspecifics, while the large spines and solid test of larger individuals make them difficult to consume (Himmelman and Steele, 1971; Jennings and Hunt, 2010; LeGault and Hunt, 2016; Scheibling and Hamm, 1991). In addition, water seems too cold for the development of paramoebiasis which regulates urchin populations in more southern regions of eastern Canada (Buchwald et al., 2015; Scheibling et al., 1999). Hence, persistently high urchin densities appear to be the main factor restricting kelp bed distribution in eastern Newfoundland and keeping this system locked in an urchin-dominated state (Johnson et al., 2019). However, the threshold urchin density necessary to maintain destructive grazing upon kelp bed is unknown; comprehensive testing of the effects of population density on urchin front formation and kelp bed destruction is needed to better understand mechanism maintaining the urchin-dominated state and the potential drivers of barrens-to-kelp community shifts in an environment such as Newfoundland subjected to chronic high wave action and persistently low sea temperature.

The present study uses a manipulative field experiment to examine the relationships between urchin density, environmental factors (namely temperature and flow acceleration, as a proxy for wave action), and kelp bed destruction in one bay of southeastern Newfoundland. Its main objective is to identify the threshold urchin density required to maintain destructive grazing of kelp beds. Two main hypotheses are being tested: 1) that the urchin density needed to maintain destructive grazing upon a kelp bed (i.e., threshold density) is lower than the natural urchin front density observed in the area, as is the case in Nova Scotia and the northern Gulf of St. Lawrence where the observed front densities are generally higher than the estimated density thresholds (Gagnon et al., 2004; Lauzon-Guay and Scheibling, 2007b; Scheibling et al., 1999); and 2) that front formation and the rate of advance of the urchin front into a kelp bed increases with increasing urchin density but decrease under low temperature and high flow acceleration. To that effect, enclosures were installed at the deeper edge of a kelp bed, stocked with specific densities of urchins varying from 25 to 125% of the natural urchin front density in the study area, and monitored using underwater videography over two summers. An adjacent unmanipulated control site was monitored over a 14-month period (which overlapped with the two summers during which the enclosures were monitored) to quantify variations in urchin density and grazing year-round.

2.3. MATERIAL AND METHODS

2.3.1. Study area

The present study was conducted on the south portion of Flat Rock Cove (47°42'08.18" N, 52°42'29.30" W), Newfoundland (Canada), opposite to the mouth of the

cove which opens to the Atlantic Ocean in the northeast direction (Figure 2.1). Hence, this portion of the cove is highly exposed to waves and swell originating from the northeast. This study area was chosen because its rocky substrate and kelp bed structure (see below) are typical of those found on exposed shores of southeastern Newfoundland. Seabed in this area is composed of bedrock platforms gently sloping seaward at an angle of 10 to 30° (Catto et al., 2003), extending from above the water surface to a depth of ~15 m. The bedrock is generally flat with scattered crevices of a few centimetres in width and depth, and small ledges (generally <50 cm in height). A continuous kelp bed composed mainly of *Alaria esculenta* and scattered *Laminaria digitata* dominates the 0-5 m depth range over ~150 m along the south shore of the cove. At the deeper edge of the kelp bed, green sea urchins, *Strongylocentrotus droebachiensis*, form grazing fronts with densities up to 400 urchins·m⁻² (preliminary observations). An extensive urchin barren with lower urchin densities (~150 urchins·m⁻²) extends from the kelp bed edge to a depth of at least 15 m. Thin encrusting coralline algae (*Lithotamnion glaciale*) covers most of the bedrock in the urchin barren. Small (<1 m²) patches of the brown seaweeds *Desmarestia viridis* and *Chordaria flagelliforma* are present in the barren near the kelp bed. Scattered stands of the grazing-resistant kelp *Agarum clathratum* are also present at depths between 6 and 10 m. Sea temperature in coastal southeastern Newfoundland generally ranges from ~0°C in winter (March to May) to ~12 to 16°C in early August (Blain and Gagnon, 2013; Caines and Gagnon, 2012) and was monitored in the study area throughout the study (see Section 2.3.4)

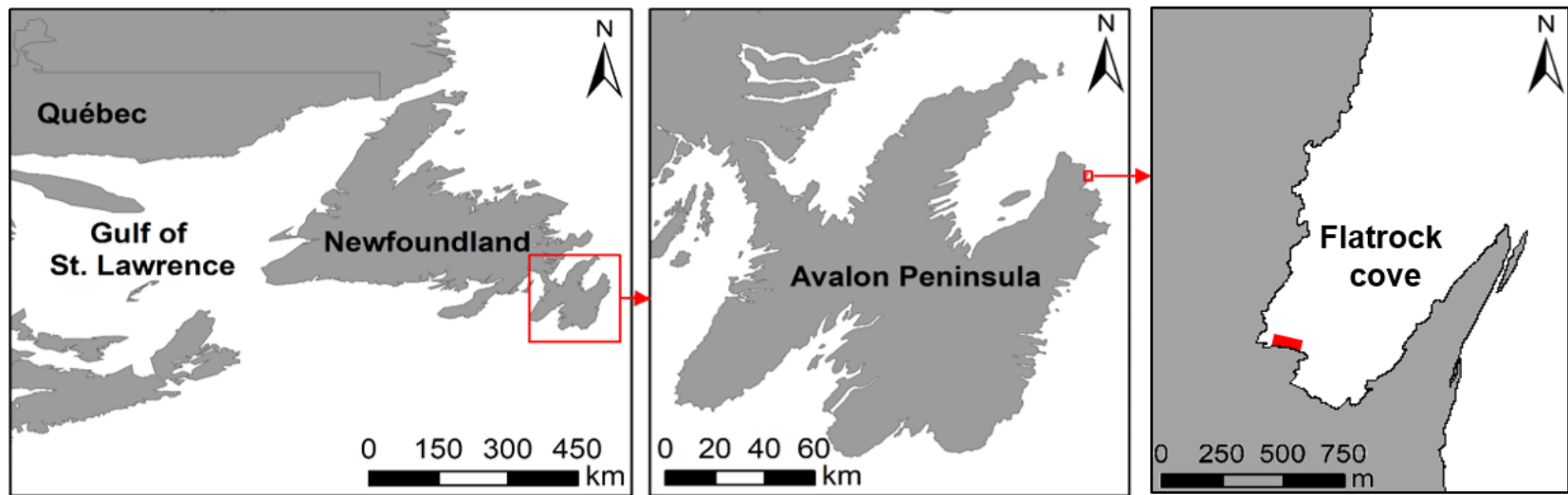


Figure 2.1. Location of the study area in Flatrock cove (Newfoundland, Canada), highlighted in red.

2.3.2. Experimental setup

To quantify the effect of urchin density on kelp bed destruction, a field experiment was conducted in which urchin densities were manipulated within enclosures placed at the interface between kelp bed and urchin barren. Enclosures were delimited by 50-cm high fences built with 1) aquaculture netting, with a mesh aperture of 2.5 cm (Polyethylene netting 1.8 mm by 50 mm); 2) heavy metal chains (link diameter 9.5 mm) sewn along the bottom of the netting to weight it down; and 3) small plastic floats (~12 x 6 cm, oval shaped) attached every metre along the top of the netting to hold the fence upright in the water column while allowing it to sway gently with wave surge (see Appendix 2.A for details). Preliminary laboratory trials in an oscillatory wave tank showed that this mesh size has little impact on water flow, but efficiently restricts the transit of urchins >3 cm in diameter as they are unable to pass through the mesh's openings and have difficulty climbing the flexible, swaying mesh. Once laid down on the seabed, the heavy chain conformed to small topographic irregularities of the bedrock, thus preventing the passage of urchins under the fence through cracks and crevices.

Fences were positioned to form elongated corridors perpendicular to the kelp-barren interface, so that each corridor measured 1 m in width and 4 m in length, extending ~2.5 m in the barren and ~1.5 m in the kelp bed (Figure 2.2.A and B). Fences were secured to the seabed with eyebolts drilled into the bedrock at the extremities and mid-length of each corridor (Figure 2.2.A). The corridors were closed at the barren extremity to prevent urchin displacement to and from the adjacent barren but were opened at the extremity situated in the kelp bed. Urchin movement towards the corridors from the kelp bed was deemed negligible since urchins are generally in low densities within kelp beds (Frey and Gagnon,

Figure 2.2. Panel A: Schematic representation of the position of fences (dashed lines) and eyebolts (circles) forming the corridors at the kelp-barren interface in the experimental sites. This example shows the configuration of the corridors at site 4 (see below) in 2015. Letters within each corridor identify the six experimental urchin density treatments at this site in 2015, where N = Natural density, H = High density, M = Medium density, L = Low density, V = Very low density, and C = Control corridor (see section 2.3.2 for details). Experimental treatments were randomly assigned to each corridor at each site following a complete-block design and re-randomized each year. **Panel B:** Picture of the corridors built at site 4 in 2015 prior to the start of the experiment (Photo: Anne P. St-Pierre). **Panel C:** Position of the four experimental sites (labeled 1 to 4) and the control site (labelled “C”) within the study area.

2015) and their displacement is greatly impeded by the presence of kelp stipes and algal whiplash (Konar, 2000; Konar and Estes, 2003; Velimirov and Griffiths, 1979). As urchins consumed kelp within the corridors, the latter were extended by the installation of additional fences to ensure that these barriers extended in the kelp bed for at least 1.5 m to limit the possibility of urchins crossing to adjacent corridors as kelp was depleted.

The layout of this experiment was based on a randomized complete blocks design (Quinn and Keough, 2002). Four blocks (hereafter called “sites”, Figure 2.2C) were established, with six corridors per block. The six experimental urchin front density treatments (described below) were randomly assigned to corridors such that each treatment occurred once within each site and each site contained all treatments. Hence, each site is considered a replicate of the experiment. The front density treatments included: 1) Natural urchin density of $350 \text{ urchins} \cdot \text{m}^{-2}$, representing the average mid-summer front density based on Gagnon et al. (2004) and preliminary observation in the study area; 2) High density [$438 \text{ urchins} \cdot \text{m}^{-2}$], representing 125% of the mid-summer average; 3) Medium density [$263 \text{ urchins} \cdot \text{m}^{-2}$], representing 75% of the mid-summer average; 4) Low density [$175 \text{ urchins} \cdot \text{m}^{-2}$], representing 50% of the mid-summer average; 5) Very low density [$88 \text{ urchins} \cdot \text{m}^{-2}$], representing 25% of the mid-summer average; and 6) Control corridor, where urchins were removed at the onset of the trial but no urchins were subsequently added. Control corridors were open at the barren extremity, thus allowing urchin to move freely between the barren and the kelp bed edge within that corridor. In this experiment, closed corridors without urchins (i.e., complete urchin removal without colonization) were not implemented as a treatment because this is not representative of the local conditions. Upon installation of the fences at each of the four sites, all urchins were removed from within the

enclosures and the experimental urchin densities were manually recreated. Divers collected urchins in the nearby barren and placed the pre-determined number of urchins within 1 m of the kelp bed edge in each corridor to mimic an urchin front. Only urchins of 3 to 6 cm in test diameter (t.d.) were used because they dominate urchin fronts at the lower limit of kelp beds in eastern Canada (Dumont et al., 2004; Gagnon et al., 2004; Himmelman, 1986) and were abundant in the study area. To ensure that the presence of seaweed other than kelp did not influence the results, patches of *Desmarestia viridis* and *Chordaria flagelliformis* present in the experimental corridors were removed prior to the start of the experiment.

In addition to the four experimental sites, a fifth site was used as an unmanipulated control area (hereafter “control site”, Figure 2.2C) in which no fences were installed. Instead, the six 1-m wide corridors within the control site were only delineated by eyebolts drilled into the bedrock ~2.5 m away from the kelp bed edge. These eyebolts helped identify the edges of the corridors during data collection. In this unmanipulated control site, urchins could move along the kelp bed edge as well as between the barren and the kelp bed, thus allowing the observation of natural, unrestricted movement patterns.

The five sites were distributed along the kelp-barren interface at a depth of 3 to 6 m over a longitudinal distance of ~50 m and positioned so that the control site was placed in the center of the study area with two experimental sites on each side (Figure 2.2C). The position of each site was chosen to minimize the distance between sites while avoiding major topographical features in the seabed (e.g., protruding rocks, large crevices) which could reduce the effectiveness of the fences in stopping urchin movements.

This experiment took place over two consecutive summers, as the experimental setup was installed and monitored in the summers of 2015 and 2016 but removed during winter.

In 2015, the experiment started on 3 August 2015 with the establishment of the urchin density treatments in the experimental corridors. Subsequently, the sites were visited bi-weekly for data collection (see below, section 2.3.4) from 5 August until 20 September 2015, at which time strong wave action damaged the experimental setup beyond repair and forced the retrieval of the fences from the seabed. In 2016, the experimental setup was installed in June, and the experiment started with the establishment of the urchin density treatments in the experimental corridors on 26 June 2016. The sites were then visited bi-weekly for data collection from 29 June until 6 October, 2016. Urchin density treatments applied to each corridor were assigned randomly within each site independently for each year. The control site, where urchin densities were not manipulated, was monitored year-round from summer 2015 to fall 2016. This site was visited bi-weekly for data collection from 5 August 2015 to 24 November 2015, three times during winter and spring due to limited site accessibility and harsh weather (4 January, 24 March, and 11 May, 2016), and bi-weekly from 29 June to 6 October 2016. Kelp beds showed similar coverage among sites at the beginning of the trials, as determined by comparisons of the proportion of seabed covered by kelp in the first metre of the kelp bed, kelp blade length, and kelp blade width among sites (one-way ANOVAs, with $\chi^2(4, n=35)=3.29$ and $p=0.51$, $\chi^2(4, n=35)=1.35$ and $p=0.85$, $\chi^2(4, n=35)=3.38$ and $p=0.50$, respectively for proportion of seabed covered, blade length, and blade width). In 2016, the kelp bed at site 3 showed important damage caused by broken fences; this site was therefore removed from further analyses.

2.3.3. Image acquisition and data extraction

Underwater videography was used to measure kelp bed destruction and monitor urchin aggregation within the study sites. Every two weeks, each corridor at each site was filmed with a submersible video camera system (Sony HDV 1080i/MiniDV with an Amphibico Endeavor housing) held by a scuba diver at a distance of approximately 1.5 to 2 m above the seabed and filming downward, hence capturing on video a width of ~1.25 m of seafloor. Videos were obtained on days of relatively low swell to facilitate filming. To record these videos, the diver started at the barren extremity of the corridor and filmed the length of the corridor by swimming at a slow and steady pace towards the kelp bed. Video recording was stopped once the diver reached at least 1 m of continuous kelp bed (without patches of exposed seabed). The video segments were digitized and converted into individual images with PanoraGen.DV v1.0, with one image corresponding to an entire individual corridor. Each image was analyzed with Image J v1.44p (National Institute of Health) to (1) quantify the rate of kelp bed destruction, and (2) monitor urchin density within each corridor.

To quantify the rate of kelp bed destruction by urchin grazing, the distance between the lower edge of the kelp bed and permanent benchmarks at the barren extremity of each corridor was measured and compared for successive collection dates. This measurement was calculated from the images as the linear distance between the corridor's barren extremity, marked by eyebolts drilled into the seabed at the corridor's corners (Figure 2.2A), and the lower edge of the first patch of kelp encountered in the corridor measuring a minimum of 50 cm in width and length (i.e., measurement perpendicular and parallel to the corridor's length, respectively). This minimum kelp patch size was chosen to represent the lower edge of the kelp bed because kelp tends to be sparser and distributed in patches

in late fall and winter rather than as a continuous bed, making the kelp bed edge more difficult to discern. Thus, a kelp patch covering at least half the width of the corridor was chosen to represent the edge of the kelp bed. Differences in the distance between the extremity of the corridors and the edge of the kelp bed on successive collections yielded an estimate of kelp retreat, used as a proxy of kelp bed destruction. Kelp retreat is commonly used as a measure of urchin grazing because the sharp transition between kelp and barrens created by urchin grazing fronts and the movement of the kelp-barren interface that they cause over time is easily measurable. Urchin grazing is distinguishable from other factors that could affect kelp survival (e.g., infestation by bryozoans, dislodgement by wave action or ice scouring, natural kelp natural senescence) which create a different mosaic visible across entire kelp beds rather than only at the interface.

To monitor changes in urchin density, the number of urchins within a 30 x 30 cm quadrat was measured at two positions within each corridor: 1) at the leading edge of the urchin front (i.e., front zone) to quantify density at the grazing front where urchins are in contact with and feeding on kelp, and 2) at a distance of ~2 m from the lower kelp bed edge towards the barren (i.e., barren zone), within the limits of the corridors, to quantify density away from the kelp bed where urchins are too far to be in contact with or feed upon kelp sporophytes. Both quadrats were drawn on the imagery of each corridor for each collection date with the software Image J v1.44p (National Institute of Health) and the number of urchins whose test was more than half within the quadrat was recorded. The absolute position of the quadrats shifted from one sampling date to the next as the kelp bed edge retreated.

2.3.4. Monitoring of environmental parameters

Temperature was recorded throughout the experiment every 30 min with a temperature logger with a precision of $\pm 0.5^{\circ}\text{C}$ (HOBO Pendant; Onset Computer Corporation) secured to an eyebolt at a depth of 5 m. Daily mean water temperature was calculated for the entire duration of the field observations, from August 2015 to October 2016 (Figure 2.3). Temperature at the site ranged from approximately -1°C in March and early April to $\sim 15^{\circ}\text{C}$ in August, with a peak of temperature reaching $\sim 19^{\circ}\text{C}$ in October 2016. Given the size (~ 50 m in width) and depth (3 to 5 m) of the study area, as well as frequent turbulence caused by waves, stratification of the water column was very unlikely and the temperature measured was considered an accurate representation of the entire study area. Temperature data was used as a predictor in the statistical analyses, as detailed in Section 2.3.5 below.

The wave environment was quantified with a modified underwater relative swell kinetics instrument (URSKI; Figurski et al., 2011, see Appendix 2.A for details) which contained a submersible accelerometer (± 0.105 g, HOBO Pendant G Acceleration, Onset Computer). The accelerometer was housed in a cylindrical, 8-cm long perforated container epoxied to one end of a 90-cm long, sealed, slightly positively buoyant ABS pipe (8 cm in diameter). The other end of the pipe was tethered with an 18-cm twine to an eyebolt drilled into the seabed. In still water, the structure stood vertically in the water column with the section containing the accelerometer at the upper, un-tethered extremity of the structure (~ 1.15 m above the seabed). In presence of water motion, the free end of the instrument was pushed and tilted with a direction and speed consistent with prevailing water flows. Every 30 seconds, the accelerometer recorded its instantaneous acceleration in response to

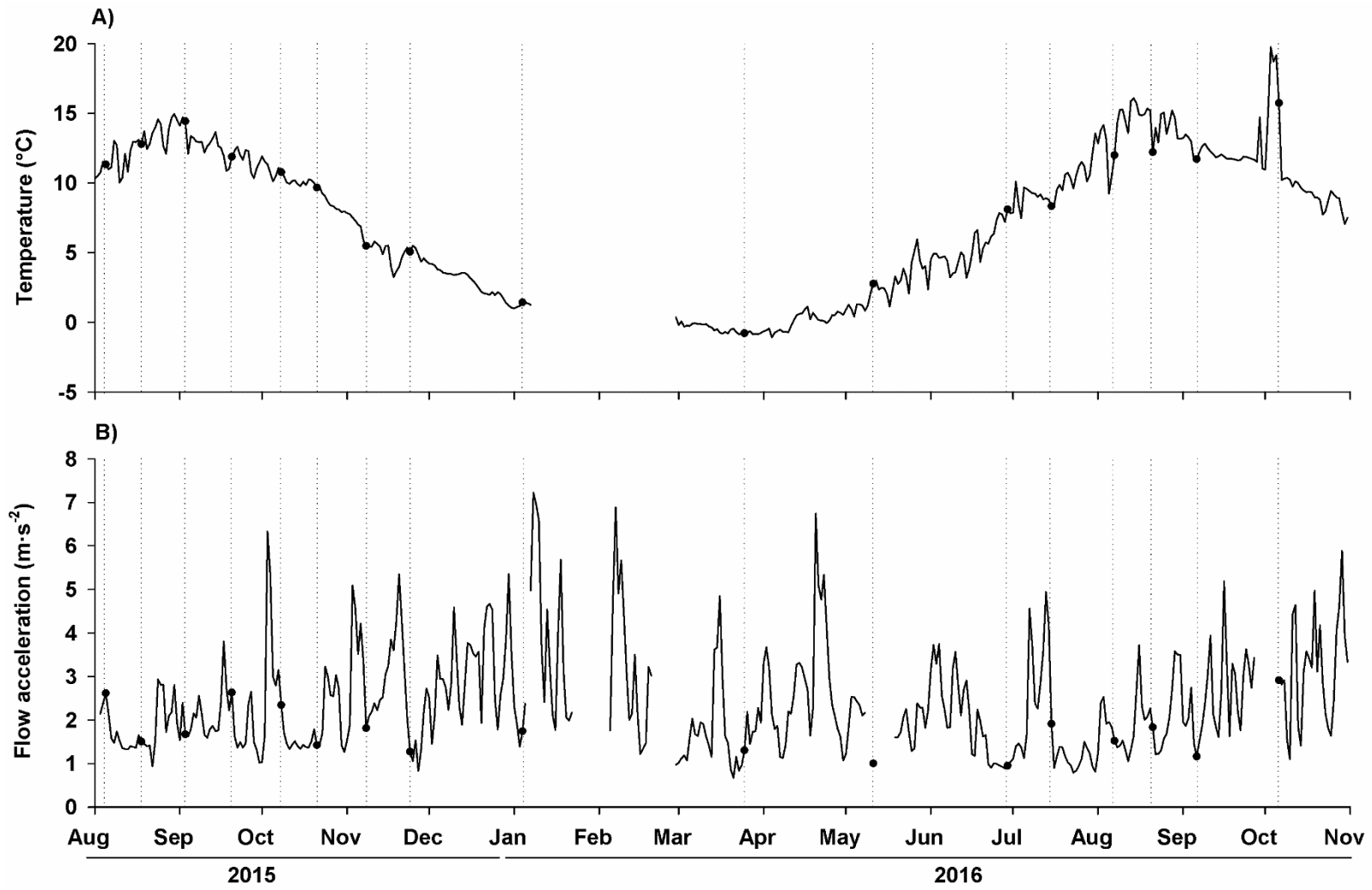


Figure 2.3. Temperature (**Panel A**, in °C) and relative Flow acceleration (**Panel B**, in $\text{m}\cdot\text{s}^{-2}$) in the study area from August 2015 to November 2016. Vertical lines identify days on which data collection (i.e., acquisition of underwater imagery and measurement of urchin densities) took place (see section 2.3.2 and 2.3.3), while black dots represent temperature and flow acceleration (in panels A and B, respectively) on each day of data collection.

passing waves in the X- (vertical), Y- (horizontal), and Z- (horizontal) axes. The sum of the instantaneous acceleration vectors in Y- and Z-axes was calculated by trigonometry and represents the flow acceleration parallel to the seabed to which sea urchins were exposed. Flow acceleration was used as a proxy of the intensity of water motion. The flow acceleration obtained by the accelerometer yields values in $\text{m}\cdot\text{s}^{-2}$, but the accelerometer could not be calibrated *in situ* with a current meter due to logistical constraints. Thus, flow accelerations presented in this study should be considered as relative rather than absolute values. Daily mean flow acceleration was calculated for the entire duration of the field observations, from August 2015 to October 2016 (Figure 2.3). Throughout the study period, flow acceleration ranged from $0.7 \text{ m}\cdot\text{s}^{-2}$ to $7.2 \text{ m}\cdot\text{s}^{-2}$. Preliminary analyses did not show considerable differences in flow acceleration at the eastern extremity, center, and western extremity of the study area. Because bottom topography and depth were highly similar across the five sites within the study area, flow acceleration was considered uniform throughout the study area. Flow acceleration data was used as a predictor in the statistical analyses, as detailed in Section 2.3.5 below.

2.3.5. Statistical analyses

Univariate analyses were conducted for the following three response variables: 1) rate of kelp bed retreat, 2) urchin density in the front zone, and 3) urchin density in the barren zone. For data obtained within the experimental setup, separate three-way ANCOVAs were conducted for each of the three response variables above, with the fixed factors Treatment (categorical, 6 levels; Natural, High, Medium, Low, and Very low densities, and Control corridor), Julian date (continuous), and Year (categorical, 2 levels;

2015 or 2016). Because the experiment was replicated at four sites, the factor Site (categorical) was used as a random blocking factor. For data from 2015, Site had 4 levels. In 2016, the kelp bed within site 3 was damaged due to broken fences and this site was consequently removed from analyses to ensure consistency. Hence, for data from 2016, the factor Site had 3 levels. For data obtained at the control site, separate two-way ANCOVAs were conducted for each of the three response variables above, with the fixed factors Julian date (continuous) and Year (categorical, 2 levels; 2015 or 2016), as well as Corridor (categorical, 6 levels) as a random blocking factor. Two-way ANCOVAs with the fixed factors Temperature (continuous) and Flow acceleration (continuous) were also applied to each of the three response variables above, separately for the data from the experimental setup (using Site as a random blocking factor) and from the control site (using Corridor as a random blocking factor). Because environmental conditions occurring over several days prior to data collection might affect the urchins' behavior and feeding, temperature and flow acceleration were averaged over the week preceding data collection (i.e., the seven days prior to measurement of kelp bed retreat in the field) and these average values were used in statistical analyses.

All ANCOVAs were conducted using the “lmer” function from the “lme4” package (Bates et al., 2015) in R 3.5.0 (R Development Core Team, 2018). For all analyses, the assumption of homogeneity of the variance was verified by examining the distribution of the residuals and the assumption of normality of the residuals was verified by examining the normal probability plot of the residuals (Snedecor and Cochran, 1989). Assumptions were met for all analyses. Comparisons of 95% confidence intervals were used to detect differences among slopes. All analyses were applied to the raw data. A significance level

of 0.05 was used in all analyses. All slope estimates are presented with standard errors (mean \pm SE) unless stated otherwise.

2.4. RESULTS

2.4.1. Rate of kelp bed retreat

Within the experimental sites during summer, the rate of kelp bed retreat was significantly affected by the factor Julian date, but not Treatment or Year (see Appendix 2.B, Table 2.B.1). The rate of kelp bed retreat increased by $0.05 \pm 0.02 \text{ m}\cdot\text{mo}^{-1}$ for each increase of one day in Julian date throughout summer (Figure 2.4). However, large variations were observed in the data. Within the control site year-round, the rate of kelp bed retreat was not significantly affected by the factors Julian date nor Year (Table 2.B.2).

In the experimental sites during summer, no effect of the factors Temperature, Flow acceleration, or their interaction was detected on the rate of kelp bed retreat (Table 2.B.3). For the data from the control site collected year-round, a significant effect of the factor Temperature was detected on the rate of kelp bed retreat (Table 2.B.4), with an increase of $0.29 \pm 0.11 \text{ m}\cdot\text{mo}^{-1}$ for each increment of 1°C in water temperature (Figure 2.5).

2.4.2. Urchin densities at the front

Within the experimental sites in summer, the density of urchins at the front was significantly affected by the triple interaction between the factors Treatment, Julian date, and Year (Table 2.B.5, Table 2.1). In the high, natural, and low density treatments, urchin density at the front decreased as Julian date increased in both 2015 and 2016. The rate of decrease in front density in these three treatments ranged from $-0.6 \text{ urchin}\cdot\text{m}^{-2}\cdot\text{d}^{-1}$ in the

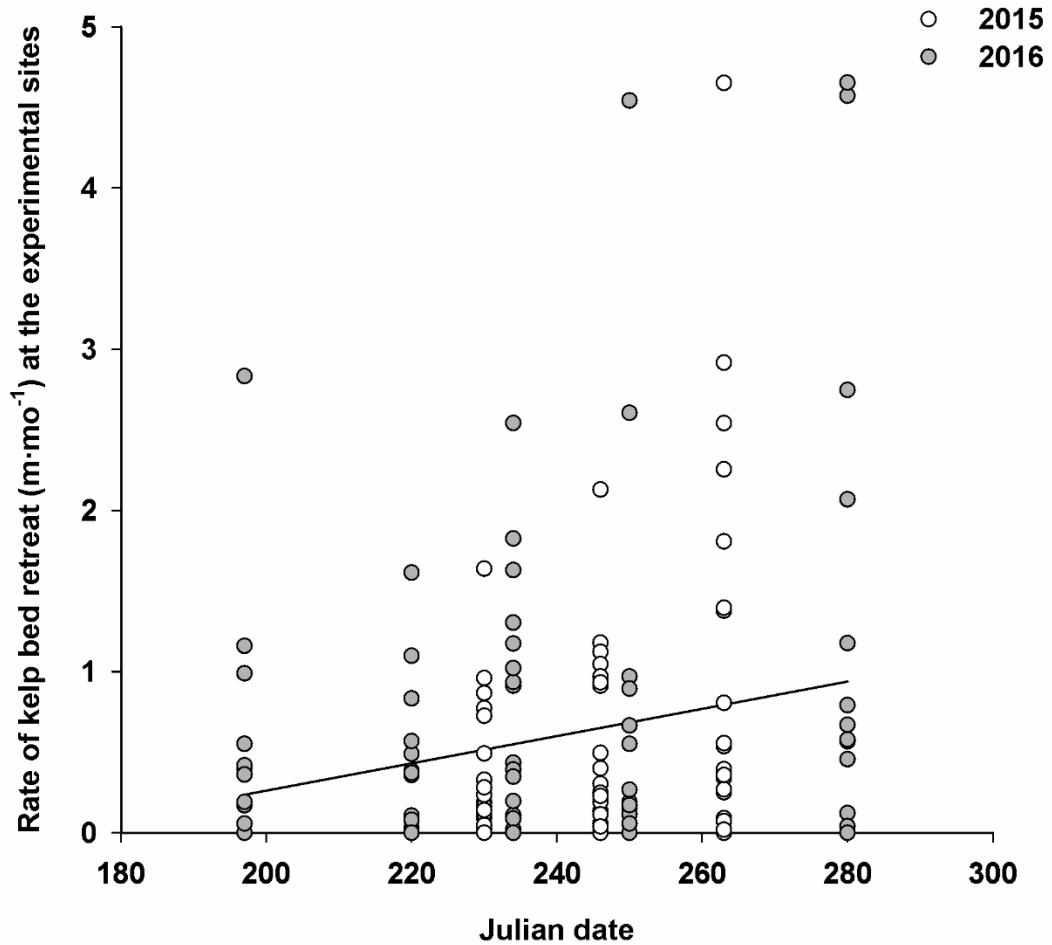


Figure 2.4. Relationship between the rate of kelp bed retreat (in $\text{m}\cdot\text{mo}^{-1}$) and Julian date for observations obtained during summer within the experimental sites ($r^2=0.046$, $p=0.004$). Because de factors Treatment and Year did not have a significant effect on the rate of kelp bed retreat within the experimental sites (see Table 2.B.1), data is pooled over the two years in which the experiment took place (2015 and 2016) and over the six experimental density treatments.

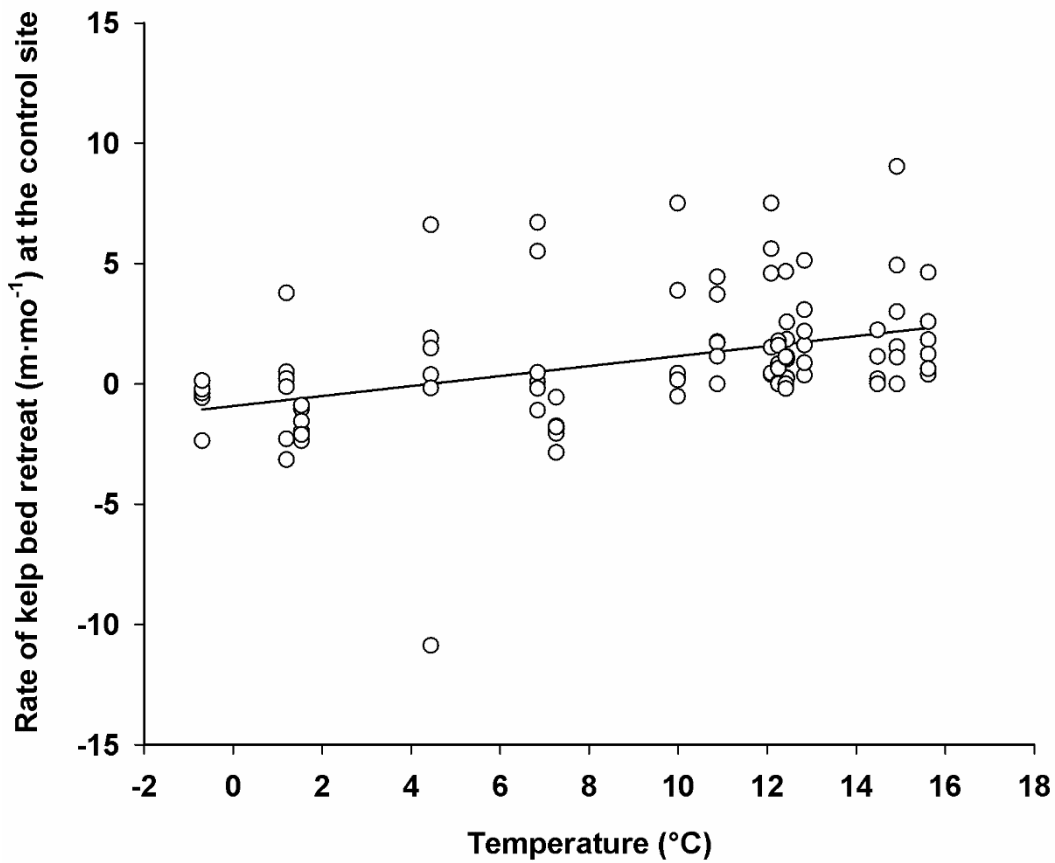


Figure 2.5. Relationship between the rate of kelp bed retreat (in $\text{m}\cdot\text{mo}^{-1}$) and temperature ($^{\circ}\text{C}$), for observations obtained year-round (i.e., from August 2015 to October 2016, see section 2.3.2) within the control site ($r^2=0.152$, $p=0.009$). Because the factor Flow acceleration did not have a significant effect on the rate of kelp bed retreat within the control site (see Appendix 2.B, Table 2.B.4), flow acceleration is not shown. Data from both years (2015 and 2016) was pooled for analyses of environmental parameters (see section 2.3.5).

Table 2.1. Estimates of slope obtained from the three-way ANCOVA examining the effect of Treatment (Natural, High, Medium, Low, and Very low densities, and Control corridor), Julian date (continuous variable), and Year (2015 and 2016) on the density of urchins at the front, which indicated a significant effect of the triple interaction between these factors (see Table 2.B.5 and Sections 2.3.5 and 2.4.2). Estimates with different letters are significantly different from each other based on comparison of the lower and upper 95% confidence interval (CI) around the slope estimate. See Figure 2.6 for a visual representation of each slope.

Year	Treatment	Slope estimate	Lower 95% CI	Upper 95% CI	Letter
2015	High	-5.182	-8.354	-2.010	a
	Natural	-3.396	-6.810	0.018	ab
	Medium	0.432	-2.136	3.000	abcd
	Low	-0.669	-3.117	1.779	abcd
	Very low	0.812	-0.758	2.382	bc
	Control corridor	1.809	0.351	3.267	d
2016	High	-1.865	-2.704	-1.025	abc
	Natural	-0.851	-1.885	0.183	bc
	Medium	-0.967	-1.822	-0.112	bc
	Low	-0.654	-1.658	0.351	bc
	Very low	-0.942	-1.400	-0.484	bc
	Control corridor	-0.521	-1.099	0.058	bc

low density treatment in 2016 (i.e., average front density decreased from 129 ± 102 urchin·m⁻² at the beginning to 56 ± 56 urchin·m⁻² at the end of the experiment) to maximum rate of -5.2 urchin·m⁻²·d⁻¹ in the high density treatment in 2015 (i.e., average front density decreased from 419 ± 103 urchin·m⁻² at the beginning to 150 ± 14 urchin·m⁻² at the end of the experiment; Table 2.1, Figure 2.6). The negative slopes in the high and natural densities treatments observed for 2015 were 1.8 to 9.9 times more pronounced than any other negative slopes (Table 2.1, Figure 2.6). In the medium and very low density treatments, as well as in the control corridors, front densities showed an increase as Julian date increased in 2015 with rates of 0.4 urchin·m⁻²·d⁻¹ (i.e., average front density increased from 183 ± 19 urchin·m⁻² at the beginning to 175 ± 56 urchin·m⁻² at the end of the experiment), 0.8 urchin·m⁻²·d⁻¹ (from 103 ± 27 urchin·m⁻² at the beginning to 111 ± 16 urchin·m⁻² at the end of the experiment), and 1.8 urchin·m⁻²·d⁻¹ (from 0 urchin·m⁻² at the beginning to 89 ± 48 urchin·m⁻² at the end of the experiment) respectively (Figure 2.6). However, front density decreased as Julian date increased in 2016 in these three treatments, with rates of -1.0 urchin·m⁻²·d⁻¹ (i.e., average front density decreased from 137 ± 16 urchin·m⁻² at the beginning to 37 ± 31 urchin·m⁻² at the end of the experiment), of -0.7 urchin·m⁻²·d⁻¹ (from 118 ± 13 urchin·m⁻² at the beginning to 0 urchin·m⁻² at the end of the experiment), and of -0.5 urchin·m⁻²·d⁻¹ (from 62 ± 57 urchin·m⁻² at the beginning to 0 urchin·m⁻² at the end of the experiment), respectively; (Figure 2.6). In 2015, null densities were only observed in the low and very low density treatments as well as the control corridors. However, null densities were observed in corridors from all treatments in 2016, particularly at the end of the season (end of August, September, and October). Within the control site year-round,

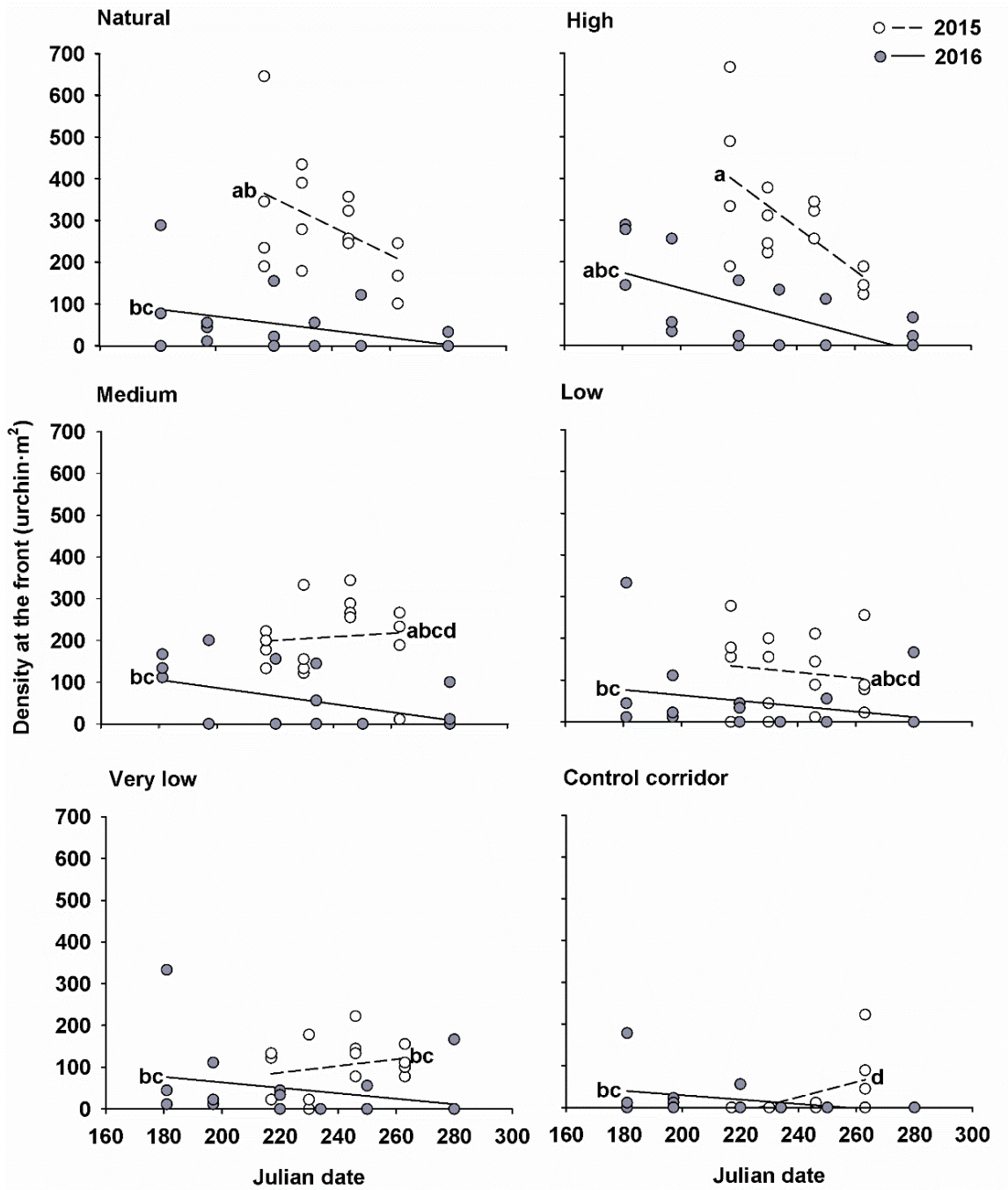


Figure 2.6. Relationship between urchin density at the front and Julian date, for observations obtained in summer within the experimental sites. Each panel represents one level of the six experimental urchin front density treatments applied, including the natural average mid-summer front density in the study area ($350 \text{ urchins} \cdot \text{m}^{-2}$), the high, medium, low, and very low densities representing respectively 125%, 75%, 50%, and 25% of the mid-summer average, and the control corridors (see section 2.3.2 for details). Data from 2015 is identified by white circles and dashed lines, while data from 2016 is identified by gray circles and full lines. Slopes not sharing the same letter are significantly different based on comparison of the 95% confidence interval for the slope estimates. Because the triple interaction between the factors Treatment, Julian date, and Year was significant ($p=0.003$, Appendix 2.B, Table 2.B.5), the 12 regression lines present in this figure are compared simultaneously.

urchin density at the front was not significantly influenced by the factors Julian date, Year, or their interaction (Table 2.B.6).

Within the experimental sites during summer, analyses showed no effect of the factors Temperature and Flow acceleration, or their interaction on urchin density at the front (Table 2.B.7). Within the control site year-round, urchin density at the front was not influenced by either Temperature or Flow acceleration, or their interaction (Table 2.B.8).

2.4.3. Urchin density in the barren

Within the experimental sites in summer, urchin density in the barren zone (i.e., at a distance of ~2 m from the lower kelp bed edge towards the barren) was significantly affected by the interaction between Julian date and Year, but not by Treatment (Table 2.B.9). Urchin density in the barren at the experimental sites increased as Julian date increased in 2015 at a rate of $0.2 \text{ urchin} \cdot \text{m}^{-2} \cdot \text{d}^{-1}$, but decreased as Julian date increased in 2016 at a rate of $-0.2 \text{ urchin} \cdot \text{m}^{-2} \cdot \text{d}^{-1}$ (Figure 2.7A). However, the data shows large variation in urchin density in the barren on both years (Figure 2.7). Within the control site year-round, urchin density in the barren zone was significantly affected by the interaction between Julian date and Year (Table 2.B.10). Urchin density in the barren at the control site increased as Julian date increased in 2015 at a rate of $1.3 \text{ urchin} \cdot \text{m}^{-2} \cdot \text{d}^{-1}$ (meaning that average barren density increased from $0 \text{ urchin} \cdot \text{m}^{-2}$ in August to $89 \pm 29 \text{ urchin} \cdot \text{m}^{-2}$ in November), but decreased as Julian date increased in 2016 at a rate of $-0.4 \text{ urchin} \cdot \text{m}^{-2} \cdot \text{d}^{-1}$ (meaning that average barren density decreased from $83 \pm 26 \text{ urchin} \cdot \text{m}^{-2}$ in January to $15 \pm 10 \text{ urchin} \cdot \text{m}^{-2}$ in October), also with large variations in the densities observed (Figure 2.7B).

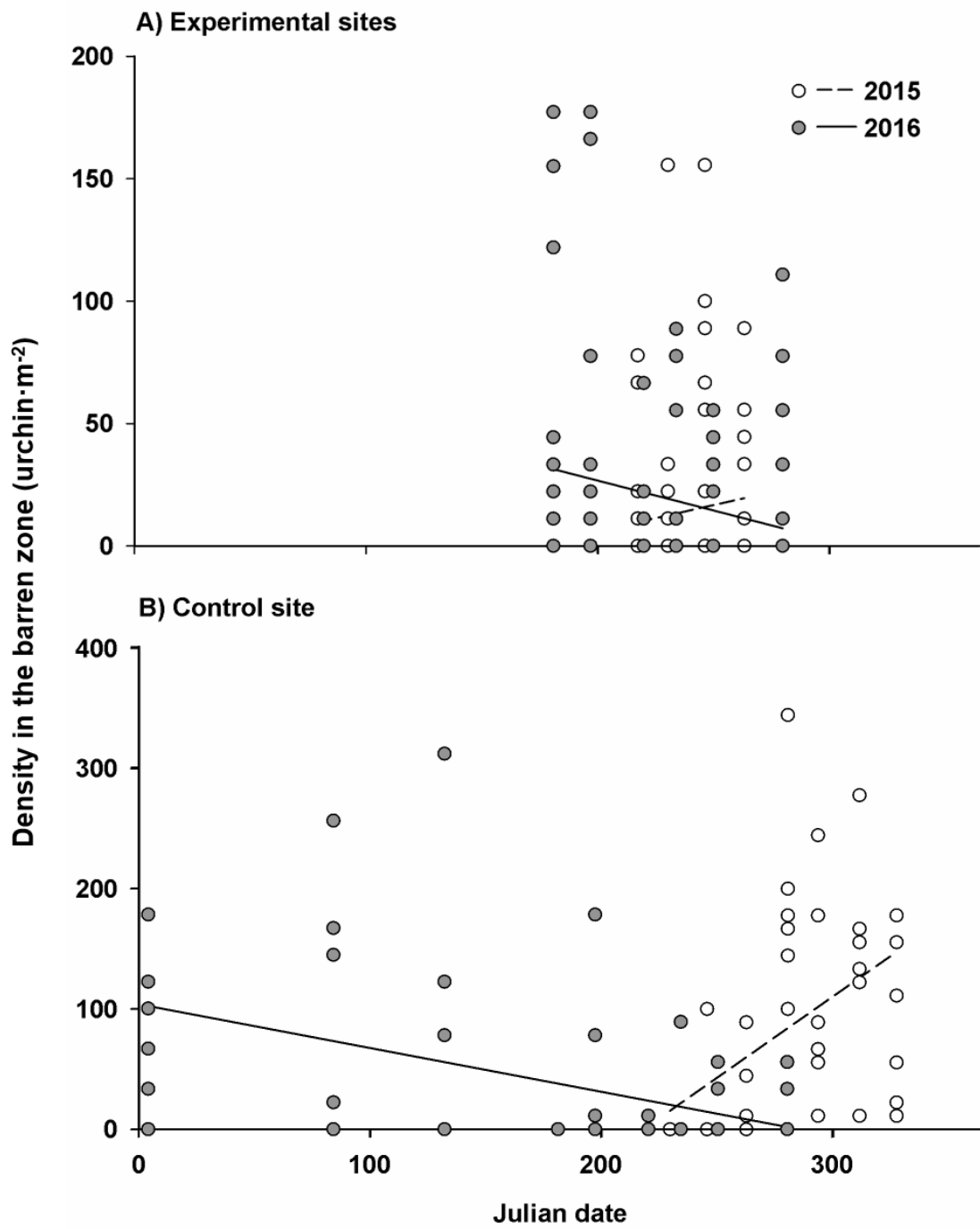


Figure 2.7. Relationship between urchin density in the barren zone (i.e., at a distance of ~2 m from the lower kelp bed edge towards the barren) and Julian date in 2015 (white circles, dashed line) and 2016 (gray circles, full line). **Panel A** presents data obtained in summer within the experimental sites ($r^2=0.014$ in 2015 and $r^2=0.037$ in 2016). The two slopes are significantly different from each other ($p=0.048$ for the interaction between factors Julian date and Year, see Appendix 2.B Table 2.B.9). Because the factor Treatment did not have a significant effect (Table 2.B.9), data are pooled over the six experimental density treatments. **Panel B** presents data obtained year-round within control site ($r^2=0.247$ in 2015 and $r^2=0.186$ in 2016). The two slopes are significantly different from each other ($p<0.001$ for the interaction between factors Julian date and Year, see Appendix 2.B Table 2.B.10).

The factors Temperature, Flow acceleration, or their interaction had no effect on urchin density in the barren zone within the experimental sites during summer (Table 2.B.11). At the control site year-round, urchin density in the barren zone was significantly affected by the interaction between the factors Temperature and Flow acceleration (Table 2.B.12). These two factors had an opposite effect, as urchin density in the barren decreased with increasing temperature and increased with increasing wave action (Figure 2.8).

2.5. DISCUSSION

The present study is the first experimental investigation of the threshold urchin density at the grazing front required to maintain kelp bed destruction in eastern Newfoundland. Results obtained within the experimental setup appeared highly variable and did not reveal a clear urchin density threshold necessary to maintain kelp bed destruction. Instead, the results suggested that the rate of kelp bed retreat in the experimental setup was not modulated by urchin density but increased over time throughout summer, being approximately 4.5 times higher in late than early summer. Temperature and flow acceleration had no effect on any of the variables measured within the experimental setup, but these factors had an interactive and opposite influence on the density of urchins in the barren of the control site, as the density observed decreased with increasing temperature but increased with increasing flow acceleration. At the control site, kelp bed retreat was affected by temperature only, being slightly negative (indicative of a slight kelp bed expansion) at temperatures below 2°C and increasing at the rate of $\sim 0.3 \text{ m}\cdot\text{mo}^{-1}$ for each increment of 1°C up to temperatures of $\sim 16^\circ\text{C}$.

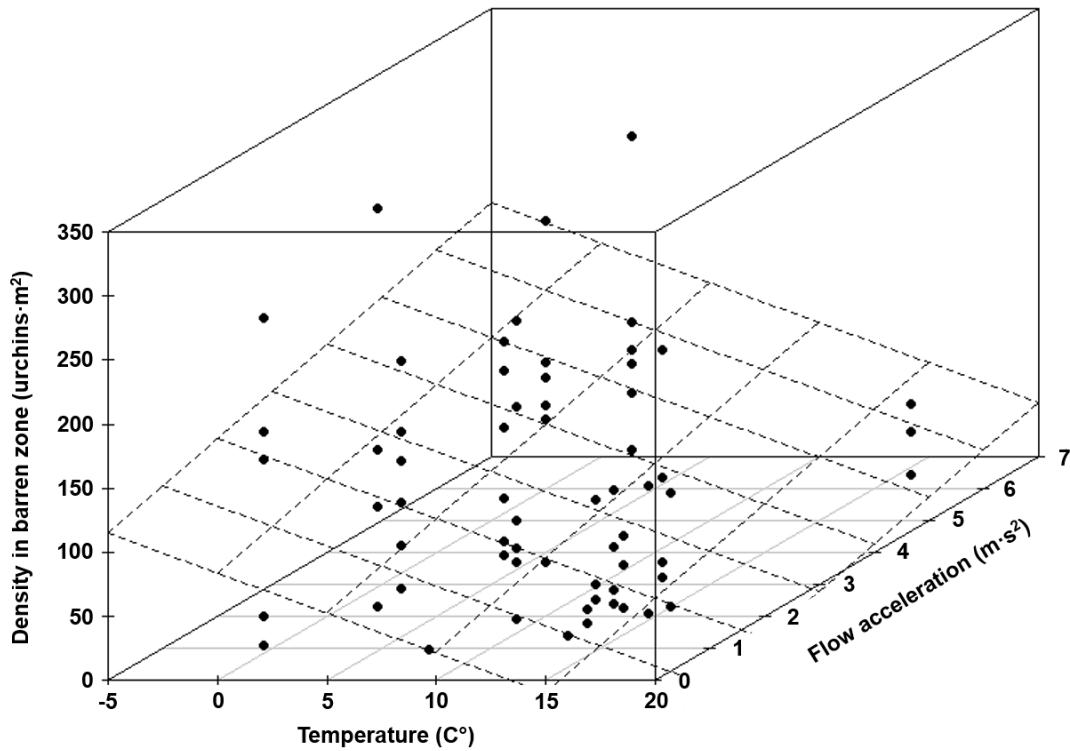


Figure 2.8. 3D plot of the multiple regression of urchin density in the barren zone (in urchins·m⁻²) with the factors Temperature (°C), and Flow acceleration (m·s⁻²) as independent variables, for observations obtained year-round (i.e., from August 2015 to October 2016, see section 2.3.2) within control site. Data from both years (2015 and 2016) was pooled for analyses of environmental parameters (see section 2.3.5 and Appendix 2.B Table 2.B.12).

Urchin front density and kelp bed consumption

Both hypotheses that (1) the urchin density needed to maintain destructive grazing upon kelp bed (i.e., threshold density) is lower than the natural urchin front density observed in the area, and (2) front formation and the rate of advance of the urchin front into the kelp bed increases with increasing urchin density but decreases under low temperature and high flow acceleration were not fully supported by the results obtained. In the present study, no correlation was detected between urchin density in the experimental setup and kelp bed retreat, suggesting that the lowest urchin density tested ($88 \text{ urchins} \cdot \text{m}^{-2}$, i.e., 25% of the natural front density in the study area) may be higher than the urchin density needed to maintain destructive grazing upon kelp beds by green sea urchins in eastern Newfoundland during summer. At the control site, the potential relationship between the rate of kelp bed retreat and urchin density at the front was visually examined but no linear trend nor threshold was immediately evident in the data. Hence, these results suggest that the threshold urchin density to maintain destructive grazing upon kelp beds is either at or below $88 \text{ urchins} \cdot \text{m}^{-2}$ and that the rate of kelp bed consumption is not modulated by urchin density above this threshold. In the barren ground near the study sites, urchin densities of $\sim 150 \text{ urchins} \cdot \text{m}^{-2}$ were observed (unpublished data), suggesting that even the urchin density several metres away from the kelp bed is high enough to cause destructive grazing of kelp beds and prevent kelp recolonization far into the barren grounds. Hence, these results support the idea that the high urchin density and their grazing pressure maintain this system locked in an urchin-dominated state and prevents large-scale shifts to a kelp-dominated state (Johnson et al., 2019).

The estimated threshold density (≤ 88 urchins·m⁻²) and the lack of relationship between urchin density and the rate of kelp bed retreat observed in the present study are similar to those reported for the northern Gulf of St. Lawrence by Gagnon et al. (2004). These authors estimated the threshold urchin density below which urchin fronts cannot significantly consume kelp beds to be ~ 102 urchins·m⁻² (or ~ 5 kg·m⁻²) and did not observe a significant relationship between urchin biomass and the rate of kelp bed retreat. Hence, observations from eastern Newfoundland (i.e., present study) and the Gulf of St. Lawrence (Gagnon et al., 2004) contrast with the trends observed in Nova Scotia, where the rate of advance of urchin fronts into kelp beds is positively correlated with front density (Lauzon-Guay and Scheibling, 2007b; Scheibling et al., 1999) and where a much lower density threshold (~ 31 urchins·m⁻²) has been estimated. Differences in the morphology and density of the dominant kelp species among regions have been suggested as a potential cause for the disparity among these regions. Indeed, the dominant kelp species in the Gulf of St. Lawrence and in southeastern Newfoundland is *Alaria esculenta* (Frey and Gagnon, 2015; Gagnon et al., 2005; Himmelman, 1991), which is much smaller and more prostrate than *Laminaria longicruris* which dominates kelp beds in Nova Scotia (Scheibling and Gagnon, 2009; Scheibling et al., 1999). Because of this morphological difference, *A. esculenta* tends to move more easily in the water column and create algal whiplash close to the seabed even under very light wave action (P. Gagnon, personal observations) which greatly inhibits urchin movement and feeding as these invertebrates are highly sensitive to physical contact with moving structures (either natural, such as macroalgae, or synthetic; Gagnon et al., 2006; Konar, 2000; Lauzon-Guay and Scheibling, 2007c; Velimirov and Griffiths, 1979). In addition, *A. esculenta* forms beds with a higher density of stipes than *L. longicruris*, and

stipe density has been shown to slow down the advance of urchins into kelp beds (Lauzon-Guay and Scheibling, 2007b). Although results from the present study found no effect of flow acceleration on the rate of kelp bed retreat and urchin aggregation at the front (discussed below), it is possible that permanently high wave action experienced at the site combined with the presence of the easily-moving *A. esculenta* fronds largely impeded the urchins from advancing into and destructively grazing the kelp bed. Hence, a higher density of urchins may be necessary to immobilise the sweeping fronds of *A. esculenta*, leading to higher threshold densities, although further studies are required to determine the exact threshold urchin density in Newfoundland.

Data compiled in a recent review of large-scale phase shifts between community states within kelp systems worldwide by Filbee-Dexter and Scheibling (2014) indicates that the threshold urchin biomass required for a transition from urchin- to kelp-dominated states (termed “reverse shift”) is generally 77 to 91% lower than the threshold for a shift from kelp- to urchin-dominated states (termed “forward shift”). In comparison, these authors estimated that the urchin biomass required to maintain a system as urchin-dominated is an order of magnitude lower than the biomass required to produce a forward shift. In the present study, because of the small spatial scale of the experiment (1-m wide corridors) and relatively short temporal span, the results obtained provide information on the conditions needed for the maintenance of a community state rather than its origin via phase shift (Petraitis and Latham, 1999). Therefore, the estimated threshold of ≤ 88 urchins·m⁻² described above does not illustrate the threshold required for a phase shift from urchin- to kelp-dominated community state, but rather the threshold urchin density below which urchins cannot destructively graze through kelp beds. Further studies will be needed to

specifically quantify the threshold urchin density causing a shift from urchin- to kelp-dominated states, but data from the present study suggest that a severe perturbation causing urchin density to decline at least below the threshold for kelp bed destruction would be needed for kelp bed expansion into urchin-dominated barren grounds to occur (i.e., urchin population decline greater than 75%). Moreover, the threshold estimated in the present study represents the urchin density necessary to destructively consume kelp beds during summer only. Because of the yearly cycle observed in kelp systems, in which urchins graze upon kelp beds largely during summer while kelp recruitment and kelp bed recovery occurs during winter when urchins are less active (DFO, 2013; Frey and Gagnon, 2015; Gagnon et al., 2004; Scheibling et al., 1999; Siikavuopio et al., 2006), this threshold may not be indicative of the minimal urchin density necessary to consume kelp beds in winter. Hence, the temporal extent studied must be taken into account when interpreting and comparing results from such threshold analyses. Within the control site, the rate of kelp bed expansion during winter was similar to the rate of kelp bed retreat in summer, suggestive of a balanced cycle of urchin grazing and kelp recovery. However, urchin grazing during winter may be limiting the expansion of the kelp bed further into the barren.

Environmental parameters

Results from the present study showed no significant correlation between temperature, flow acceleration, and any of the response variables measured in the experimental setup (i.e., rate of kelp bed retreat, urchin front density, urchin density in the barren). However, the influence of environmental parameters was observed in the control site. Results from the control site partly support the hypothesis that both kelp bed

destruction and the formation of urchin front are reduced at low temperature and high wave action. The positive correlation observed between kelp bed retreat and temperature at the control site is consistent with the increasing feeding rate of the green sea urchin in eastern Newfoundland with increasing temperature up to a threshold of 12°C (Frey and Gagnon, 2015). Despite this threshold, the rate of kelp bed retreat in the present study continued to increase with temperature past 12°C, as was observed during another field study in the same region (Frey and Gagnon, 2015) and may be caused by the natural senescence of kelp sporophytes. Increasing temperature causes degradation and mortality of kelp sporophytes, especially in *Alaria esculenta* for which the lethal temperature is estimated at 16°C (Munda and Lüning, 1977). Frey and Gagnon (2015) reported deterioration of kelp sporophytes in eastern Newfoundland starting in mid August, as water temperature reached an annual peak in late summer, and continuing into fall. In addition to changes in water temperature over time, the trends in wave action observed in the present study (strong storms in October in 2015, gradually increasing severity of wave action from August to November in 2016 as indicated by high flow accelerations) may also have contributed to damaging kelp fronds. Therefore, it is not possible to disentangle the effects of urchin grazing from the effects of high late-summer temperature on kelp bed degradation in this field experiment by measuring the rate of kelp bed retreat only. For example, studies quantifying the degradation of kelp beds through summer in the absence of urchin grazing pressure (e.g., through large-scale urchin exclusion experiments) would be needed to estimate the proportion of kelp degradation linked to adverse effects of temperature and wave action on kelp sporophyte.

Within the control site, densities of urchins in the barren zone (~2 m away from the kelp bed) decreased with increasing temperature and increased with increasing flow acceleration, with an interactive effect of these two environmental parameters. Urchin feeding and movement are known to increase with water temperature and to decrease with increasing wave action (Feehan et al., 2012; Frey and Gagnon, 2015, 2016; Lauzon-Guay and Scheibling, 2007c). Therefore, in situations of high water flow and low temperatures when feeding is deterred, urchins may be prone to move away from the kelp bed to avoid the whiplash of kelp blades which could dislodge them (Frey and Gagnon, 2016; Himmelman and Steele, 1971; Konar, 2000; Velimirov and Griffiths, 1979). As urchin movement is slowed in high wave action, urchins may minimize the distance travelled which explains the increases in urchin densities in the barren close to the kelp bed observed in this study. When temperature and flow conditions improve, these urchins would then be able to move towards the kelp bed and quickly initiate feeding. Although not statistically significant, a slight increase in urchin density at the front was observed with increasing temperature and decreasing flow, further supporting the idea that urchins respond to changes in environmental parameters by moving towards or away from the kelp bed depending on the suitability of the conditions for grazing. Surprisingly, temperature and flow acceleration did not affect urchin density (either at the front or in the barren) in the experimental setup. Other abiotic factors, such as microhabitat heterogeneity or kelp debris distribution, should be investigated to identify other potential drivers of front and barren density patterns.

Limitations of the study

Two types of controls were used in the present study; first, each experimental site contained a control corridor, which was emptied of urchins at the start of the experiment but allowed the movement of urchins from the barren towards the kelp bed by an opening at the barren end. Secondly, an unmanipulated control site was monitored, where no corridors were installed thus allowing the movement of urchins both between the barren and kelp bed and along the kelp bed edge without obstruction. It was expected that urchin densities within the control corridors would gradually increase to match those in the control site because of directional movement of individual urchins towards food sources (Garnick, 1978; Mann et al., 1984; Scheibling and Hamm, 1991) although urchin displacement is largely random (Dumont et al., 2006; Lauzon-Guay and Scheibling, 2007a; Lauzon-Guay et al., 2006). It was expected that urchins would move into the open corridors to take advantage of the readily available kelp resources as Lauzon-Guay and Scheibling (2007b) showed that urchins redistribute their densities at the front to concentrate in areas of highest food availability, especially when kelp is being depleted in adjacent areas. However, urchin front densities within the control corridors remained low in both summer (19.0 ± 8.6 urchins·m⁻²) compared to the control site (93.7 ± 11.1 urchins·m⁻², up to 355 urchins·m⁻²), suggesting that redistribution was limited. Yet, it cannot be excluded that the presence of fences may have limited recolonization of the control corridors despite the large opening at the barren end of each control corridor. Since whiplash created by macroalgae or flexible synthetic structures swaying in the water column and brushing against urchins inhibits urchin movement (Konar, 2000; Lauzon-Guay and Scheibling, 2007c; Velimirov and Griffiths, 1979), it is possible that the movement of the fences limited urchin displacement

within the experimental setup, including the open-ended control corridors. After removal of the fences in fall 2015, urchin densities at the front appeared more evenly distributed in the study sites (A. P. St-Pierre, personal observations), supporting the findings of Lauzon-Guay and Scheibling (2007b) regarding the redistribution of urchins along kelp bed edges and suggesting that along-edge movement is more important for the spatial redistribution of urchin densities at the front than barren-to-edge movement.

Important interannual variations were observed in urchin density at the front (within the experimental sites) and density in the barren zone (within the experimental sites and the control site). Interannual differences in kelp bed distribution were also observed, as kelp beds within Flatrock Bay seemed more fragmented in 2016 than in 2015. As urchin grazing and front advance are known to be negatively correlated with kelp density (Lauzon-Guay and Scheibling, 2007b), interannual differences in urchin aggregation behavior may be partly explained by differences in the density and distribution of kelp patches as discussed above. However, these differences may also partly be an artefact stemming from the different range of collection dates each year. This possibility is particularly likely for data from the control site, where sampling dates in 2015 ranged from August to November, but extended from January to October in 2016, thus spanning a wider range of seasonal and temperature variations in the latter year. This suggests that the timescale over which investigations are conducted may impact the results, given the interannual differences observed as well as the yearly cycle of kelp bed retreat from grazing (summer) and kelp bed recovery (winter). Additional studies in Flatrock Bay would be necessary to quantify the variability in kelp cover over several years and measure its influence on kelp-urchin dynamics.

The present study is the first manipulative experiment conducted in southeastern Newfoundland aiming to understand how urchin density affects kelp bed destruction and urchin aggregation to provide insights into the factors regulating kelp-urchin dynamics in this region. It suggests that the threshold urchin front density necessary to maintain destructive grazing of kelp beds during summer is at or below $88 \text{ urchins}\cdot\text{m}^{-2}$ and that increasing urchin density above this threshold does not further modulate the rate of kelp bed consumption. Given that this threshold is lower than the urchin density observed in the barren adjacent to the study sites, urchin densities within the study area appear to be too high to allow the expansion of kelp beds into the barren grounds and thus may be maintaining this system locked in an urchin-dominated state, similar to what has been suggested in the northern Gulf of St. Lawrence (Gagnon et al., 2004; Johnson et al., 2019). Further studies are required to test the generality of the results over broader spatial and temporal scales in eastern Newfoundland and to investigate if more intense variations in urchin densities (i.e., lower densities affecting a greater area) could influence the stability of the kelp-urchin system in this region and generate a phase shift from urchin- to kelp-dominated states.

2.6. ACKNOWLEDGEMENTS

We are grateful to D. Bélanger, S. Trueman, K. Millar, R. Knight, C. Hounsell, A. Lomond, M. Maeland, S. Munro, R. Bowering, K. Brenton, K. Graham, D. Mallowney, N. Brown, and S. Hacker Teper, for help with field and laboratory work, as well as D. Schneider and L. Charron for statistical advice. We are grateful to Y. Wiersma and J. Fisher for constructive comments on earlier versions of this manuscript. This research was funded

by Natural Sciences and Engineering Research Council of Canada (NSERC Discovery Grant), Canada Foundation for Innovation (CFI-Leaders Opportunity Funds), and Research & Development Corporation of Newfoundland and Labrador (IgniteR&D) grants to P. Gagnon. A. P. St-Pierre was supported by an NSERC Post-Graduate Scholarship.

2.7. REFERENCES

- Bates, D., Maechler, M., Bolker, B., Walker, S., 2015. Fitting Linear Mixed-Effects Models Using lme4. *J Stat Softw* 67, 1-48.
- Bekkby, T., Rinde, E., Erikstad, L., Bakkestuen, V., 2009. Spatial predictive distribution modelling of the kelp species *Laminaria hyperborea*. *ICES J Mar Sci* 66, 2106-2115.
- Blain, C., Gagnon, P., 2013. Interactions between thermal and wave environments mediate intracellular acidity (H₂SO₄), growth, and mortality in the annual brown seaweed *Desmarestia viridis*. *J Exp Mar Biol Ecol* 440, 176-184.
- Breen, P.A., Mann, K.H., 1976. Destructive grazing of kelp by sea urchins in eastern Canada. *J Fish Res Board of Canada* 33, 1278-1283.
- Buchwald, R.T., Feehan, C.J., Scheibling, R.E., Simpson, A.G., 2015. Low temperature tolerance of a sea urchin pathogen: Implications for benthic community dynamics in a warming ocean. *J Exp Mar Biol Ecol* 469, 1-9.
- Burrows, D., Balciunas, J., 1997. Biology, distribution and host-range of the sawfly, *Lophyrotoma zonalis* (Hym. Pergidae), a potential biological control agent for the paperbark tree, *Melaleuca quinquenervia*. *Entomophaga* 42, 299-313.
- Caines, S., Gagnon, P., 2012. Population dynamics of the invasive bryozoan *Membranipora membranacea* along a 450-km latitudinal range in the subarctic northwestern Atlantic. *Mar Biol* 159, 1817-1832.
- Catto, N.R., Scruton, D., Ollerhead, L., 2003. The coastline of eastern Newfoundland. Science, Oceans and Environment Branch, Department of Fisheries and Oceans. Report prepared for the Newfoundland and Labrador Ministry of Environment and Conservation.
- Clua, É., Grosvalet, F., 2001. Mixed-species feeding aggregation of dolphins, large tunas and seabirds in the Azores. *Aquat Living Resour* 14, 11-18.
- Dayton, P.K., 1985. Ecology of kelp communities. *Annu. Rev. Ecol. Syst.* 16, 215-245.

- DFO, 2013. Assessment of Information on Irish Moss, Rockweed, and Kelp Harvests in Nova Scotia. Department of Fisheries and Ocean Canada. Sci Advis Sec Sci Advis Rep 2013/004.
- Dumont, C., Himmelman, J.H., Russell, M.P., 2004. Size-specific movement of green sea urchins *Strongylocentrotus droebachiensis* on urchin barrens in eastern Canada. Mar Ecol Prog Ser 276, 93-101.
- Dumont, C.P., Himmelman, J.H., Russell, M.P., 2006. Daily movement of the sea urchin *Strongylocentrotus droebachiensis* in different subtidal habitats in eastern Canada. Mar Ecol Prog Ser 317, 87-99.
- Estes, J., Danner, E., Doak, D., Konar, B., Springer, A., Steinberg, P., Tinker, M., Williams, T., 2004. Complex trophic interactions in kelp forest ecosystems. Bull Mar Sci 74, 621-638.
- Feehan, C., Scheibling, R.E., Lauzon-Guay, J., 2012. Aggregative feeding behavior in sea urchins leads to destructive grazing in a Nova Scotian kelp bed. Mar Ecol Prog Ser 444, 69-83.
- Fiedler, P.C., Bernard, H.J., 1987. Tuna aggregation and feeding near fronts observed in satellite imagery. Cont Shelf Res 7, 871-881.
- Figurski, J.D., Malone, D., Lacy, J.R., Denny, M., 2011. An inexpensive instrument for measuring wave exposure and water velocity. Limnol Oceanogr-Meth 9, 204-214.
- Filbee-Dexter, K., Scheibling, R.E., 2014. Sea urchin barrens as alternative stable states of collapsed kelp ecosystems. Mar Ecol Prog Ser 495, 1-25.
- Frey, D.L., Gagnon, P., 2015. Thermal and hydrodynamic environments mediate individual and aggregative feeding of a functionally important omnivore in reef communities. Plos One 10, e0118583.
- Frey, D.L., Gagnon, P., 2016. Spatial dynamics of the green sea urchin *Strongylocentrotus droebachiensis* in food-depleted habitats. Mar Ecol Prog Ser 552, 223-240.
- Gagnon, P., Himmelman, J.H., Johnson, L.E., 2004. Temporal variation in community interfaces: kelp-bed boundary dynamics adjacent to persistent urchin barrens. Mar Biol 144, 1191-1203.
- Gagnon, P., Johnson, L.E., Himmelman, J.H., 2005. Kelp patch dynamics in the face of intense herbivory: Stability of *Agarum clathratum* (Phaeophyta) stands and associated flora on urchin barrens. J Phycol 41, 498-505.

- Gagnon, P., St-Hilaire-Gravel, L.V., Himmelman, J.H., Johnson, L.E., 2006. Organismal defenses versus environmentally mediated protection from herbivores: unraveling the puzzling case of *Desmarestia viridis* (Phaeophyta). *J Exp Mar Biol Ecol* 334, 10-19.
- Garnick, E., 1978. Behavioral ecology of *Strongylocentrotus droebachiensis* (Muller) (Echinodermata-Echinoidea) - Aggregating behavior and chemotaxis. *Oecologia* 37, 77-84.
- Grand, T.C., Dill, L.M., 1999. The effect of group size on the foraging behaviour of juvenile coho salmon: reduction of predation risk or increased competition? *Anim Behav* 58, 443-451.
- Gueron, S., Liron, N., 1989. A model of herd grazing as a travelling wave, chemotaxis and stability. *J Math Biol* 27, 595-608.
- Himmelman, J.H., 1970. Some aspects of the ecology of *Strongylocentrotus droebachiensis* in eastern Newfoundland, M. Sc. thesis, Memorial University.
- Himmelman, J.H., 1984. Urchin feeding and macroalgal distribution in Newfoundland, eastern Canada. *Nat Can* 111, 337-348.
- Himmelman, J.H., 1986. Population biology of green sea urchins on rocky barrens. *Mar Ecol Prog Ser* 33, 295-306.
- Himmelman, J.H., 1991. Diving observations of subtidal communities in the northern Gulf of St. Lawrence. *Can Special Pub Fish Aquat Sci* 113, 319-332.
- Himmelman, J.H., Steele, D.H., 1971. Foods and predators of the green sea urchin *Strongylocentrotus droebachiensis* in Newfoundland waters. *Mar Biol* 9, 315-322.
- Hoffmayer, E.R., Franks, J.S., Driggers III, W.B., Oswald, K.J., Quattro, J.M., 2007. Observations of a feeding aggregation of whale sharks, *Rhincodon typus*, in the north central Gulf of Mexico. *Gulf Caribb Res* 19, 69-73.
- Jennings, L.B., Hunt, H.L., 2010. Settlement, recruitment and potential predators and competitors of juvenile echinoderms in the rocky subtidal zone. *Mar Biol* 157, 307-316.
- Johnson, C.R., Mann, K.H., 1988. Diversity, patterns of adaptation, and stability of Nova Scotian kelp beds. *Ecol Monogr* 58, 129-154.
- Johnson, L.E., MacGregor, K.A., Narvaez, C.A., Suskiewicz, T.S., 2019. Subtidal rocky shores of the north-west Atlantic Ocean: The complex ecology of a simple ecosystem, in: Williams, G.A., Bohn, K., Firth, L.B., Hawkins, S.J. (Eds.), *Interactions in the Marine Benthos: Global Patterns and Processes*. Cambridge University Press, Cambridge, pp. 90-127.

- Kayal, M., Vercelloni, J., De Loma, T.L., Bosserelle, P., Chancerelle, Y., Geoffroy, S., Stievenart, C., Michonneau, F., Penin, L., Planes, S., 2012. Predator crown-of-thorns starfish (*Acanthaster planci*) outbreak, mass mortality of corals, and cascading effects on reef fish and benthic communities. *Plos One* 7.
- Keats, D.W., 1991. Refugial *Laminaria* abundance and reduction in urchin grazing in communities in the north-west Atlantic. *J Mar Biol Assoc Uk* 71, 867-876.
- Kerrison, P.D., Stanley, M.S., Edwards, M.D., Black, K.D., Hughes, A.D., 2015. The cultivation of European kelp for bioenergy: Site and species selection. *Biomass Bioenerg* 80, 229-242.
- Konar, B., 2000. Seasonal inhibitory effects of marine plants on sea urchins: structuring communities the algal way. *Oecologia* 125, 208-217.
- Konar, B., Estes, J.A., 2003. The stability of boundary regions between kelp beds and deforested areas. *Ecology* 84, 174-185.
- Lang, C., Mann, K.H., 1976. Changes in sea urchin populations after the destruction of kelp beds. *Mar Biol* 36, 321-326.
- Lauzon-Guay, J.-S., 2007. Spatial dynamics of feeding fronts of sea urchins (*Strongylocentrotus droebachiensis*), Dissertation/Thesis, ProQuest, UMI Dissertations Publishing.
- Lauzon-Guay, J.-S., Scheibling, R.E., 2007a. Seasonal variation in movement, aggregation and destructive grazing of the green sea urchin (*Strongylocentrotus droebachiensis*) in relation to wave action and sea temperature. *Mar Biol* 151, 2109-2118.
- Lauzon-Guay, J.-S., Scheibling, R.E., Barbeau, M.A., 2008. Formation and propagation of feeding fronts in benthic marine invertebrates: a modeling approach. *Ecology* 89, 3150-3162.
- Lauzon-Guay, J.S., Scheibling, R.E., 2007b. Behaviour of sea urchin *Strongylocentrotus droebachiensis* grazing fronts: food-mediated aggregation and density-dependent facilitation. *Mar Ecol Prog Ser* 329, 191-204.
- Lauzon-Guay, J.S., Scheibling, R.E., 2007c. Seasonal variation in movement, aggregation and destructive grazing of the green sea urchin (*Strongylocentrotus droebachiensis*) in relation to wave action and sea temperature. *Mar Biol* 151, 2109-2118.
- Lauzon-Guay, J.S., Scheibling, R.E., Barbeau, M.A., 2006. Movement patterns in the green sea urchin, *Strongylocentrotus droebachaensis*. *J Mar Biol Assoc Uk* 86, 167-174.
- Lauzon-Guay, J.S., Scheibling, R.E., Barbeau, M.A., 2009. Modelling phase shifts in a rocky subtidal ecosystem. *Mar Ecol Prog Ser* 375, 25-39.

- LeGault, K., Hunt, H., 2016. Cannibalism among green sea urchins *Strongylocentrotus droebachiensis* in the laboratory and field. *Mar Ecol Prog Ser* 542, 1-12.
- Ling, S., Scheibling, R., Rassweiler, A., Johnson, C., Shears, N., Connell, S., Salomon, A., Norderhaug, K., Pérez-Matus, A., Hernández, J., 2015. Global regime shift dynamics of catastrophic sea urchin overgrazing. *Phil Trans R Soc B* 370, 20130269.
- Mann, K.H., Wright, J.L.C., Welsford, B.E., Hatfield, E., 1984. Responses of the sea urchin *Strongylocentrotus droebachiensis* (O.F. Müller) to water-borne stimuli from potential predators and potential food algae. *J Exp Mar Biol Ecol* 79, 233-244.
- Munda, I.M., Lüning, K., 1977. Growth performance of *Alaria esculenta* off Helgoland. *Helgoland Wiss Meer* 29, 311.
- Norderhaug, K.M., Christie, H.C., 2009. Sea urchin grazing and kelp re-vegetation in the NE Atlantic. *Mar Biol Res* 5, 515-528.
- Petraitis, P.S., Latham, R.E., 1999. The importance of scale in testing the origins of alternative community states. *Ecology* 80, 429-442.
- Quinn, G.P., Keough, M.J., 2002. Experimental design and data analysis for biologists. Cambridge University Press.
- R Development Core Team, 2018. R: A language and environment for statistical computing. R Foundation for Statistical Computing, Vienna, Austria. URL <https://www.R-project.org/>.
- Scheibling, R.E., Gagnon, P., 2009. Temperature-mediated outbreak dynamics of the invasive bryozoan *Membranipora membranacea* in Nova Scotian kelp beds. *Mar Ecol Prog Ser* 390, 1-13.
- Scheibling, R.E., Hamm, J., 1991. Interactions between sea urchins (*Strongylocentrotus droebachiensis*) and their predators in field and laboratory experiments. *Mar Biol* 110, 105-116.
- Scheibling, R.E., Hatcher, B.G., 2007. Ecology of *Strongylocentrotus droebachiensis*, in: Lawrence, J.M. (Ed.), *Edible Sea Urchins: Biology and Ecology*, Amsterdam, pp. 353-392.
- Scheibling, R.E., Hennigar, A.W., Balch, T., 1999. Destructive grazing, epiphytism, and disease: the dynamics of sea urchin-kelp interactions in Nova Scotia. *Can J Fish Aquat Sci* 56, 2300-2314.
- Siikavuopio, S.I., Christiansen, J.S., Dale, T., 2006. Effects of temperature and season on gonad growth and feed intake in the green sea urchin (*Strongylocentrotus droebachiensis*). *Aquaculture* 255, 389-394.

- Silliman, B.R., McCoy, M.W., Angelini, C., Holt, R.D., Griffin, J.N., van de Koppel, J., 2013. Consumer fronts, global change, and runaway collapse in ecosystems. *Annu Rev Ecol Evol Syst* 44, 503-538.
- Silliman, B.R., Van De Koppel, J., Bertness, M.D., Stanton, L.E., Mendelsohn, I.A., 2005. Drought, snails, and large-scale die-off of southern US salt marshes. *Science* 310, 1803-1806.
- Snedecor, G.W., Cochran, W.G., 1989. *Statistical methods*, eight ed. Iowa State University Press, Ames.
- Stander, P.E., 1992. Foraging dynamics of lions in a semi-arid environment. *Can J Zool* 70, 8-21.
- Steneck, R.S., Graham, M.H., Bourque, B.J., Corbett, D., Erlandson, J.M., Estes, J.A., Tegner, M.J., 2002. Kelp forest ecosystems: biodiversity, stability, resilience and future. *Environ Conserv* 29, 436-459.
- Studd, M., Montgomerie, R.D., Robertson, R.J., 1983. Group size and predator surveillance in foraging house sparrows (*Passer domesticus*). *Can J Zool* 61, 226-231.
- Velimirov, B., Griffiths, C., 1979. Wave-induced kelp movement and its importance for community structure. *Bot Mar* 22, 169-172.
- Wilson, W., Richards, S., 2000. Consuming and grouping: resource-mediated animal aggregation. *Ecol Lett* 3, 175-180.
- Wright, J.T., Dworjanyn, S.A., Rogers, C.N., Steinberg, P.D., Williamson, J.E., Poore, A.G.B., 2005. Density-dependent sea urchin grazing: differential removal of species, changes in community composition and alternative community states. *Mar Ecol Prog Ser* 298, 143-156.

CHAPTER III

Kelp-bed dynamics across scales: Enhancing mapping capability with remote sensing and GIS ¹

¹ St-Pierre, A.P., Gagnon, P., 2020. Kelp-bed dynamics across scales: Enhancing mapping capability with remote sensing and GIS. *J Exp Mar Biol Ecol* 522, 151246.

3.1. ABSTRACT

Kelp are important drivers of productivity and biodiversity patterns in cold-water and nutrient-rich rocky reefs. Scuba- and boat-based methods are routinely used to study submerged kelp beds. However, these time-consuming and labor-intensive methods enable monitoring of kelp beds or the factors and processes that control their distribution over only small spatial (few 100s of m²) and temporal (<5 years) extents. Remote sensing and geographic information system (GIS) technologies are increasingly used to compare marine species distribution over multiple spatiotemporal scales. However, there is currently no clear framework and limited demonstration of their potential for studies of broad-scale changes in completely submerged kelp beds. The present study aims to establish the foundation of a simple, accessible, and robust set of remote sensing and GIS-based methods to address key questions about the stability of subtidal kelp beds across multiple spatial and temporal scales. It tests the suitability of conventional image classification methods for mapping kelp from digital aerial (acquired on board a helicopter) and satellite (SPOT 7) imagery of ~250 ha of seabed around four islands in the Mingan Archipelago (northern Gulf of St. Lawrence, Canada). Three classification methods are compared: 1) a software-led unsupervised classification in which pixels are grouped into clusters based on similarity in spectral signature among pixels; 2) a software-led supervised classification in which pixels are assigned to categories based on similarity in the spectral signature of pixels and that of reference data from each category; and 3) a visual classification carried out by a trained observer. Supervised classification of satellite imagery and visual classification of aerial imagery were the top methods to map kelp, with overall accuracies of 89% and 90%, respectively. Unsupervised classification of both types of imagery showed poor

discrimination between kelp and non-kelp benthic classes. Kelp bed edges were more difficult to identify on satellite than aerial imagery because the former presented poorer contrasts and a lower spatial resolution. Kelp bed edges identified with visual classification appeared artificially jagged for both types of imagery, mainly because of the coarse (225-m²) spatial units used for this classification. Kelp bed edges were smoother on maps created with the unsupervised and supervised classifications, which used 1-m-pixel images. The present study demonstrates that conventional remote sensing and GIS methods can accurately map submerged kelp beds over large spatial domains in the Mingan Archipelago or in other benthic systems with similar oceanic conditions and a largely dichotomous (kelp-barrens) biological makeup.

3.2. INTRODUCTION

Kelp (large brown seaweeds of the order Laminariales) are key drivers of productivity and biodiversity patterns in cold-water and nutrient-rich, shallow rocky reefs (Dayton, 1985; Tegner and Dayton, 2000). Kelp typically form structurally complex aggregates, known as kelp beds or forests, which provide critical habitat to a variety of fish and invertebrates (Estes et al., 2004; Ling, 2008; Steneck et al., 2002). Worldwide, large-scale shifts from kelp-dominated to urchin-dominated community states have occurred following increases in the intensity of urchin grazing on kelp, or as a result of climate-driven shifts in species distribution (Ling et al., 2015; Steneck et al., 2002; Vásquez et al., 2007; Wernberg et al., 2016). Although these shifts between community states affect 10s to 100s of km² of coastal habitats (Filbee-Dexter and Scheibling, 2014; Krumhansl et al., 2016; Moy and Christie, 2012), most studies of subtidal kelp systems, including distributional aspects, have

been conducted over small spatial (few hundreds of metres) and temporal (less than five years) scales mainly because of the limitations of the time-consuming and labor-intensive scuba techniques typically employed (Gagnon et al., 2004; Lauzon-Guay and Scheibling, 2007; Scheibling et al., 1999; Van Rein et al., 2009). Such studies provide valuable information about local kelp bed dynamics. However, distributional patterns of kelp and the underlying ecological drivers may vary across scale (Cavanaugh et al., 2010; Schneider, 2001; Turner et al., 1989; Van Rein et al., 2009), and hence repeated measurements of kelp abundance and the ecological drivers of change at broad spatial and temporal scales are desirable over inferences from small scale patterns.

In the northern Gulf of St. Lawrence (Canada), mixed kelp beds dominated by *Alaria esculenta* (Linneaus) and *Laminaria digitata* (Hudson) often form a fringe from the lower intertidal to depths of ~7 m. Dense (up to 400 individuals m⁻²) aggregations of green sea urchins, *Strongylocentrotus droebachiensis* (Müeller), known as urchin fronts, typically form at the lower edge of the beds, more so in summer. Urchin fronts destructively graze the beds as they move in shallower water, leaving behind extensive barrens largely devoid of fleshy macroalgae (Gagnon et al., 2003; Gagnon et al., 2004; Himmelman, 1991). The Mingan Archipelago is a group of more than 40 islands along the northern shore of the Gulf of St. Lawrence, between Anticosti Island and Québec's Middle North Shore. The shallow seascape around these islands presents the biological characteristics described above, with a spatial dominance of barrens over kelp beds within the first ~10 m of water (Gagnon et al., 2003; Gagnon et al., 2004; Himmelman, 1991).

Scuba-based research carried out around many islands since the early 1980s, suggests that urchin barrens can persist for decades, mainly because of sustained urchin grazing (see Gagnon et al., 2003; Gagnon et al., 2004; Gagnon et al., 2005; Himmelman, 1991; Narvaez Diaz, 2018). This situation differs from that in more southerly regions of eastern Canada with warmer waters, in particular Nova Scotia, where outbreaks of a pathogenic amoeba have sporadically decimated urchin populations, causing large-scale shifts in kelp/barrens community states (Filbee-Dexter and Scheibling, 2012, 2014; Lauzon-Guay et al., 2009). The presumed stability of the kelp bed and barrens states across the Mingan Archipelago is not backed by a rigorous, broad-scale assessment of temporal changes in the spatial extent of each community state. Also, factors that control the broad-scale stability, or lack thereof, of these community states are largely unknown. Synoptic approaches that depend less on scuba techniques, more on mass acquisition and analysis of data, must be developed to properly address the frequency, causes, and consequences of community phase shifts in this and other systems, at scales that enable significant gains in ecological knowledge and ability to manage marine resources.

Broad-scale marine habitat mapping programs increasingly rely on remote sensing and geographic information system (GIS) technologies (Finkl and Makowski, 2014; Green et al., 2000; McCarthy et al., 2017), which provide several key advantages over traditional scuba-based techniques. First, acquisition of imagery (or other types of data) with airborne or spaceborne sensors can be much quicker and cover much larger areas, including in remote locations (Cavanaugh et al., 2010; Deysher, 1993; Green et al., 2000; Van Rein et al., 2009). Orbiting satellites revisit the same locations on the earth's surface at regular intervals, thus acquiring core information for community change analysis (Brooks et al.,

2015; Lyons et al., 2011; Yang and Yang, 2009). High-resolution satellite images covering a variety of spatial domains are publicly (and sometimes freely) available (e.g., Worldview-1 to 4 [0.31 to 0.46-m pixels], Quickbird [0.65-m pixels], SPOT7 [1.5-m pixels], PlanetScope [3-m pixels], and RapidEye [5-m pixels]), therefore facilitating access to core data. Secondly, images can be georeferenced, projected, and analyzed in a GIS, and spatially matched with environmental factors to explore the causes and consequences of changes of a given community component (Garza-Pérez et al., 2004; Kendrick et al., 2000; Lathrop et al., 2001; Silva et al., 2008). Despite these advantages, mapping of subtidal benthic communities based on optical imagery acquired from above the sea surface can be challenging, mainly because of the exponential attenuation of sunlight passing through the water column (Green et al., 2000; Jerlov, 1976). This phenomenon, which further varies with the type of oceanic water (Jerlov, 1976; Maritorena et al., 1994; Mobley, 1994) ultimately alters the spectral values of the seabed and benthos recorded by the camera and, in turn, the ability to correctly classify benthic community types (Ackleson, 2003; Gagnon et al., 2008; Green et al., 2000). Because of this challenge, studies of submerged vegetation from remotely acquired optical imagery have largely been in benthic habitats overtopped by optically shallow (low-turbidity) waters (Andréfouët et al., 2004; Gullström et al., 2006; Hedley et al., 2012; Hochberg and Atkinson, 2003; Hu et al., 2015; Kendrick et al., 2000; Lyons et al., 2011).

Most studies that have used optical remote sensing to map kelp have focused on tall species (e.g., the giant kelp, *Macrocystis pyrifera*) that form forests and grow tissues at or near the sea surface, therefore substantially reducing the risk of misclassification (Bell et al., 2015a; Bell et al., 2015b; Cavanaugh et al., 2010; Cavanaugh et al., 2011; Friedlander

et al., 2018; Grove et al., 2002; Nijland et al., 2019; Stekoll et al., 2007). The greater challenge of detecting largely submerged, low-lying kelp species from above the sea surface, like is the case in the Mingan Archipelago, might partly explain the rarity of studies that have mapped completely submerged kelp beds with optical remote sensing (Casal et al., 2011; Malthus and Karpouzli, 2003; Simms and Dubois, 2001; Vahtmäe et al., 2012). Water column correction techniques can be applied to improve the accuracy of classification maps of benthic habitats (Hoang et al., 2015; Sagawa et al., 2012; Zoffoli et al., 2014), yet their complexity may limit their implementation. Remote sensing and GIS technologies evolve rapidly (Finkl and Makowski, 2014; Frohn and Lopez, 2017; McCarthy et al., 2017), becoming increasingly powerful and complex. As highlighted by Andréfouët (2008), the perspective and objectives of “map producers” (e.g., remote sensing specialists) whose main goal is to develop highly effective methods, differ from those of “map users” (e.g., scientists and managers) who are primarily interested in creating trustable and adaptable products (e.g., habitat classification maps and accuracy metrics) in simple ways. As map users, those with a prime interest in studying submerged kelp bed dynamics, i.e., marine benthic ecologists, may not be familiar with, or have access to, specialized, cutting-edge remote sensing technologies. These non-specialists would therefore benefit from a demonstration of the gain in information that simple and accessible remote sensing and GIS technologies can provide.

The present study is the first of a series aimed at developing and presenting a simple and accessible, yet robust set of remote sensing and GIS-based approaches to address key questions about the stability of kelp beds across multiple spatial and temporal scales. The series uses the Mingan Archipelago as a study system because of its relative simplicity (see

details in section 3.3.1) and the opportunity that previous scuba-based studies offer to compare patterns and drivers of kelp stability across scales (Gagnon et al., 2003; Gagnon et al., 2004; Gagnon et al., 2005; Himmelman and Dutil, 1991; Narvaez Diaz, 2018). The present study's main objective is to identify the most reliable methodology to quantify the distribution of completely submerged kelp that subsequent studies can use to generate core information to quantify biological and ecological patterns and their natural drivers. This objective is accomplished by testing the suitability of three conventional classification methods for kelp detection and mapping: 1) a software-led unsupervised classification in which clusters of pixels are identified based on the similarity in spectral signature among pixels and the user subsequently assigns the clusters to a cover class (in the present case, either "kelp" or "non-kelp"); 2) a software-led supervised classification in which the user provides field reference data to identify the spectral characteristics of each cover class, then each pixel is assigned to a class by the software based on spectral similarity; and 3) a visual classification in which a trained observer identifies the presence of either cover class on the imagery across a grid of points. Each classification method was applied to digital aerial (acquired on board a helicopter) and satellite (SPOT 7) imagery covering nearly 250 ha of seabed around four islands. The imagery was acquired at times of optimal sea-state conditions to facilitate image classification. Each method's operational and logistical advantages and limitations are discussed to guide the choice of a particular methodology for systems similar to the Mingan Archipelago's but where access to resources may differ.

3.3. MATERIALS AND METHODS

3.3.1. Study system

The study system encompassed the seabed around four islands in the Mingan Archipelago: Île à Firmin (westernmost), Île du Havre, Île aux Goélands, and Petite île au Marteau (easternmost; Figure 3.1). The seabed in this system is mainly composed of bedrock and boulders, with occasional patches of cobble, gravel, or sand in areas with low hydrodynamic forces (Gagnon et al., 2004). This system was chosen because it presents characteristics facilitating the application and validation of the methods described below. First, kelp beds composed mainly of *Alaria esculenta* and *Laminaria digitata*, and to a lesser extent *Agarum clathratum* (Dumortier), *Saccharina longicuris* (Bachelot de la Pylaie), and *Saccorhiza dermatodea* (Bachelot de la Pylaie), develop at depths of 0 to 7 m and are generally more abundant on southern, wave-exposed sides of the islands (Gagnon et al., 2004). These thick, dark-colored beds are followed in deeper water by green sea urchin (*Strongylocentrotus droebachiensis*) barrens colonized by a thin, light-colored layer of live and dead encrusting coralline algae, mainly *Lithothamnion glaciale* (Kjellman) (Figure 3.2.B, Gagnon et al., 2004). Such a dichotomous division of the benthos into two biologically and spectrally distinct community types, hereafter termed “kelp” and “non-kelp”, is compatible with the application of a simple image classification method. Second, the transition between kelp beds and barrens is often clear-cut, mainly because of grazing by urchin fronts advancing over the lower edge of the beds (Figure 3.2, Gagnon et al., 2004). Sharp transitions between these two spectrally different community types further facilitate identification on imagery (Figure 3.2.D and 3.2.E). Third, seabed slope is gentle, on average ~3% as calculated from bathymetry data, with no major sudden shifts in topography. Such a mild, gradual change in slope and the shallow depth range (0 to 7 m) on which the present study focuses limit effects of attenuation of light by the water column

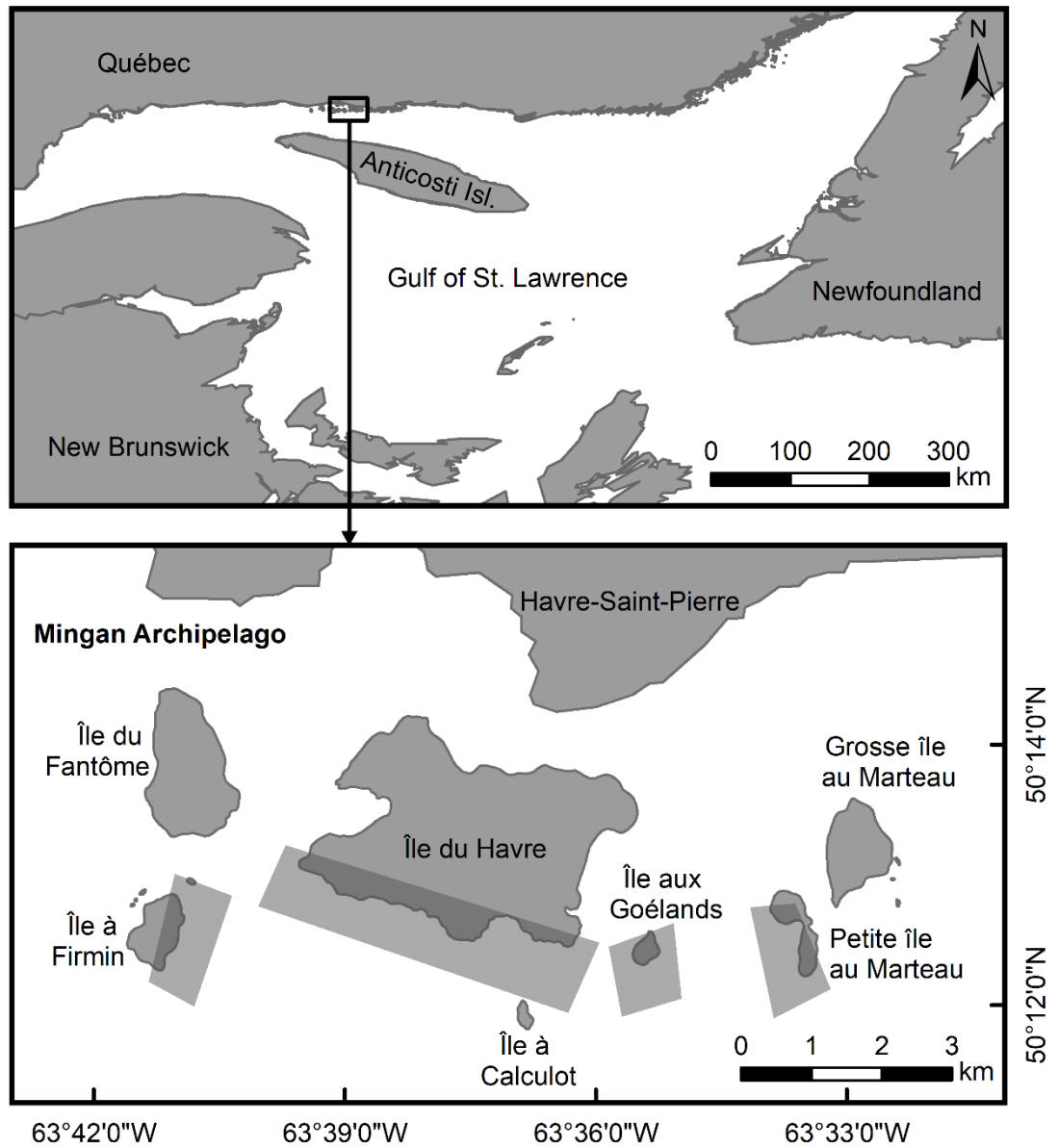
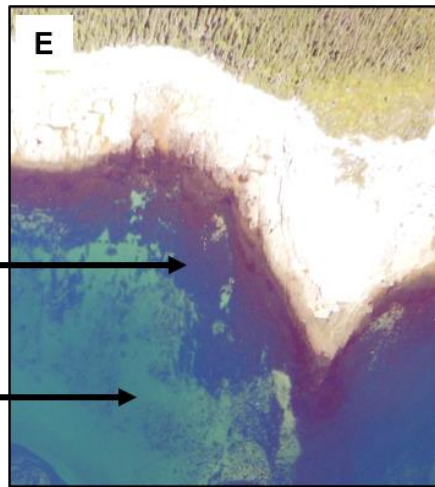
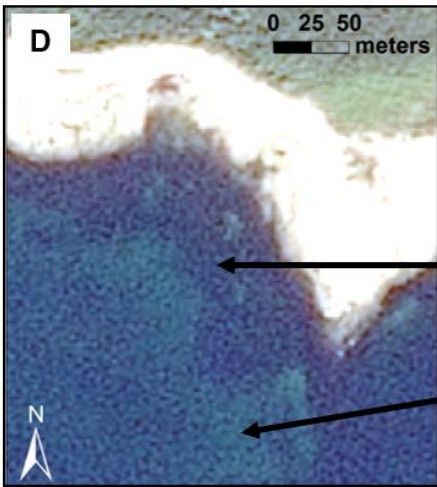


Figure 3.1. Location of study areas (shaded polygons) at Île à Firmin, Île du Havre, Île aux Goélands, and Petite île au Marteau in the western sector of the Mingan Archipelago, northern Gulf of St. Lawrence, eastern Canada.



Kelp

Non-kelp

Figure 3.2. **A)** Kelp bed [mainly *Alaria esculenta*] at a depth of ~2 m within the Île du Havre study area (photo: Anne P. St-Pierre). **B)** Green sea urchin (*Strongylocentrotus droebachiensis*) barrens with a few kelp patches at a depth of 6 m within the Île du Havre study area (photo: Anne P. St-Pierre). **C)** Sharp transition between the lower edge of a kelp bed and upper edge of an urchin barrens caused by an urchin grazing front advancing over kelp at a depth of ~2 m within the Île du Havre study area (photo: Anne P. St-Pierre). **D)** Satellite [SPOT 7] image of a portion of the Île du Havre study area. **E)** Aerial image of the same portion shown in D (photo: Patrick Gagnon).

on benthic spectral signatures (Green et al., 1996; Green et al., 2000), therefore eliminating the need to apply water column correction. All these characteristics reduce the likelihood of misclassifying both community types.

Monospecific stands of the grazing-resistant, perennial kelp *A. clathratum* and annual brown seaweed *Desmarestia viridis* (Müller) that cover up to a few 10s of m² can develop in the barrens at depths of up to 15 m (Gagnon et al., 2003; Gagnon et al., 2004; Gagnon et al., 2005). *Agarum clathratum* stands are considered a stable component of barrens, whereas stands of *D. viridis* are ephemeral, with annual recruitment and die-off in late winter and early fall, respectively (Blain and Gagnon, 2014; Gagnon et al., 2003; Gagnon et al., 2004; Gagnon et al., 2005). These stands typically develop in areas of low to moderate wave action, along the lower edge of *A. esculenta* beds (*A. clathratum*) or in the barrens (*A. clathratum* and *D. viridis*; Gagnon et al., 2003; Gagnon et al., 2004; Gagnon et al., 2005). While *A. clathratum* and *D. viridis* are not consumed by sea urchins and grow outside of mixed kelp beds in this region, they are not generally considered as part of kelp beds. However, these seaweeds could not be distinguished from mixed kelp beds on the imagery. As discussed later (see Discussion), there was low potential for misclassification of *D. viridis* stands as kelp and other non-kelp macroalgae were rare within the study area, covering only ~6% of the seabed (see section 3.2.3). In total, 248.4 ha of seabed were classified, with respectively 15, 62, 13, and 10% of this surface at Île à Firmin, Île du Havre, Île aux Goélands, and Petite île au Marteau.

To identify the most accurate classification method (out of the three methods tested) for kelp detection and mapping in the Mingan Archipelago system, the procedures applied were grouped under four modules detailed in the sections below and summarized

schematically (Figure 3.3): (1) image acquisition and pre-processing [section 3.3.2]; (2) ground truthing [section 3.3.3]; (3) image classification [section 3.3.4]; and (4) accuracy assessment [section 3.3.5]. These modules combine satellite (*Satellite Pour l'Observation de la Terre*; SPOT 7), aerial (digital), and underwater (digital) seabed imagery of the study area, as well as bathymetric data and conventional image classification techniques and accuracy assessment metrics. Some of the key remote sensing and GIS terms employed are underlined and defined in a separate section (Appendix 3.A).

3.3.2. Image acquisition and pre-processing

The two types of remotely sensed imagery used in the present study - one SPOT 7 satellite image and multiple aerial photographs acquired with a basic digital camera - align with the overarching goal of establishing simple and reliable ways to map subtidal kelp cover over large tracts of seabed. Original imagery differed in spatial coverage (175 to 1015 times larger on SPOT 7 than on aerial images), spatial resolution (14 to 320 times lower on the SPOT 7 image), and contrast (lower on the SPOT 7 image). These differences enabled the comparison of the accuracy of classification maps derived from a readily available commercial product (SPOT 7 image) and imagery that is logistically more challenging and time-consuming to acquire and process (aerial photographs). The SPOT 7 image, acquired on 11 August, 2016, in the hour preceding low tide, encompassed the entire study system. It was taken after four days with low winds ($16.4 \pm 1.1 \text{ km h}^{-1}$, based on data from Environment Canada [<http://climate.weather.gc.ca>]) and no precipitation and contained no cloud cover or surface waves. Aerial photographs were acquired sequentially with overlap from Petite île au Marteau to Île à Firmin on board a helicopter flown at an altitude of

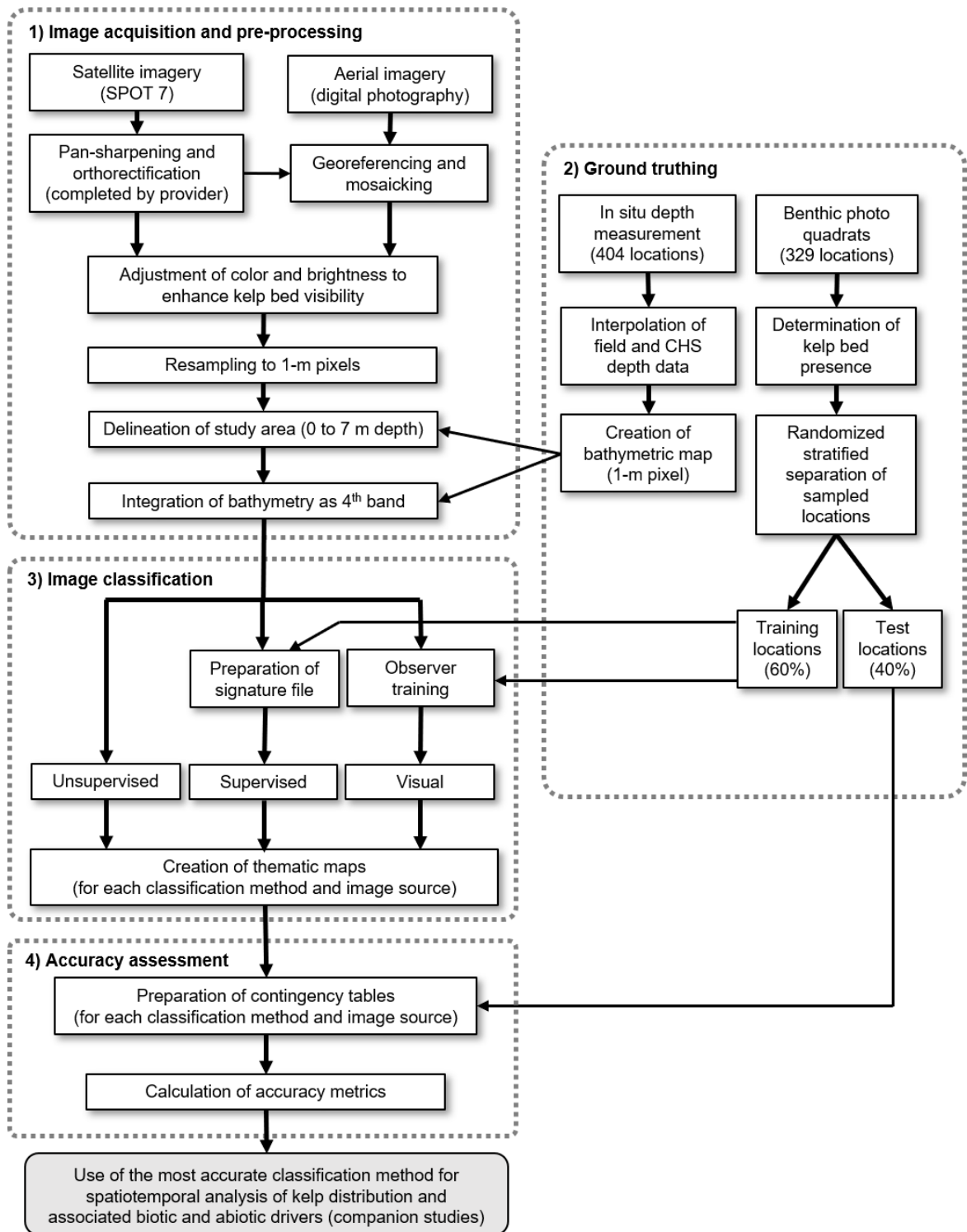


Figure 3.3. Break down of steps in each of the four methodological modules used in the present study. **(1)** Image acquisition and pre-processing: satellite imagery of the study area was used as a base map to georectify [dashed arrow within box 1] corresponding aerial imagery. Both sets of images were digitally balanced to enhance contrast between kelp and other benthic components. Bathymetric mask was applied to restrict analysis to shallow (0 to 7 m deep) seabed. **(2)** Ground truthing: bathymetric data acquired in situ with an echosounder and from the Canadian Hydrographic Service [CHS] were used to support delineation of each study area and image classification [dashed arrows from box 2 to box 1]. Benthic photo quadrats acquired within each study area were used to validate the presence and absence of kelp on satellite and aerial imagery and support image classification and accuracy assessment [dashed arrows from box 2 to boxes 3 and 4]. **(3)** Image classification: pre-processed satellite and aerial imagery and ground truth data were used to create maps of kelp distribution from three different classification methods: unsupervised, supervised, and visual. **(4)** Accuracy assessment: classification accuracy for each of the six thematic maps created was calculated based on test location ground truth data [dashed arrow from box 2 to box 4].

~300 m. They were taken with a hand-held digital camera (Nikon Coolpix AW130) at low tide on 8 July, 2016, after four days of low winds ($14.1 \pm 0.8 \text{ km h}^{-1}$, based on data from Environment Canada [<http://climate.weather.gc.ca>]) and no precipitation. None of the images contained cloud cover or surface waves. We deliberately chose dates and times of image acquisition for each image source with best possible sea conditions (i.e., low waves, low winds, low turbidity) to facilitate image classification. These conditions minimized the amount of suspended particles in the water column and glare from sunlight reflection at the sea surface, enabling viewing the seabed clearly to depths of up to ~8 m on both satellite and aerial images (Figure 3.2.D and 3.2.E). Water-column data enabling quantifying water turbidity were not available. Yet, water clarity was highest for the region at this time of the year (P. Gagnon, personal observations over multiple years). Logistical considerations prevented acquiring aerial photographs on a day for which a SPOT image was available. Based on previous research and observations of kelp recruitment periods and urchin grazing in the area, the temporal gap between the acquisition of the two types of imagery is deemed small enough not to create a significant difference in kelp distribution (Gagnon et al., 2003; Gagnon et al., 2004; Gagnon et al., 2005).

One key aspect affecting the quality of image classification is the spectral resolution of images. In theory, a higher spectral resolution yields greater spectral differences among image pixels with different objects or biota, thus increasing separability (Green et al., 2000). Spectral resolution refers to the number and width of spectral bands in an image, such that images with multiple spectral bands (channels) generally have a greater spectral resolution and are preferred over panchromatic (one band) images (Green et al., 2000). Furthermore, in optically deep waters like was the case in the present study, short (blue and

green) wavelengths penetrate deeper than long (red and near-infrared) ones (Jerlov, 1976; Maritorena et al., 1994; Mobley, 1994). Consequently, sensors with a greater number of bands recording in the shorter wavelengths typically produce more useful imagery of completely submerged benthic features than sensors with a greater number of bands recording in the longer wavelengths (infrared wavelengths are completely filtered out within the first few centimetres of water, and hence useless; Lillesand et al., 2014). Yet, the expertise and software and hardware needed to process and classify images also increase with the number of spectral bands (Bioucas-Dias et al., 2013; Green et al., 2000). Accordingly, images with only few bands may provide sufficient resolution when dealing with low habitat complexity, like in the present study.

Both satellite and aerial images were true color composite images. The SPOT 7 image was pan sharpened to a spatial resolution (pixel size) of 1.5 m and orthorectified by the image provider (Land Info Worldwide Mapping LLC, Colorado, USA). The three bands forming the satellite image covered the 455 to 525 nm (blue), 530 to 590 nm (green), and 625 to 890 nm (red) ranges. Spatial resolution of aerial photographs varied between 7 and 20 cm depending on camera (helicopter) height and angle. Although the aerial photographs were 3-band (blue, green, and red) color composite images, the specific wavelengths recorded in each band is unknown. Aerial photographs were georectified and mosaicked (Lillesand et al., 2014) to create a single image of the four islands using the SPOT 7 image as the registration template and six to 14 photographs per island (based on the size of the study area and quality of the photographs) with side overlap among photographs. During mosaicking, 10 to 15 ground control points per photograph were used and a projective transformation was applied. This transformation was chosen over other common types of

transformation because it yielded the lowest root mean square residual error (between 1.2 to 9.5 m), and the best visual match to the satellite imagery. During mosaicking, contrast and brightness of each aerial photograph were adjusted with ArcGIS' Contrast and Brightness function to facilitate kelp detection and reduce variation among photographs. Contrast and brightness were also adjusted on the SPOT 7 image to facilitate kelp detection. To facilitate data processing and analysis, all individual layers were converted to a common map coordinate system (Universal Transverse Mercator Projection, Zone 20N, North American Datum 1983). All raster datasets were resampled to a 1-m grid cell size with the nearest neighbour resampling algorithm (Lillesand et al., 2014). Atmospheric and radiometric corrections, which correct for or calibrate irregularities in pixel values due to atmospheric distortion or instrumentation errors, were not applied because only one satellite image was used (Andréfouët, 2008; Green et al., 2017; Song et al., 2001). These corrections should be applied to calibrate pixel values prior to analysis when using multiple satellite images acquired at the same or different times. (Green et al., 2017; Lillesand et al., 2014). The SPOT 7 image and mosaics of aerial photographs were cropped to keep only seabed between 0 and 7 m deep (see section 3.3.3). Light attenuation in the water column was indirectly accounted for by adding bathymetry as a 4th band to both types of imagery as a means of improving classification with the unsupervised and supervised classification methods (see section 3.3.3).

3.3.3. Ground truthing

Bathymetry

Preliminary analysis of bathymetric charts for the Mingan Archipelago obtained from the Canadian Hydrographic Service (CHS) revealed inaccuracies in the 0 to 5 m depth range. Bathymetry across the study area was therefore acquired with a boat-mounted depth sounder (Lowrance Hook5 recreational fishfinder, vertical precision of 0.1 m) equipped with a GPS unit. A horizontal accuracy below 5 m was estimated for the GPS unit by comparing the position of features on the SPOT 7 image (e.g., docks, roads, rocky features across the study area) with *in situ* measurements of their position with the depth sounder's GPS unit. In total, 404 depth soundings were acquired, with 83, 226, 57, and 38 soundings at Île à Firmin, Île du Havre, Île aux Goélands, and Petite île au Marteau, respectively. Bathymetric data were corrected for tidal elevation at the time of measurement. This was done by subtracting tidal amplitude (precision of 0.1 m, based on water level observations by the Department of Fisheries and Oceans Canada [www.waterlevels.gc.ca]) from *in situ* depth measurements. A bathymetric chart encompassing the four study areas was created with ordinary kriging based on the self-acquired, corrected bathymetric data and the 10-m isobath on CHS' 2002 bathymetric chart. This map, which had a grid cell size of 1 m (Figure 3.4), was incorporated to the GIS platform used to classify images (see section 3.3.4), both to crop the SPOT 7 image and mosaic of aerial photographs (hereafter termed "aerial mosaic") to the targeted 0 to 7 m depth range, and as a means of potentially improving classification accuracy (Gagnon et al., 2008). The SPOT 7 image and the aerial mosaic contained three bands (layers) of spectral information for each image pixel; one for each of the red, green, and blue wavelengths. The addition of the 4th non-spectral bathymetric band (see above) created a 4-band raster.

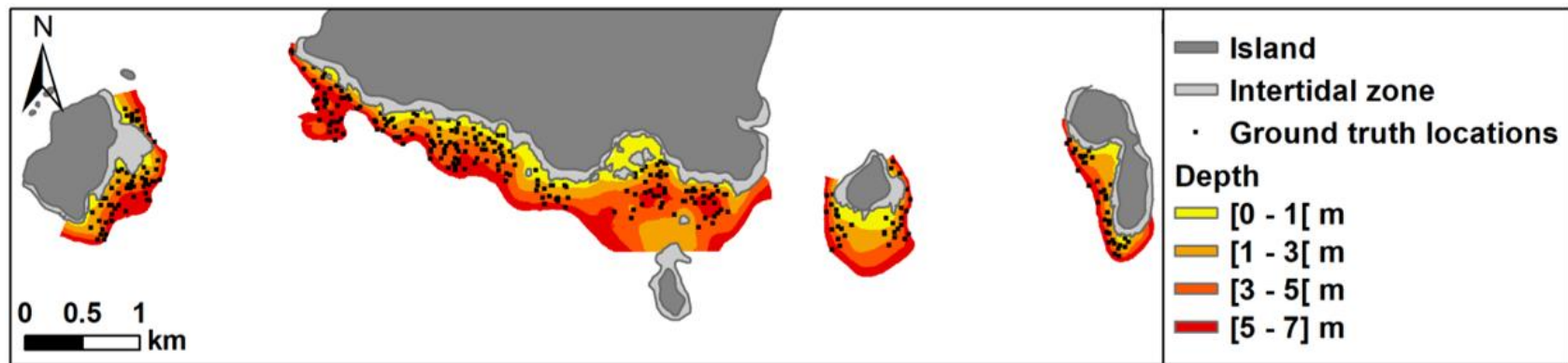


Figure 3.4. Bathymetry of the study system used to map kelp from satellite and aerial imagery with locations of ground truth data acquisition (see summary of methodological details in Figure 3.3).

Complementary data

The three image classification methods used required *in situ* data about the presence and absence of kelp for training purposes (in the case of supervised and visual classifications) and to calculate classification accuracies (see sections 3.3.4 and 3.3.5). Kelp occurrence at multiple locations across the four study areas was determined between 23 July and 29 July, 2016. To facilitate field work, sampling locations in each study area were pre-determined with a random point generator (Create Random Points tool in ArcGIS v10.3.1, Esri, 2015). The number of locations in each area was proportional to the size of the area, with a minimum distance of 15 m between locations to ensure that two ground truthing locations did not fall within a single grid intersect used for image classification (see section 3.3.4). The nearly even distribution of the locations enabled a spatially balanced sampling design. However, 86 of the 415 pre-determined locations (~21%), were not sampled because they were deeper than the 7-m limit or too shallow to be safely accessed with the boat used for the survey. Of the 329 locations sampled 63, 197, 34, and 35 were at Île à Firmin, Île du Havre, Île aux Goélands, and Petite île au Marteau, respectively. At each location, a down-facing drop camera system (GoPro Hero 3 in an underwater housing, attached to a metal frame) was lowered to ~1 m above the seabed. The height of the camera allowed photographing the seabed within an 80 x 80-cm plot. In total, 231 locations contained one or more kelp sporophytes and 98 had none. The 329 locations were divided into: 1) a training dataset [60% of the locations] used to guide the supervised classification and to train an observer in recognizing kelp on the imagery prior to visual classification; and 2) a test dataset [40% of the locations] used to quantify the accuracy of

each classification method (see section 3.3.5). To ensure that both datasets were spatially balanced among the four study areas and evenly represented each benthic cover class (“kelp” and “non-kelp”), a stratified randomized selection method was applied to divide the locations into training and test datasets. This was done by randomly selecting (without replacement) and assigning to the training dataset 60% of the locations from each benthic cover class within the study area of each of the four islands and assigning the remaining 40% to the test dataset.

3.3.4. Image classification

Three image classification methods commonly used in benthic habitat mapping studies (Brown et al., 2011; Green et al., 2000) were considered: 1) unsupervised [software-led]; 2) supervised [software-led]; and 3) visual [observer-led]. Each method was applied to both the satellite imagery and aerial mosaic for comparison purposes. All methods employed a binary classification scheme, whereby the image was divided into either of two benthic classes: “kelp” or “non-kelp”. Kelp species could not be discriminated given the type and resolution of the images.

Unsupervised classification was carried out in ArcGIS v10.3.1 with the Interactive Self-Organizing (ISO) Cluster Unsupervised Classification algorithm (Esri, 2015) and default settings (minimal number of pixel in a valid class = 20, sample interval = 10). This algorithm separates pixels of input raster images into a user-defined number of clusters based on similarities of pixels’ spectral signatures. It is generally recommended that the number of clusters be at least five times that of cover (benthic) classes (two in the present study), and that each cluster contains at least 10 times as many pixels as the number of

bands in the imagery (four in the present study; Green et al., 2000; Lillesand et al., 2014). For each type of imagery, outputs were created with various numbers of clusters (10, 15, 20, 30, and 40), with 20 providing the best spatial distribution of the two target classes based on visual comparisons with the imagery and complementary field data. Each cluster created by the ISO Cluster algorithm was subsequently assigned to either of the two benthic classes (kelp or non-kelp) by the user based on visual comparison with the original imagery and field data to create a thematic map of the spatial distribution of both benthic classes.

Supervised classification was carried out in ArcGIS v10.3.1 with the Maximum Likelihood Classification (MLC) tool (Esri, 2015). This technique consists of two steps. First, the training dataset created from ground truth data (see section 3.3.3) is used to identify, on the imagery, multiple areas representative of each benthic class. The digital signature of each area, which is based on the numerical values contained in the four bands [red, green, blue, and bathymetry] of each pixel that form the area, is used to create a signature file, which defines the mean numerical values (and their variance) for each benthic class, on each type of imagery. Second, the MLC tool assigns each pixel in the input raster image to a benthic class based on the similarity between the pixel's digital signature and the signature of the classes identified in the signature file. Once all pixels have been assigned to classes, the MLC tool produces a thematic map showing the distribution of the two benthic classes.

Visual classification was carried out by an observer (A. P. St-Pierre) trained to recognize kelp presence and absence on the imagery from the position and cover type of ground-truthed locations. A grid with evenly spaced points was overlaid on each type of images. The distance between adjacent points, 15 m, was consistent with the approximate

scale of earlier studies of kelp bed dynamics in the Mingan Archipelago (Gagnon et al., 2004; Gagnon et al., 2005). The 225-m² (15 x 15 m) area surrounding each point was categorized as “kelp” when 50% or more of the area contained kelp or as “non-kelp” when kelp was less than 50%. Visual classification is based on human perception of shapes, color, and contrasts within an image rather than on numerical values contained in the various bands of information of individual image pixels, and thus is more easily applied to small areas rather than individual pixels. Consequently, the observer must be trained to recognize the visual characteristics of kelp on the imagery prior to conducting the classification. Observer training in the present study was achieved by overlying the training dataset created from the ground truth data on the imagery to identify areas where the field data confirmed the presence or absence of kelp. The observer compared the color, brightness, tone, and shape of known kelp and non-kelp areas, and applied this knowledge to classify the rest of the imagery by matching brightness, tone, and contrasts. In general, the dark (blue-brown) areas, covered in kelp, contrasted sharply with the surrounding light (greenish) areas, devoid of kelp (Figure 3.2.D and 3.2.E). Thematic maps were prepared based on the classification of each point in the grid, for the satellite and aerial imagery separately.

3.3.5. Accuracy of classification

To identify which combination of classification method and image source yielded the most precise kelp distribution map, the accuracy of the six thematic maps produced with the unsupervised, supervised, and visual classification methods (applied to the satellite and aerial imagery separately) was quantified and compared with accuracy metrics commonly

used in the field of remote sensing (Green et al., 2000; Lillesand et al., 2014). This was first done qualitatively by examining the thematic maps visually, to evaluate if patterns suggestive of artefacts from the original imagery (e.g., sharp differences in contrast between images) were present. The proportion of the study area classified into each benthic class was calculated for each thematic map and compared. The similarity among thematic maps was assessed by calculating the proportion of spatial overlap in the distribution of each benthic class, to identify the location and extent of areas consistently classified as kelp or non-kelp by all classification methods. The proportion of spatial overlap was also calculated for all possible pairs of thematic maps. To quantitatively assess classification accuracy, contingency tables, also known as confusion or error matrices, were constructed based on the test dataset (40% of the ground truth data) and used to calculate accuracy measures traditionally used in the field of remote sensing (Lillesand et al., 2014). In contingency tables, the agreement between the true benthic class observed at a location *in situ* (based on analysis of ground truth data) and the benthic class attributed to the same location by the classification is assessed for each location sampled in the field and compiled for each benthic class individually. Hence, the proportion of correctly or incorrectly classified locations in a class can be compared with that of the other classes (see Appendix 3.B for contingency tables from the present study). Overall accuracy and kappa coefficient were both calculated from each of the six contingency tables. Overall accuracy, which ranges from 0 to 100%, indicates the proportion of correctly classified locations (all classes included). Kappa coefficient, which ranges from -1 to 1, indicates how well the classification agrees with ground truth data, with values ≤ 0 indicating chance agreement (a meaningless classification) and values of 1 a perfect agreement between ground truth

and classified data. Producer's accuracy and user's accuracy were used to compare the accuracy of detection of each benthic class separately. Producer's accuracy is the proportion of locations correctly classified in a given class, whereas user's accuracy is the proportion of locations classified in a given class that are actually present under the same class on the seabed. See Landis and Koch (1977) and Lillesand et al. (2014) for further discussion of these statistics.

3.4. RESULTS

3.4.1. Visual assessment of thematic maps

The satellite imagery (which encompassed the entire study area) appeared grainy, with relatively coarse spatial resolution and poor contrast between benthic features (Figure 3.5.A). Kelp and non-kelp pixels on the thematic map created from unsupervised classification were highly segregated, forming small, discontinuous clusters scattered across the seabed around the four islands (Figure 3.5.B). With the supervised classification, kelp formed larger, more continuous patches, which also better matched their true distribution on the satellite image (Figures 3.5.A and 3.5.C). In comparison, kelp cover appeared higher with the visual classification, with long and jagged boundaries (Figures 3.5.A and 3.5.D).

The aerial imagery exhibited better contrasts and delineations between spectrally different benthic features than the satellite imagery (Figures 3.5.A and 3.6.A). However, contrary to the satellite imagery, there was considerable variation in color, tone, and contrast from one photograph to the next (Figure 3.6.A) despite efforts to spectrally

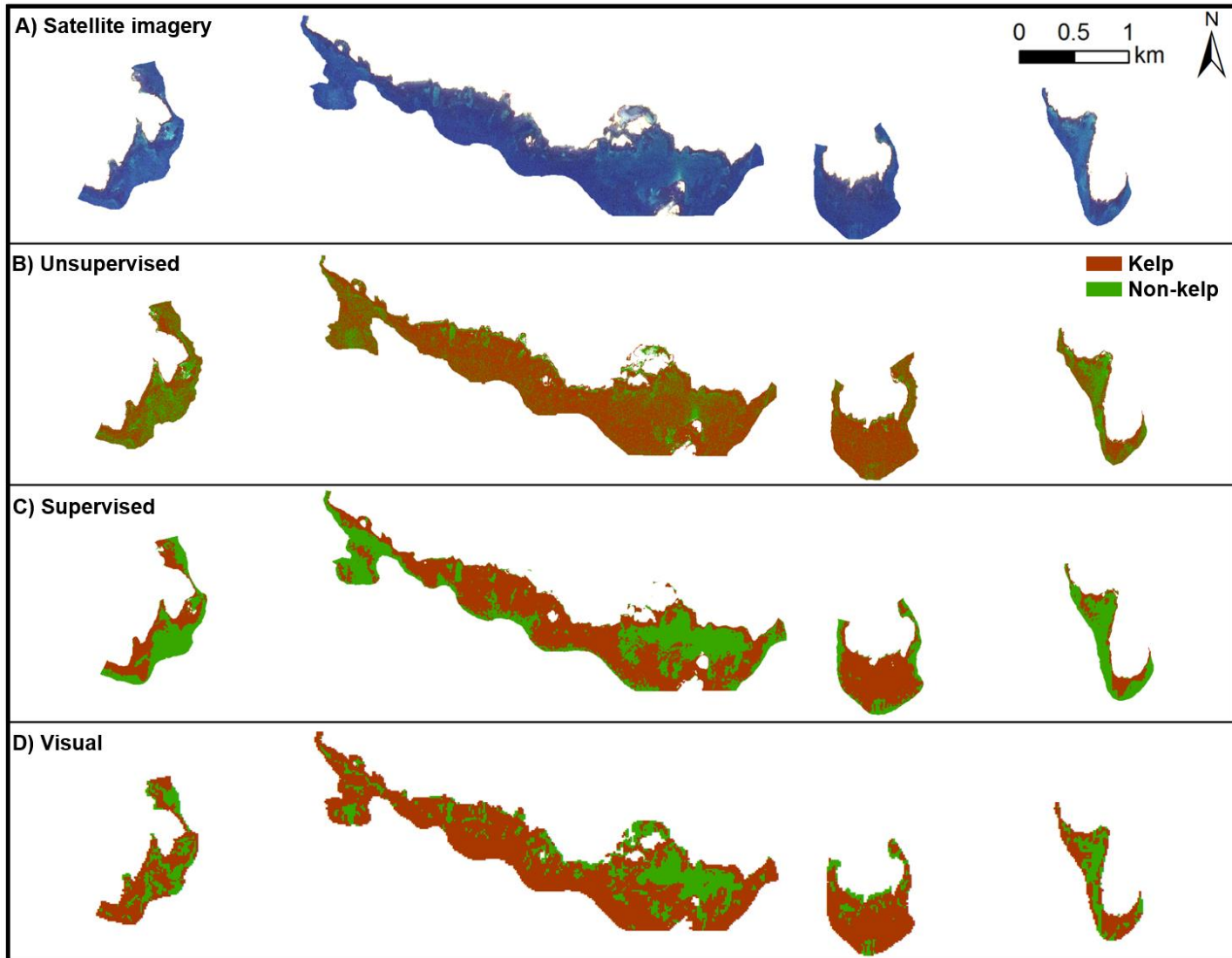


Figure 3.5. Satellite (SPOT 7) imagery of the study system in the Mingan Archipelago (from west to east; île à Firmin, île du Havre, île aux Goélands, and Petite île au Marteau) (A) and associated thematic maps obtained with the three image classification methods tested: unsupervised (B), supervised (C), and visual (D).

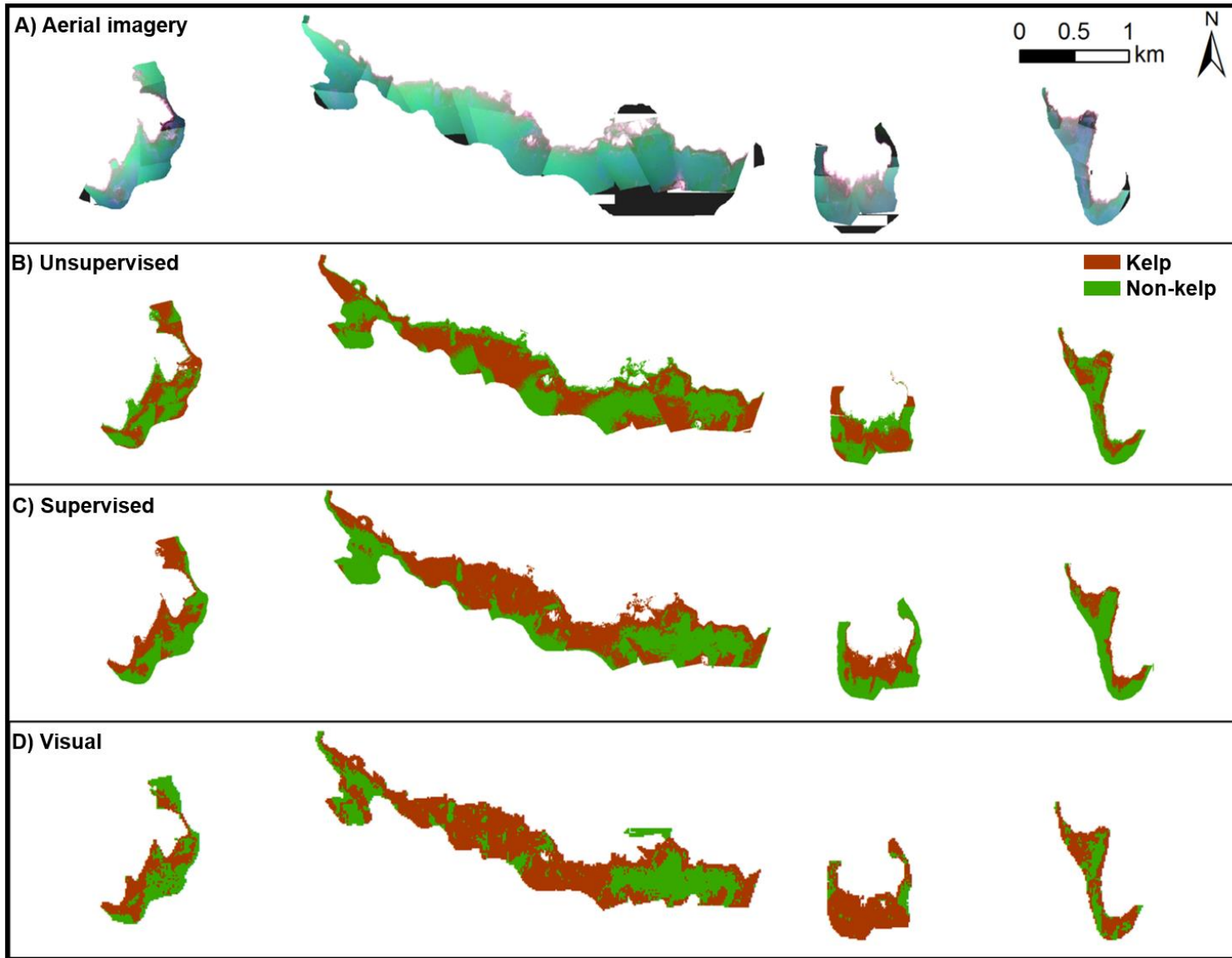


Figure 3.6. Aerial imagery (mosaic of aerial photographs) of the study system in the Mingan Archipelago (from west to east; île à Firmin, île du Havre, île aux Goélands, and Petite île au Marteau) (A) and associated thematic maps obtained with the three image classification methods tested: unsupervised (B), supervised (C), and visual (D).

equalize them during mosaicking. The consequences of this spectral variation were particularly apparent in the thematic map obtained from the unsupervised classification on which: (1) large tracts of seabed classified as kelp contained no kelp on the aerial imagery and vice-versa; and (2) delineations between areas with or without kelp sometimes followed the margins between adjacent photographs (Figure 3.6.B). Kelp distribution with the supervised classification more closely matched that on the aerial imagery, although some artifacts similar to those noted for the unsupervised method remained, particularly around Île à Firmin and along the eastern half of Île du Havre (Figure 3.6.C). As observed with the satellite imagery, kelp cover appeared higher with the visual classification, with coarse boundaries encompassing smaller areas with no kelp on the aerial imagery (Figures 3.5.D, 3.6.A, and 3.6.D).

3.4.2. Spatial overlap in distribution of benthic classes

Overall, the six classification methods similarly classified 32% of the study area as kelp (25%) or non-kelp (7%; Table 3.1). The remaining 68% was classified differently by at least one classification method and was scattered across the area, particularly at the deeper end (5-7 m) with 86% of the seabed classified differently (Figures 3.4 and 3.7, Table 3.1). The proportion of seabed classified as kelp varied among classification methods, from 52% in the unsupervised classification of aerial imagery to 74% in the visual classification of satellite imagery (Table 3.2). With a spatial overlap of 81% in seabed classified as kelp, supervised classification of satellite imagery and visual classification of aerial imagery yielded the most similar kelp bed distributions, followed closely by visual classifications

Table 3.1. Depth-specific proportions of the study area classified as kelp or non-kelp by the six classification methods used (unsupervised, supervised, and visual applied to both types of imagery) or classified differently by at least one classification method.

Depth	Cover		
	Kelp	Non-kelp	Different
0 – 1 m	30.6%	0.8%	68.6%
1 – 3 m	43.7%	7.0%	49.3%
3 – 5 m	22.2%	9.0%	68.8%
5 – 7 m	6.3%	7.5%	86.2%
Overall	25.3%	7.2%	67.5%

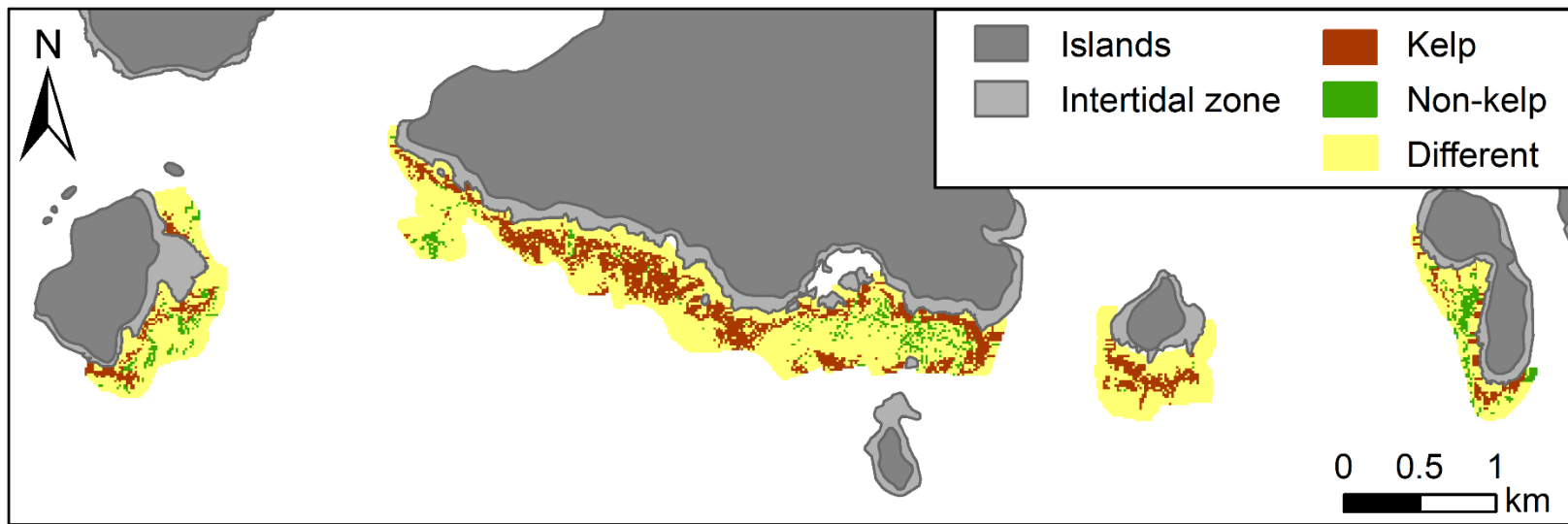


Figure 3.7. Location and extent of seabed consistently classified as kelp or non-kelp by the six classification methods used (unsupervised, supervised, and visual applied to both types of imagery) or classified differently by at least one classification method.

Table 3.2. Coincidence matrix showing the proportion (%) of overlap in seabed classified as kelp or non-kelp (kelp; non-kelp) within each pair of comparison of classification methods used. Bolded values in the bottom row indicate overall proportions of the seabed classified as kelp or non-kelp with each classification method.

	Satellite			Aerial		
	Unsupervised	Supervised	Visual	Unsupervised	Supervised	Visual
Satellite						
Unsupervised	-	-	-	-	-	-
Supervised	68.1; 45.9	-	-	-	-	-
Visual	78.9; 46.8	73.0; 52.5	-	-	-	-
Aerial						
Unsupervised	56.6; 35.9	63.5; 55.7	58.3; 36.2	-	-	-
Supervised	58.9; 37.8	77.2; 79.6	62.6; 41.2	70.0; 66.7	-	-
Visual	73.5; 38.8	81.3; 70.6	80.4; 58.3	64.0; 50.9	73.8; 63.2	-
Overall	70.8; 29.2	58.3; 41.7	73.5; 26.5	52.0; 48.0	53.3; 46.7	65.5; 34.5

of both types of imagery at 80% overlap in kelp distribution (Table 3.2). As to seabed classified as non-kelp, supervised classification applied to both types of imagery yielded the most congruent results with 80% overlap (Table 3.2). The most dissimilar patterns of kelp and non-kelp distributions were with the unsupervised classification method applied to both types of imagery, with spatial overlaps of 57% and 36%, respectively (Table 3.2).

3.4.3. Accuracy of classifications

Unsupervised classification applied to satellite and aerial imageries yielded the lowest overall accuracy (respectively 70% and 66%) and kappa coefficient (respectively 0.261 and 0.273) among the six classification methods used (Table 3.3). Supervised and visual classifications outperformed unsupervised classifications, as shown by gains of 14% to 24% in overall accuracy (Table 3.3). Visual classification of aerial imagery was the most accurate method (overall accuracy: 90%; kappa coefficient: 0.757), followed closely by supervised classification of satellite imagery (overall accuracy: 89%; kappa coefficient: 0.744; Table 3.3).

Visual classification of aerial imagery and supervised classification of satellite imagery exhibited the highest producer's accuracy for the kelp (97%) and non-kelp (95%) classes, respectively, as well as the highest user's accuracy for the non-kelp (91%) and kelp (98%) classes, respectively (Table 3.3). Producer's accuracy was lowest with unsupervised classification of kelp on aerial imagery (68%) and of non-kelp on satellite imagery (44%; Table 3.3). User's accuracy was lowest with unsupervised classification of kelp on satellite imagery (76%) and of non-kelp on aerial imagery (46%; Table 3.3).

Table 3.3. Classification methods used for mapping kelp and non-kelp benthic classes and associated measures of accuracy.

Producer's, user's, and overall accuracies are in %. Numbers in parentheses are the 95% confidence intervals.

	Producer's accuracy		User's accuracy		Overall accuracy	Kappa coefficient
	Kelp	Non-kelp	Kelp	Non-kelp		
Satellite						
Unsupervised	81.1 (±8.6)	43.9 (±16.4)	76.0 (±9.1)	51.4 (±18.0)	69.5 (±8.3)	0.261
Supervised	85.6 (±7.8)	95.0 (±8.0)	97.5 (±4.1)	74.5 (±12.9)	88.5 (±5.9)	0.744
Visual	92.2 (±6.1)	53.7 (±16.5)	81.4 (±8.0)	75.9 (±17.3)	80.1 (±7.2)	0.499
Aerial						
Unsupervised	67.5 (±10.3)	62.5 (±16.3)	80.0 (±9.8)	46.3 (±14.2)	65.8 (±8.6)	0.273
Supervised	80.0 (±8.8)	82.5 (±13.0)	91.1 (±6.9)	64.7 (±14.1)	80.8 (±7.2)	0.581
Visual	96.6 (±4.3)	75.6 (±14.4)	89.6 (±6.6)	91.2 (±11.0)	90.0 (±5.5)	0.757

3.5. DISCUSSION

Spaceborne or airborne infrared imagery is increasingly used to map floating canopies of kelp forests at the sea surface (Bell et al., 2015b; Cavanaugh et al., 2010; Nijland et al., 2019; Stekoll et al., 2007). Canopy maps are then used to estimate subsurface kelp distribution and biomass as well as the influences of various physicochemical factors on them (Bell et al., 2015a; Cavanaugh et al., 2010; Cavanaugh et al., 2011; Friedlander et al., 2007). Completely submerged kelp beds are more difficult to detect because infrared wavelengths emitted by the sun filter out completely by the time they reach kelp near the seabed. Shorter wavelengths that better penetrate water have been used to map submerged kelp beds (Casal et al., 2011; Hoang et al., 2015; Sagawa et al., 2012; Simms and Dubois, 2001; Vahtmäe et al., 2012). However, progress in this area has been relatively slow with only a handful of studies that have specifically quantified and compared the ability to create accurate maps of submerged kelp bed distribution with simple remote sensing and GIS tools (Casal et al., 2011; Gagnon et al., 2008; Uhl et al., 2016). By comparing several accessible, yet simple and robust methods, the present study helps guide map users (*sensu* Andréfouët, 2008) in the choice of suitable approaches to map completely submerged kelp beds in optically deep, yet bathymetrically shallow benthic systems.

The present study demonstrates that satellite and aerial optical imagery, together with basic image classification methods, can produce accurate maps of submerged kelp bed over large (several km²) tracts of seabed. Overall accuracies of maps from supervised classification of satellite imagery (89%), and visual classification of aerial imagery (90%) matched those of studies of submerged aquatic vegetation in temperate and tropical waters (Gagnon et al., 2008; Green et al., 2000; Mumby and Edwards, 2002; Pasqualini et al.,

2005; Valta-Hulkkonen et al., 2003). These accuracies were also above the 85% threshold generally judged satisfactory for management purposes (Anderson, 1976; Congalton and Green, 2008; Hayes and Sader, 2001). Although in principle both methods can be used interchangeably, some logistical considerations, discussed below, might favor the choice of one method over the other.

Image classification based on unsupervised clustering methods only require minimal user input (typically assigning class names to spectral clusters output by software) and field reference data (Thomson, 1998). Unsupervised methods are particularly accurate when spectral differences among classes are well defined (Rozenstein and Karnieli, 2011; Thomson, 1998). However, this is rarely the case in aquatic habitats since light attenuation by water reduces spectral separability (Green et al., 2000). The application of water column correction techniques can increase the accuracy of unsupervised and supervised classifications (Hoang et al., 2015; Mumby et al., 1998; Sagawa et al., 2012; Zoffoli et al., 2014). However, such techniques are generally too complex to be easily implemented by map users. Unsupervised methods often yield accurate classifications for lakes, wetlands, and seagrass meadows (Dogan et al., 2009; Gullström et al., 2006; Luo et al., 2016), but are generally outperformed by supervised methods in other marine habitats (Calvert et al., 2015; Gagnon et al., 2008; McCarthy and Halls, 2014). In the present study, the selected approach of unsupervised classification of either type of imagery showed poor discrimination between kelp and non-kelp benthic classes, indicating that this method is inadequate to detect submerged kelp beds in the Mingan Archipelago. This method should therefore be used with caution to study kelp bed distribution in systems with similar biological makeup and oceanic conditions.

Supervised classification methods typically produce readily interpretable thematic maps of only the cover classes of interest, and usually outperform unsupervised classification when the training dataset encompasses the spectral variation in each cover classes (Calvert et al., 2015; Green et al., 2000; Lillesand et al., 2014). Supervised techniques perform less well when the spectral signature of one or more classes is highly variable or classes show little spectral differences (Green et al., 2000; Lillesand et al., 2014; Lu and Weng, 2007). Thus, supervised methods may require more field sampling to ensure that reference data capture variability in the signature of each target class. For the Mingan Archipelago, where kelp and non-kelp benthic classes are spectrally quite distinct, supervised classification performed well, especially with the satellite imagery. Supervised classification of satellite imagery was only ~2% less accurate than visual classification of aerial imagery, the most accurate method (90%). These results are consistent with those of Casal et al. (2011) who mapped kelp beds along the Galician coast with accuracies of 80 to 90% with visual or supervised classifications of satellite imagery (SPOT 4).

Visual classification is somewhat subjective because it centers on the ability of an observer to visually separate benthic classes. Yet, this method has proved highly successful to identify benthic features in different types of subtidal systems worldwide (Andrew and O'Neill, 2000; Drake, 1996; Kendrick et al., 2000; Walker, 2009). As with contextual editing and object-oriented classification (Baatz et al., 2008; Green et al., 2000; Whiteside and Ahmad, 2005), visual classification has the advantage of accounting simultaneously for patch shape, size, and contrast. By relying on the detection of changes in color, in the present case sharp contrasts at kelp bed edges, this method is more robust to cross-image changes in light intensity caused, for example, by variation in water turbidity. In the present

study, visual identification of kelp bed edges was more difficult on satellite than aerial imagery because of poorer contrasts on the former and coarseness of the original satellite imagery (6-m pixels color imagery, pansharpened to 1.5-m pixels, and resampled to 1-m pixel). Moreover, kelp bed edges identified with visual classification appeared artificially jagged for both types of imagery, mainly as a result of the minimum mapping unit (MMU; Saura, 2002) of 225 m² in the classification grid used with this method. Kelp bed edges were much smoother on the maps created with the unsupervised and supervised classifications, which were based on 1-m-pixel images and thus had a much smaller MMU. The size of the grid in the visual classification was intentionally large, to strike an acceptable balance between the minimal spatial scale over which to assess kelp presence (or absence) and the amount of time required to classify the imagery. Yet, because the MMU determines the amount of details within a map, the user's goals and analysis of the information mapped should guide the choice of appropriate MMU and classification method (Saura, 2002). Both the spatial scale of kelp assessment and classification time can be adjusted based on needs and resources. Visual classification necessitated 30 to 45 h of work for each type of imagery (including observer training), while unsupervised and supervised classifications were generally completed within 6 to 10 h.

In the present study, supervised and unsupervised classifications yielded more accurate maps of kelp distribution with satellite than aerial imagery. Aerial imagery presented better contrasts and more contextual details than the satellite imagery, which generally yields higher accuracy in automated classification (Green et al., 2000). However, in the present case variation in contrast and color among the aerial photographs could not be completely corrected for during mosaicking, introducing noise picked up by the

unsupervised and supervised classifications. Conversely, satellite imagery showed less pronounced but more uniform contrasts across the study area, making it more suitable than aerial imagery for supervised and unsupervised classification.

Ground truth data is essential to define spectral classes for supervised classification, train the observer for visual classification, and assess image classification accuracy (Green et al., 2000; Lillesand et al., 2014). In the present study, four people completed boat-based ground truthing in about 100 h, including time to familiarize with the sampling gear. This approach enabled sampling a relatively large tract of seabed (~250 ha) much quicker than if scuba-based mapping techniques had been used (Frey and Gagnon, 2015; Gagnon et al., 2004; Lauzon-Guay, 2007; Rinde et al., 2014; Scheibling et al., 1999). Urchin fronts in eastern Canada, including in the Mingan Archipelago, can destroy kelp beds at a rate as high as 4 m month⁻¹ during summer (Gagnon et al., 2004; Lauzon-Guay, 2007; Scheibling et al., 1999). These fast changes in community states stress the necessity of synchronizing ground truthing and image acquisition not to introduce extraneous data variability, an aspect largely disregarded in previous studies (Anderson et al., 2007; Simms and Dubois, 2001). Ground truth data in the present study were collected in mid-July, whereas above sea-level imagery was acquired in early July (aerial) and early August (satellite), respectively. Given the small temporal window (~1 month) over which all data were acquired, kelp loss to urchin grazing likely contributed very little to the errors of classification reported.

The study area was limited to shallow (<7 m deep) seabed because light scattering and attenuation by the water column prevented visual separation of kelp and non-kelp benthic classes in deeper water (Green et al., 2000). For the same reason, Simms and

Dubois (2001) also limited their assessment of kelp biomass from satellite imagery of the Gulf of St. Lawrence to <7 m deep. Echo sounders or automated underwater vehicles (AUVs) equipped with cameras could help map macrophyte distribution on deeper seabed (Bewley et al., 2012; Calvert et al., 2015; Marzinelli et al., 2015; Minami et al., 2010). Spectral resolution of both satellite and aerial imagery was insufficient to separate kelp species within beds or kelp beds from monospecific stands of *Desmarestia viridis*. Thus, stands of *D. viridis* were likely classified as kelp, potentially overestimating kelp cover. However, *D. viridis* occurred in less than 10% of the 329 benthic photo quadrats acquired around the four islands and was observed without kelp only in 2% of the benthic photo quadrats. These results suggest that a negligible portion of the imagery classified as kelp was actually *D. viridis*. Non-kelp macroalgae, including *D. viridis* and turf algae, were rare within the study area, covering altogether only ~6% of the seabed. Furthermore, 26% of the photo quadrats contained strictly non-kelp macroalgae, and the latter covered only ~17% of the photo quadrats' area. Hence, these quadrats contained mainly bare rock, which the image classification methods used identified as non-kelp. The low abundance of non-kelp macroalgae and predominantly small (a few 10s of cm²) clusters they formed, suggest that their misclassification as kelp was negligible. More advanced sensors, such as multispectral or hyperspectral imagers with a higher spectral resolution, could increase the ability to identify and map benthic vegetation, yet would necessitate a more specialized workforce, software, and hardware (Gagnon et al., 2008; Lathrop et al., 2006; Uhl et al., 2016; Valle et al., 2015). The two benthic classes used were sufficient to map the relatively simple and largely dichotomous structure of the benthic system studied. A greater number

of classes may be needed to create accurate maps of kelp distribution in systems with more complex benthic structures (e.g., Casal et al., 2011), in which case images with a better spectral resolution than that in the present study (including a greater coverage of the blue to yellow wavelengths) could be required (Green et al., 2000; Mumby and Edwards, 2002).

In the present study, the acquisition of satellite and aerial imagery was planned and executed with the goal of acquiring imagery at times of optimal sea state and water clarity to maximize image quality and the accuracy of the classification maps produced from it (Green et al., 2000; Green et al., 2017). Therefore, all images were acquired at low tide on cloudless days (to maximize light penetration to, and reflection from, the seabed), prior to zenith (to minimize glare on the imagery), and following several days with low winds and no precipitation (to limit water turbulence and freshwater runoffs). Satellite and aerial images were each acquired on a single day, with less than a month separating both days. These precautions provided the best images possible for our study system, while enabling trustable comparisons between any set of maps. Our results suggest that the classification methods tested could be used to study temporal changes in the distribution and abundance of submerged kelp, provided that consistently high quality can be achieved across an image time series, which, as mentioned above, is best achieved under optimal sea conditions. For studies of change over time, collection of ground-truth data at the time of each image acquisition would be an asset to increase confidence in the information extracted from map products (Green et al., 2000; Lillesand et al., 2014). Preliminary tests with imagery acquired across a range of sea state and turbidity may be required to identify the minimal environmental requirements for accurate classification.

Scuba- and boat-based sampling methods are used extensively for benthic habitat mapping and monitoring (Filbee-Dexter et al., 2016; Himmelman, 1991; Lauzon-Guay et al., 2009; Matarrese et al., 2004; Polovina et al., 1995; Smale and Moore, 2017; Van Rein et al., 2009; Vásquez et al., 2007). These time-consuming and labor-intensive methods are useful to study small-scale (i.e., a few 100s of m² over <5 y) ecological patterns, but present two major limitations for larger-scale applications. First, the methods used for small-scale benthic monitoring often are inadequate to work at large extents because of practical limitations. Second, factors and processes that drive species distribution often differ across scales, and thus results from small-scale studies can rarely be extrapolated to larger scales with confidence (Edwards, 2004; Levin, 1992; Schneider, 2001; Turner et al., 2001). Yet, the development of reliable models of benthic community and ecosystem dynamics is largely based on repeated quantification of species distribution over increasingly large spatiotemporal scales (Lecours et al., 2015; Wiens, 1989). Multiscale monitoring is particularly important for systems that exhibit multiple stable states and for management purposes (Groffman et al., 2006; Moffett et al., 2015; Petraitis and Dudgeon, 2004). Because remote sensing and GIS enable mapping and comparing species distribution over multiple spatial and temporal scales, they are increasingly used to assess the stability and resilience of marine systems (Knudby et al., 2013; Knudby et al., 2014; Moffett et al., 2015; Scopélitis et al., 2009).

Kelp-barrens systems often exhibit characteristics of multiple stable state systems, including sudden shifts in, and sharp boundaries between, kelp- and urchin-dominated community states (Filbee-Dexter and Scheibling, 2014; Ling et al., 2015; Moffett et al., 2015). Accurate knowledge of the factors and processes that control the stability and

resilience of kelp-barrens systems is crucial to predict and mitigate large-scale shifts of these ecologically and economically important systems (Groffman et al., 2006; Moffett et al., 2015; Petraitis and Dudgeon, 2004). The present study identifies supervised classification of satellite imagery and visual classification of aerial imagery as the top two methods to map kelp distribution, and from there study kelp-barrens dynamics, in the Mingan Archipelago. More broadly, it demonstrates that conventional remote sensing and GIS methods can be used to accurately map and monitor submerged kelp beds over large, yet largely unexplored, spatial and temporal domains. This operational improvement should provide “non-specialist map users” (*sensu* Andréfouët, 2008) like most kelp ecologists, with the ability to address novel questions relating to alternative stable state theory, including the effects of landscape heterogeneity on the stability of community states and basins of attraction (St-Pierre et al., in prep).

3.6. ACKNOWLEDGEMENTS

We are grateful to R. Hovey, M. P. St-Pierre, B. Dumas, H. Hawk, I. Garrido, P. Bruning, C. Narvaez-Diaz, and L. E. Johnson for their help in preparing and conducting field work. We are grateful to Y. Wiersma, J. Fisher, and two anonymous reviewers for constructive comments that helped improve the manuscript. This research was funded by Natural Sciences and Engineering Research Council of Canada (NSERC Discovery Grant), Canada Foundation for Innovation (CFI-Leaders Opportunity Funds), and Research & Development Corporation of Newfoundland and Labrador (IgniteR&D) grants to P. Gagnon. A. P. St-Pierre was supported by an NSERC Post-Graduate Scholarship (PGS).

3.7. REFERENCES

- Ackleson, S.G., 2003. Light in shallow waters: A brief research review. *Limnol Oceanogr* 48, 323-328.
- Anderson, J.R., 1976. A land use and land cover classification system for use with remote sensor data. US Government Printing Office.
- Anderson, R., Rand, A., Rothman, M., Share, A., Bolton, J., 2007. Mapping and quantifying the South African kelp resource. *Afr J Mar Sci* 29, 369-378.
- Andréfouët, S., 2008. Coral reef habitat mapping using remote sensing: a user vs producer perspective. Implications for research, management and capacity building. *J Spat Sci* 53, 113-129.
- Andréfouët, S., Payri, C., Hochberg, E.J., Hu, C., Atkinson, M.J., Muller-Karger, F.E., 2004. Use of in situ and airborne reflectance for scaling-up spectral discrimination of coral reef macroalgae from species to communities. *Mar Ecol Prog Ser* 283, 161-177.
- Andrew, N., O'Neill, A., 2000. Large-scale patterns in habitat structure on subtidal rocky reefs in New South Wales. *Mar Freshwater Res* 51, 255-263.
- Baatz, M., Hoffmann, C., Willhauck, G., 2008. Progressing from object-based to object-oriented image analysis In: Blaschke T., Lang S., Hay G.J. (eds) *Object-Based Image Analysis. Lecture Notes in Geoinformation and Cartography*. Springer, Berlin, Heidelberg.
- Bell, T.W., Cavanaugh, K.C., Reed, D.C., Siegel, D.A., 2015a. Geographical variability in the controls of giant kelp biomass dynamics. *J. Biogeogr.* 42, 2010-2021.
- Bell, T.W., Cavanaugh, K.C., Siegel, D.A., 2015b. Remote monitoring of giant kelp biomass and physiological condition: An evaluation of the potential for the Hyperspectral Infrared Imager (HyspIRI) mission. *Remote Sens Environ* 167, 218-228.
- Bewley, M., Douillard, B., Nourani-Vatani, N., Friedman, A., Pizarro, O., Williams, S., 2012. Automated species detection: An experimental approach to kelp detection from sea-floor AUV images, *Proc Australas Conf Rob Autom*.
- Bioucas-Dias, J.M., Plaza, A., Camps-Valls, G., Scheunders, P., Nasrabadi, N., Chanussot, J., 2013. Hyperspectral remote sensing data analysis and future challenges. *IEEE Geosc Rem Sen M* 1, 6-36.
- Blain, C., Gagnon, P., 2014. Canopy-forming seaweeds in urchin-dominated systems in eastern Canada: structuring forces or simple prey for keystone grazers? *Plos One* 9.

- Brooks, C., Grimm, A., Shuchman, R., Sayers, M., Jessee, N., 2015. A satellite-based multi-temporal assessment of the extent of nuisance *Cladophora* and related submerged aquatic vegetation for the Laurentian Great Lakes. *Remote Sens Environ* 157, 58-71.
- Brown, C.J., Smith, S.J., Lawton, P., Anderson, J.T., 2011. Benthic habitat mapping: a review of progress towards improved understanding of the spatial ecology of the seafloor using acoustic techniques. *Estuar Coast Shelf Sci* 92, 502-520.
- Calvert, J., Strong, J.A., McGonigle, C., Quinn, R., 2015. An evaluation of supervised and unsupervised classification techniques for marine benthic habitat mapping using multibeam echosounder data. *ICES J Mar Sci; J du Conseil* 72, 1498-1513.
- Casal, G., Sánchez-Carnero, N., Sánchez-Rodríguez, E., Freire, J., 2011. Remote sensing with SPOT-4 for mapping kelp forests in turbid waters on the south European Atlantic shelf. *Estuar Coast Shelf Sci* 91, 371-378.
- Cavanaugh, K.C., Siegel, D.A., Kinlan, B.P., Reed, D.C., 2010. Scaling giant kelp field measurements to regional scales using satellite observations. *Mar Ecol Prog Ser* 403, 13-27.
- Cavanaugh, K.C., Siegel, D.A., Reed, D.C., Dennison, P.E., 2011. Environmental controls of giant-kelp biomass in the Santa Barbara Channel, California. *Mar Ecol Prog Ser* 429, 1-17.
- Congalton, R.G., Green, K., 2008. Assessing the accuracy of remotely sensed data: principles and practices. CRC press.
- Dayton, P.K., 1985. Ecology of kelp communities. *Annu Rev Ecol Syst* 16, 215-245.
- Deysler, L.E., 1993. Evaluation of remote sensing techniques for monitoring giant kelp populations. *Hydrobiologia* 260, 307-312.
- Dogan, O.K., Akyurek, Z., Beklioglu, M., 2009. Identification and mapping of submerged plants in a shallow lake using quickbird satellite data. *J Environ Manage* 90, 2138-2143.
- Drake, S., 1996. Visual interpretation of vegetation classes from airborne videography: an evaluation of observer proficiency with minimal training. *Photogramm Eng Remote Sensing* 62, 969.
- Edwards, M.S., 2004. Estimating scale-dependency in disturbance impacts: El Niños and giant kelp forests in the northeast Pacific. *Oecologia* 138, 436-447.
- Esri, 2015. ArcGIS Desktop; Release 10.3.1, Redland, CA.

- Estes, J., Danner, E., Doak, D., Konar, B., Springer, A., Steinberg, P., Tinker, M., Williams, T., 2004. Complex trophic interactions in kelp forest ecosystems. *Bull Mar Sci* 74, 621-638.
- Filbee-Dexter, K., Feehan, C.J., Scheibling, R.E., 2016. Large-scale degradation of a kelp ecosystem in an ocean warming hotspot. *Mar Ecol Prog Ser* 543, 141-152.
- Filbee-Dexter, K., Scheibling, R.E., 2012. Hurricane-mediated defoliation of kelp beds and pulsed delivery of kelp detritus to offshore sedimentary habitats. *Mar Ecol Prog Ser* 455, 51-64.
- Filbee-Dexter, K., Scheibling, R.E., 2014. Sea urchin barrens as alternative stable states of collapsed kelp ecosystems. *Mar Ecol Prog Ser* 495, 1-25.
- Finkl, C.W., Makowski, C., 2014. Remote sensing and modeling: Advances in coastal and marine resources. Springer.
- Frey, D.L., Gagnon, P., 2015. Thermal and hydrodynamic environments mediate individual and aggregative feeding of a functionally important omnivore in reef communities. *Plos One* 10, e0118583.
- Friedlander, A.M., Ballesteros, E., Bell, T.W., Giddens, J., Henning, B., Hüne, M., Muñoz, A., Salinas-de-León, P., Sala, E., 2018. Marine biodiversity at the end of the world: Cape Horn and Diego Ramírez islands. *Plos One* 13, e0189930.
- Friedlander, A.M., Brown, E.K., Monaco, M.E., 2007. Coupling ecology and GIS to evaluate efficacy of marine protected areas in Hawaii. *Ecol Appl* 17, 715-730.
- Frohn, R.C., Lopez, R.D., 2017. Remote sensing for landscape ecology: New metric indicators: monitoring, modeling, and assessment of ecosystems. CRC Press.
- Gagnon, P., Himmelman, J.H., Johnson, L.E., 2003. Algal colonization in urchin barrens: defense by association during recruitment of the brown alga *Agarum cribrosum*. *J Exp Mar Biol Ecol* 290, 179-196.
- Gagnon, P., Himmelman, J.H., Johnson, L.E., 2004. Temporal variation in community interfaces: kelp-bed boundary dynamics adjacent to persistent urchin barrens. *Mar Biol* 144, 1191-1203.
- Gagnon, P., Johnson, L.E., Himmelman, J.H., 2005. Kelp patch dynamics in the face of intense herbivory: Stability of *Agarum clathratum* (Phaeophyta) stands and associated flora on urchin barrens. *J Phycol* 41, 498-505.
- Gagnon, P., Scheibling, R.E., Jones, W., Tully, D., 2008. The role of digital bathymetry in mapping shallow marine vegetation from hyperspectral image data. *Int J Remote Sens* 29, 879-904.

- Garza-Pérez, J., Lehmann, A., Arias-González, J., 2004. Spatial prediction of coral reef habitats: integrating ecology with spatial modeling and remote sensing. *Mar Ecol Prog Ser* 269, 141-152.
- Green, E., Mumby, P., Edwards, A., Clark, C., 1996. A review of remote sensing for the assessment and management of tropical coastal resources. *Coast Manage* 24, 1-40.
- Green, E., Mumby, P., Edwards, A., Clark, C., 2000. Remote sensing: Handbook for tropical coastal management. United Nations Educational, Scientific and Cultural Organization (UNESCO).
- Green, K., Congalton, R.G., Tukman, M., 2017. Imagery and GIS: Best Practices for Extracting Information from Imagery. Esri Press Redlands, CA.
- Groffman, P.M., Baron, J.S., Blett, T., Gold, A.J., Goodman, I., Gunderson, L.H., Levinson, B.M., Palmer, M.A., Paerl, H.W., Peterson, G.D., 2006. Ecological thresholds: the key to successful environmental management or an important concept with no practical application? *Ecosystems* 9, 1-13.
- Grove, R.S., Zabloudil, K., Norall, T., Deysher, L., 2002. Effects of El Nino events on natural kelp beds and artificial reefs in southern California. *ICES J Mar Sci; J du Conseil* 59, S330-S337.
- Gullström, M., Lundén, B., Bodin, M., Kangwe, J., Öhman, M.C., Mtolera, M.S., Björk, M., 2006. Assessment of changes in the seagrass-dominated submerged vegetation of tropical Chwaka Bay (Zanzibar) using satellite remote sensing. *Estuar Coast Shelf Sci* 67, 399-408.
- Hayes, D.J., Sader, S.A., 2001. Comparison of change-detection techniques for monitoring tropical forest clearing and vegetation regrowth in a time series. *Photogramm Eng Remote Sensing* 67, 1067-1075.
- Hedley, J.D., Roelfsema, C.M., Phinn, S.R., Mumby, P.J., 2012. Environmental and sensor limitations in optical remote sensing of coral reefs: Implications for monitoring and sensor design. *Remote Sens* 4, 271-302.
- Himmelman, J.H., 1991. Diving observations of subtidal communities in the northern Gulf of St. Lawrence. *Can Special Pub Fish Aquat Sci* 113, 319-332.
- Himmelman, J.H., Dutil, C., 1991. Distribution, population-structure and feeding of subtidal seastars in the Northern Gulf of St-Lawrence. *Mar Ecol-Prog Ser* 76, 61-72.
- Hoang, T.C., O'Leary, M.J., Fotedar, R.K., 2015. Remote-Sensed Mapping of Sargassum spp. Distribution around Rottnest Island, Western Australia, Using High-Spatial Resolution WorldView-2 Satellite Data. *J Coast Res* 32, 1310-1321.

- Hochberg, E.J., Atkinson, M.J., 2003. Capabilities of remote sensors to classify coral, algae, and sand as pure and mixed spectra. *Remote Sens Environ* 85, 174-189.
- Hu, C., Feng, L., Hardy, R.F., Hochberg, E.J., 2015. Spectral and spatial requirements of remote measurements of pelagic *Sargassum* macroalgae. *Remote Sens Environ* 167, 229-246.
- Jerlov, N.G., 1976. *Marine optics*. Elsevier.
- Kendrick, G., Hegge, B., Wyllie, A., Davidson, A., Lord, D., 2000. Changes in seagrass cover on Success and Parmelia Banks, Western Australia between 1965 and 1995. *Estuar Coast Shelf Sci* 50, 341-353.
- Knudby, A., Jupiter, S., Roelfsema, C., Lyons, M., Phinn, S., 2013. Mapping coral reef resilience indicators using field and remotely sensed data. *Remote Sens* 5, 1311-1334.
- Knudby, A., Pittman, S.J., Maina, J., Rowlands, G., 2014. Remote sensing and modeling of coral reef resilience. In: Finkl C., Makowski C. (eds) *Remote Sensing and Modeling*. Coastal Research Library, vol 9. Springer.
- Krumhansl, K.A., Okamoto, D.K., Rassweiler, A., Novak, M., Bolton, J.J., Cavanaugh, K.C., Connell, S.D., Johnson, C.R., Konar, B., Ling, S.D., Micheli, F., Norderhaug, K.M., Pérez-Matus, A., Sousa-Pinto, I., Reed, D.C., Salomon, A.K., Shears, N.T., Wernberg, T., Anderson, R.J., Barrett, N.S., Buschmann, A.H., Carr, M.H., Caselle, J.E., Derrien-Courtet, S., Edgar, G.J., Edwards, M., Estes, J.A., Goodwin, C., Kenner, M.C., Kushner, D.J., Moy, F.E., Nunn, J., Steneck, R.S., Vásquez, J., Watson, J., Witman, J.D., Byrnes, J.E.K., 2016. Global patterns of kelp forest change over the past half-century. *Proc Natl Acad Sci USA* 113, 13785-13790.
- Landis, J.R., Koch, G.G., 1977. The measurement of observer agreement for categorical data. *biometrics*, 159-174.
- Lathrop, R.G., Montesano, P., Haag, S., 2006. A multi-scale segmentation approach to mapping seagrass habitats using airborne digital camera imagery. *Photogramm Eng Remote Sensing* 72, 665-675.
- Lathrop, R.G., Styles, R.M., Seitzinger, S.P., Bognar, J.A., 2001. Use of GIS mapping and modeling approaches to examine the spatial distribution of seagrasses in Barnegat Bay, New Jersey. *Estuaries and Coasts* 24, 904-916.
- Lauzon-Guay, J.-S., 2007. Spatial dynamics of feeding fronts of sea urchins (*Strongylocentrotus droebachiensis*), Dissertation/Thesis, ProQuest, UMI Dissertations Publishing.

- Lauzon-Guay, J.S., Scheibling, R.E., 2007. Seasonal variation in movement, aggregation and destructive grazing of the green sea urchin (*Strongylocentrotus droebachiensis*) in relation to wave action and sea temperature. *Mar Biol* 151, 2109-2118.
- Lauzon-Guay, J.S., Scheibling, R.E., Barbeau, M.A., 2009. Modelling phase shifts in a rocky subtidal ecosystem. *Mar Ecol Prog Ser* 375, 25-39.
- Lecours, V., Devillers, R., Schneider, D.C., Lucieer, V.L., Brown, C.J., Edinger, E.N., 2015. Spatial scale and geographic context in benthic habitat mapping: review and future directions. *Mar Ecol Prog Ser* 535, 259-284.
- Levin, S.A., 1992. The problem of pattern and scale in ecology: the Robert H. MacArthur award lecture. *Ecology* 73, 1943-1967.
- Lillesand, T., Kiefer, R.W., Chipman, J., 2014. Remote sensing and image interpretation. John Wiley & Sons.
- Ling, S., 2008. Range expansion of a habitat-modifying species leads to loss of taxonomic diversity: a new and impoverished reef state. *Oecologia* 156, 883-894.
- Ling, S., Scheibling, R., Rassweiler, A., Johnson, C., Shears, N., Connell, S., Salomon, A., Norderhaug, K., Pérez-Matus, A., Hernández, J., 2015. Global regime shift dynamics of catastrophic sea urchin overgrazing. *Phil Trans R Soc B* 370, 20130269.
- Lu, D., Weng, Q., 2007. A survey of image classification methods and techniques for improving classification performance. *Int J Remote Sens* 28, 823-870.
- Luo, X., Wang, Y., Luczhovich, J., 2016. Mapping submerged aquatic vegetation in albemarle sound, North Carolina, USA using Landsat-8 and SONAR data, Geoscience and Remote Sensing Symposium (IGARSS), 2016 IEEE International. IEEE, pp. 3802-3805.
- Lyons, M., Phinn, S., Roelfsema, C., 2011. Integrating Quickbird multi-spectral satellite and field data: mapping bathymetry, seagrass cover, seagrass species and change in Moreton Bay, Australia in 2004 and 2007. *Remote Sens* 3, 42-64.
- Malthus, T.J., Karpouzli, E., 2003. Integrating field and high spatial resolution satellite-based methods for monitoring shallow submersed aquatic habitats in the Sound of Eriskay, Scotland, UK. *Int J Remote Sens* 24, 2585-2593.
- Maritorena, S., Morel, A., Gentili, B., 1994. Diffuse reflectance of oceanic shallow waters: Influence of water depth and bottom albedo. *Limnol Oceanogr* 39, 1689-1703.
- Marzinelli, E.M., Williams, S.B., Babcock, R.C., Barrett, N.S., Johnson, C.R., Jordan, A., Kendrick, G.A., Pizarro, O.R., Smale, D.A., Steinberg, P.D., 2015. Large-scale

- geographic variation in distribution and abundance of Australian deep-water kelp forests. *Plos One* 10, e0118390.
- Matarrese, A., Mastrototaro, F., D'onghia, G., Maiorano, P., Tursi, A., 2004. Mapping of the benthic communities in the Taranto seas using side-scan sonar and an underwater video camera. *Chem Ecol* 20, 377-386.
- McCarthy, M.J., Colna, K.E., El-Mezayen, M.M., Laureano-Rosario, A.E., Méndez-Lázaro, P., Otis, D.B., Toro-Farmer, G., Vega-Rodriguez, M., Muller-Karger, F.E., 2017. Satellite Remote Sensing for Coastal Management: A Review of Successful Applications. *Environ Manage* 60, 323-339.
- McCarthy, M.J., Halls, J.N., 2014. Habitat mapping and change assessment of coastal environments: an examination of WorldView-2, QuickBird, and IKONOS satellite imagery and airborne LiDAR for mapping barrier island habitats. *ISPRS Int J Geo-Inf* 3, 297-325.
- Minami, K., Yasuma, H., Tojo, N., Fukui, S.-i., Ito, Y., Nobetsu, T., Miyashita, K., 2010. Estimation of kelp forest, *Laminaria* spp., distributions in coastal waters of the Shiretoko Peninsula, Hokkaido, Japan, using echosounder and geostatistical analysis. *Fisheries Sci* 76, 729-736.
- Mobley, C.D., 1994. Light and water: radiative transfer in natural waters. Academic press.
- Moffett, K.B., Nardin, W., Silvestri, S., Wang, C., Temmerman, S., 2015. Multiple stable states and catastrophic shifts in coastal wetlands: Progress, challenges, and opportunities in validating theory using remote sensing and other methods. *Remote Sens* 7, 10184-10226.
- Moy, F.E., Christie, H., 2012. Large-scale shift from sugar kelp (*Saccharina latissima*) to ephemeral algae along the south and west coast of Norway. *Mar Biol Res* 8, 309-321.
- Mumby, P., Clark, C., Green, E., Edwards, A., 1998. Benefits of water column correction and contextual editing for mapping coral reefs. *Int J Remote Sens* 19, 203-210.
- Mumby, P.J., Edwards, A.J., 2002. Mapping marine environments with IKONOS imagery: enhanced spatial resolution can deliver greater thematic accuracy. *Remote Sens Environ* 82, 248-257.
- Narvaez Diaz, C., 2018. Green urchin demography in a subarctic ecosystem: patterns and processes, PhD thesis, Université Laval.
- Nijland, W., Reshitnyk, L., Rubidge, E., 2019. Satellite remote sensing of canopy-forming kelp on a complex coastline: A novel procedure using the Landsat image archive. *Remote Sens Environ* 220, 41-50.

- Pasqualini, V., Pergent-Martini, C., Pergent, G., Agreil, M., Skoufas, G., Sourbes, L., Tsirika, A., 2005. Use of SPOT 5 for mapping seagrasses: An application to *Posidonia oceanica*. *Remote Sens Environ* 94, 39-45.
- Petraitis, P.S., Dudgeon, S.R., 2004. Detection of alternative stable states in marine communities. *J Exp Mar Biol Ecol* 300, 343-371.
- Polovina, J.J., Haight, W.R., Moffitt, R.B., Parrish, F.A., 1995. The role of benthic habitat, oceanography, and fishing on the population dynamics of the spiny lobster, *Panulirus marginatus* (Decapoda, Palinuridae), in the Hawaiian Archipelago. *Crustaceana*, 203-212.
- Rinde, E., Christie, H., Fagerli, C.W., Bekkby, T., Gundersen, H., Norderhaug, K.M., Hjermann, D.Ø., 2014. The influence of physical factors on kelp and sea urchin distribution in previously and still grazed areas in the NE Atlantic. *Plos One* 9, e100222.
- Rozenstein, O., Karnieli, A., 2011. Comparison of methods for land-use classification incorporating remote sensing and GIS inputs. *Appl Geogr* 31, 533-544.
- Sagawa, T., Mikami, A., Aoki, M.N., Komatsu, T., 2012. Mapping seaweed forests with IKONOS image based on bottom surface reflectance, *Remote Sensing of the Marine Environment II*. International Society for Optics and Photonics, p. 85250Q.
- Saura, S., 2002. Effects of minimum mapping unit on land cover data spatial configuration and composition. *Int J Remote Sens* 23, 4853-4880.
- Scheibling, R.E., Hennigar, A.W., Balch, T., 1999. Destructive grazing, epiphytism, and disease: the dynamics of sea urchin-kelp interactions in Nova Scotia. *Can J Fish Aquat Sci* 56, 2300-2314.
- Schneider, D.C., 2001. The rise of the concept of scale in ecology: The concept of scale is evolving from verbal expression to quantitative expression. *AIBS Bulletin* 51, 545-553.
- Scopélitis, J., Andréfouët, S., Phinn, S., Chabanet, P., Naim, O., Tourrand, C., Done, T., 2009. Changes of coral communities over 35 years: integrating in situ and remote-sensing data on Saint-Leu Reef (la Réunion, Indian Ocean). *Estuar Coast Shelf Sci* 84, 342-352.
- Silva, T.S., Costa, M.P., Melack, J.M., Novo, E.M., 2008. Remote sensing of aquatic vegetation: theory and applications. *Environ Monit Assess* 140, 131-145.
- Simms, E., Dubois, J.-M., 2001. Satellite remote sensing of submerged kelp beds on the Atlantic coast of Canada. *Int J Remote Sens* 22, 2083-2094.

- Smale, D.A., Moore, P.J., 2017. Variability in kelp forest structure along a latitudinal gradient in ocean temperature. *J Exp Mar Biol Ecol* 486, 255-264.
- Song, C., Woodcock, C.E., Seto, K.C., Lenney, M.P., Macomber, S.A., 2001. Classification and Change Detection Using Landsat TM Data: When and How to Correct Atmospheric Effects? *Remote Sens Environ* 75, 230-244.
- Stekoll, M., Deysher, L., Hess, M., 2007. A remote sensing approach to estimating harvestable kelp biomass, Eighteenth International Seaweed Symposium. Springer, pp. 97-108.
- Steneck, R.S., Graham, M.H., Bourque, B.J., Corbett, D., Erlandson, J.M., Estes, J.A., Tegner, M.J., 2002. Kelp forest ecosystems: biodiversity, stability, resilience and future. *Environ Conserv* 29, 436-459.
- Tegner, M., Dayton, P., 2000. Ecosystem effects of fishing in kelp forest communities. *ICES J Mar Sci; J du Conseil* 57, 579-589.
- Thomson, A., 1998. Supervised versus unsupervised methods for classification of coasts and river corridors from airborne remote sensing. *Int J Remote Sens* 19, 3423-3431.
- Turner, M.G., Gardner, R.H., O'Neill, R.V., 2001. Landscape ecology in theory and practice: patterns and process. EUA: Springer.
- Turner, M.G., O'Neill, R.V., Gardner, R.H., Milne, B.T., 1989. Effects of changing spatial scale on the analysis of landscape pattern. *Landsc Ecol* 3, 153-162.
- Uhl, F., Bartsch, I., Oppelt, N., 2016. Submerged kelp detection with hyperspectral data. *Remote Sens* 8, 487.
- Vahtmäe, E., Kutser, T., Kotta, J., Pärnoja, M., Möller, T., Lennuk, L., 2012. Mapping Baltic Sea shallow water environments with airborne remote sensing. *Oceanology* 52, 803.
- Valle, M., Pala, V., Lafon, V., Dehouck, A., Garmendia, J.M., Borja, Á., Chust, G., 2015. Mapping estuarine habitats using airborne hyperspectral imagery, with special focus on seagrass meadows. *Estuar Coast Shelf Sci* 164, 433-442.
- Valta-Hulkkonen, K., Pellikka, P., Tanskanen, H., Ustinov, A., Sandman, O., 2003. Digital false colour aerial photographs for discrimination of aquatic macrophyte species. *Aquat Bot* 75, 71-88.
- Van Rein, H., Brown, C., Quinn, R., Breen, J., 2009. A review of sublittoral monitoring methods in temperate waters: a focus on scale. *Underwat Technol* 28, 99-113.
- Vásquez, J.A., Vega, J.M.A., Buschmann, A.H., 2007. Long term variability in the structure of kelp communities in northern Chile and the 1997–98 ENSO, in:

- Anderson, R., Brodie, J., Onsøyen, E., Critchley, A.T. (Eds.), Eighteenth International Seaweed Symposium: Proceedings of the Eighteenth International Seaweed Symposium, held in Bergen, Norway, 20 – 25 June 2004. Springer Netherlands, Dordrecht, pp. 279-293.
- Walker, B.K., 2009. Benthic habitat mapping of Miami-Dade County: Visual interpretation of LADS bathymetry and aerial photography. Florida DEP report #RM069. Miami Beach, FL. Pp. 47.
- Wernberg, T., Bennett, S., Babcock, R.C., de Bettignies, T., Cure, K., Depczynski, M., Dufois, F., Fromont, J., Fulton, C.J., Hovey, R.K., 2016. Climate-driven regime shift of a temperate marine ecosystem. *Science* 353, 169-172.
- Whiteside, T., Ahmad, W., 2005. A comparison of object-oriented and pixel-based classification methods for mapping land cover in northern Australia, Proceedings of SSC2005 Spatial intelligence, innovation and praxis: The national biennial Conference of the Spatial Sciences Institute, pp. 1225-1231.
- Wiens, J.A., 1989. Spatial scaling in ecology. *Functional ecology* 3, 385-397.
- Yang, D., Yang, C., 2009. Detection of seagrass distribution changes from 1991 to 2006 in Xincun Bay, Hainan, with satellite remote sensing. *Sensors* 9, 830-844.
- Zoffoli, M., Frouin, R., Kampel, M., 2014. Water column correction for coral reef studies by remote sensing. *Sensors* 14, 16881-16931.

CHAPTER IV

Kelp-bed dynamics across scales: Assessing distribution patterns with spatial pattern metrics and modelling

4.1. ABSTRACT

Spatial pattern metrics are used to investigate the links between a species' distribution patterns and underlying ecological drivers at multiple spatiotemporal scales. These metrics, in combination with remotely acquired imagery offer a novel approach for the study of kelp-urchin systems and enable the study of drivers of kelp distribution at broad (>km²) spatial scales difficult to achieve through traditional scuba-based methods. This study uses aerial imagery of 2.85 km² of shallow (<7 m) seabed around five islands in the Mingan Archipelago (northern Gulf of St. Lawrence, Canada) to (1) quantify kelp distribution patterns with spatial pattern metrics and (2) examine correlations between kelp presence and physical and biotic parameters. The imagery was classified visually and divided into two benthic classes based on cover type: kelp and non-kelp. Kelp covered 62% of the study area, with substantial variation (46% to 87%) among islands. Kelp and non-kelp patches varied in size from 225 to 891,225 m², while exhibiting considerable variation in geometric complexity. Over 80% of the kelp patches were relatively small (< 1350 m²), although the fewer, larger patches contained most (98%) of the kelp-covered seabed and were located in shallower water, near the coastline. Both the kelp and non-kelp benthic classes were highly aggregated as suggested by clumpiness indices of 0.67 and 0.59, respectively. Variability in spatial pattern metrics and kelp coverage among spatial scales indicate that kelp distribution is not uniform among islands in the Mingan Archipelago and suggest that the spatial extent over which observations are obtained strongly influences the patterns detected. Increasing depth, urchin density, and relative exposure to waves independently led to a decrease in kelp presence, with depth having the strongest correlation, followed by urchin density and relative exposure. By increasing knowledge of

the physical and biological factors regulating the distribution and configuration of kelp beds at spatial scales largely unexplored to date, this study is a step towards a comprehensive understanding of scale-dependent processes regulating submerged kelp bed dynamics.

4.2. INTRODUCTION

Landscape ecology aims to identify the relationships between patterns in species distribution and ecological processes over a range of spatial and temporal scales (Fu et al., 2011; Turner et al., 2001; Turner et al., 1989). To that effect, many spatially explicit approaches have been developed to quantify spatial patterns in terrestrial landscape components (e.g., forest patches; Haines-Young and Chopping, 1996; Uuemaa et al., 2013). In particular, approaches combining remote sensing, distribution maps, and spatial pattern metrics (also known as landscape metrics; Gustafson, 1998; Mcgarigal and Marks, 1995; Wedding et al., 2011) were developed to assess the composition and spatial configuration of landscapes and can be easily applied over extensive areas (up to thousands of km²). Spatial pattern metrics provide a quantitative assessment of the abundance, diversity, shape, connectivity, and clustering of landscape components, which is fundamental for the understanding of the spatial structure and dynamics of landscapes (Cushman et al., 2008; Frohn and Lopez, 2017; McGarigal et al., 2012). These metrics have been routinely used to monitor forests (Maier et al., 2008; Matte et al., 2015), mangroves (Manson et al., 2003; Romero-Berny et al., 2015) and wetland habitats (Kelly et al., 2011; Li et al., 2005), to identify the causes and consequences of changes in spatial distribution patterns on community structure and biodiversity.

Seascape ecology, the marine counterpart of landscape ecology, generally applies approaches developed in terrestrial systems to marine communities (Boström et al., 2011; Irlandi et al., 1999; Pittman, 2017; Wedding et al., 2011). One advantage of these approaches is their applicability over spatial scales much greater than what is generally feasible through traditional techniques; indeed, traditional *in situ* monitoring methods applied to benthic systems are often spatially and temporally limited because of the technical and logistical challenges of working in submerged systems (e.g., scuba-based methods, as in Gagnon et al., 2004; Lauzon-Guay and Scheibling, 2007; Van Rein et al., 2009). Because ecological processes are scale dependent (Lecours et al., 2015; Levin, 1992; Schneider, 2001), studies conducted at various spatiotemporal scales are crucial to gain a better understanding of scale-dependency in species distribution patterns and their drivers. For systems exhibiting alternate stable states in particular, the conceptual and analytical framework of seascape ecology is key to investigate complex questions relative to seascape structure and function, and to identify scale-dependent drivers of stability and change that can lead to shifts in community states (Boström et al., 2011; Moffett et al., 2015).

Approaches from seascape ecology, in particular the use of spatial pattern metrics, are a promising tool for the study of submerged kelp-urchin systems. These systems found on shallow rocky reefs are composed of two distinct benthic communities: 1) kelp beds, where large brown seaweed (Laminariales) create extensive 3-D structures enhancing habitat complexity, productivity, and biodiversity (Dayton, 1985a; Steneck et al., 2002; Tegner and Dayton, 2000), and 2) urchin barrens, where sea urchins are numerous, erect macroalgae are sparse, and habitat complexity is low (reviewed in Filbee-Dexter and Scheibling, 2014). Kelp-urchin systems are considered as candidates for alternate stable

states because cyclical large-scale shifts between kelp-dominated and urchin-dominated states have been documented in many regions, affecting areas of up to several km² and strongly reducing the productivity and structural complexity of these benthic systems (Filbee-Dexter and Scheibling, 2014; Simenstad et al., 1978; Steneck et al., 2013). Urchin barrens are often considered as a collapsed state of the kelp-urchin system (Filbee-Dexter and Scheibling, 2014). Despite the ecological importance of kelp beds, studies of the drivers of submerged kelp distribution to date have remained limited to relatively small spatial extents (m² to 10s of m²) because of the labor-intensive and time-consuming scuba-based techniques generally used.

In eastern Canada, studies employing such techniques identified grazing by green sea urchin, *Strongylocentrotus droebachiensis*, as main driver of submerged kelp distribution at the scale of m to 10s of m due to its intensive and destructive grazing of kelp beds (Frey and Gagnon, 2015; Gagnon et al., 2004; Scheibling et al., 1999). Metre-scale observations suggest winter ice scouring also affects kelp distribution in this region (Gagnon et al., 2004; Keats et al., 1985). In Norway, kelp distribution has been shown to vary with depth, light conditions, and exposure to waves (Bekkby et al., 2009; Lüning, 1990; Rinde and Sjøtun, 2005). Although studies conducted in this region encompassed broad spatial extents (hundreds of km² in some studies of latitudinal trends), they still generally rely on point-based data collection (quadrat collections, presence/absence, or density measurements) limited to a few 10s of m at discrete sites (Moy and Christie, 2012; Rinde et al., 2014; Rinde and Sjøtun, 2005). Research focusing on broader, continuous spatial extents (km²) is needed to identify whether kelp distribution and spatial patterning are driven by abiotic factors (i.e., depth, slope, exposure to waves), herbivore pressure (urchins grazing), or a

combination of both when examined over broad spatial scales. Such investigations should benefit the study of boundary dynamics and alternate stable states in kelp-urchin systems by improving the understanding of scale-dependent processes affecting kelp distribution patterns; they will require the simultaneous use of a large enough spatial coverage and sufficiently precise spatial resolution, which can be addressed with remote sensing and seascape ecology approaches.

Recently, St-Pierre and Gagnon (2020) showed that simple image classification techniques applied to remotely sensed imagery can accurately detect shallow (<7 m) submerged kelp beds in the Mingan Archipelago (northern Gulf of St. Lawrence, Canada). These authors identified the visual classification of aerial imagery and the supervised classification of satellite imagery as the top two methods for kelp detection, yielding overall accuracies >89% (St-Pierre and Gagnon, 2020) which are highly satisfactory for ecological analyses and management purposes (Congalton and Green, 2008; Hayes and Sader, 2001). The Mingan Archipelago possess a generally clear water column and largely dichotomous division of the seabed (between kelp-covered and kelp-devoid areas) which facilitate kelp bed detection on remotely sensed imagery. Hence, this archipelago constitutes an ideal study system for the investigation of spatial patterning in kelp bed distribution at broad spatial scales (i.e., km²) largely unexplored to date.

The present study uses remotely sensed imagery of shallow subtidal (< 7 m) zones of the Mingan Archipelago to (1) quantify spatial patterns in the distribution of kelp-covered and kelp-devoid benthic communities using spatial pattern metrics, and (2) examine correlations between kelp presence over a broad spatial scale and physical and biotic factors using modelling techniques. First, the spatial characteristics of kelp beds are obtained by

computing spatial pattern metrics quantifying the proportional abundance, shape, area, and clustering of kelp beds. These metrics are compared among islands within the archipelago. Secondly, the relative influence of depth, bottom slope, exposure to waves, and urchin density on kelp distribution is assessed by comparing 11 models built from combinations (additive or multiplicative) of these four factors based on ecological hypotheses. For example, based on studies from other regions, it is hypothesized that increasing depth reduces the probability of kelp presence due to decreasing light availability and water movement, which can be detrimental to kelp growth and allow for intensive urchin grazing (Bekkby et al., 2009; Hepburn et al., 2007; Lauzon-Guay and Scheibling, 2007). It is also hypothesized that increased urchin density decreases the probability of kelp presence due to grazing pressure (Frey and Gagnon, 2015; Lauzon-Guay et al., 2008; Wright et al., 2005). More complex models address hypotheses related to the combined effects of the factors studied, such that increasing water movement from the interactive effect of depth, slope, and exposure to waves increase the probability of kelp presence by limiting urchin movement and feeding (Frey and Gagnon, 2015, 2016; Kawamata, 1998; Laur et al., 1986).

4.3. MATERIAL AND METHODS

4.3.1. Study area

The study area encompasses the subtidal fringe along the coast of five islands in the Mingan Archipelago (Québec, Canada): Île Niapiskau (westernmost), Île à Firmin, Île du Havre, Île aux Goélands, and Petite île au Marteau (easternmost; Figure 4.1). The biological community in the study area is largely dichotomous, being dominated at shallow (0-7 m)

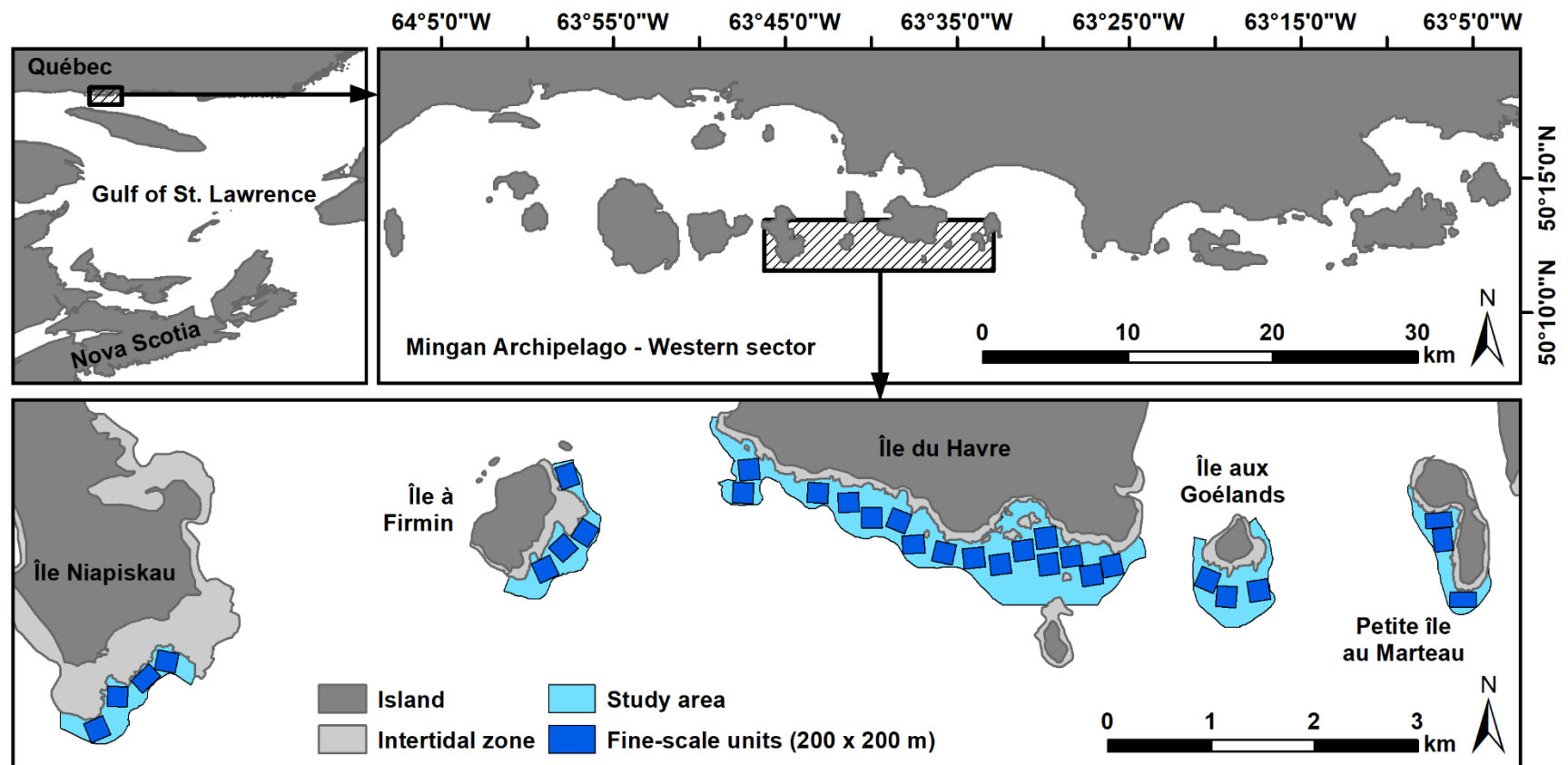


Figure 4.1. Location of the study area (pale blue) and of fine-scale study units (dark blue) at Île Niapiskau, Île à Firmin, Île du Havre, Île aux Goélands, and Petite île au Marteau, in the western sector of the Mingan Archipelago, northern Gulf of St. Lawrence, eastern Canada.

depths by mixed kelp beds (mainly *Alaria esculenta*, but also *Laminaria digitata*, *Saccharina longicuris*, and *Saccorhiza dermatodea*), and followed in deeper water by green sea urchin (*Strongylocentrotus droebachiensis*) barrens (Figure 4.2; Gagnon et al., 2004). By forming grazing fronts at the lower edge of kelp beds, sea urchins create a clearly defined boundary between kelp-covered and kelp-devoid seabed which is distinguishable from remotely sensed imagery (St-Pierre and Gagnon, 2020). This clear division between benthic communities is ideal for the application of spatial pattern metrics, which requires the presence of discrete patches of different cover types (in this case, patches of kelp and non-kelp benthic cover classes, see section 4.3.3). Since kelp beds are more abundant in the shallow subtidal zone (0-7 m) on the generally south-facing, wave-exposed coast of these islands (Gagnon et al., 2004), the present study focuses on these areas where kelp beds are more likely to be found (Figure 4.1). Within the study area, most of the seabed is composed of bedrock and boulders, with sporadic patches of cobble, gravel, or sand in areas of presumably lower hydrodynamic forces. The study area covers 2.85 km² and extends over a longitudinal distance of ~14 km. The area studied at Île Niapiskau, Île à Firmin, Île du Havre, Île aux Goélands, and Petite île au Marteau, represents respectively 12.8, 12.9, 54.3, 10.9, and 9.1% of the total study area.

Monospecific stands of the grazing-resistant perennial kelp *Agarum clathratum*, and of the annual brown seaweed *Desmarestia viridis* are observed within the study area in zones of moderate wave action. These stands cover up to a few 10s of m² in the barrens at depths of up to 15 m, developing along the lower edge (*A. clathratum*) or outside (*A. clathratum* and *D. viridis*) of kelp beds (Gagnon et al., 2003; Gagnon et al., 2004;

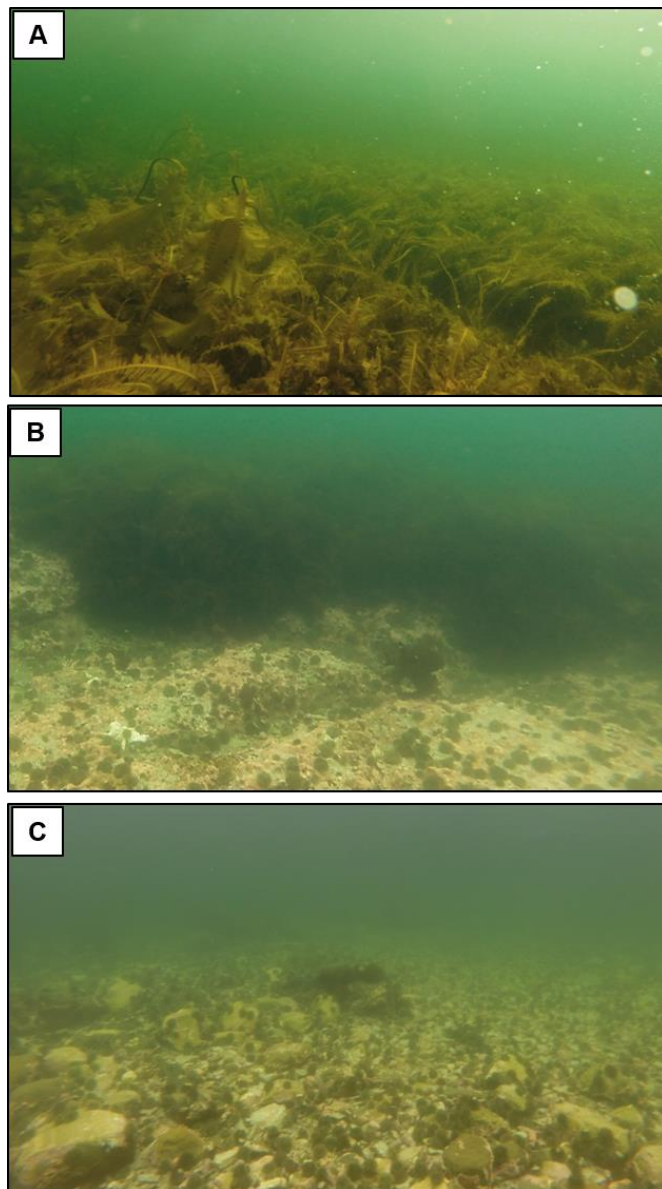


Figure 4.2. **A)** Kelp bed [mainly *Alaria esculenta*] at a depth of ~2 m at Île Niapiskau. **B)** Sharp transition between the lower edge of the kelp bed and upper edge of an urchin barrens caused by an urchin grazing front advancing over kelp at a depth of ~2 m. **C)** Green sea urchin (*Strongylocentrotus droebachiensis*) barrens with a few kelp patches at a depth of 6 m (Photos: Anne P. St-Pierre).

Gagnon et al., 2005). Although stands of *A. clathratum* and *D. viridis* could not be spectrally distinguished from kelp beds on the remotely sensed imagery, preliminary analysis of ground truth data suggests that misclassification of these stands as kelp beds is negligible (estimated at ~2%, as discussed in St-Pierre and Gagnon, 2020).

4.3.2. Image acquisition and field measurements

Aerial imagery was used to characterize the distribution of kelp beds within the study area. Procedures for the acquisition, georectification, and mosaicking of the aerial imagery are detailed in St-Pierre and Gagnon (2020). Essentially, digital photographs were acquired on 8 July, 2016, with a hand-held camera (Nikon Coolpix AW130), on board a helicopter flown at an altitude of ~300 m after four days of low winds and no precipitation. The photographs' resolution and area of the field of view varied from 8 to 17 cm per pixel and from 0.08 to 0.52 km², respectively. A satellite image (SPOT 7) of the area acquired on 11 August, 2016 (i.e., one month after acquisition of aerial imagery), was used to georectify the digital photographs and combine them into a mosaic encompassing the five islands' study areas in ArcMap 10.3.1 (Esri, 2015). Depending on the size of each island's study area and quality of the photographs (e.g., due to glare, variable overlap between adjacent images, or angle of view), 6 to 14 photographs per island were used to build the mosaic. Contrast and brightness were enhanced on each aerial photograph individually during the mosaicking process to increase the visibility and reduce variations in color between the mosaicked photographs.

Using the methodology detailed in St-Pierre and Gagnon (2020), a bathymetric map of the study area was prepared by interpolation (ordinary kriging, 1-m grid cell size) in

ArcMap 10.3.1 (Esri, 2015). This interpolation was based on 504 *in situ* depth measurements obtained across the entire study area and the location of the 10-m isobath obtained from bathymetric charts (Canadian Hydrographic Services, published in 2002). Using this bathymetric map, the mosaic of photographs was trimmed to discard all areas outside the 0 to 7 m depth range (Figure 4.3) in ArcMap 10.3.1 (Esri, 2015), because the present study focuses only on these areas where kelp presence is most probable (see section 4.3.1). To facilitate data processing and analysis, the mosaic and bathymetric map were converted to a common map coordinate system (Universal Transverse Mercator Projection, Zone 20N, North American Datum 1983), and the mosaic of photographs was resampled to a 1-m grid cell size using a nearest-neighbour resampling algorithm.

Underwater imagery collected at each of 360 locations throughout the study area between 23 July and 29 July, 2016, was used to 1) determine kelp presence/absence and use this information as ground reference for image classification and accuracy calculation (see St-Pierre and Gagnon, 2020 for details), and 2) measure urchin density. At each location, a photograph covering an 80 x 80 cm portion of the seabed was taken using a drop camera system consisting of a GoPro Hero 3 camera in an underwater housing secured face-down ~1 m above the seafloor onto a metal frame. The bottom portion frame was visible on each photograph and equipped with a visible scale to allow measurement of urchin size from the photographs (see below). Urchin density was measured by counting the number of urchins visible on each photograph and used in statistical analyses of kelp distribution (see section 4.3.5). Sampling locations were randomly selected within each island's study area in proportion to the size of the latter, to yield a spatially balanced sampling design. Kelp was present at 233 of the 360 locations surveyed (65%).

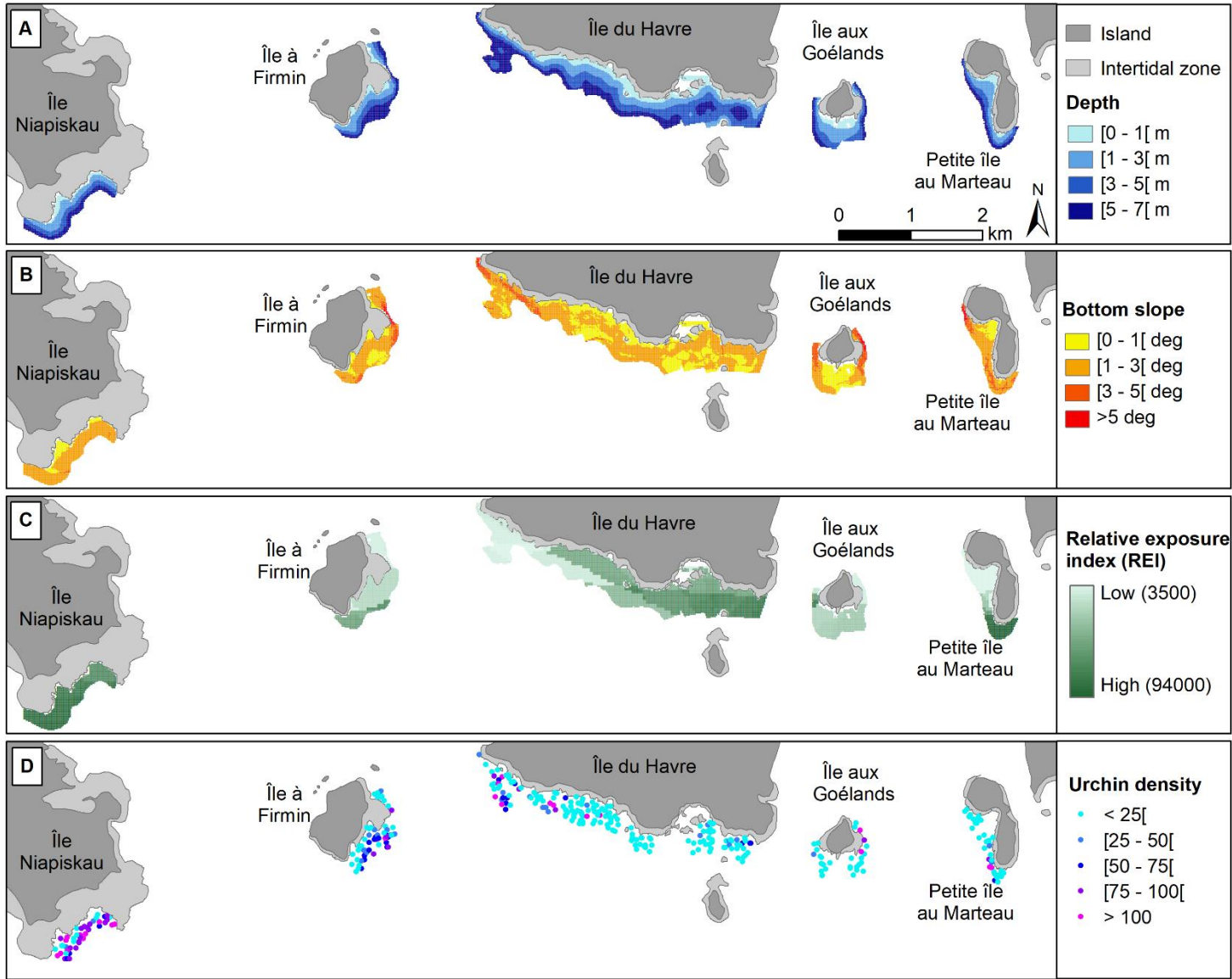


Figure 4.3. Map of the specific study area on the southward-facing subtidal fringe of five islands in the Mingan Archipelago, showing the bathymetry (within the 0 to 7 m depth range, **Panel A**), bottom slope (in degrees, **Panel B**), relative exposure index (REI, **Panel C**), and urchin density (in urchins·m⁻² **Panel D**). Urchin density is shown only for the 360 locations surveyed during ground truthing.

4.3.3. Data extraction from aerial imagery

The aerial imagery of the seabed was divided into kelp and non-kelp benthic classes using the proven visual classification method described in St-Pierre and Gagnon (2020). This method was deemed the most accurate for the classification of aerial imagery from the Mingan Archipelago's shallow subtidal zone (St-Pierre and Gagnon, 2020). In short, a sampling grid with intersects spaced at 15-m intervals was overlaid on the mosaicked imagery. The 225-m² area (15 x 15 m) surrounding each grid intersect was examined individually and assigned to either of two benthic classes: 1) "kelp", if over 50% of it was covered by kelp, or 2) "non-kelp", if less than 50% of it was covered by kelp. A grid intersect was excluded from the classification if over 50% of the area surrounding it was outside of the study area or was indistinguishable (e.g., due to glare). Less than 2% of the intersects were excluded. In total, 12,654 grid intersects were included in the analyses. The classification was conducted by a single observer to ensure consistency and yielded an overall accuracy of 89.6% and a Kappa coefficient of 0.77, both deemed largely satisfactory.

4.3.4. Kelp coverage and spatial pattern metrics

To investigate the effect of the extent of sampling area on observed kelp distribution, kelp coverage was calculated over three spatial extents: 1) the entire study area [$\sim 2,8$ km² of seabed], 2) each island separately [varying from 0.26 to 1.55 km²], and 3) fine-scale units of ~ 200 x 200 m [$\sim 40,000$ m²] randomly distributed without overlap and completely within the study area (Figure 4.1). The size of the fine-scale units was chosen to represent the spatial extent of local mapping projects which could be conducted within a reasonable

time frame using intensive SCUBA or boat-based surveys, based on the authors' personal experience and common kelp bed mapping techniques (Chapter 1; Gagnon et al., 2004; Kimura et al., 2012). This yielded a total of 30 fine-scale units distributed among islands based on the size of each island's study area. The fine-scale units at Petite île au Marteau were rectangular rather than square (still ~40,000 m²) because the study area at this island was too narrow to accommodate 200 x 200 m square units.

To quantify the spatial configuration of kelp and non-kelp features, a series of spatial pattern metrics were calculated with FRAGSTATS software version 4 (McGarigal et al., 2012). In the present study, a "patch" is defined as an element in the seascape delineated as a distinct entity, i.e., a discrete, contiguous area identified as either kelp or non-kelp. The eight-neighbour rule was used in this analysis, whereby any of the eight cells surrounding a pixel were considered part of a patch if they had the same value as the central pixel. The eight-neighbour rule was chosen over the four-neighbour rule as it was judged more representative of the distribution and connectivity of kelp patches in the field. The borders of the imagery were not considered as edges because they are not true boundaries between patches created by biological communities; rather, these boundaries are created by the extent of the mosaicked photographs. The background (pixels outside of the study area) was considered as no data instead of a zero (0) value, and thus was ignored in the calculations (McGarigal et al., 2012). A parsimonious suite of six meaningful and complementary metrics was selected to minimize redundancy among metrics (Cushman et al., 2008; see Table 4.1 for details), which included: 1) Largest patch index, which yields the percentage of seascape comprised by the largest patch of each benthic class; 2) Patch

Table 4.1. Spatial pattern metrics examined in the present study. All metrics were calculated with FRAGSTATS (v.4, Amherst, MA; McGarigal et al., 2012).

Metric	Abbreviated FRAGSTATS command	Range	Unit	Description
Largest patch index	LPI	0–100	Percent (%)	Percent of seascape comprised by the largest patch of each benthic class.
Patch area	AREA	0–∞	Square metres (m ²)	Area of each patch in each benthic class. Minimum, mean, and maximum patch areas are reported.
Patch density	PD	1–∞	(N/A)	Number of patches in each benthic class divided by the size of the area studied (in km ²), which measures the extent of subdivision or fragmentation of a benthic class.
Shape index	SHAPE	1–∞	(N/A)	Measure of patch complexity based on the ratio of the patch's perimeter to the perimeter of a standard shape (square) of the same surface area. Mean value for each benthic class is reported.
Mean nearest neighbour distance	ENN	0–∞	Metres (m)	Measure of the Euclidean distance to the nearest neighbouring patch of the same benthic class. Mean value for each benthic class is reported.
Clumpiness index	CLUMPY	-1–1	(N/A)	Measure of aggregation within each benthic class, where -1 represents patches maximally disaggregated, 0 represents a random distribution, and 1 represents maximal aggregation.

area, calculated for each individual patch; 3) Patch density, which reports the number of patches per km² in each benthic class; 4) Shape index, which quantifies the complexity of a given patch; 5) Mean nearest neighbour distance, which is the average distance between patches of the same benthic class; and 6) Clumpiness index, which measures patch aggregation within each benthic class. These metrics are descriptive tools which, taken together, provide an insight into the ecological processes occurring within the studied seascape. The chosen metrics assess categorical map patterns (or patch mosaics) but do not intrinsically quantify or correct for spatial autocorrelation in the distribution of patches (see McGarigal et al., 2012 for further details regarding the use and limitations of these metrics). Exploration of spatial pattern metrics were conducted separately for 1) the entire study area, and 2) each island's study area, to compare the patterns observed at two contrasting scales. Spatial pattern metrics were not calculated for the fine scale units because the quantity and complexity of data generated would have made it nearly impossible to contrast results meaningfully among units.

4.3.5. Relationships between environmental factors and kelp distribution

To investigate the relationship between environmental factors and kelp distribution, model selection (Burnham and Anderson, 2002) was applied to determine which combination of four explanatory variables best describes kelp distribution in the Mingan Archipelago. These explanatory variables, explained in more details below, are 1) depth, 2) bottom slope, 3) relative exposure to waves, and 4) urchin density. Because urchin density can fluctuate between >500 urchins·m⁻² in grazing fronts and <10 urchins·m⁻² in barren areas less than 30 m away (Gagnon et al., 2003; Gagnon et al., 2004, A. P. St-Pierre,

personal observation), interpolation of this variable between locations sampled in the field would not be an accurate representation of actual field densities. Therefore, statistical analyses were conducted using only the 360 grid intersects for which urchin densities were calculated using underwater imagery (see section 4.3.2) and values of depth, bottom slope, and exposure to waves were extracted only for these grid intersects.

Depth

The precise bathymetric map of the study area (see section 4.3.2, Figure 4.3A) was used to calculate depth at each of the 360 grid intersects used for model selection. Using the Focal Statistics tool in ArcMap 10.3.1 (Esri, 2015), average depth was calculated for the 225 m² of seafloor surrounding each grid intersect. Average depth of the seafloor surrounding an intersect was used in analyses instead of depth directly below the intersect to better represent the area surveyed for kelp presence in its entirety.

Bottom slope

Bottom slope (0 to 90°, Figure 4.3B) was calculated with the Slope tool in Arc Map 10.3.1 (Esri, 2015), based on the interpolated bathymetric map. Using the Focal Statistics tool in ArcMap 10.3.1, average slope was calculated for the 225-m² area surveyed around each 360 grid intersects used for model selection. Average slope of the seafloor surrounding an intersect was used in analyses instead of the slope directly below the intersect to better represent the area surveyed for kelp presence in its entirety.

Relative exposure to waves

A relative exposure index (REI, Figure 4.3C) was used as a proxy of exposure to waves and calculated following the procedure outlined by Garcon et al. (2010) which combines mean wind velocity, mean wind direction, and effective fetch. Daily wind data recorded at the meteorological station of Havre St Pierre Airport (~10 km from the study area) in the 12 mo before acquisition of aerial imagery (i.e., July 2015 to June 2016) was obtained from the web archives of Environment Canada (http://climate.weather.gc.ca/historical_data/search_historic_data_e.html). This data was used to calculate 1) the yearly average of maximum wind gust velocity (V) from the daily maximum wind speed ($\text{m}\cdot\text{s}^{-1}$); and 2) the directional percentage frequency (P_i) of winds, calculated as the proportion of days (%) during which wind occurs from each of the 16 compass directions (see below). Wind velocity and directional percentage frequency were calculated over a 12-month period to capture the range of conditions occurring across seasons. Effective fetch (F) is defined as the distance from a site to the nearest wave-obstructing obstacle (U.S. Army Corps of Engineers, 1984). For any given point intersect, effective fetch was calculated along each of 16 compass directions (i.e., 1 to 16 compass headings, from N, NNE, NE, etc. in 22.5° increments from 0 to 360°) using the Fetch tool in the Waves toolbox (Rohweder et al., 2012) in ArcGIS 10.3.1 (Esri, 2015). REI was calculated for each of the 360 grid intersects used in analysis by applying the following equation (Garcon et al., 2010; Keddy, 1982):

$$REI = \sum_{i=1}^{16} (V \cdot P_i \cdot F_i)$$

where i is the i^{th} of 16 compass headings, V is the mean wind velocity in m s^{-1} , P_i is the wind direction frequency (%), and F_i is the effective fetch in kilometres. It is important to note that the REI here does not take water depth into account and is therefore a measure of exposure at the water's surface only. Possible interactions between depth and exposure were considered when preparing the models to be compared (see below).

Urchin density

Urchin densities were calculated from the underwater imagery collected at 360 locations during ground truthing (see section 4.3.2, Figure 4.3D). Densities were calculated based on the number of urchins of >2 cm in diameter visible on the 80 x 80 cm photograph of the seabed acquired at each sampling location, as urchins of <2 cm in diameter were not readily visible on the imagery.

Model selection

A mixed model approach was applied to examine the relative influence of depth, bottom slope, exposure to waves (estimated by the REI), and urchin density on kelp presence. Binomial generalized linear mixed models (GLMM) with a combination of these four factors as fixed exploratory variables and Island as a random variable (categorical factor) were fitted to kelp presence data. To restrict the number of models to ecologically meaningful ones, the combinations of fixed factors to be tested in each model was chosen based on specific ecological hypotheses related to the factors studied (see Table 4.2), rather than testing all possible combinations of factors. These models assume that kelp presence

Table 4.2. Hypotheses and corresponding models used in model selection to investigate the relationship between kelp distribution and a combination of four explanatory variables, i.e., depth, bottom slope, relative exposure index (REI, a measure of exposure to waves), and urchin density (see section 4.3.5). The + symbol indicates an additive effect between parameters, while the * symbol indicates an interactive effect between parameters.

Model number	Hypothesis tested	Fixed factors
1	Kelp presence decreases with increasing depth (because of decreasing light availability).	Depth
2	Kelp presence decreases with increasing urchin density (due to the grazing pressure of the urchin).	Urchin density
3	Kelp presence decreases with increasing depth and increasing urchin density, with an additive effect of both parameters.	Depth + Urchin density
4	Kelp presence increases with increasing wave action caused by the interaction between depth and relative exposure index (note that REI calculated in the present study and is a measure of exposure at the sea surface only, although wave action decreases with depth).	Depth*REI
5	Kelp presence increases with wave action (an interactive effect of depth and relative exposure) and slope (additive effect).	Depth*REI + Slope
6	Kelp presence decreases with wave action (an interactive effect of depth and relative exposure) and slope (additive effect) and decreases with increasing urchin density.	Depth*REI + Slope + Urchin density
7	Kelp presence increases with wave action (an interactive effect of depth and relative exposure) and decreases with urchin density.	Depth*REI + Urchin density
8	Urchin density and wave action (calculated as the interaction of depth and relative exposure) have an interactive, negative effect on kelp presence.	Depth*REI*Urchin density
9	Kelp presence decreases with increasing depth and with increasing relative exposure, without interaction between parameters.	Depth + REI
10	Kelp presence decreases with increasing depth and urchin density, but increases with increasing relative exposure, without interactive effect between parameters.	Depth + REI + Urchin density
11	Kelp presence decreases with increasing depth, slope, and urchin density, but increases with increasing relative exposure, without interactive effect between parameters.	Depth + REI + Slope + Urchin density

is dependent on local factors and do not include the potential effect of kelp bed proximity. Further studies would be required to investigate the effects of kelp patch proximity on recruitment in our study area before such variable could be adequately included in the model (which falls outside the scope of the present study). To select between competing models, the Akaike's information criterion (AIC) was calculated for each model and compared. AIC is an estimate of model fit which accounts for model complexity by applying penalties based on the number of factors present in a model (Burnham and Anderson, 2002). Hence, in model comparisons using AIC, the most informative model is the one which yields the lowest AIC. Models with an AIC difference (Δ_i , i.e., the difference between the AIC value of model i , where i represents any of the models tested, and the lowest AIC value among all models tested) of less than 2 have substantial support (Anderson, 2007) and are considered not meaningfully different from each other, indicating the presence of pretending variables which are not informative (Burnham and Anderson, 2002; Leroux, 2019). Therefore, the best fitting model was selected as the most parsimonious model out of those with a $\Delta_i < 2$.

Generalized linear mixed models were fitted in R 3.3.2 (R Development Core Team, 2018) using the functions "glmer" in the "lme4" package (Bates et al., 2014). Residuals of the best fitting model were examined graphically for normality, independence, and homoscedasticity, and did not display violations of these assumptions. Given the large difference in range of values among the four explanatory variables, all explanatory variables were rescaled prior to running GLMMs. Scaling of each explanatory variable consisted of subtracting the explanatory variable's median from each original value (centering) and dividing by the standard deviation. Applying this scaling and centering

method also allowed the coefficient estimates (i.e., slope coefficients) to be directly comparable, thus enabling comparisons in the magnitude of the effect of each explanatory variable (Welham et al., 2015). Odds ratios represent the rate of change in the odds of an event occurring (i.e., kelp presence) given a change of one unit of the explanatory variable and are calculated as the antilog of the coefficient estimate (e^{estimate} or $e^{\beta 1}$, Quinn and Keough, 2002). Since the variables were scaled before analysis, the units of the odds ratios from the model output are one standard deviation of the variable rather than the original unit of the variable. Odds ratios were calculated from the parameter estimates from the most informative model, and subsequently back-transformed to be reported on each explanatory variable's original scale.

4.4. RESULTS

Kelp coverage and spatial pattern metrics

At the broadest spatial scale studied (entire study area), kelp was present over 62.5% of the seabed (Figure 4.4 and 4.5). At the intermediate spatial scale (each island taken separately), kelp coverage showed differences of up to 41.0% among islands, being the lowest at Île Niapiskau with 46.3% coverage and highest at Île aux Goélands with 87.3% coverage (Figure 4.5). Within the finest-scale units (200 x 200 m), kelp coverage showed greater variability than the coverage measured at the intermediate scale (islands); kelp coverage varied from 2.7% in one fine-scale unit at Île du Havre to 100% in one unit at Île aux Goélands (Figure 4.5).

Largest patch index values indicate that, at all islands except Île Niapiskau, the largest contiguous kelp patch covered between 42.6% (Petite île au Marteau) and 81.7% (Île du

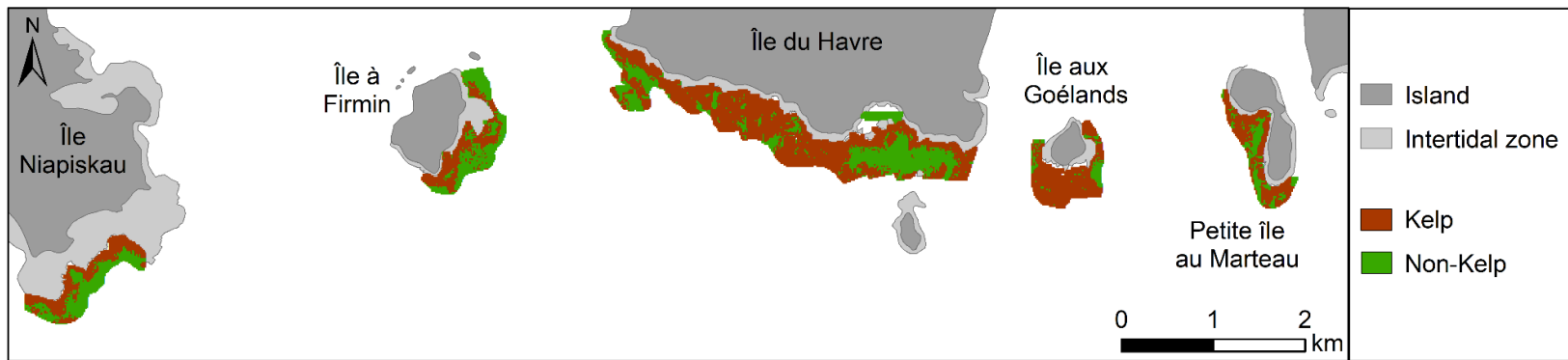


Figure 4.4. Map issued from the visual classification of the aerial imagery acquired around the five studied islands in the Mingan Archipelago showing the distribution of the kelp (brown) and non-kelp (green) benthic classes.

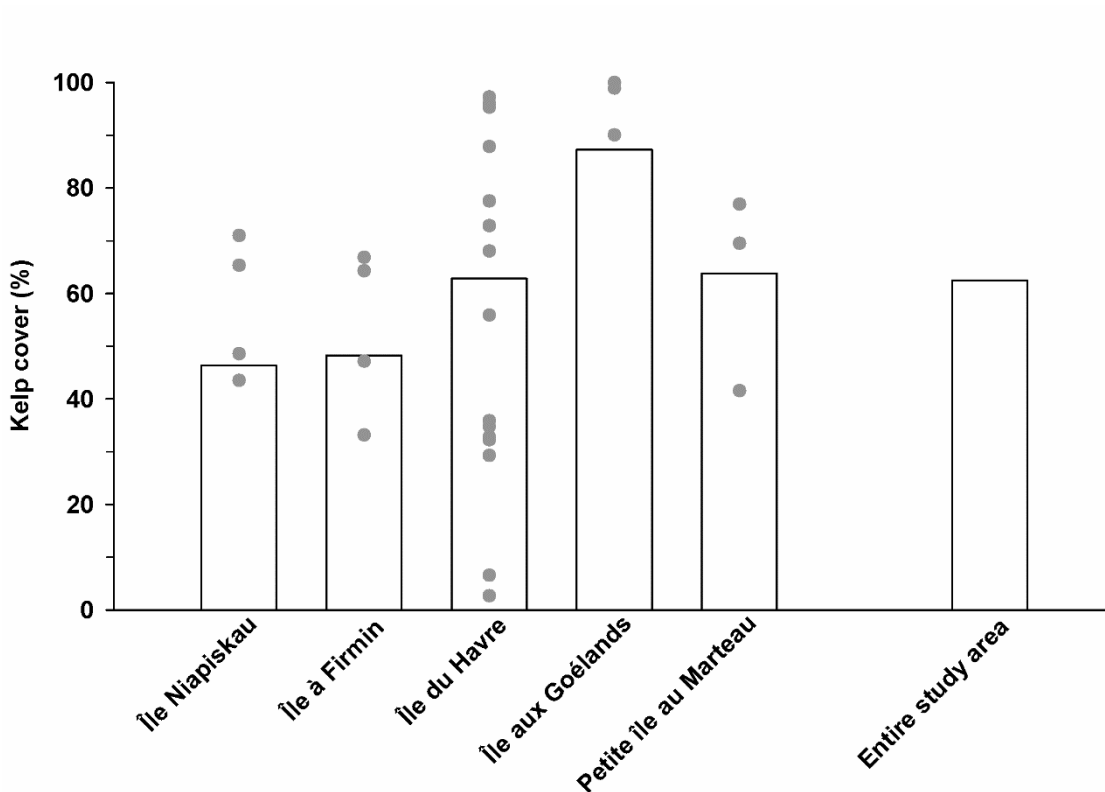


Figure 4.5. Comparison of kelp cover (%) as measured within the study area of each island (columns), and within fine-scale units of approximately 200 x 200 m (~40,000 m²; gray circles). The number of fine-scale units at each island was determined proportionally to the size of each island's study area, for a total of 30 sites (with 4 at Île Niapiskau, 4 at Île à Firmin, 16 at Île du Havre, 3 at Île aux Goélands, and 3 at Petite île au Marteau). The bar furthest to the right represents the overall kelp cover (62.5%) calculated over the entire study area.

Havre) of each island's study area (Figure 4.6A). In contrast, the largest kelp patch observed at Île Niapiskau covered only 24.4% of that island's study area. Largest patch index for the non-kelp benthic class varied between 5.9% (Île aux Goélands) and 33.4% (Île à Firmin), except at Île Niapiskau where the largest patch index for non-kelp reached 53.3%.

Patch area was highly variable for both benthic classes. Kelp patch area varied from 225 m² (all islands except Petite île au Marteau, where minimum was 450 m²) to 891,225 m² (Île du Havre, Figure 4.6B and 4.7). Among islands, maximum kelp patch area showed variation of up to one order of magnitude (Figure 4.7). Similar variations were observed in non-kelp patches, with a minimum of 225 m² (all islands) and a maximum of 311,850 m² (Île du Havre, Figure 4.7C). Maximum non-kelp patch size varied considerably among islands, being 17 times greater at Île du Havre than Île aux Goélands. Maximum non-kelp patch size at Île Niapiskau, Île à Firmin, and Petite île au Marteau varied between 46,575 m² and 193,500 m² (Figure 4.6B and 4.7). At Île du Havre, Île aux Goélands, Petite île au Marteau, and in the entire study area, kelp patches were on average 6.5 times larger than non-kelp patches; 16.8 to 24.6 patches·km⁻² for the kelp benthic class and 51.7 to 74.3 patches·km⁻² for the non-kelp benthic class; Figure 4.6C). Contrary to this trend, the mean patch area for kelp was 48 and 27% lower than non-kelp patches at Île Niapiskau and Île à Firmin, respectively. Standard error around the values of mean patch area were substantial for both benthic classes at all islands, suggesting large variation in patch size for kelp and non-kelp patches throughout the study area (Figure 4.6B). Frequency distribution of patch size from both benthic classes shows that 81 and 77% of patches were smaller than 1350

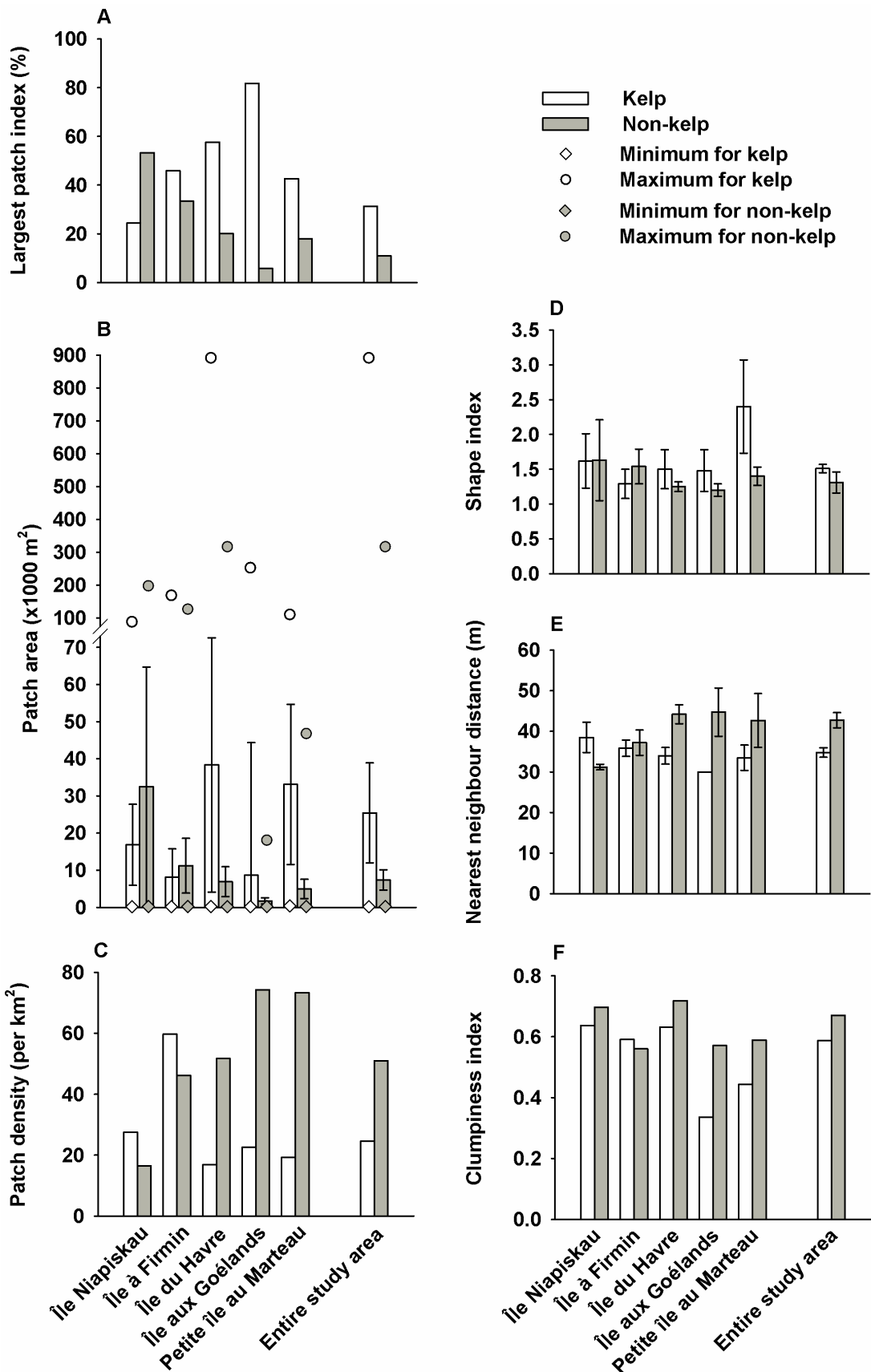


Figure 4.6. Spatial pattern metrics for the kelp (white) and non-kelp (gray) benthic classes. Metrics were calculated individually for each of the five islands and for the entire study area. **Panel A** shows the largest patch index (%). **Panel B** shows patch area where bars represent the mean (in m², ± SE) and symbols represent minimum (diamond) and maximum (circles) values. **Panel C** shows patch density (number of patches per km²). **Panel D** shows shape index (unitless, mean ± SE). **Panel E** shows Euclidian nearest neighbour distance (in m, mean ± SE). **Panel F** shows clumpiness index (unitless). Details regarding each metric are presented in Table 4.1.

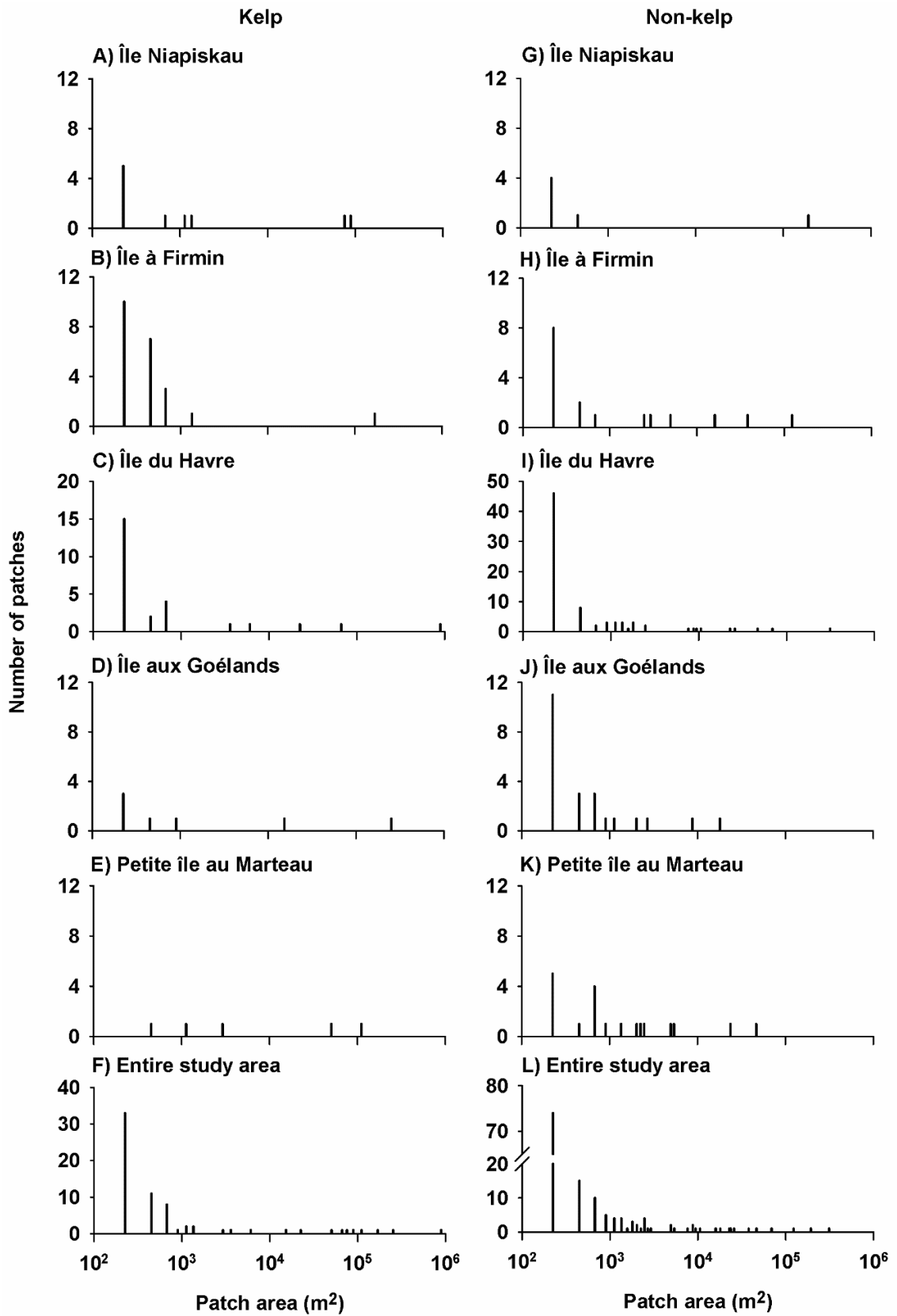


Figure 4.7. Frequency distribution of patch size (surface area, in m²) for the kelp (left side panels, from A to F) and non-kelp benthic classes (right side panels, from G to L) for each island and the entire study area. Note the exponential scale of the abscissas and various scales along the ordinates.

m² in the kelp and non-kelp benthic classes, respectively, with only 1 to 15 larger patches present per island (Figures 4.7).

Mean shape index differed among islands, with more complex kelp patches observed at Petite île au Marteau (2.4 ± 0.7) and Île Niapiskau (1.6 ± 0.4) compared to the other islands. Île Niapiskau also presented the most complex non-kelp patches with shape indices averaging 1.6 ± 0.6 , followed by Île à Firmin with 1.5 ± 0.3 . Shape indices over the entire area were similar for the kelp and non-kelp benthic classes, with values of 1.5 ± 0.1 and 1.3 ± 0.2 respectively (Figure 4.6D).

Mean (Euclidean) nearest neighbour distance among patches of the same benthic class calculated over the entire study area were of 34.8 ± 1.2 and 42.7 ± 1.9 m for the kelp and non-kelp benthic classes, respectively (Figure 4.6E). This metric was relatively stable among islands, ranging from 30.0 to 38.5 m and from 31.2 to 44.7 m for the kelp and non-kelp benthic classes, respectively (Figure 6E). Clumpiness indices yielded values of 0.59 and 0.67 over the entire study area for kelp and non-kelp cover respectively, indicating a relatively high degree of aggregation for both benthic classes (Figure 4.6F). Clumpiness indices varied among islands from 0.34 (Île aux Goélands) to 0.64 (Île Niapiskau) for the kelp benthic class, and from 0.56 (Île à Firmin) to 0.72 (Île du Havre) for the non-kelp benthic class. The clumpiness index of the kelp benthic class was 9, 13, 69, and 32% higher than the non-kelp benthic class at Île Niapiskau, Île du Havre, Île aux Goélands, and Petite île au Marteau, respectively (Figure 4.6F). At Île à Firmin, the clumpiness index of the non-kelp benthic class was 5% lower than that of the kelp benthic class (Figure 4.6F).

Model selection

Results from model selection (Table 4.3) indicated that three models had low AIC values and were equally well fitting the dataset ($\Delta_i < 2$). Of these three models, Model 10 which includes the additive effects of the variables depth, REI, and urchin density was the most parsimonious and therefore was used for subsequent analyses (Table 4.3, see section 4.3.5 for details). Regression coefficient estimates (i.e., slope coefficients) from this model, which represent the log-odds of the presence of kelp, yielded values of -1.32, -0.86, and -1.01 for the variables depth, REI, and urchin density, respectively. Comparison of the coefficient estimates is possible because the exploratory variables were scaled prior to analyses. In this case, coefficient estimates from Model 10 showed that depth had the strongest influence on kelp presence (Table 4.4), being 1.5 times greater than the influence of REI, and 1.3 times greater than that of urchin density (Table 4.4). The influence of urchin density on kelp presence was 1.2 times higher than the effect of REI (Table 4.4). Based on odds ratios, Model 10 indicates that for every increase of one metre in depth, the odds of kelp presence declined by 0.15 (Table 4.4). Similarly, for every increase of one unit in REI and of one urchin·m⁻² (urchin density), the odds of kelp presence declined by 0.00002 and 0.008, respectively (Table 4.4).

4.5. DISCUSSION

Characterizing species-habitat relationships at multiple scales is crucial for a comprehensive understanding of the scale-dependent ecological processes driving species distribution (Lecours et al., 2015; Petraitis and Latham, 1999). For instance, the

Table 4.3. Outcome of model selection applied to determine the relative influence of four explanatory variables (Depth, Relative Exposure Index [REI], Slope, and Urchin density) on kelp presence (see Section 4.3.5 for details). AIC_i is the value of the Akaike Information Criterion (AIC) calculated for model i (where i represents any of the 11 models tested), and Δ_i is the difference between the AIC of the best fitting model and that of model i . k represents the number of parameters, $\text{Exp}(-0.5\Delta_i)$ represents the relative likelihood of model i , and w_i represents the Akaike weights. The + symbol indicates additive effects, while the * symbol indicates interactive effects among model factors. Model 10 (bold) was selected as the most informative.

Model number	Fixed explanatory variables in each model	k	AIC_i	Δ_i	$\text{Exp}(-0.5\Delta_i)$	w_i
Model 11	Depth + REI + Slope + Urchin density	6	315.2	0	1.000	0.395
Model 10	Depth + REI + Urchin density	5	315.7	0.4	0.803	0.317
Model 6	Depth * REI + Slope + Urchin density	7	317.2	2.0	0.370	0.146
Model 7	Depth * REI + Urchin density	6	317.6	2.4	0.302	0.119
Model 8	Depth * REI * Urchin density	9	321.0	5.8	0.054	0.022
Model 3	Depth + Urchin density	4	345.6	30.3	0.000	0.000
Model 9	Depth + REI	4	362.9	47.7	0.000	0.000
Model 4	Depth * REI	5	364.4	49.2	0.000	0.000
Model 5	Depth * REI + Slope	6	366.0	50.8	0.000	0.000
Model 1	Depth	3	386.2	71.0	0.000	0.000
Model 2	Urchin density	3	388.5	73.3	0.000	0.000

Table 4.4. Coefficient estimate (β), p -values, and odds ratios for the explanatory variables in Model 10, which was selected as the most informative by comparison of Akaike’s Information Criterion (AIC; see Table 4.3 and Section 4.3.5). Odds ratios indicate the relative change in the odds of kelp being present at a given location, for an increase of one unit in the exploratory variable. As the explanatory variables were scaled and centered prior to analyses, the odds ratios represent the change in odd for an increase of one standard deviation of the exploratory variable. The odds ratios were back-transformed to present the change in odds for an increase of one unit of the explanatory variable (first column from the right). All changes in odds represent declines in the odds of kelp being present, since the coefficient estimates are of negative values.

Exploratory variable	β (\pmSE)	p-value	Change in odds per one standard deviation of the exploratory variable (i.e., odds ratio; e^β)	Standard deviation of the initial data	Change in odds per unit of the exploratory variable
Intercept	0.8718	<0.001	-	-	-
Depth	-1.32 (\pm 0.19)	<0.001	0.266	1.79 m	0.15 per m
REI	-0.86 (\pm 0.17)	<0.001	0.423	24750.54 units	0.00002 per unit
Urchin density	-1.01 (\pm 0.16)	<0.001	0.366	44.67 urchins·m ⁻²	0.008 per urchin·m ⁻²

combination of fine- and broad-scale approaches showed that distribution patterns of giant kelp at the scale of 10s to 100s of km² are strongly influenced by oceanographic factors (e.g., El Niño events or North Pacific Gyre Oscillations, Cavanaugh et al., 2011; Edwards, 2004), while biological and physical factors occurring at the scale of a few metres are the main drivers of local distribution patterns (e.g., grazing, substrate stability, and canopy shading, Dayton, 1985a; Dayton et al., 1992). Approaches developed in terrestrial ecology to measure landscape heterogeneity using spatial pattern metrics are increasingly applied to link distribution patterns in habitat-forming marine benthic species and their drivers at various spatial scales (Boström et al., 2011; Huntington et al., 2010; Wedding et al., 2011). For submerged kelp-urchin systems, these metrics enable the assessment of seascape patterns at broad spatial scales (km²) largely unexplored to date; they provide a new perspective for the study of boundary dynamics and community shifts which could not be obtained through traditional methods and which is crucial to assess the long-term stability and resilience (or lack thereof) of these systems. The present study contributes to the understanding of kelp distribution patterns and their drivers in the northern Gulf of St. Lawrence by exploring new approaches using spatial analyses and modelling techniques applied at a broad spatial scale (km²). Results indicate that kelp distribution (based on kelp coverage and spatial pattern metrics) is not uniform among islands in the Mingan Archipelago and suggest that the spatial extent over which observations are obtained strongly influences the patterns detected. Results from model selection indicate that both biotic and abiotic factors influence kelp distribution, since increasing depth, urchin density, and relative exposure to waves were all independently correlated to a decrease in the odds of kelp presence, with depth having the strongest effect.

Substantial variation in kelp coverage was observed in the fine-scale units (200 x 200 m) studied, with some units being practically devoid of kelp (2.7% kelp cover) while others had continuous (100%) kelp coverage. When measured over the intermediate spatial scale (i.e., each island separately), variations in kelp coverage were less pronounced, ranging from 46.3 to 87.3% among islands. Overall kelp coverage calculated for the entire study area was of 62.5%. Based on these observations of kelp coverage and the fact that spatial pattern metrics varied greatly among islands (particularly largest patch index, patch area, and patch density), the present study suggests the spatial extent over which a study is conducted strongly influences the patterns observed in terms of coverage and distribution patterns. Hence, extrapolating observations of kelp distribution from fine-scale (10s or 100s m²) monitoring projects to greater spatial extents (km²) may lead to unreliable estimates. Care should be taken in determining the spatial extent and resolution needed in studies of kelp bed distribution. Also, spatial pattern metrics are highly dependent on the resolution and minimal mapping unit employed during image classification (Fassnacht et al., 2006; Kendall et al., 2011; Saura, 2002). Because the grid intersects used during image classification in the present study covered 225 m², kelp and non-kelp features of a smaller size were not identified. Thus, only patterns of kelp distribution encompassing at least several 100s of m² can be obtained from interpretation of these metrics.

In the present study, patch size and density of both kelp and non-kelp benthic classes displayed wide variations within islands and among islands. Within islands, the smallest patches observed covered only one grid intersect (225 m²) and the largest formed long, connected areas with a varying degree of geometric complexity. Among islands, maximum kelp patch area showed variation of up to one order of magnitude and mean kelp patch area

showed up to 475% difference. These variations in patch size and density among islands may stem from differences in environmental parameters such as depth and exposure to waves (discussed below), substrate, or topography, although further data is required to assess the effects of the latter two. Differences in urchin density among island may also influence kelp patch size, as urchin grazing is known to modulate the extent of kelp beds at the scale of m to 10s of m (Frey and Gagnon, 2015; Gagnon et al., 2004; Scheibling et al., 1999). In this study, a strong negative correlation was observed between urchin density and largest patch index calculated for the kelp class, although mean kelp patch showed no clear trend with urchin density among islands (data not shown). At the largest spatial scale studied (entire study area), over 80% of all kelp patches measured less than 1350 m² (6 grid intersects), suggesting that the study area is characterized by numerous small kelp patches with only few large patches. However, these few large patches contain most (98%) of the kelp-covered seabed. As large kelp patches form continuous and unfragmented habitat, they may contribute to a higher biodiversity of kelp-associated species and be more resilient to grazing than smaller patches (Norderhaug et al., 2005; Reeves et al., 2015; Sievers et al., 2016). For instance, biomass and abundance of fish are positively correlated with kelp patch area in Californian kelp forests (Deza and Anderson, 2010). It is unclear from the data at hand whether kelp beds were initially forming large unfragmented patches and were subsequently divided (e.g., by urchin grazing) or if the kelp beds developed directly as variably sized patches, for example due to localized differences in substrate.

Similar to patch size, the degree of aggregation of habitat patches influences diversity patterns, animal movement, and genetic diversity (Alberto et al., 2010; Bender et al., 2003; Billot et al., 2003; Jackson and Fahrig, 2014). In the present study, clumpiness indices (a

measure of aggregation) showed that kelp patches are aggregated to a degree that varied among islands, as indices calculated for each of the five islands varied between 0.34 and 0.64, while the study area as a whole had a relatively high degree of aggregation with an index value of 0.59. Aggregation of kelp patches may be modulated by spore dispersal patterns, as kelp spores generally tend to remain within a few m to 10s of m of their parental patch but can be dispersed over several hundred m (Fredriksen et al., 1995; Gaylord et al., 2002; Norton, 1992). Thus, the strength and direction of currents transporting spores may differ among and within islands, creating patterns in which new kelp patches form close by or far away from the parent patch. As is the case for patch size, the aggregation of kelp patches may also depend on the intensity of urchin grazing pressure which determines the position of kelp bed edges (Frey and Gagnon, 2015; Gagnon et al., 2004; Konar et al., 2014; Scheibling et al., 1999). Although intensive urchin grazing may increase the distance between neighbouring patches (thus decreasing the clumpiness index), data from the present study suggest a positive correlation between average urchin density and clumpiness indices at each island (data not shown). Further studies are needed to elucidate the mechanisms driving this trend. Other physical factors such as substrate type, topography, and local currents should be investigated as potential drivers of kelp patch aggregation, as they modulate both kelp settlement and urchin activity (Feehan et al., 2012; Flukes et al., 2012; Laur et al., 1986; Muth, 2012).

Model selection results showed that increasing depth, urchin density, and relative exposure to waves all independently lead to a decrease in kelp presence, with depth having the strongest effect followed by urchin density and exposure to waves. The relationship between depth and kelp presence can be easily visualized on the kelp distribution map

created in the present study, as extensive kelp patches are generally present along the coast while smaller dispersed patches more frequently form in deeper areas. These results support observations from studies in the northeast Atlantic, which showed kelp are more frequent in shallow water (Bekkby et al., 2009; Rinde et al., 2014; Svendsen and Kain, 1971). Increased kelp presence near the surface may stem from better light conditions and increased water motion which stimulate nutrient intake and photosynthesis (Hepburn et al., 2007; Hurd, 2000). The greater water motion near the surface compared to deeper area may also affect kelp presence indirectly because wave-induced movement of algal fronds deters displacement and feeding in several urchin species including *S. droebachiensis* (Dayton, 1985b; Himmelman and Steele, 1971; Konar, 2000; Velimirov and Griffiths, 1979). Given this relationship, it was surprising that the interaction between depth and relative wave exposure did not improve modelling outcomes. Since the study area only encompassed shallow (0-7 m) zones generally exposed to the open waters of the Gulf of St. Lawrence, it is possible that this interaction may become more significant if a wider range of depths and exposure levels were studied.

Although water motion can have positive effects on kelp growth (Hepburn et al., 2007; Hurd, 2000; Sjutun and Fredriksen, 1995), strong wave action can also lead to blade damage and dislodgement from the substratum (Krumhansl and Scheibling, 2011; Thomsen et al., 2004). Contrary to the initial hypothesis, the present study shows kelp presence decreases with increasing exposure to waves. In the northeast Atlantic, studies by Bekkby et al. (2009), Rinde et al. (2014), and Pedersen et al. (2012) reported a positive correlation between wave exposure and kelp presence. In these studies, kelp presence was compared among sites within a wide gradient of wave exposure, from sheltered to highly

exposed coasts. In contrast, the present study focuses on the exposed shores within the Mingan Archipelago, therefore targeting wave exposed areas since kelp is rarely present on protected shores in this area (Gagnon et al., 2004, P. Gagnon, personal observations; Himmelman, 1991). Favorable growth conditions and difficulty of access by urchins have been suggested to explain the enhanced kelp presence in areas of high wave exposure in other regions (Lauzon-Guay and Scheibling, 2007; Merzouk and Johnson, 2011; Rinde et al., 2014). Yet, results from the present study suggest that moderately exposed shores (i.e., the lower end of the exposure gradient studied here) are more favorable than highly exposed areas for kelp species growing in the Mingan Archipelago. This may be due to damage to sporophytes, dislodgement, or impeded settlement of kelp recruits caused by strong waves and increased ice scouring in areas of high exposure (Filbee-Dexter and Scheibling, 2012; Krumhansl and Scheibling, 2011; Saunders and Metaxas, 2008).

The hypothesis that increased urchin density decreases the likelihood of kelp presence was supported by results from the present study, since urchin density was identified as the second most important variable influencing kelp presence, after depth. As urchin densities often reach up to 300 urchins·m⁻² in feeding aggregations near kelp beds in the Mingan Archipelago (Gagnon et al., 2004; Himmelman and Nédélec, 1990), the fact that the odds of kelp presence declined by 0.008 for each increase of a single urchin per m² confirms that urchin grazing is an important driver of kelp distribution in that region. In barren areas, the presence of urchin limits kelp resettlement and may preclude the formation of large, connected kelp patches (Breen and Mann, 1976; Chapman, 1981; Gagnon et al., 2004; Scheibling et al., 1999). A clear example of this is found at Île Niapiskau, which presents the lowest percent cover of kelp and smaller, less connected patches than the other

islands studied, as well as the highest value for largest patch index and percent cover for the non-kelp benthic class. Île Niapiskau also had the highest urchin density; ground-truth data at this island showed an average urchin density of $77 \text{ urchins} \cdot \text{m}^{-2}$, with 12 locations out of the 45 surveyed containing over $100 \text{ urchins} \cdot \text{m}^{-2}$. In comparison, urchin densities at each of the other four islands studied averaged 18 to $33 \text{ urchins} \cdot \text{m}^{-2}$, with only 1 to 8 locations per island having densities $>100 \text{ urchins} \cdot \text{m}^{-2}$. These findings suggest that high urchin density limits the formation of large, continuous kelp patches in the Mingan Archipelago, although more testing is needed to identify the threshold urchin density required to produce such effects and the drivers of differences in urchin density among islands.

Large-scale phase shifts between kelp-dominated and urchin-dominated states have been observed worldwide (Krumhansl et al., 2016; Ling et al., 2015; Steneck et al., 2002), including in Nova Scotia (Filbee-Dexter and Scheibling, 2014; Lauzon-Guay et al., 2009). These shifts are mainly caused by dramatic variations in urchin density and because they occur over extensive areas (up to 10s of km^2), they have a profound effect on biodiversity patterns which can be maintained over decades (Filbee-Dexter and Scheibling, 2014; Ling et al., 2015; Steneck et al., 2002; Steneck et al., 2013). In the Mingan Archipelago, several field-based research projects on benthic invertebrates and algae have occurred over the past 30 years (see work by J.H. Himmelman, L.E. Johnson, and their students). Based on these projects, the shallow benthic communities in this region has been generally described as including relatively small, shallow kelp beds near coastlines and extensive urchin barrens in deeper areas, without having undergone major shifts in the spatial dominance of either kelp or urchins at a broader (km^2) scale. Hence, the kelp-urchin system in this region

appears to be relatively stable over time. The apparent temporal stability of this system at broad (km²) spatial scales may be explained by the fact that kelp distribution is correlated with depth and exposure to waves (i.e., two abiotic parameters which do not vary temporally) as shown in the present study. As urchin density modulates annual and seasonal variations in the position of the kelp-barren interface at small spatial scales (few 10s m²; Gagnon et al., 2004), this factor (which was also correlated with kelp presence in the present study), may have a more local influence and lead to the differences in kelp bed patterning observed among islands, while the effects of depth and exposure to waves may affect broader spatial and temporal scales.

Given the global (Krumhansl et al., 2016) and regional (Filbee-Dexter et al., 2016; Moy and Christie, 2012; Pehlke and Bartsch, 2008) kelp forest declines observed over the past decades, understanding the causes and consequences of spatial patterns in kelp distribution in these systems is crucial from ecological and management standpoints. The present study is the first investigation of spatial patterns in the distribution of completely submerged kelp beds. Results of spatial pattern metrics demonstrate that kelp beds form an irregular seascape with patches of diverse sizes in shallow subtidal zones in the Mingan Archipelago. Modelling results show a strong correlation between kelp presence and depth, urchin density, and relative exposure to waves, but no significant effect of bottom slope or any interactions among parameters on kelp distribution. This study increases knowledge of the physical and biological factors regulating kelp distribution at a broad spatial scale and is a step forward towards a comprehensive understanding of scale-dependent processes regulating submerged kelp bed distribution. Spatial pattern metrics applied to the study of subtidal kelp ecosystems are a promising technique for monitoring these ecosystems over

extended spatial and temporal scales (e.g., years), as well as evaluating the effects of natural and anthropogenic disturbances on kelp bed distribution and recovery to better inform management practices.

4.6. ACKNOWLEDGEMENTS

We are grateful to R. Hovey, M. P. St-Pierre, B. Dumas, H. Hawk, I. Garrido, P. Bruning, C. Narvaez-Diaz, and L.E. Johnson for their help in preparing and conducting field work. We are grateful to Y. Wiersma, D. Schneider, and K. Bøe for helpful statistical discussions throughout this project. We are grateful to Y. Wiersma and J. Fisher for constructive comments on earlier versions of this manuscript. This research was funded by Natural Sciences and Engineering Research Council of Canada (NSERC Discovery Grant), Canada Foundation for Innovation (CFI-Leaders Opportunity Funds), and Research & Development Corporation of Newfoundland and Labrador (IgniteR&D) grants to P. Gagnon. A. P. St-Pierre was supported by an NSERC Post-Graduate Scholarship (PGS).

4.7. REFERENCES

- Alberto, F., Raimondi, P.T., Reed, D.C., Coelho, N.C., Leblois, R., Whitmer, A., Serrão, E.A., 2010. Habitat continuity and geographic distance predict population genetic differentiation in giant kelp. *Ecology* 91, 49-56.
- Anderson, D.R., 2007. *Model based inference in the life sciences: a primer on evidence*. Springer Science & Business Media.
- Bates, D., Maechler, M., Bolker, B., Walker, S., 2014. *lme4: Linear mixed-effects models using Eigen and S4*. R package version 1, 1-23.

- Bekkby, T., Rinde, E., Erikstad, L., Bakkestuen, V., 2009. Spatial predictive distribution modelling of the kelp species *Laminaria hyperborea*. *Ices J Mar Sci* 66, 2106-2115.
- Bender, D.J., Tischendorf, L., Fahrig, L., 2003. Using patch isolation metrics to predict animal movement in binary landscapes. *Landsc Ecol* 18, 17-39.
- Billot, C., Engel, C.R., Rousvoal, S., Kloareg, B., Valero, M., 2003. Current patterns, habitat discontinuities and population genetic structure: the case of the kelp *Laminaria digitata* in the English Channel. *Mar Ecol Prog Ser* 253, 111-121.
- Boström, C., Pittman, S.J., Simenstad, C., Kneib, R.T., 2011. Seascape ecology of coastal biogenic habitats: advances, gaps, and challenges. *Mar Ecol Prog Ser* 427, 191-217.
- Breen, P.A., Mann, K.H., 1976. Destructive grazing of kelp by sea urchins in eastern Canada. *Journal of the Fisheries Research Board of Canada* 33, 1278-1283.
- Burnham, K.P., Anderson, D.R., 2002. Model selection and multimodel inference: a practical information-theoretic approach. Springer Science & Business Media.
- Cavanaugh, K.C., Siegel, D.A., Reed, D.C., Dennison, P.E., 2011. Environmental controls of giant-kelp biomass in the Santa Barbara Channel, California. *Mar Ecol Prog Ser* 429, 1-17.
- Chapman, A.R.O., 1981. Stability of sea urchin dominated barren grounds following destructive grazing of kelp in St. Margaret's Bay, Eastern Canada. *Mar Biol* 62, 307-311.
- Congalton, R.G., Green, K., 2008. Assessing the accuracy of remotely sensed data: principles and practices. CRC press.
- Cushman, S.A., McGarigal, K., Neel, M.C., 2008. Parsimony in landscape metrics: strength, universality, and consistency. *Ecol Indic* 8, 691-703.
- Dayton, P.K., 1985a. Ecology of kelp communities. *Annu. Rev. Ecol. Syst.* 16, 215-245.
- Dayton, P.K., 1985b. The structure and regulation of some South American kelp communities. *Ecol Monogr* 55, 447-468.
- Dayton, P.K., Tegner, M.J., Parnell, P.E., Edwards, P.B., 1992. Temporal and spatial patterns of disturbance and recovery in a kelp forest community. *Ecol Monogr* 62, 421-445.
- Deza, A.A., Anderson, T.W., 2010. Habitat fragmentation, patch size, and the recruitment and abundance of kelp forest fishes. *Mar Ecol Prog Ser* 416, 229-240.
- Edwards, M.S., 2004. Estimating scale-dependency in disturbance impacts: El Niños and giant kelp forests in the northeast Pacific. *Oecologia* 138, 436-447.

- Esri, 2015. ArcGIS Desktop; Release 10.3.1, Redland, CA.
- Fassnacht, K.S., Cohen, W.B., Spies, T.A., 2006. Key issues in making and using satellite-based maps in ecology: A primer. *Forest Ecol Manag* 222, 167-181.
- Feehan, C., Scheibling, R.E., Lauzon-Guay, J., 2012. Aggregative feeding behavior in sea urchins leads to destructive grazing in a Nova Scotian kelp bed. *Mar Ecol Prog Ser* 444, 69-83.
- Filbee-Dexter, K., Feehan, C.J., Scheibling, R.E., 2016. Large-scale degradation of a kelp ecosystem in an ocean warming hotspot. *Mar Ecol Prog Ser* 543, 141-152.
- Filbee-Dexter, K., Scheibling, R.E., 2012. Hurricane-mediated defoliation of kelp beds and pulsed delivery of kelp detritus to offshore sedimentary habitats. *Mar Ecol Prog Ser* 455, 51-64.
- Filbee-Dexter, K., Scheibling, R.E., 2014. Sea urchin barrens as alternative stable states of collapsed kelp ecosystems. *Mar Ecol Prog Ser* 495, 1-25.
- Flukes, E., Johnson, C., Ling, S., 2012. Forming sea urchin barrens from the inside out: an alternative pattern of overgrazing. *Mar Ecol Prog Ser* 464, 179-194.
- Fredriksen, S., Sjøtun, K., Lein, T.E., Rueness, J., 1995. Spore dispersal in *Laminaria hyperborea* (Laminariales, Phaeophyceae). *Sarsia* 80, 47-53.
- Frey, D.L., Gagnon, P., 2015. Thermal and hydrodynamic environments mediate individual and aggregative feeding of a functionally important omnivore in reef communities. *Plos One* 10, e0118583.
- Frey, D.L., Gagnon, P., 2016. Spatial dynamics of the green sea urchin *Strongylocentrotus droebachiensis* in food-depleted habitats. *Mar Ecol Prog Ser* 552, 223-240.
- Frohn, R.C., Lopez, R.D., 2017. Remote sensing for landscape ecology: New metric indicators: monitoring, modeling, and assessment of ecosystems. CRC Press.
- Fu, B., Liang, D., Lu, N., 2011. Landscape ecology: Coupling of pattern, process, and scale. *Chin Geogr Sci* 21, 385.
- Gagnon, P., Himmelman, J.H., Johnson, L.E., 2003. Algal colonization in urchin barrens: defense by association during recruitment of the brown alga *Agarum cribrosum*. *J Exp Mar Biol Ecol* 290, 179-196.
- Gagnon, P., Himmelman, J.H., Johnson, L.E., 2004. Temporal variation in community interfaces: kelp-bed boundary dynamics adjacent to persistent urchin barrens. *Mar Biol* 144, 1191-1203.

- Gagnon, P., Johnson, L.E., Himmelman, J.H., 2005. Kelp patch dynamics in the face of intense herbivory: Stability of *Agarum clathratum* (Phaeophyta) stands and associated flora on urchin barrens. *J Phycol* 41, 498-505.
- Garcon, J.S., Grech, A., Moloney, J., Hamann, M., 2010. Relative Exposure Index: an important factor in sea turtle nesting distribution. *Aquat Conserv: Mar Freshw Ecosyst* 20, 140-149.
- Gaylord, B., Reed, D.C., Raimondi, P.T., Washburn, L., McLean, S.R., 2002. A physically based model of macroalgal spore dispersal in the wave and current-dominated nearshore. *Ecology* 83, 1239-1251.
- Gustafson, E.J., 1998. Quantifying landscape spatial pattern: what is the state of the art? *Ecosystems* 1, 143-156.
- Haines-Young, R., Chopping, M., 1996. Quantifying landscape structure: a review of landscape indices and their application to forested landscapes. *Prog Phys Geogr* 20, 418-445.
- Hayes, D.J., Sader, S.A., 2001. Comparison of change-detection techniques for monitoring tropical forest clearing and vegetation regrowth in a time series. *Photogramm Eng Rem S* 67, 1067-1075.
- Hepburn, C.D., Holborow, J.D., Wing, S.R., Frew, R.D., Hurd, C.L., 2007. Exposure to waves enhances the growth rate and nitrogen status of the giant kelp *Macrocystis pyrifera*. *Mar Ecol Prog Ser* 339, 99-108.
- Himmelman, J.H., 1991. Diving observations of subtidal communities in the northern Gulf of St. Lawrence. *Can Special Pub Fish Aquat Sci* 113, 319-332.
- Himmelman, J.H., Nédélec, H., 1990. Urchin foraging and algal survival strategies in intensely grazed communities in eastern Canada. *Can J Fish Aquat Sci* 47, 1011-1026.
- Himmelman, J.H., Steele, D.H., 1971. Foods and predators of the green sea urchin *Strongylocentrotus droebachiensis* in Newfoundland waters. *Mar Biol* 9, 315-322.
- Huntington, B.E., Karnauskas, M., Babcock, E.A., Lirman, D., 2010. Untangling natural seascape variation from marine reserve effects using a landscape approach. *Plos One* 5, e12327.
- Hurd, C.L., 2000. Water motion, marine macroalgal physiology, and production. *J Phycol* 36, 453-472.

- Irlandi, E. A., Orlando, B. A., & Ambrose Jr, W. G., 1999. Influence of seagrass habitat patch size on growth and survival of juvenile bay scallops, *Argopecten irradians concentricus* (Say). *J Exp Mar Biol Ecol*, 235(1), 21-43.
- Jackson, N.D., Fahrig, L., 2014. Landscape context affects genetic diversity at a much larger spatial extent than population abundance. *Ecology* 95, 871-881.
- Kawamata, S., 1998. Effect of wave-induced oscillatory flow on grazing by a subtidal sea urchin *Strongylocentrotus nudus* (A-Agassiz). *J Exp Mar Biol Ecol* 224, 31-48.
- Keats, D., South, G., Steele, D., 1985. Algal biomass and diversity in the upper subtidal at a pack-ice disturbed site in eastern Newfoundland. *Mar Ecol Prog Ser*, 151-158.
- Keddy, P.A., 1982. Quantifying within-lake gradients of wave energy - Interrelationships of wave energy, substrate particle-size and shoreline plants in axe lake, Ontario. *Aquat Bot* 14, 41-58.
- Kelly, M., Tuxen, K.A., Stralberg, D., 2011. Mapping changes to vegetation pattern in a restoring wetland: Finding pattern metrics that are consistent across spatial scale and time. *Ecol Indic* 11, 263-273.
- Kendall, M.S., Miller, T.J., Pittman, S.J., 2011. Patterns of scale-dependency and the influence of map resolution on the seascape ecology of reef fish. *Mar Ecol Prog Ser* 427, 259-274.
- Kimura, S., Cox, G., Carroll, J., Pengilley, S., Harmer, A., 2012. Going the distance: Use of diver propulsion units, underwater acoustic navigation, and three-way wireless communication to survey kelp forest habitats, *Diving For Science* 2012.
- Konar, B., 2000. Seasonal inhibitory effects of marine plants on sea urchins: structuring communities the algal way. *Oecologia* 125, 208-217.
- Konar, B., Edwards, M.S., Estes, J.A., 2014. Biological interactions maintain the boundaries between kelp forests and urchin barrens in the Aleutian Archipelago. *Hydrobiologia* 724, 91-107.
- Krumhansl, K.A., Okamoto, D.K., Rassweiler, A., Novak, M., Bolton, J.J., Cavanaugh, K.C., Connell, S.D., Johnson, C.R., Konar, B., Ling, S.D., Micheli, F., Norderhaug, K.M., Pérez-Matus, A., Sousa-Pinto, I., Reed, D.C., Salomon, A.K., Shears, N.T., Wernberg, T., Anderson, R.J., Barrett, N.S., Buschmann, A.H., Carr, M.H., Caselle, J.E., Derrien-Courtel, S., Edgar, G.J., Edwards, M., Estes, J.A., Goodwin, C., Kenner, M.C., Kushner, D.J., Moy, F.E., Nunn, J., Steneck, R.S., Vásquez, J., Watson, J., Witman, J.D., Byrnes, J.E.K., 2016. Global patterns of kelp forest change over the past half-century. *Proc Natl Acad Sci USA* 113, 13785-13790.

- Krumhansl, K.A., Scheibling, R.E., 2011. Detrital production in Nova Scotian kelp beds: patterns and processes. *Mar Ecol Prog Ser* 421, 67-82.
- Laur, D., Ebeling, A., Reed, D., 1986. Experimental evaluations of substrate types as barriers to sea urchin (*Strongylocentrotus* spp.) movement. *Mar Biol* 93, 209-215.
- Lauzon-Guay, J.-S., Scheibling, R.E., Barbeau, M.A., 2008. Formation and propagation of feeding fronts in benthic marine invertebrates: a modeling approach. *Ecology* 89, 3150-3162.
- Lauzon-Guay, J.S., Scheibling, R.E., 2007. Seasonal variation in movement, aggregation and destructive grazing of the green sea urchin (*Strongylocentrotus droebachiensis*) in relation to wave action and sea temperature. *Mar Biol* 151, 2109-2118.
- Lauzon-Guay, J.S., Scheibling, R.E., Barbeau, M.A., 2009. Modelling phase shifts in a rocky subtidal ecosystem. *Mar Ecol Prog Ser* 375, 25-39.
- Lecours, V., Devillers, R., Schneider, D.C., Lucieer, V.L., Brown, C.J., Edinger, E.N., 2015. Spatial scale and geographic context in benthic habitat mapping: review and future directions. *Mar Ecol Prog Ser* 535, 259-284.
- Leroux, S.J., 2019. On the prevalence of uninformative parameters in statistical models applying model selection in applied ecology. *Plos One* 14, e0206711.
- Levin, S.A., 1992. The problem of pattern and scale in ecology: the Robert H. MacArthur award lecture. *Ecology* 73, 1943-1967.
- Li, X., Jongman, R.H., Hu, Y., Bu, R., Harms, B., Bregt, A.K., He, H.S., 2005. Relationship between landscape structure metrics and wetland nutrient retention function: A case study of Liaohhe Delta, China. *Ecol Indic* 5, 339-349.
- Ling, S., Scheibling, R., Rassweiler, A., Johnson, C., Shears, N., Connell, S., Salomon, A., Norderhaug, K., Pérez-Matus, A., Hernández, J., 2015. Global regime shift dynamics of catastrophic sea urchin overgrazing. *Phil Trans R Soc B* 370, 20130269.
- Lüning, K., 1990. Seaweeds: their environment, biogeography, and ecophysiology. John Wiley & Sons.
- Maier, B., Tiede, D., Dorren, L., 2008. Characterising mountain forest structure using landscape metrics on LiDAR-based canopy surface models, Object-Based Image Analysis. Springer, pp. 625-643.
- Manson, F.J., Loneragan, N.R., Phinn, S.R., 2003. Spatial and temporal variation in distribution of mangroves in Moreton Bay, subtropical Australia: a comparison of pattern metrics and change detection analyses based on aerial photographs. *Estuar Coast Shelf Sci* 57, 653-666.

- Matte, A.L.L., Muller, S.C., Becker, F.G., 2015. Forest expansion or fragmentation? Discriminating forest fragments from natural forest patches through patch structure and spatial context metrics. *Austral Ecol* 40, 21-31.
- McGarigal, K., Cushman, S.A., Ene, E., 2012. FRAGSTATS v4: Spatial pattern analysis program for categorical and continuous maps, Computer software program produced by the authors at the University of Massachusetts, Amherst. Available at the following web site: <http://www.umass.edu/landeco/research/fragstats/fragstats.html>.
- Mcgarigal, K., Marks, B.J., 1995. Spatial pattern analysis program for quantifying landscape structure. Gen. Tech. Rep. PNW-GTR-351. US Department of Agriculture, Forest Service, Pacific Northwest Research Station, 1-122.
- Merzouk, A., Johnson, L.E., 2011. Kelp distribution in the northwest Atlantic Ocean under a changing climate. *J Exp Mar Biol Ecol* 400, 90-98.
- Moffett, K.B., Nardin, W., Silvestri, S., Wang, C., Temmerman, S., 2015. Multiple stable states and catastrophic shifts in coastal wetlands: Progress, challenges, and opportunities in validating theory using remote sensing and other methods. *Remote Sens* 7, 10184-10226.
- Moy, F.E., Christie, H., 2012. Large-scale shift from sugar kelp (*Saccharina latissima*) to ephemeral algae along the south and west coast of Norway. *Mar Biol Res* 8, 309-321.
- Muth, A.F., 2012. Effects of zoospore aggregation and substrate rugosity on kelp recruitment success. *J Phycol* 48, 1374-1379.
- Norderhaug, K.M., Christie, H., Fosså, J.H., Fredriksen, S., 2005. Fish–macrofauna interactions in a kelp (*Laminaria hyperborea*) forest. *J Mar Biol Assoc Uk* 85, 1279-1286.
- Norton, T., 1992. Dispersal by macroalgae. *Br Phycol J* 27, 293-301.
- Pedersen, M.F., Nejrup, L.B., Fredriksen, S., Christie, H., Norderhaug, K.M., 2012. Effects of wave exposure on population structure, demography, biomass and productivity of the kelp *Laminaria hyperborea*. *Mar Ecol Prog Ser* 451, 45-60.
- Pehlke, C., Bartsch, I., 2008. Changes in depth distribution and biomass of sublittoral seaweeds at Helgoland (North Sea) between 1970 and 2005. *Clim Res* 37, 135-147.
- Petraitis, P.S., Latham, R.E., 1999. The importance of scale in testing the origins of alternative community states. *Ecology* 80, 429-442.
- Pittman, S.J., 2017. Seascape ecology. John Wiley & Sons.
- Quinn, G.P., Keough, M.J., 2002. Experimental design and data analysis for biologists. Cambridge University Press.

- R Development Core Team, 2018. R: A language and environment for statistical computing. R Foundation for Statistical Computing, Vienna, Austria. URL <https://www.R-project.org/>.
- Reeves, S., Ling, S., Kriegisch, N., Johnson, C., 2015. Mechanisms of kelp bed resilience and recovery on urbanised coasts, Australian Marine Sciences Association 2015 Conference.
- Rinde, E., Christie, H., Fagerli, C.W., Bekkby, T., Gundersen, H., Norderhaug, K.M., Hjermann, D.Ø., 2014. The influence of physical factors on kelp and sea urchin distribution in previously and still grazed areas in the NE Atlantic. *Plos One* 9, e100222.
- Rinde, E., Sjøtun, K., 2005. Demographic variation in the kelp *Laminaria hyperborea* along a latitudinal gradient. *Mar Biol* 146, 1051-1062.
- Rohweder, J., Rogala, J., Johnson, B., Anderson, D., Clark, S., Chamberlin, F., Potter, D., Runyon, K., 2012. Application of wind fetch and wave models for habitat rehabilitation and enhancement projects—2012 update. US Army Corps of Engineers, Contract report.
- Romero-Berny, E.I., Acosta-Velazquez, J., Tovilla-Hernandez, C., Schmook, B., Gomez-Ortega, R., 2015. Land coverage changes and fragmentation of mangroves in the Soconusco region, Chiapas, Mexico, 1994-2011. *Rev Geogr Am Cent*, 153-169.
- Saunders, M., Metaxas, A., 2008. High recruitment of the introduced bryozoan *Membranipora membranacea* is associated with kelp bed defoliation in Nova Scotia, Canada. *Mar Ecol Prog Ser* 369, 139-151.
- Saura, S., 2002. Effects of minimum mapping unit on land cover data spatial configuration and composition. *Int J Remote Sens* 23, 4853-4880.
- Scheibling, R.E., Hennigar, A.W., Balch, T., 1999. Destructive grazing, epiphytism, and disease: the dynamics of sea urchin-kelp interactions in Nova Scotia. *Can J Fish Aquat Sci* 56, 2300-2314.
- Schneider, D.C., 2001. The rise of the concept of scale in ecology: The concept of scale is evolving from verbal expression to quantitative expression. *AIBS Bulletin* 51, 545-553.
- Sievers, K., Barr, R., Maloney, J., Driscoll, N., Anderson, T., 2016. Impact of habitat structure on fish populations in kelp forests at a seascape scale. *Mar Ecol Prog Ser* 557, 51-63.
- Simenstad, C.A., Estes, J.A., Kenyon, K.W., 1978. Aleuts, sea otters, and alternate stable-state communities. *Science* 200, 403-411.

- Sjotun, K., Fredriksen, S., 1995. Growth allocation in *Laminaria hyperborea* (Laminariales, Phaeophyceae) in relation to age and wave exposure. *Mar Ecol Prog Ser* 126, 213-222.
- St-Pierre, A.P., Gagnon, P., 2020. Kelp-bed dynamics across scales: Enhancing mapping capability with remote sensing and GIS. *J Exp Mar Biol Ecol* 522, 151246.
- Steneck, R.S., Graham, M.H., Bourque, B.J., Corbett, D., Erlandson, J.M., Estes, J.A., Tegner, M.J., 2002. Kelp forest ecosystems: biodiversity, stability, resilience and future. *Environ Conserv* 29, 436-459.
- Steneck, R.S., Leland, A., McNaught, D.C., Vavrinec, J., 2013. Ecosystem flips, locks, and feedbacks: The lasting effects of fisheries on Maine's kelp forest ecosystem. *Bull Mar Sci* 89, 31-55.
- Svendsen, P., Kain, J.M., 1971. The taxonomic status, distribution, and morphology of *Laminaria cucullata* Sensus Jorde and Klavestad. *Sarsia* 46, 1-22.
- Tegner, M., Dayton, P., 2000. Ecosystem effects of fishing in kelp forest communities. *ICES J Mar Sci; J du Conseil* 57, 579-589.
- Thomsen, M.S., Wernberg, T., Kendrick, G.A., 2004. The effect of thallus size, life stage, aggregation, wave exposure and substratum conditions on the forces required to break or dislodge the small kelp *Ecklonia radiata*. *Bot Mar* 47, 454-460.
- Turner, M.G., Gardner, R.H., O'Neill, R.V., 2001. *Landscape ecology in theory and practice: patterns and process*. EUA: Springer.
- Turner, M.G., O'Neill, R.V., Gardner, R.H., Milne, B.T., 1989. Effects of changing spatial scale on the analysis of landscape pattern. *Landsc Ecol* 3, 153-162.
- U.S. Army Corps of Engineers, 1984. *Shore Protection Manual*. Coastal Engineering Research Center, Fort Belvoir, Va.
- Uuemaa, E., Mander, Ü., Marja, R., 2013. Trends in the use of landscape spatial metrics as landscape indicators: A review. *Ecol Indic* 28, 100-106.
- Van Rein, H., Brown, C., Quinn, R., Breen, J., 2009. A review of sublittoral monitoring methods in temperate waters: a focus on scale. *Underwat Technol* 28, 99-113.
- Velimirov, B., Griffiths, C., 1979. Wave-induced kelp movement and its importance for community structure. *Bot Mar* 22, 169-172.
- Wedding, L.M., Lepczyk, C.A., Pittman, S.J., Friedlander, A.M., Jorgensen, S., 2011. Quantifying seascape structure: extending terrestrial spatial pattern metrics to the marine realm. *Mar Ecol Prog Ser* 427, 219-232.

- Welham, S.J., Gezan, S.A., Clark, S., Mead, A., 2015. Statistical methods in biology: Design and analysis of experiments and regression. Chapman and Hall/CRC.
- Wright, J.T., Dworjanyn, S.A., Rogers, C.N., Steinberg, P.D., Williamson, J.E., Poore, A.G.B., 2005. Density-dependent sea urchin grazing: differential removal of species, changes in community composition and alternative community states. *Mar Ecol Prog Ser* 298, 143-156.

CHAPTER V

Kelp-bed dynamics across scales: Stability and drivers of kelp distribution patterns over broad spatiotemporal scales

5.1. ABSTRACT

Drivers of stability and change in benthic systems operate at multiple spatiotemporal scales. In submerged kelp bed systems, most studies to date have been limited to fine spatiotemporal scales due to the scuba-based monitoring techniques applied, which limits our understanding of the occurrence and drivers of broader patterns. The present study applies remote sensing and landscape ecology approaches to investigate spatial configuration and persistence of kelp beds over broad spatial (km²) and temporal (decades) extents in the Mingan Archipelago (Gulf of St. Lawrence, Canada). Aerial imagery covering 2.85 km² of shallow (<7 m) seabed surrounding five islands was acquired every five to 11 years between 1983 and 2016 (six sampling years in total). The imagery was visually classified and divided into two benthic classes based on cover type: kelp and non-kelp. Spatial pattern metrics were used to quantify the spatial characteristics of kelp beds in each of the six years studied (including kelp coverage, number of kelp patches, mean patch area, and largest patch index) and to examine the correlations between these metrics and atmospheric or oceanographic conditions. Results showed that kelp cover increased from 1999 to 2016 and that harsh oceanographic conditions in late winter to spring (e.g., long ice-covered season, high North Atlantic Oscillation index) lead to a decrease in kelp cover, smaller mean patch size, and increased number of patches. The distribution of kelp-covered areas was relatively stable over time, with 75% of the total area exhibiting two changes in cover type or less over the entire study period. Analysis of the effects of depth, bottom slope, and exposure to waves on the persistence of kelp beds and variability in cover type showed a significant effect of depth only, indicating that shallow seabed withstands fewer changes in cover type over time compared to deeper areas and that kelp beds

persisting through time are found in shallow areas. The present study offers a novel, broad-scale perspective of the variability in distribution patterns of completely submerged kelp beds in the northern Gulf of St. Lawrence and the drivers of long-term stability in kelp-urchin systems.

5.2. INTRODUCTION

Understanding the biotic and abiotic drivers of species distribution is necessary to predict shifts in community structure and ecosystem functioning (Boulangeat et al., 2012; Leach et al., 2016; Meier et al., 2010). Given that biological and environmental processes regulating species distribution are scale-dependent (Schneider, 2009; Turner et al., 1989), investigations of species distribution patterns should encompass various spatial and temporal scales (Hobbs, 2003; Lecours et al., 2015). However, technical limitations often dictate the scale at which studies are conducted, leading to sporadic and spatially limited sampling (Lecours et al., 2015; Wheatley and Johnson, 2009). This is especially true in marine benthic studies where data gathering is generally costly and time consuming (e.g., when applying scuba techniques). Yet, quantifying temporal trends in species distribution across broad spatial (km^2 to 10s of km^2) and temporal (multiple years) extents is essential to assess the stability and resilience of marine systems and to build strong inferences of the impacts of changing environmental conditions on benthic communities (Magurran et al., 2010; Reed et al., 2015; Thrush et al., 2009). This is particularly important to predict change in systems where alternate stable states exist, because state shifts lead to dramatic changes in biological composition, productivity, and ecosystem services (Beisner et al., 2003; Moffett et al., 2015; Petraitis and Latham, 1999).

In cold-water shallow rocky reef environments, kelp-urchin systems are generally considered as candidates for alternate stable states (Filbee-Dexter and Scheibling, 2014; Konar and Estes, 2003; Simenstad et al., 1978; Steneck et al., 2013). In these systems, large-scale shifts may occur between two states: 1) a kelp bed state, characterized by the spatial dominance of large brown seaweed (Laminariales) creating structurally complex, productive, and biodiverse habitats, and 2) an urchin barren state in which the benthic floor is mostly devoid of erect fleshy macroalgae, is dominated by sea urchins, and presents relatively lower habitat complexity and biodiversity (reviewed in Filbee-Dexter and Scheibling, 2014). In a recent meta-analysis of regional and global trends in kelp abundances over the past half-century, Krumhansl et al. (2016) examined worldwide ecoregions where kelp occurs and identified that 38% of these ecoregions showed declines in kelp populations, 27% showed increases, and 35% showed no detectable changes. These changes in kelp distribution have various causes and, in some cases, were linked to large-scale shifts between kelp bed and urchin barren states (Krumhansl et al., 2016 and references within). However, Krumhansl et al. (2016) observed a high degree of variability in the direction and magnitude of kelp distribution changes among and within ecoregions. Because of this variability, these authors suggest that kelp dynamics are strongly influenced by local stressors (i.e., affecting specific sites or regions, such as pollution, harvesting, competition with invasive species, or variations in urchin densities) rather than global drivers. Yet, because of the poor spatial and temporal resolution of the available data in many ecoregions, estimates of kelp distribution changes calculated by Krumhansl et al. (2016) may not reflect drivers of kelp change at relevant scales.

In eastern Canada and northern Europe, sea urchin densities are the main driver of kelp distribution at the metre scale (Gagnon et al., 2004; Lauzon-Guay and Scheibling, 2007a) and variations in urchin density can lead to state shifts between urchin-dominated and kelp-dominated states (Lauzon-Guay et al., 2009; Steneck et al., 2002). In addition, environmental factors such as ice scouring (Gagnon et al., 2004; Keats et al., 1985), wave action (Bekkby et al., 2009; Frey and Gagnon, 2015), and temperature (Fredersdorf et al., 2009; Fredriksen et al., 1995) have also been shown to modulate kelp distribution. However, assessments of kelp distribution patterns in these systems have been limited to small spatial (few 100s m² at most) and temporal (<5 years) extents given the limitations of scuba sampling techniques generally used to monitor kelp beds (e.g., Frey and Gagnon, 2015; Gagnon et al., 2004; Lauzon-Guay and Scheibling, 2007b). Correlations between environmental factors and kelp distribution patterns at broader spatiotemporal scales remain largely unexplored yet necessary to gain a clearer understanding of scale-dependent processes modulating kelp bed stability and distribution patterns (Edwards, 2004).

Approaches relying on remote sensing and landscape ecology are increasingly used to address multiscale questions pertaining to the spatial configuration, drivers, and persistence of species distribution patterns (Boström et al., 2011; Uuemaa et al., 2013). In particular, spatial pattern metrics are routinely applied in terrestrial systems to quantify the spatial arrangement and connectivity of habitat patches over broad spatial extents from maps or remotely sensed imagery (Turner et al., 2001). The use of spatial pattern metrics is rising in marine seascape studies as they provide a suitable approach to quantify seascape configuration, monitor temporal changes, and explore correlations between the spatial configuration of habitats and environmental conditions through space and time (Boström

et al., 2011; Wedding et al., 2011). For kelp-urchin systems, such approaches present an opportunity to identify drivers of stability and change in kelp distribution patterns and test the tenets of alternate stable states theory at spatiotemporal scales unattainable through traditional (scuba-based) monitoring techniques.

The kelp-urchin system in the Mingan Archipelago (northern Gulf of St. Lawrence) is an ideal study system for the investigation of the temporal stability and spatial configuration of kelp beds over broad (km²) expanses of seabed. A mainly dichotomous division of the seabed is observed in this system, with mixed kelp beds near coastlines and green sea urchin (*Strongylocentrotus droebachiensis*) barrens extending from the edge of kelp beds to >15 m (Chapters 2 & 3, Gagnon et al., 2004; Gagnon et al., 2005). Because of this and the generally clear water column, kelp beds can be easily identified using remote sensing techniques. Indeed, a companion study conducted in this area demonstrated that completely submerged shallow (<7 m) kelp beds can be accurately detected and mapped by applying a visual classification technique to aerial imagery, yielding 90% overall accuracy (St-Pierre and Gagnon, 2020). From the precise kelp distribution map thus created, the spatial configuration of kelp beds can then be assessed using spatial pattern metrics. These techniques have been applied successfully to quantify spatial patterns in the distribution of kelp in the Mingan Archipelago from aerial imagery obtained at a single occasion (Chapter IV). By applying the same proven techniques to a time-series of aerial imagery, it becomes possible to investigate the stability of kelp beds and their resilience to changing environmental conditions. Hence, the availability of a time-series of aerial images encompassing the shallow subtidal zone of several islands of the Mingan Archipelago (acquired in part by Parks Canada's surveys of coastline erosion in this area) dating back

to 1983 provides a unique opportunity to quantify the stability of kelp beds in this region over several decades. In addition, sound knowledge of the factors modulating kelp distribution at the metre scale within the Mingan Archipelago over short time periods (<3 years, Gagnon et al., 2004; Gagnon et al., 2005) allows for strong comparison of the patterns and drivers of kelp distribution across scales.

The present study is the first to apply approaches based on remote sensing and landscape ecology to monitor submerged kelp bed dynamics with both the fine spatial resolution and broad spatiotemporal coverage necessary to assess the stability of kelp systems beyond current knowledge. Using aerial imagery from the Mingan Archipelago between 1983 and 2016 (six sampling occasions in total), the first aim of this study is to assess correlations between kelp distribution patterns and environmental conditions. Kelp distribution was measured at each sampling occasion by calculating spatial pattern metrics quantifying the proportional abundance, shape, area, and clustering of kelp beds. An exploratory analysis of the correlations between these metrics and atmospheric or oceanographic conditions was conducted to identify potential drivers of kelp distribution patterns. The second aim of this study is to quantify the temporal stability of kelp beds and to measure the relative influence of physical site characteristics (depth, bottom slope, and exposure to waves) on kelp bed persistence by applying model comparison techniques.

5.3. MATERIAL AND METHODS

5.3.1. Study site

The Mingan Archipelago consists of a chain of ~20 islands and 1000 islets scattered over >150 km along the north shore of the Gulf of St. Lawrence (Québec, Canada). This

study focuses on five islands from the western portion of the archipelago, spread over a longitudinal distance of ~14 km: Île Niapiskau (westernmost), Île à Firmin, Île du Havre, Île aux Goélands, and Petite île au Marteau (easternmost; Figure 1). A summary description of the study site is presented below, with more details in Chapter IV. The Mingan Archipelago was chosen for the present study due to 1) the reasonable knowledge of kelp dynamics at the metre scale in this region from previous studies (Gagnon et al., 2004; Gagnon et al., 2005; Himmelman, 1991) offering a basis for comparison of broader scale studies; and 2) the availability of high-resolution aerial imagery acquired in that region every five to 11 years since 1983 (see section 5.3.2), in part by Parks Canada for coastal erosion monitoring. In the Mingan Archipelago, kelp beds are more abundant on the islands' generally south-facing shores (i.e., exposed to the open waters of the Gulf of St. Lawrence), in shallow (0-7 m) subtidal zones (Gagnon et al., 2004). Because the objective of the present study was to examine the factors driving kelp distribution in areas where kelp beds dominate, the study area was confined to the 0-7 m depth zone on the south-facing shores of the five islands mentioned above to focus the sampling effort in areas where kelp beds presence is most probable (Figure 5.1). Boulders and bedrock are the main substrate types throughout the study area, with sporadic patches of cobbles, gravel, or sand.

Two subtidal communities dominate the shallow (0-7 m) nearshore zone: 1) mixed kelp beds, mainly of *Alaria esculenta* but often including *Laminaria digitata*, *Saccharina longicuris*, *Agarum cribosum*, and *Saccorhiza dermatodea*, and 2) green sea urchin (*Strongylocentrotus droebachiensis*) barrens extending from the edge of kelp beds to >15 m. The transition between kelp beds and barrens is generally clearly defined because

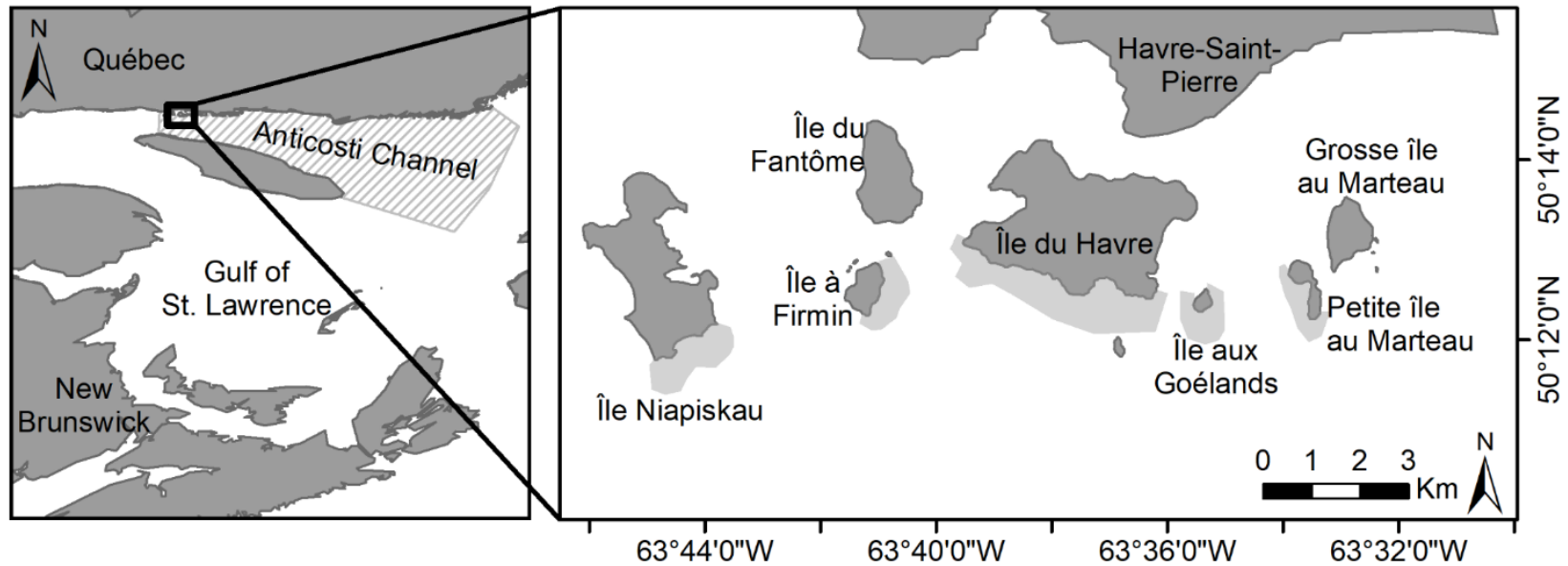


Figure 5.1 General location of the western sector of the Mingan Archipelago (boxed) within the Gulf of St. Lawrence (eastern Canada) and of the Anticosti Channel oceanographic region (hatched) as defined by Galbraith et al. (2017). The enlarged area shows the location of the study area (shaded subtidal areas) at Île Niapiskau, Île à Firmin, Île du Havre, Île aux Goélands, and Petite île au Marteau.

of aggregations of green sea urchins (called grazing fronts) at the lower edge of kelp beds which destructively graze upon kelp, leaving behind barren areas. Because this sharp transition can be identified on aerial imagery, the study area can easily be divided into two benthic classes, i.e., kelp and non-kelp benthic classes, using a simple image classification technique (see below and St-Pierre and Gagnon, 2020).

5.3.2. Acquisition, pre-processing, and classification of aerial imagery

The aerial imagery used to monitor the distribution of kelp in shallow (< 7 m) areas of the Mingan Archipelago was acquired at 6 occasions since 1983. The imagery was acquired over a single day during summer (early July to early August) in 1983, 1988, 1999, 2004, 2009, and 2016. The imagery consisted of scan-digitized black and white aerial photograph obtained from a plane flying at an altitude of ~1550 m (1983, 1988, and 1999, provided by Parks Canada), color digital photographs obtained with a hand-held camera from a helicopter flying at an altitude of ~300 m (2004 and 2016), and panchromatic digital images acquired with a plane flying at an altitude of ~4175 m (2009, provided by Parks Canada). All imagery was acquired on cloudless, windless days. Pixel size and the area covered by a single photograph varied among photographs and years (8 cm to 1 m, and 0.08 km² to ~14 km², respectively). Although color images were available for some sampling years, all imagery was converted to black and white using the Grayscale function in ArcMap 10.3.1 (Esri, 2015) to avoid potential classification discrepancies between black and white and color pictures. Imagery from each year was georectified, mosaicked, resampled to 1-m pixels, and trimmed to discard all areas outside the target 0-7 m depth range following the procedures and rationale detailed in St-Pierre and Gagnon (2020).

In a companion study, St-Pierre and Gagnon (2020) demonstrated that visual classification of aerial imagery was the most accurate method for the detection of shallow (<7 m) subtidal kelp beds, yielding an overall accuracy of 90%. Hence, the same proven visual classification method was applied here. Essentially, a sampling grid with intersects spaced at 15-m intervals was overlaid on top of each mosaic of aerial images. A trained observer examined the 225-m² area (15 x 15 m) surrounding each grid intersect and assigned it to either of two benthic classes: 1) “kelp”, if over 50% of it was covered by kelp, or 2) “non-kelp”, if less than 50% of it was covered by kelp. If over 50% of the area surrounding a grid intersect was outside the limit of the study area, the grid intersect was discarded. Only grid intersects visible on the imagery from all six years were retained for further analysis, yielding a total of 10,308 grid intersects each year. The grid was overlaid in the exact same position on top of each mosaic to ensure that a given grid intersect covered the same area of the seabed at each collection. Potential misclassification of non-kelp seaweed (e.g., *Desmarestia viridis*) as kelp beds is considered to be negligible (discussed in St-Pierre and Gagnon, 2020). All classifications were conducted by the same observer to ensure consistency.

As this visual classification method relies on the ability of an observer to identify kelp and non-kelp benthic classes on imagery, the observer was trained to differentiate these two benthic classes based on their visual characteristics by comparing locations covered by and devoid of kelp identified from ground truth data acquired in 2016 (detailed in St-Pierre and Gagnon, 2020). Preliminary analyses confirmed that an observer trained to recognize kelp from color imagery obtains a similar accuracy when classifying black and white imagery (Appendix 5.A, section 1). In addition, preliminary analyses confirmed that

the knowledge gained by an observer trained to recognize kelp beds on aerial imagery from a single year can accurately classify (1) imagery from a nearby area acquired in the same year but for which ground truth data was not used during the observer's training (Appendix 5.A, section 2), and (2) imagery from the same area acquired in different years for which ground truth data was not used in the training process (Appendix 5.A, section 3).

5.3.3. Spatial pattern metrics and correlations with oceanographic and atmospheric conditions

To assess variation in the spatial characteristics of kelp and non-kelp benthic classes over time, spatial pattern metrics were calculated using the software FRAGSTATS version 4 (McGarigal et al., 2012). For this analysis, "patch" refers to a discrete, contiguous landscape element, such as a distinct entity identified as either kelp or non-kelp during image classification. The seven metrics selected for analysis are: 1) percentage of seabed covered by the benthic class (in %), 2) largest patch index (in %), 3) patch area (in m²), 4) number of patches, 5) shape index (unitless), 6) mean Euclidean nearest neighbour distance (in m), and 7) clumpiness index (unitless). Further details pertaining to these metrics are presented in Chapter IV. The metrics chosen for this analysis form a parsimonious and complementary combination which describes the geometric characteristics and spatial arrangement of patches of either cover type, while minimizing redundancy between metrics (Cushman et al., 2008). Metrics were calculated separately for each year sampled. For metrics calculations within FRAGSTATS, the eight-neighbour rule was applied, and the borders of the mosaicked photographs do not represent true boundaries between patches created by biological communities. Background pixels with no value were considered as

no data and thus were ignored in calculations (McGarigal et al., 2012). Spatial pattern metrics were calculated for both the kelp and the non-kelp benthic classes; however, since the emphasis of this study is on kelp distribution patterns, results pertaining to the non-kelp benthic class are not discussed but are appended (Appendix 5.B).

To study the relationships between the spatial distribution of kelp beds each year and variations in oceanographic and atmospheric conditions, each metric was plotted against physical oceanographic data obtained from long-term data series. In this exploratory analysis, the oceanographic and atmospheric parameters studied included: 1) monthly and seasonal averages of sea surface temperature for the summer months (May to September, i.e., period during which urchin grazing on kelp is high); 2) the number of weeks with sea surface temperature above 10°C (considered warmer than average for the region); 3) maximum ice volume and anomalies in ice volume (relative to the 1981–2010 climatology; Galbraith et al., 2017); 4) first and last day of ice occurrence; 5) duration of the ice season (in days); 6) sum of standardized anomalies in sea surface temperature (relative to the 1981–2010 climatology; Galbraith et al., 2017); and 7) North Atlantic Oscillation (NAO) index calculated over different time periods (yearly, spring, and winter indices). These oceanographic and atmospheric parameters were chosen because they may influence various aspects of kelp's life cycle. For instance, kelp growth is modulated by changes in temperature, light availability, and salinity arising from variations in sea temperature and ice cover because they can affect cell physiology and photosynthesis (Fredersdorf et al., 2009). Sea temperature may also influence urchin grazing, especially in summer when these grazers are more active, and indirectly affect kelp distribution (Frey and Gagnon, 2015; Lauzon-Guay and Scheibling, 2007b). Physical damages to kelp sporophytes can be

inflicted by strong, repeated storm events or ice scouring, which can degrade kelp blades or forcibly detach holdfasts (Keats et al., 1985). Increased water movement, such as that created by waves and storms, can also yield higher release and dispersal of zoospores than calm conditions in some kelp species (Gordon and Brawley, 2004; Reed et al., 1988). Changes in current strengths, temperature, and salinity may also influence propagule dispersal and survival (Fredriksen et al., 1995). While correlations with water turbidity and phytoplankton concentrations would have been of interest for the present study, these data were not available for the study area over all six collection dates and were therefore not included in analyses. Further details regarding these parameters and their source are provided in Table 5.1. When possible, data reported for the Anticosti Channel was used as it encloses the study sites (Figure 5.1). For parameters where data specific to the Anticosti Channel was unavailable, data averaged over the Gulf of St. Lawrence was used (Table 5.1). The oceanographic and atmospheric conditions were quantified for the year of image acquisition (i.e., 1983, 1988, 1999, 2004, 2009, and 2016, up to the date of image acquisition each year), as well as one year prior to image acquisition (i.e., 1982, 1987, 1998, 2003, 2008, and 2015) to investigate potential temporally-lagged effects of these parameters on kelp distribution, for example if extreme weather events could have a long-term effect on kelp distribution. Correlations between each spatial pattern metric and each oceanographic or atmospheric parameter were examined separately for data acquired during the year of image acquisition and the years prior to acquisition. All correlations were assessed by calculating Pearson's coefficient of correlation and p -value ($\alpha=0.05$). Only statistically significant correlations are described below and presented graphically, but results for all correlations tested are presented in Appendix 5.C.

Table 5.1 Environmental parameters assessed for their correlation with spatial pattern metrics. “C” indicates that the data was acquired concurrent to the year of imagery acquisition (i.e., 1983, 1988, 1999, 2004, 2009, 2016). “P” indicates data acquired for the year preceding image acquisition (i.e., 1982, 1987, 1998, 2003, 2008, 2015). The North Atlantic Oscillation (NAO) index used for averaging consists of monthly values calculated by the National Oceanic and Atmospheric Administration (NOAA) using a station-based definition based on pressure differences between Lisbon (Portugal) and Reykjavik (Iceland). Further details regarding the calculation of this index can be found on NOAA’s Climate Prediction Center website: <https://www.cpc.ncep.noaa.gov/data/teledoc/nao.shtml>.

Environmental parameter	Time of acquisition	Description	Data source
Sea surface temperature (SST)			
May average	C, P	Monthly average SST for the month of May calculated via Advanced Very High Resolution Radiometer (AVHRR) remote sensing, or from buoy data for 1983 (AVHRR data not available) for the Anticosti Channel region.	Galbraith et al. (2017); DFO (2018)
June average	C, P	Monthly average SST for the month of June calculated via AVHRR satellite images or from buoy data for 1983 (AVHRR data not available) for the Anticosti Channel region.	Galbraith et al. (2017); DFO (2018)
July average	C, P	Monthly average SST for the month of July calculated via AVHRR satellite images or from buoy data for 1983 (AVHRR data not available) for the Anticosti Channel region.	Galbraith et al. (2017); DFO (2018)
August average	P	Monthly average SST for the month of August calculated via AVHRR satellite images or from buoy data for 1983 (AVHRR data not available) for the Anticosti Channel region.	Galbraith et al. (2017); DFO (2018)
September average	P	Monthly average SST for the month of September calculated via AVHRR satellite images or from buoy data for 1983 (AVHRR data not available) for the Anticosti Channel region.	Galbraith et al. (2017); DFO (2018)

May to July average	C, P	SST averaged from May to July, based on values from the Anticosti Channel calculated via AVHRR satellite images or from buoy data for 1983 (AVHRR data not available) for the Anticosti Channel region.	Galbraith et al. (2017); DFO (2018)
Number of weeks above 10°C	P	Number of weeks with SST above 10°C each year, calculated for the Anticosti Channel region.	Galbraith et al. (2017); DFO (2018)
Sum of standardized anomalies in sea surface temperature	C, P	Composite sea-surface temperature index measuring the overall state of the system (positive and negative values representing warm and cold conditions, respectively), calculated for the Gulf of St. Lawrence. Anomalies are calculated relative to the 1985–2010 climatology.	Galbraith et al. (2017); DFO (2018)
Ice cover			
Anomaly in ice volume	C, P	Normalized anomalies in ice volume, i.e., deviation from the 1981-2010 average, calculated for the Gulf of St. Lawrence.	Galbraith et al. (2017)
Maximum ice volume	C, P	Maximum volume of ice recorded.	Galbraith et al. (2017)
Date of first ice occurrence	C, P	First day of ice occurrence in Julian days, with minimum threshold being 5% of the largest ice volume ever recorded in the Anticosti Channel region.	Galbraith et al. (2017)

Date of last ice occurrence	C, P	Last day of ice occurrence in Julian days, with minimum threshold being 5% of the largest ice volume ever recorded in the Anticosti Channel region.	Galbraith et al. (2017)
Duration of ice season	C, P	Number of days during which ice was present, i.e., when a threshold of 5% of the largest ice volume ever recorded was exceeded in the Anticosti Channel region.	Galbraith et al. (2017)
North Atlantic Oscillation (NAO) index			
Yearly	C, P	Averaged for the 12 months before image acquisition (August to July).	NOAA (2018)
Spring	C, P	Averaged for the 4 months before image acquisition (April to July).	NOAA (2018)
Winter	C, P	Averaged for the winter before image acquisition (December to March).	NOAA (2018)

5.3.4. Effects of site characteristics on the stability of kelp bed distribution

Kelp stability and cover type variability indices

Two indices were used to assess the effects of site characteristics (depth, bottom slope, and exposure to waves, see below) on the distribution of kelp beds over time. First, a kelp stability index (KSI) was calculated based on the presence or absence of kelp at each grid intersect on the aerial imagery of each year. Each intersect in each year received a value of 1 if classified as “kelp” and a value of 0 if classified as “non-kelp” (see Section 5.3.2). The KSI was calculated as the sum of the value given a grid intersect in each year, such that a sum of 6 indicated the presence of a temporally stable kelp bed (i.e., kelp beds were present in all six years studied) and 0 indicated the presence of a temporally stable non-kelp area (i.e., kelp beds were absent in all six years studied). Intermediate values (1 to 5) indicated that the cover type had changed over time at least once. The KSI indicates where kelp beds tend to be found repeatedly (i.e., over several collections), and helps identify areas of temporally stable persistent kelp beds, but provides little information on the frequency at which benthic cover type changed. For example, a KSI of 3 for a given grid intersect could indicate that kelp was present for the first three collection years and absent for the last three collections (i.e., one change in cover types between the 3rd and 4th collections), but could also mean that kelp was present every other collection year, thus changing cover type between each collection (i.e., five changes in cover type). To assess this variation, the cover type variability index (CTVI) was calculated by counting the number of times that the cover type identified in one grid intersect changed between one year and the subsequent year studied. A change in cover type between one studied year and the next was given a value of 1 and the absence of change was given a value of 0. Thus, a

CTVI of 0 indicated that no changes in cover type occurred for a given grid intersect over the studied time period, while a value of 5 indicated that the cover type change between each pair of successive years studied (i.e., between 1983 and 1988, between 1988 and 1999, between 1999 and 2004, between 2004 and 2009, and between 2009 and 2016). These two indices allowed the identification of areas where kelp beds tend to be more present and temporally stable, as well as areas where kelp may be present frequently but where cover type vary among collection years. The length of the gap between collection years was not included in the indices, as it was not mathematically possible to do so while keeping the indices' outcome interpretable and biologically meaningful.

Site characteristics

The KSI and CTVI were used in statistical analyses to assess the effects of depth, slope, and exposure to wave action on each index separately. These three site characteristics were chosen because they do not change over time and are known to directly or indirectly affect kelp growth and urchin grazing at small (m to 10s of m) spatial scales (de Bettignies et al., 2013; Frey and Gagnon, 2015; Lauzon-Guay and Scheibling, 2007b; Reed et al., 2011). Hence, it was hypothesized that their effect may also occur at broader scales. Depth, bottom slope (in degrees, 0 to 90°), and a relative exposure index (REI) were calculated for each grid intersect following the procedures outlined in Chapter IV. Essentially, values of depth and bottom slope were obtained from a bathymetric map and averaged over the 225-m² area around a given grid intersect. Relative exposure index (REI) was calculated for each grid intersect by applying the procedure outlined by Garcon et al. (2010) and detailed in Chapter IV. This index combines mean wind velocity, direction, and effective fetch by

applying the following equation (Fonseca and Bell, 1998; Garcon et al., 2010; Keddy, 1982):

$$REI = \sum_{i=1}^{16} (V \cdot P_i \cdot F_i)$$

where i is the i^{th} of 16 compass headings, V is the mean wind velocity in $\text{m}\cdot\text{s}^{-1}$, P_i is the wind direction frequency (%), and F_i is the effective fetch in kilometres. Mean wind velocity and wind direction frequency were calculated based on daily wind reading at Havre Saint Pierre Airport (~10 km north of the study area) recorded during the 12 months before image acquisition in 1988, 1999, 2004, 2009, and 2016. Effective fetch (F), defined as the distance from a site to the nearest wave-obstructing obstacle (U.S. Army Corps of Engineers, 1984), was calculated along each of 16 compass directions (i.e., 1 to 16 compass headings, from N, NNE, NE, etc. in 22.5° increments from 0 to 360°) for each grid intersect.

Statistical analysis

The KSI, CTVI, and site characteristics were calculated for each grid intersect individually. However, it was not possible to use the data at this resolution for statistical analyses due to technical difficulties, including strong deviations from statistical assumptions (mainly normality of residuals and independence) arising despite the use of correct generalized linear models and spatial autocorrelation structures as determined from graphical inspection of the models' residuals and semi-variograms. These difficulties likely stemmed from the high level of similarity between adjacent grid intersects. To bypass this problem, the data were aggregated into larger units (see below) subsequently used for analyses, which allowed the models to better fit assumptions. Data aggregation was done

by grouping grid intersects using a regular grid of square polygons of 45 m width. This size of squares for aggregation was chosen because it yielded at least 100 square units per islands which were then used for analysis (1145 squares in total, with 115, 157, 611, 137, and 125 squares at Île Niapiskau, Île à Firmin, Île du Havre, Île aux Goélands, and Petite île au Marteau, respectively) and consistently had nine grid intersects within each square (except at the edges of the study area, see below). The values of KSI, CTVI, depth, slope, and REI for each square unit were obtained by averaging the values from each grid intersect within a square. Only the average value of the square unit was used for statistical analysis. Due to the irregular shape of the study area, fewer grid intersects were sometimes present in squares at the edges of the study area. To avoid biases at the edges of the study area caused by variation in the number of grid intersects used for averaging, only squares containing more than five grid intersects were used in analyses.

A mixed model approach was applied to examine whether KSI and CTVI are influenced by depth, bottom slope, and exposure to waves (estimated by the REI). A series of linear mixed models (LMM) were fitted to the KSI and CTVI data separately, with a combination of these three site characteristics as fixed effects, “Island” as a random effect (categorical factor with five levels; referring to the study area of which island the grid intersect is situated), and an exponential correlation structure. This correlation structure was included in the models to account for spatial autocorrelation between nearby squares. With an exponential correlation structure, the correlation between any two data points (in this case, any two square units) is assumed to decrease exponentially with increasing distance between the data points. This correlation structure was chosen as it corresponded to that observed in semi-variograms obtained from the raw data. All possible combinations

of the three site characteristics as explanatory variables (both additive and multiplicative interactions) were used to construct and compare a total of 14 models (Tables 5.2 and 5.3). Akaike's information criterion (AIC) was calculated for each model and used to select the most informative model. AIC is an estimate of model fit which accounts for model complexity by applying penalties based on the number of factors present in a model (Burnham and Anderson, 2002). AIC differences (Δ_i) were calculated as the difference between the AIC value of a given model (i.e., model i) and the lowest AIC value obtained among all models. The best fitting model was selected as the most parsimonious out of those with a $\Delta_i < 2$, because models with less than $\Delta_i < 2$ have substantial support (Anderson, 2007) and are considered not meaningfully different from each other, indicating the presence of pretending variables (Burnham and Anderson, 2002; Leroux, 2019). All LMMs were fitted in R 3.3.2 (R Development Core Team, 2018) using the functions `lme` in the 'nlme' package (Bates et al., 2014). Residuals of the best fitting model were examined graphically for normality, independence, and homogeneity of variances, and did not display any violations of these assumptions. Because of the large difference in range of values among the three explanatory variables, all explanatory variables were rescaled prior to running LMMs and model selection. Scaling consisted of subtracting the explanatory variable's median from each original value (centering) and dividing by the standard deviation. Applying this scaling and centering method allowed the coefficient estimates (i.e., slope coefficients) to be directly comparable, thus enabling comparisons in the magnitude of the effect of each explanatory variable (Welham et al., 2015).

Table 5.2. Outcome of model selection for the Kelp Stability Index (KSI). AIC_i is the value of the Akaike Information Criterion (AIC) calculated for model i , and Δ_i is the difference between the AIC of the best fitting model and that of model i . Value of k represents the number of parameters in each model. $\text{Exp}(-0.5\Delta_i)$ represents the relative likelihood of model i , and w_i represents the Akaike weights. The “+” symbol indicates additive effects, while the “*” symbol indicates interactive effects among model factors. Model 1 (bold) was selected as the most informative model and used for subsequent analyses, because it is the most parsimonious among models with $\Delta_i < 2$. REI refers to the relative exposure index (see Section 5.3.4).

Model number	Fixed factors	k	AIC_i	Δ_i	$\text{Exp}(-0.5\Delta_i)$	w_i
01	Depth	5	3101.38	0.00	1.00	0.72
04	Depth + REI	6	3105.35	3.97	0.14	0.10
12	REI * Slope + Depth	8	3106.16	4.78	0.09	0.07
05	Depth + Slope	6	3106.65	5.27	0.07	0.05
07	Depth * REI	7	3108.26	6.88	0.03	0.02
08	Depth * Slope	7	3108.45	7.06	0.03	0.02
11	Depth * REI * Slope	11	3109.90	8.52	0.01	0.01
10	Depth + REI + Slope	7	3110.63	9.25	0.01	0.01
13	Depth * Slope + REI	8	3112.36	10.98	0.00	0.00
14	Depth * REI + Slope	8	3113.61	12.23	0.00	0.00
03	Slope	5	3235.12	133.74	0.00	0.00
09	REI * Slope	7	3237.31	135.93	0.00	0.00
06	REI + Slope	6	3238.85	137.46	0.00	0.00
02	REI	5	3240.34	138.96	0.00	0.00

Table 5.3. Outcome of model selection for the Cover Type Variability Index (CTVI). AIC_i is the value of the Akaike Information Criterion (AIC) calculated for model i , and Δ_i is the difference between the AIC of the best fitting model and that of model i . Value of k represents the number of parameters in each model. $\text{Exp}(-0.5\Delta_i)$ represents the relative likelihood of model i , and w_i represents the Akaike weights. The “+” symbol indicates additive effects, while the “*” symbol indicates interactive effects among model factors. Model 1 (bold) was selected as the most informative model and used for subsequent analyses, because it is the most parsimonious among models with $\Delta_i < 2$.

Model number	Fixed factors in each model	k	AIC_i	Δ_i	$\text{Exp}(-0.5\Delta_i)$	w_i
01	Depth	5	2529.92	0.00	1.00	0.61
04	Depth + REI	6	2531.39	1.48	0.48	0.29
05	Depth + Slope	6	2535.36	5.44	0.07	0.04
07	Depth * REI	7	2537.01	7.10	0.03	0.02
10	Depth + REI + Slope	7	2537.2	7.31	0.03	0.02
02	REI	5	2537.53	7.62	0.02	0.01
03	Slope	5	2538.45	8.53	0.01	0.01
06	REI + Slope	6	2540.54	10.63	0.01	0.00
12	REI * Slope + Depth	8	2541.53	11.61	0.00	0.00
08	Depth * Slope	7	2541.63	11.72	0.00	0.00
14	Depth * REI + Slope	8	2542.91	12.99	0.00	0.00
13	Depth * Slope + REI	8	2543.60	13.68	0.00	0.00
09	REI * Slope	7	2544.84	14.92	0.00	0.00
11	Depth * REI * Slope	11	2559.04	29.12	0.00	0.00

5.4. RESULTS

5.4.1. Overview of spatial pattern metrics

Kelp coverage across the study area varied among years, from a minimum of 44% in 1983 to a maximum of 62% in 2016 (Table 5.4). Maps of kelp presence for each of the six years studied are presented in Appendix 5.D. Kelp coverage showed an increase over four consecutive sampling occasions since 1999. The amount of change in kelp coverage (in %) was calculated for each possible pair of images; it ranged from a decrease of 11% (between 1988 and 2016) and an increase of 18% (between 1983 and 2016), but no significant correlation was observed between the number of years between two images and the change in kelp coverage (Pearson's $r = 0.08$, p -value = 0.774; Figure 5.2). Largest patch indices for the kelp benthic class showed strong variations among years, with a low of 10% observed in 1988 and a high of 31% in 2016 (Table 5.4). Kelp patch area varied considerably within and among years; the lowest mean patch area was observed in 1988 with $10,710 \pm 3043$ (SE) m^2 , while the highest mean patch area was observed in 2016 with $32,130 \pm 16,670$ m^2 (Table 5.4). Years 1983 and 1988 were characterized by small, numerous kelp patches, as opposed to the larger, fewer kelp patches observed from 1999 to 2016, particularly in the latter (Table 5.4). Shape indices, mean nearest neighbour distance, and clumpiness indices calculated for the kelp benthic class showed little variation among years (Table 5.4).

5.4.2. Correlation between spatial pattern metrics and environmental parameters

Assessment of the correlations between spatial pattern metrics calculated for the kelp benthic class and environmental parameters from the same year as image acquisition

Table 5.4. Outcome of the spatial pattern metrics calculated for the kelp benthic class on imagery from each of the six years studied. Mean values are presented with standard error (\pm SE).

Year	Percent cover (%)	Largest patch index (%)	Patch area (m ²)			Number of patches	Mean shape index	Mean nearest neighbour distance (m)	Clumpiness index
			Min.	Mean	Max.				
1983	44.19	15.37	225	13,665 \pm 5443	356,400	75	1.59 \pm 0.10	40.56 \pm 1.81	0.65
1988	52.18	10.28	225	10,710 \pm 3043	238,500	113	1.55 \pm 0.10	36.10 \pm 1.20	0.50
1999	48.39	11.42	225	22,006 \pm 7553	264,825	51	1.89 \pm 0.18	42.26 \pm 2.85	0.59
2004	52.33	21.26	225	20,228 \pm 8901	492,975	60	1.65 \pm 0.14	42.67 \pm 2.40	0.63
2009	59.43	30.76	225	24,182 \pm 12,872	713,475	57	1.64 \pm 0.13	38.67 \pm 2.27	0.63
2016	62.34	31.14	225	32,130 \pm 16,670	722,250	45	1.64 \pm 0.19	42.23 \pm 2.91	0.61

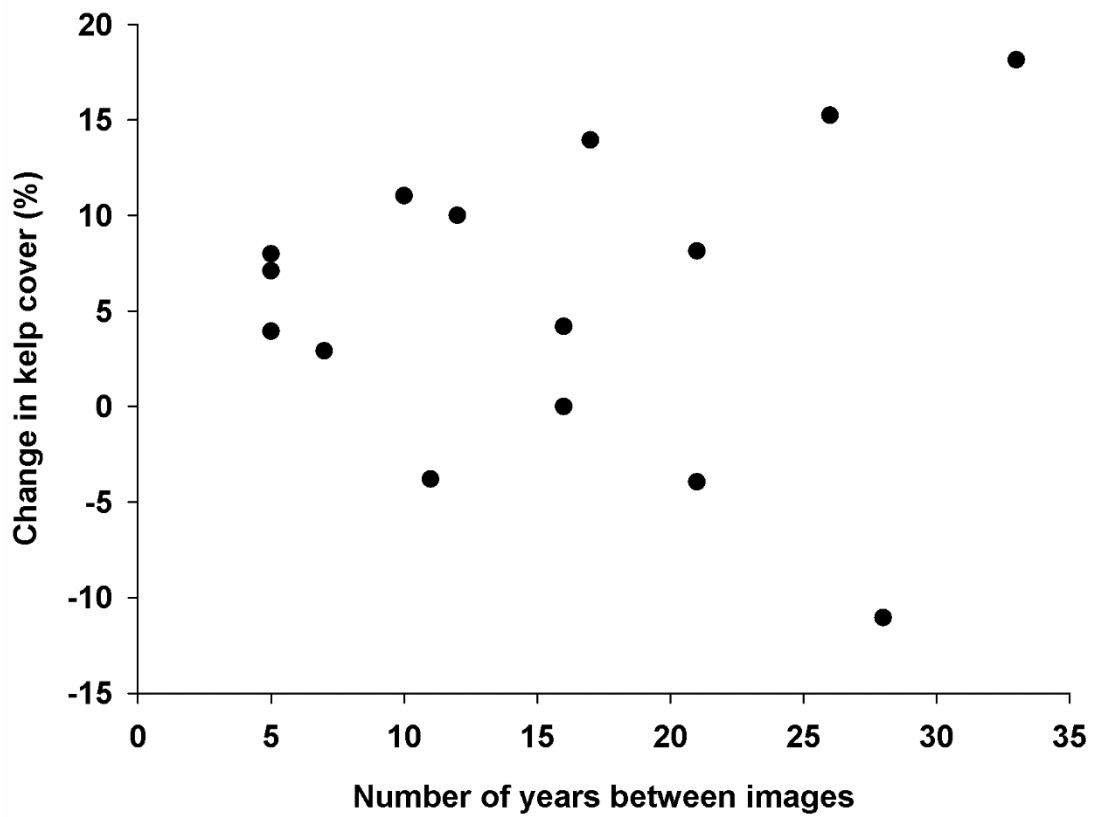


Figure 5.2. Relationship between the amount of change in kelp cover (in %) for each possible pair of images and the number of years between collection date of the images.

indicated six correlations as statistically significant (Table 5.D.1, Figure 5.3). Several spatial pattern metrics were correlated with the spring NAO indices, ice conditions, and sea surface temperature. Kelp percent coverage was negatively correlated with NAO indices calculated for the spring (April to July; Pearson's $r = -0.868$, $p = 0.025$ Table 5.D.1, Figure 5.3A), indicating that kelp coverage decreases after periods of increased storm frequency and colder temperatures characteristic of high NAO indices. Ice coverage had a significant impact on the number and size of kelp patch, as mean kelp patch area was negatively correlated with the duration of the ice-covered season (Pearson's $r = -0.866$, $p = 0.026$ Table 5.D.1, Figure 5.3B) and the number of kelp patches was positively correlated with the date of last ice occurrence (Pearson's $r = 0.840$, $p = 0.036$ Table 5.D.1, Figure 5.3C). Shape indices were positively correlated with the sum of standardized anomalies in surface temperature (Pearson's $r = 0.878$, $p = 0.022$ Table 5.D.1, Figure 5.3D), indicating that warm conditions are correlated with more complex patch shapes, and clumpiness indices were positively correlated with the average sea surface temperature measured in July (Pearson's $r = 0.818$, $p = 0.047$ Table 5. D.1, Figure 5.3E). Although mean nearest neighbour distance between kelp patches was significantly correlated with the date of last ice occurrence (Pearson's $r = -0.882$, $p = 0.020$ Table 5.D.1), this correlation was not further investigated nor presented graphically because values calculated for mean nearest neighbour distance were very low and stable temporally (from 36.10 ± 1.20 m to 42.67 ± 2.40 m) thus variations in mean nearest neighbour distance are likely of little biological significance.

Assessment of the relationships between spatial pattern metrics calculated for the kelp benthic class and oceanographic or atmospheric parameters from the year prior to

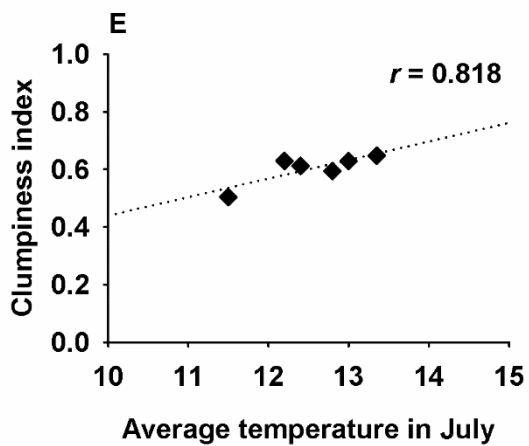
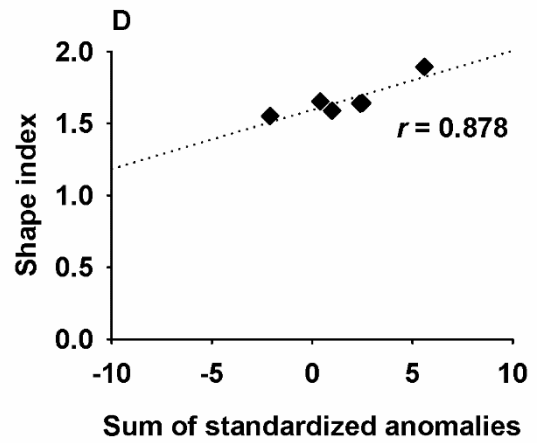
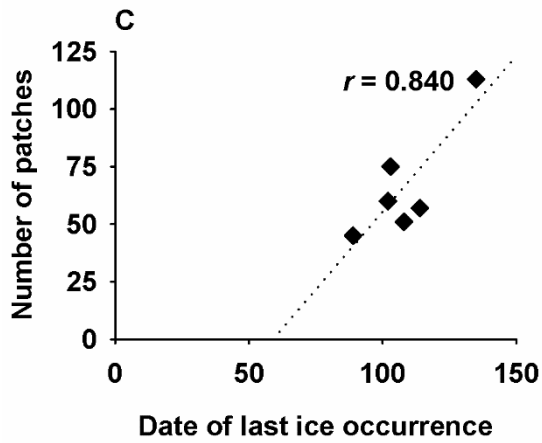
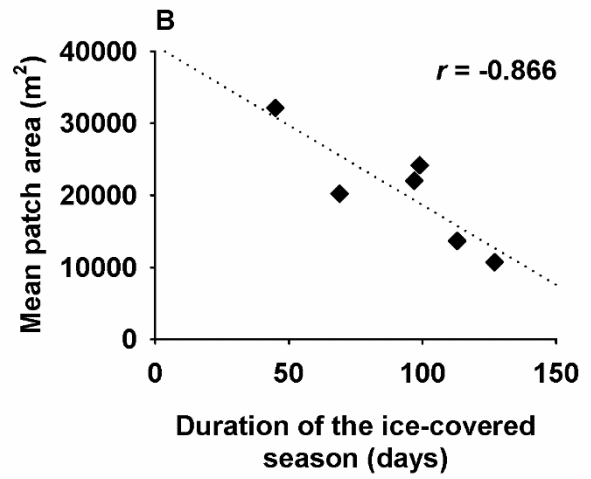
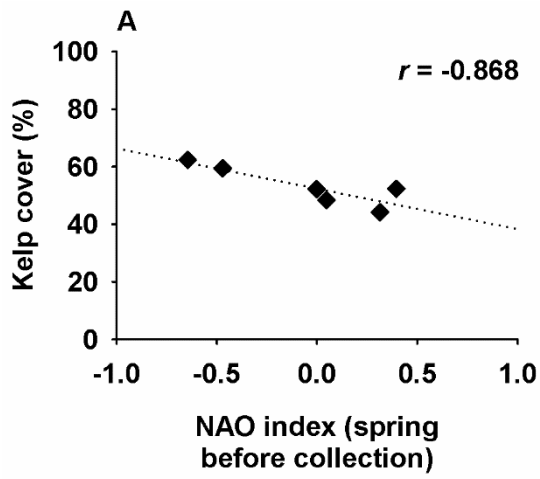


Figure 5.3. Relationships between spatial pattern metrics calculated for the kelp benthic class and environmental parameters measured in the same years as the collections occurred. Only statistically significant correlations are shown ($p < 0.05$, see Appendix C, Table 5.C.1). Pearson correlation coefficient (r) is indicated for each correlation ($n = 6$). NAO index refers to the North Atlantic Oscillation Index (see Section 5.3.3).

image acquisition identified five statistically significant correlations (Table 5.D.2, Figure 5.4). In this analysis, sea surface temperature, the NAO index, and ice coverage were identified as factors modulating kelp distribution. Sea surface temperature was correlated to several metrics; kelp percent coverage and largest patch indices for kelp were positively correlated with average August sea surface temperature calculated in the year prior to image acquisition (Pearson's $r = 0.921$, $p = 0.026$ and Pearson's $r = 0.981$, $p = 0.003$, respectively, Table 5.D.2, Figure 5.4A and 5.4B), while mean kelp patch area was positively correlated with average September sea surface temperature calculated in the year prior to image acquisition (Pearson's $r = 0.877$, $p = 0.022$ Table 5.D.2, Figure 5.4C). Mean kelp patch area was also correlated with the NAO indices for the spring (April to July) in the year prior to image acquisition (Pearson's $r = 0.816$, $p = 0.048$ Table 5.D.2, Figure 5.4D). Number of kelp patches was negatively correlated with the date of first ice occurrence (Pearson's $r = -0.869$, $p = 0.025$ Table 5.D.2, Figure 5.4E).

5.4.3. KSI and CTVI distributions

Of the 10,308 grid intersects classified, 17% had a Kelp Stability Index (KSI) of 6, indicating that a given grid intersect was classified as a kelp-covered in all six years studied, while 15% had a KSI of 0, indicating that a given grid intersect was classified as non-kelp in all six years studied (Figures 5.5 and 5.6). KSI shows variation both among islands and within the study area of each island. At three of the five islands studied (Île Niapiskau, Île à Firmin, and Petite île au Marteau), high KSI values tend to be found near the coastline while lower values are found in deeper areas away from shore (Figure 5.5). This trend was less clear at Île du Havre and Île aux Goélands, where KSI values appear to be distributed

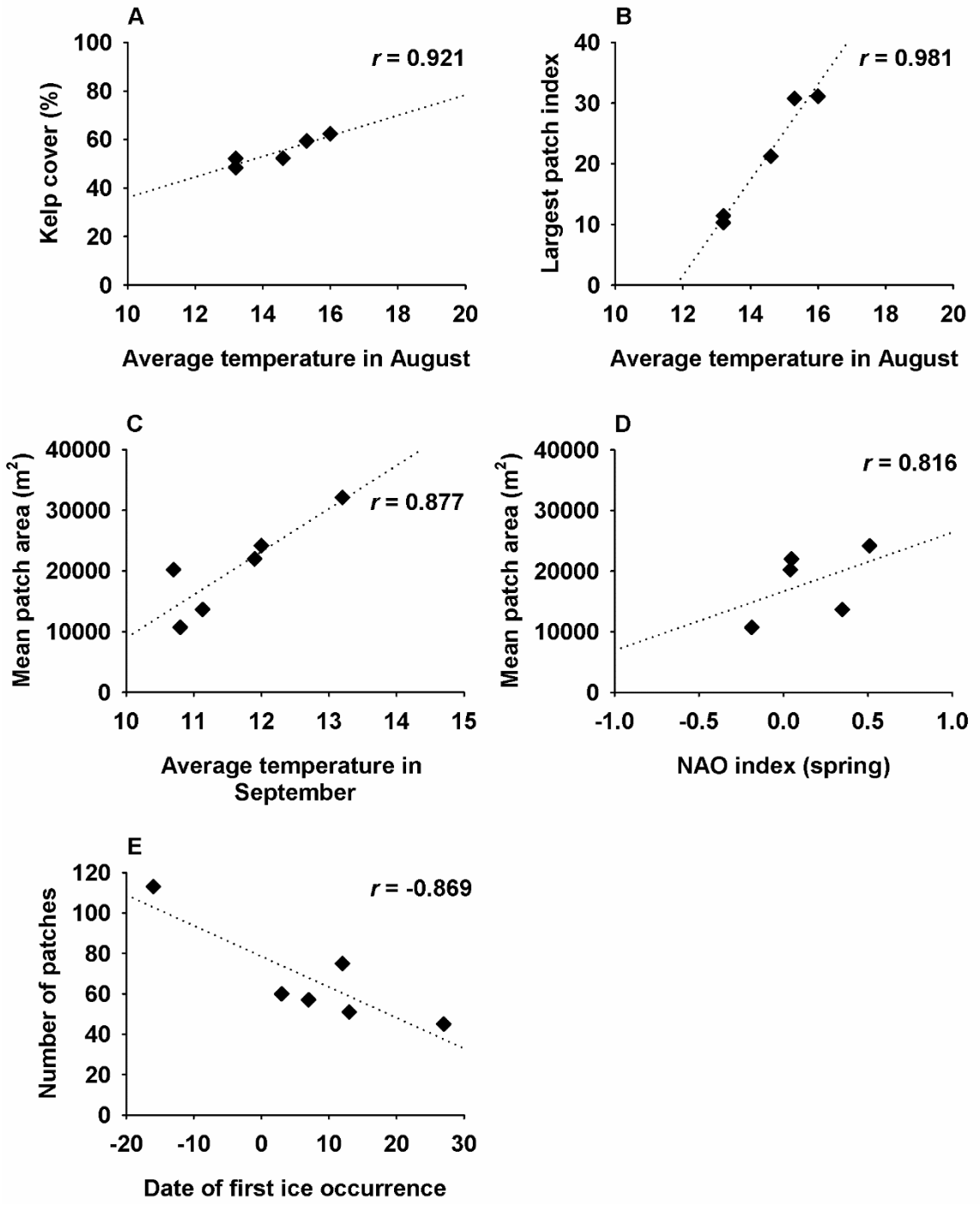
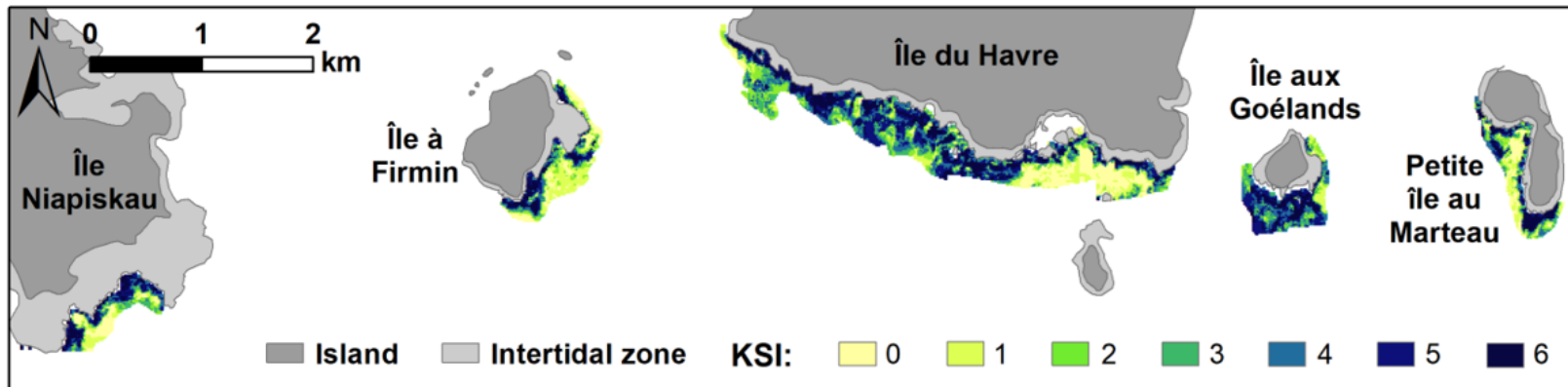


Figure 5.4. Relationships between spatial pattern metrics calculated for the kelp benthic class and environmental parameters measured in the year prior to each collection occurring. Only statistically significant correlations are shown ($p < 0.05$, see Appendix 5.C, Table 5.C.2). Pearson correlation coefficient (r) is indicated for each correlation. ($n = 6$, except for panel B where $n = 5$). NAO index refers to the North Atlantic Oscillation Index (see Section 5.3.3).

A) Kelp Stability Index (KSI)



B) Cover Type Variability Index (CTVI)

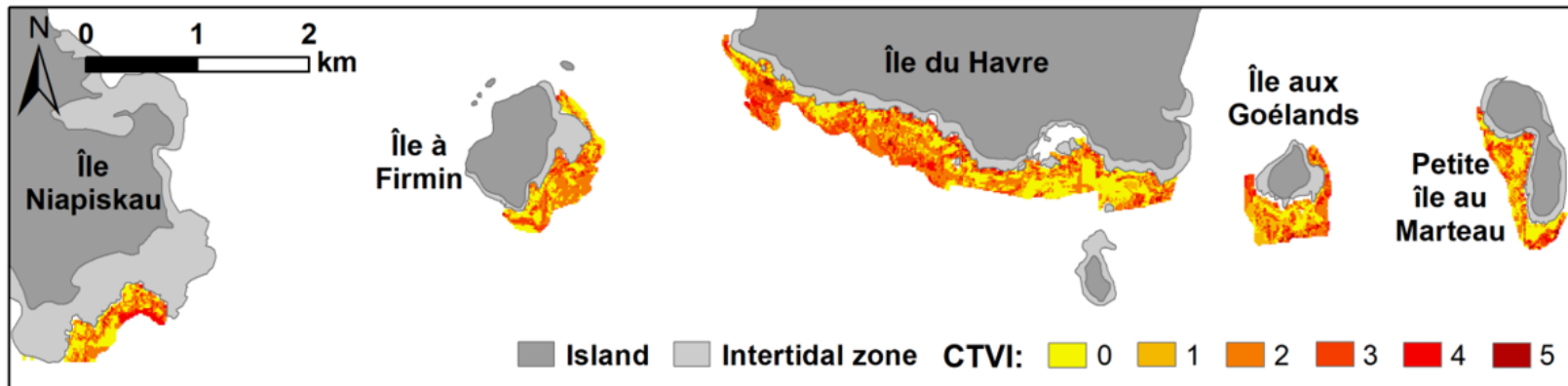


Figure 5.5. Panel A: Spatial distribution of the Kelp Stability Index (KSI) values across the study area. KSI was calculated as the sum of the presence/absence values from each grid intersect on the imagery from each year, such that a value of 6 indicated the presence of a temporally stable kelp bed (i.e., kelp beds were present in all six years studied) and 0 indicated the presence of a temporally stable non-kelp area (i.e., kelp beds were absent in all six years studied). Intermediate values indicated that the cover type had changed over time at least once (see Section 5.3.4). **Panel B:** Spatial distribution of the Cover Type Variability Index (CTVI) values across the study area. CTVI was calculated by counting the number of times that the cover type identified in one grid intersect changed between one year and the subsequent year studied. Thus, a CTVI of 0 indicates that no changes in cover type occurred for a given grid intersect over the studied time period, while a value of 5 indicates that the cover type changed between each pair of successive years studied (see Section 5.3.4).

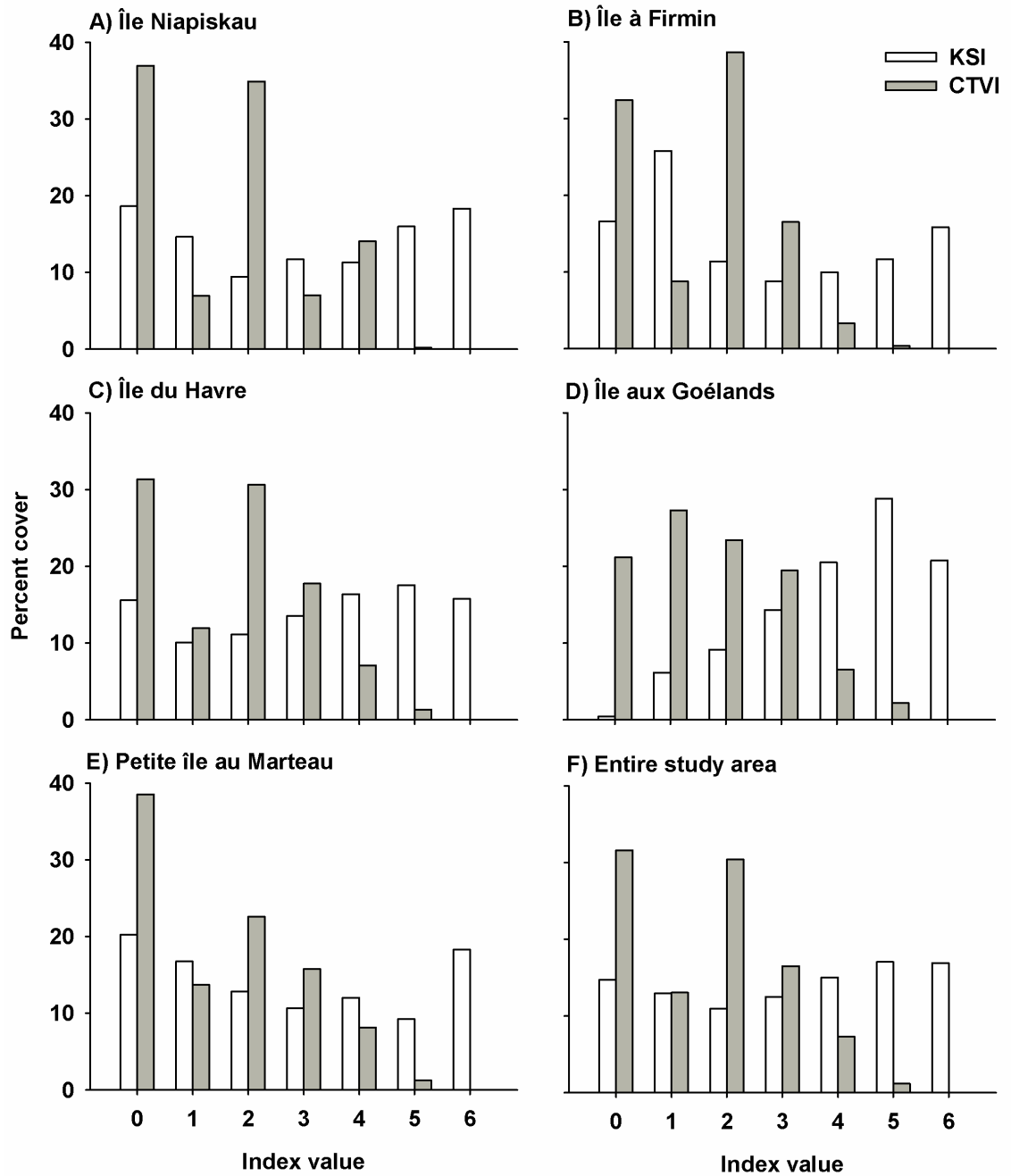


Figure 5.6. Percent cover of each value of the Kelp Stability Index (KSI) and Cover Type Variability Index (CTVI) for each island and for the study area as a whole. Note that the KSI values range from 0 to 6, while the CTVI values range from 0 to 5 (see Section 5.3.4 and Figure 5.5 for details regarding these two indices).

more evenly across the depth range. All possible KSI values (0 to 6) were present in similar proportions across the entire study area, with each possible value covering 10 to 17% of the seabed (Figure 5.6F). KSI values were also present in similar proportion at Île Niapiskau, Île du Havre, and Petite île au Marteau (Figure 5.6A, C, and E). In contrast, low KSI values (KSI = 1) were more frequent at Île à Firmin (covering 26% of the seabed at this island, Figure 5.6B), while high KSI values (KSI = 5 or 6) were more frequent Île aux Goélands (covering 29 and 21% of the seabed at this island, respectively, Figure 5.6D).

Inspection of the Cover Type Stability Indices (CTVI) showed that 45% of the study area presented a low variation in cover type over time (CTVI = 0 or 1), while 8% presented high variation (CTVI = 4 or 5; Figures 5.5 and 5.6). Across the entire study area, CTVI values of 0 were the most frequent as they covered 32% of the seabed, while CTVI values of 5 were the least frequent, covering 1% of the seabed (Figure 5.6). Trends in the spatial distribution of the CTVI values are difficult to distinguish visually on the map (Figure 5.5). CTVI values of 0 and 2 were the most frequently observed at all islands (covering between 23 and 36% of the seabed), except at Île aux Goélands where CTVI values of 1 were the most frequent (covering 27% of the seabed) followed by CTVI values of 2 and 0 (covering 23 and 21% of the seabed, respectively).

5.4.4. Model selection

Results from model selection applied to the Kelp Stability Index (KSI) data indicated that Model 01, which only includes depth as fixed factor, was the most informative model (Table 5.2). Coefficient estimate from this model showed that KSI decreases by 0.62 for every increase of 1 m in depth. (Table 5.5). Hence, the KSI

Table 5.5. Coefficient estimates for Model 01, which only contained the variable Depth (selected as the most informative by comparison of Akaike’s Information Criterion (AIC); see Table 5.3 and 5.5 and Section 5.3.4), applied to Kelp Stability Index (KSI) and to the Cover Type Variability Index (CTVI). As the data was scaled prior to analyses, both the scaled and back-transformed coefficients are presented, with 95% confidence intervals (CI).

Exploratory variable	Scaled coefficient			Standard deviation of initial data	Back-transformed coefficient		
	Estimate	Lower 95% CI	Upper 95% CI		Estimate	Lower 95% CI	Upper 95% CI
<i>KSI</i>							
Intercept	3.44	2.94	3.94	NA	NA	NA	NA
Depth	-1.13	-1.31	-0.95	1.83 m	-0.62	-0.72	-0.52
<i>CTVI</i>							
Intercept	1.65	1.49	1.81	NA	NA	NA	NA
Depth	0.19	0.09	0.28	1.83 m	0.10	0.05	0.15

is inversely related to depth, meaning that kelp beds persisting through time (high KSI) are found at shallow depths while non-kelp areas persisting through time (low KSI) are in deeper areas.

Results from the model selection applied to the Cover Type Variability Index (CTVI) data indicated that Model 01, which only includes depth as fixed factor, was the most informative model (Table 5.3). Coefficient estimate from this model showed that CTVI increases by 0.10 for every increase of 1 m in depth. (Table 5.5). Hence, the CTVI is positively related to depth, meaning that areas of shallow depth generally withstand fewer changes in cover type over time (low CTVI) compared to deeper areas where changes are more frequent (high CTVI).

5.5. DISCUSSION

Recognition of the concept of scale in ecology has led to the identification of scale-dependent biological and environmental processes regulating species distribution in numerous ecosystems (Lecours et al., 2015; Levin, 1992; Schneider, 2001). Yet, identifying these scale-dependent processes remains a challenge in ecological studies as technical limitations often force a trade-off in data collection between the spatial scale at which studies are conducted, and the accuracy and precision of the data acquired (Brennan et al., 2002; Lecours et al., 2015; Wheatley and Johnson, 2009). New perspectives into the scale-dependency of processes driving species distribution can be gained either by the adoption of multiscale approaches or by exploring species-environment relationships at scales generally overlooked in a given system.

The present study addresses the lack of broad-scale information regarding the distribution patterns of submerged kelp beds by applying landscape ecology approaches rather than the restrictive traditional scuba-based monitoring methods generally used in such systems. By using archival aerial imagery and GIS techniques to monitor kelp bed distribution in the Mingan Archipelago (northern Gulf of St. Lawrence, Canada) over the course of 33 years, this study revealed patterns in kelp bed spatial distribution at an unprecedented spatiotemporal scale. Overall, significant correlations were detected between oceanographic conditions measured in late winter and spring and the spatial configuration of kelp beds (namely kelp coverage, patch size, and patch number). Over time, an increase in kelp bed coverage was observed from 1999 to 2016. In addition, examination of the Kelp Stability Index (KSI) and Cover Type Variability Index (CTVI) showed that the distribution of kelp-covered areas is temporally stable, with only 8% of the study area exhibiting a highly variable cover type. These two indices are modulated by depth but not by bottom slope nor exposure to waves.

Effects of environmental conditions on kelp distribution patterns

In eastern Canada, kelp sporophytes are perennial and beds are known to withstand canopy loss in late summer and fall, followed by recruitment during winter and bed expansion during the following cold months until late spring (DFO, 2013; Krumhansl and Scheibling, 2011; Scheibling et al., 1999). Results from the present study suggest that environmental conditions measured in winter and late spring drive kelp bed configuration observed in summer. Indeed, positive North Atlantic Oscillation (NAO) indices in late spring (April to July), which cause increased storm frequency and colder temperatures in

eastern Canada (Hurrell, 1995), as well as long-lasting ice cover lead to decreased kelp coverage and smaller, numerous kelp patches. Ice scouring and high wave action (e.g., caused by storms), can abrade kelp sporophytes and make them more vulnerable to breakage, detachment from the substratum, and canopy loss (Castorani et al., 2018; Filbee-Dexter and Scheibling, 2012; Keats et al., 1985). Increased damage to kelp sporophytes during periods of high storm frequency (i.e., high NAO index) causing sporadic increases in wave action, and long ice-covered season would explain the decreased kelp coverage and more fragmented seascape observed during summer. In addition, light attenuation caused by the presence of ice may provide sub-optimal growth conditions. Although kelp are well adapted to low-light conditions, growth and survival respond to changes in light availability (Sjøtun et al., 2006) and may be negatively affected by prolonged light limitations under thick, long-lasting ice (Dunton, 1985; Gendron, 1989; Krause-Jensen et al., 2012). A similar effect of ice coverage on kelp distribution has been observed in Greenland, where the duration of the ice-free period is a strong predictor of the latitudinal gradient in Arctic kelp production and depth expansion (Krause-Jensen et al., 2012). Changes to climatic conditions and ice regimes are expected to affect kelp survival and distribution in several Arctic regions (reviewed in Filbee-Dexter et al., 2019) and may have similar effects in temperate areas such as the Mingan Archipelago where kelp distribution is also linked to ice cover.

Late-winter and spring conditions measured one year prior to image acquisition (15 to 18 months before) showed no correlation with kelp distribution. However, sea surface temperature in late summer (August and September, i.e., 11 to 12 months prior to image acquisition) was correlated with increases in kelp coverage, mean patch area, and largest

patch index measured in summer almost a year later. This result is counterintuitive given that high water temperature slow kelp growth and induce natural senescence in some kelp species; for example, *A. esculenta*, which is abundant at the study site, undergo natural senescence at temperature of 16-17°C (Fredersdorf et al., 2009; Munda and Lüning, 1977). Based on this relationship, decreases in kelp coverage following episodes of high temperature were expected. Yet, one indirect mechanism by which late summer temperature may modulate kelp distribution patterns is through the regulation of its grazer's activity. The green sea urchin, *Strongylocentrotus droebachiensis*, is a major consumer of kelp in eastern Canada (Gagnon et al., 2004; Scheibling et al., 1999), whose grazing activity is regulated by water temperature (Frey and Gagnon, 2015; Lauzon-Guay and Scheibling, 2007b). Indeed, Frey and Gagnon (2015) showed that grazing increases with temperature but drops markedly above a threshold of 12-15°C in a population of urchins in eastern Newfoundland where summer temperature generally peaks at ~16°C in summer (Chapter 1; Blain and Gagnon, 2013), similar to temperatures in the Mingan Archipelago (Galbraith et al., 2017; Himmelman et al., 2008). Hence, it is hypothesized that decreased grazing pressure from urchins under high late summer temperatures may leave a higher number of kelp sporophytes un-grazed, allowing for greater expansion of kelp beds through the winter and yielding the observed high kelp coverage and large patch sizes the following summer.

Correlations presented here show a strong relationship between summer kelp distribution patterns over a broad spatial extent (km²) and oceanographic conditions during winter and spring months. These results suggest that oceanographic conditions have a direct effect on kelp distribution rather than an indirect effect derived from the modulation of urchin grazing pressure because urchins are least active in winter and spring due to cold

temperatures and increased wave action (Chapter II; Frey and Gagnon, 2015). Similar effects of large-scale oceanographic conditions have been described in the Pacific, where El Niño events and the North Pacific Gyre Oscillations modulate the distribution and biomass of giant kelp (*Macrocystis pyrifera*) over broad spatial extents (10s to 100s of km²) and decadal time scales by regulating wave disturbance and nutrient availability (Bell et al., 2015; Cavanaugh et al., 2011; Edwards, 2004).

Comparison of the results from metre-scale studies taking place in the Mingan Archipelago which identified urchin grazing as the main driver of kelp presence (Gagnon et al., 2003; Gagnon et al., 2004; Gagnon et al., 2005) and the kilometre-scale patterns observed in the present study may suggest that biological drivers (i.e., urchin grazing) regulate small-scale distribution of kelp while oceanographic conditions affect large-scale kelp distribution patterns. However, the link between water temperature, urchin grazing, and changes in large-scale kelp distribution patterns described above contradicts this idea and suggests that overlooking the links between direct, local effects (e.g., grazing) and indirect, large-scale effects (effect of temperature on grazing) may lead to a simplistic interpretation. Further investigation of scale-dependency in the effects of biotic and abiotic drivers are needed to fully comprehend their relative contribution to kelp distribution patterns, for example by investigating the effects of harsh winter conditions (especially the presence and movement of the ice cover) on kelp growth and recruitment at the metre scale, or by assessing the correlations between kelp distribution patterns and changes in urchin populations over broad spatial scales.

Drivers of kelp bed stability

Two indices were used in the present study to examine kelp distribution over time: 1) the Kelp Stability Index (KSI) which identifies where kelp beds are found repeatedly (i.e., over several collections), and 2) the Cover Type Variability Index (CTVI) which calculates the number of changes in cover type among collections (see section 5.3.4 for details). Examination of these indices showed that 45% of the study area presented a stable cover type through time (i.e., cover type changing once or less). Kelp beds in the Mingan Archipelago were more temporally persistent in shallower parts of the study area (higher KSI) whereas the cover type is more variable in deep areas (CTVI increases with depth). This is consistent with a previous study (Chapter IV) which showed depth as the most important factor explaining kelp presence at broad spatial scale (km²) in the Mingan Archipelago. This trend in kelp persistence may be caused by greater light availability in shallow water favoring kelp growth or by higher wave action and water flow near the surface limiting the activity and grazing of sea urchins. Indeed, urchin movement and feeding are deterred by seaweed motion created by high water flows or intense wave action (Himmelman and Steele, 1971; Konar, 2000; Velimirov and Griffiths, 1979), suggesting that modulation of kelp distribution by urchin grazing is limited to the deeper, more wave-protected edges of kelp beds (Gagnon et al., 2004; Ling et al., 2015; Scheibling et al., 1999). Surprisingly, exposure to wave action and bottom slope, which affect hydrodynamic conditions and urchin grazing (Frey and Gagnon, 2015; Lauzon-Guay and Scheibling, 2007b), were not found to impact the KSI or CTVI. While high exposure to wave action generally provides kelp with a refuge from grazing pressure compared to more sheltered sites (Hepburn et al., 2007; Pedersen et al., 2012; Rinde et al., 2014; Sivertsen, 1997), the

present study shows that small variations in exposure and bottom slope have little effect on the long-term persistence of kelp beds along exposed shorelines.

The presence of more persistent kelp beds at shallow depth suggests that sporadic disturbance from ice scouring occurring near the surface has less weight on regulating the temporal persistence of kelp beds than continued urchin grazing occurring at greater depths. As spore dispersal is limited to short distances in most kelp species (Fredriksen et al., 1995; Norton, 1992), these persistent kelp patches in shallow water may be an important source of spores maintaining recruitment in nearby deeper areas where cover type varies over time. Further studies are needed to quantify the contribution of these shallow persistent kelp patches to recruitment in nearby kelp-devoid areas.

Kelp coverage in the Mingan Archipelago changed by <8% between consecutive sampling years. A gradual increase in kelp coverage was observed from 1999 to 2016 (from 48 to 62%). This finding is consistent with those of Krumhansl et al. (2016) who estimated that kelp bed coverage is either stable or increasing for the Gulf of St. Lawrence ecoregion (although this estimate was based on metre-scale experimental data only). The local increase in kelp coverage observed here contrasts with trends in nearby regions of Nova Scotia (89% average decrease in kelp canopy cover since 1982; Filbee-Dexter et al., 2016) and the Gulf of Maine (shifts to filamentous and turf algae between mid-1990 and mid-2000; Dijkstra et al., 2017; Steneck et al., 2013). In these two regions, fluctuations in urchin grazing pressure and increasing temperature favoring the settlement of epiphytes, which in turn cause kelp overgrowth leading to breakage and dislodgement, are the main causes of decline in kelp distribution (Filbee-Dexter et al., 2016; Filbee-Dexter and Scheibling, 2012; Steneck et al., 2013). Hence, the gradual increase in kelp coverage from 1999 to 2016 in

the Mingan Archipelago may be linked to difference in urchin and epiphytes population dynamics compared to more southern regions. First, urchin populations in the Mingan Archipelago persist at very high densities (Gagnon et al., 2004; Himmelman, 1991; Narvaez Diaz, 2018) due to the limited top-down control mechanisms as both urchin predators and urchin diseases are rare in the area (Himmelman et al., 1983; Johnson et al., 2019; Scheibling, 1997). Secondly, colder water temperatures in the Mingan Archipelago (summer maximum $\sim 16^{\circ}$; Galbraith et al., 2017) can limit the growth of epiphytes on kelp fronds. In particular, temperature-mediated outbreaks of the introduced epiphytic bryozoan *Membranipora membranacea* which cause major decreases in kelp canopy cover in eastern Canada (Saunders and Metaxas, 2008; Scheibling and Gagnon, 2009; Scheibling et al., 1999) are still rare in the northern Gulf of St. Lawrence, where this bryozoan nears the northern edge of its distribution range (Caines and Gagnon, 2012). Hence, stability of the Mingan Archipelago's kelp may be caused by a lack of large-scale variations in urchin and epiphytes population.

Limitations and future directions

The observed trend in kelp coverage from 1999 to 2016 is characterised by a slow, gradual increase over time rather than a sharp, large-scale shift. The latter would have been expected in situations of sudden release of the kelp from grazing pressure, for example following mass urchin mortalities as observed in kelp-urchin systems presenting multiple stable states (reviewed in Filbee-Dexter and Scheibling, 2014; Steneck et al., 2013). The fact that only minor changes in overall kelp coverage were observed between successive collections (8% change in kelp cover at most) suggests that no large-scale state shifts have

occurred over the studied period and supports the idea that the Mingan Archipelago is locked in an urchin-dominated state without alternate cycles (Johnson et al., 2019). However, the temporal gap between successive image collection in the present study, varying from 5 to 11 years, limits interpretation of the trends observed. These uneven gaps make it possible that a large-scale shift between urchin-dominated and kelp-dominated community states may have occurred without being detected. In Nova Scotia, forward shifts from urchin-dominated to kelp-dominated states can occur over the course of 18 months (Johnson and Mann, 1988), but urchin populations then require roughly a decade to recover densities capable of producing a backward shift to an urchin-dominated state (Steneck et al., 2002). Assuming a similar timeline would apply in the Mingan Archipelago and given the 5 to 11-year gap between consecutive image acquisitions in the present study, it appears unlikely that a full cycle from urchin-dominated to kelp-dominated state and back to urchin-dominated state could have occurred without being detected. Also, it was not possible to include the length of the temporal gap between image acquisitions in the calculation of the kelp indices (KSI and CTVI) while retaining biologically meaningful and logical index values. Hence, these indices consider kelp distribution to be static between collections, meaning that a kelp bed observed at a given location in one collection could disappear and reappear before the next collection and still be recorded as temporally stable between the two sampling occasions. Low sampling frequencies (i.e., long time intervals between collections) increase the possibility of change being undetected and can underestimate the rate of change in the variable observed (Leecaster and Weisberg, 2001; Miller-Rushing et al., 2008). Thus, future studies applying a similar methodology as the one presented here

should aim to collect imagery at more regular intervals, ideally yearly, to avoid this potential bias.

The present study is the most spatially and temporally broad analysis of the drivers modulating kelp distribution and stability in the Gulf of St. Lawrence to date. By exploring kelp distribution patterns at a broad spatiotemporal scale, this study shows that ice and wave conditions during the peak period for kelp growth and bed expansion (i.e., late winter and spring) drive kelp bed configuration in summer. This suggests that variations in ice coverage expected from climate changes will likely have a strong influence on kelp distribution patterns in the Gulf of St. Lawrence. Also, late summer temperature influenced kelp distribution patterns, likely through the modulation of urchin grazing, suggesting that the urchins' influence on kelp distribution is present at large (km^2) as well as small (m^2) spatial scales. The presence of more temporally persistent kelp beds at shallow depth suggests that sporadic disturbances from ice scouring occurring near the surface have less weight on dictating the temporal persistence of kelp beds than continued urchin grazing occurring at greater depths. The local, gradual increase in kelp coverage from 1999 to 2016 and the lack of large-scale shifts in kelp distribution during the study period distinguish the Mingan Archipelago from more southern regions of the Northwest Atlantic, as an example of a resilient, non-cyclical kelp-urchin system. Together, these results offer a novel broad-scale perspective of the variability in the distribution patterns of completely submerged kelp and the long-term stability of kelp-urchin systems. Similar time-series analyses based on remotely acquired imagery and landscape ecology approaches should be applied in kelp systems where alternate stable states are known to occur, to test the generality of the findings obtained in the Mingan Archipelago's stable system.

5.6. ACKNOWLEDGEMENTS

We are grateful to R. Hovey, M. P. St-Pierre, B. Dumas, H. Hawk, I. Garrido, P. Bruning, and C. Narvaez-Diaz for their help in preparing and conducting field work. We are grateful to Y. Wiersma, A. Bates, and K. Bøe for helpful statistical discussions throughout this project. We are thankful to the staff of Parks Canada's Mingan Archipelago National Park Reserve for help in finding suitable aerial imagery for this project and for the authorization to use these images in our research. This research was funded by Natural Sciences and Engineering Research Council of Canada (NSERC Discovery Grant), Canada Foundation for Innovation (CFI-Leaders Opportunity Funds), and Research & Development Corporation of Newfoundland and Labrador (IgniteR&D) grants to P. Gagnon. A. P. St-Pierre was supported by an NSERC Post-Graduate Scholarship (PGS).

5.7. REFERENCES

- Anderson, D.R., 2007. Model based inference in the life sciences: a primer on evidence. Springer Science & Business Media.
- Bates, D., Maechler, M., Bolker, B., Walker, S., 2014. lme4: Linear mixed-effects models using Eigen and S4. R package version 1, 1-23.
- Beisner, B., Haydon, D., Cuddington, K., 2003. Alternative stable states in ecology. *Front Ecol Environ* 1, 376-382.
- Bekkby, T., Rinde, E., Erikstad, L., Bakkestuen, V., 2009. Spatial predictive distribution modelling of the kelp species *Laminaria hyperborea*. *ICES J Mar Sci* 66, 2106-2115.
- Bell, T.W., Cavanaugh, K.C., Reed, D.C., Siegel, D.A., 2015. Geographical variability in the controls of giant kelp biomass dynamics. *J Biogeogr* 42, 2010-2021.
- Blain, C., Gagnon, P., 2013. Interactions between thermal and wave environments mediate intracellular acidity (H₂SO₄), growth, and mortality in the annual brown seaweed *Desmarestia viridis*. *J Exp Mar Biol Ecol* 440, 176-184.

- Boström, C., Pittman, S.J., Simenstad, C., Kneib, R.T., 2011. Seascape ecology of coastal biogenic habitats: advances, gaps, and challenges. *Mar Ecol Prog Ser* 427, 191-217.
- Boulangeat, I., Gravel, D., Thuiller, W., 2012. Accounting for dispersal and biotic interactions to disentangle the drivers of species distributions and their abundances. *Ecol Lett* 15, 584-593.
- Brennan, J.M., Bender, D.J., Contreras, T.A., Fahrig, L., 2002. Focal patch landscape studies for wildlife management: Optimizing sampling effort across scales, in: Liu, J., Taylor, W.W. (Eds.), *Integrating Landscape Ecology into Natural Resource Management*. Cambridge University Press, Cambridge, pp. 68-91.
- Burnham, K.P., Anderson, D.R., 2002. *Model selection and multimodel inference: a practical information-theoretic approach*. Springer, New York.
- Caines, S., Gagnon, P., 2012. Population dynamics of the invasive bryozoan *Membranipora membranacea* along a 450-km latitudinal range in the subarctic northwestern Atlantic. *Mar Biol* 159, 1817-1832.
- Castorani, M.C., Reed, D.C., Miller, R.J., 2018. Loss of foundation species: disturbance frequency outweighs severity in structuring kelp forest communities. *Ecology* 99, 2442-2454.
- Cavanaugh, K.C., Siegel, D.A., Reed, D.C., Dennison, P.E., 2011. Environmental controls of giant-kelp biomass in the Santa Barbara Channel, California. *Mar Ecol Prog Ser* 429, 1-17.
- Cushman, S.A., McGarigal, K., Neel, M.C., 2008. Parsimony in landscape metrics: strength, universality, and consistency. *Ecol Indic* 8, 691-703.
- de Bettignies, T., Wernberg, T., Lavery, P.S., 2013. Size, not morphology, determines hydrodynamic performance of a kelp during peak flow. *Mar Biol* 160, 843-851.
- DFO, 2013. *Assessment of Information on Irish Moss, Rockweed, and Kelp Harvests in Nova Scotia*. Department of Fisheries and Ocean Canada. *Sci Advis Sec Sci Advis Rep* 2013/004.
- DFO, 2018. *Coastal Time Series (CTS): database of daily average temperatures from inshore moored thermographs for the East Coast of Canada*. <http://www.bio.gc.ca/science/data-donnees/base/data-donnees/cts-en.php>.
- Dijkstra, J.A., Harris, L.G., Mello, K., Litterer, A., Wells, C., Ware, C., 2017. Invasive seaweeds transform habitat structure and increase biodiversity of associated species. *J Ecol* 105, 1668-1678.

- Dunton, K.H., 1985. Growth of dark-exposed *Laminaria saccharina* (L.) Lamour. and *Laminaria solidungula* J. Ag.(laminariales: phaeophyta) in the alaskan Beaufort sea. *J Exp Mar Biol Ecol* 94, 181-189.
- Edwards, M.S., 2004. Estimating scale-dependency in disturbance impacts: El Niños and giant kelp forests in the northeast Pacific. *Oecologia* 138, 436-447.
- Esri, 2015. ArcGIS Desktop; Release 10.3.1, Redland, CA.
- Filbee-Dexter, K., Feehan, C.J., Scheibling, R.E., 2016. Large-scale degradation of a kelp ecosystem in an ocean warming hotspot. *Mar Ecol Prog Ser* 543, 141-152.
- Filbee-Dexter, K., Scheibling, R.E., 2012. Hurricane-mediated defoliation of kelp beds and pulsed delivery of kelp detritus to offshore sedimentary habitats. *Mar Ecol Prog Ser* 455, 51-64.
- Filbee-Dexter, K., Scheibling, R.E., 2014. Sea urchin barrens as alternative stable states of collapsed kelp ecosystems. *Mar Ecol Prog Ser* 495, 1-25.
- Filbee-Dexter, K., Wernberg, T., Fredriksen, S., Norderhaug, K.M., Pedersen, M.F., 2019. Arctic kelp forests: Diversity, resilience and future. *Glob Planet Change* 172, 1-14.
- Fonseca, M.S., Bell, S.S., 1998. Influence of physical setting on seagrass landscapes near Beaufort, North Carolina, USA. *Mar Ecol Prog Ser* 171, 109-121.
- Fredersdorf, J., Müller, R., Becker, S., Wiencke, C., Bischof, K., 2009. Interactive effects of radiation, temperature and salinity on different life history stages of the Arctic kelp *Alaria esculenta* (Phaeophyceae). *Oecologia* 160, 483-492.
- Fredriksen, S., Sjøtun, K., Lein, T.E., Rueness, J., 1995. Spore dispersal in *Laminaria hyperborea* (Laminariales, Phaeophyceae). *Sarsia* 80, 47-53.
- Frey, D.L., Gagnon, P., 2015. Thermal and hydrodynamic environments mediate individual and aggregative feeding of a functionally important omnivore in reef communities. *Plos One* 10, e0118583.
- Gagnon, P., Himmelman, J.H., Johnson, L.E., 2003. Algal colonization in urchin barrens: defense by association during recruitment of the brown alga *Agarum cribrosum*. *J Exp Mar Biol Ecol* 290, 179-196.
- Gagnon, P., Himmelman, J.H., Johnson, L.E., 2004. Temporal variation in community interfaces: kelp-bed boundary dynamics adjacent to persistent urchin barrens. *Mar Biol* 144, 1191-1203.
- Gagnon, P., Johnson, L.E., Himmelman, J.H., 2005. Kelp patch dynamics in the face of intense herbivory: Stability of *Agarum clathratum* (Phaeophyta) stands and associated flora on urchin barrens. *J Phycol* 41, 498-505.

- Galbraith, P.S., Chassé, J., Caverhill, C., Nicot, P., Gilbert, D., Petigrew, B., Lefaiivre, D., Brickman, D., Devine, L., Lafleur, C., 2017. Physical oceanographic conditions in the Gulf of St. Lawrence in 2016. DFO Can. Sci. Advis. Sec. Res. Doc. 2017/044. v + 91 p.
- Garcon, J.S., Grech, A., Moloney, J., Hamann, M., 2010. Relative Exposure Index: an important factor in sea turtle nesting distribution. *Aquat Conserv: Mar Freshw Ecosyst* 20, 140-149.
- Gendron, L., 1989. Seasonal growth of the kelp *Laminaria longicuris* in Baie des Chaleurs, Québec, in relation to nutrient and light availability. *Bot Mar* 32, 345-354.
- Gordon, R., Brawley, S.H., 2004. Effects of water motion on propagule release from algae with complex life histories. *Mar Biol* 145, 21-29.
- Hepburn, C.D., Holborow, J.D., Wing, S.R., Frew, R.D., Hurd, C.L., 2007. Exposure to waves enhances the growth rate and nitrogen status of the giant kelp *Macrocystis pyrifera*. *Mar Ecol Prog Ser* 339, 99-108.
- Himmelman, J.H., 1991. Diving observations of subtidal communities in the northern Gulf of St. Lawrence. *Can Special Pub Fish Aquat Sci* 113, 319-332.
- Himmelman, J.H., Dumont, C.P., Gaymer, C.F., Vallieres, C., Drolet, D., 2008. Spawning synchrony and aggregative behaviour of cold-water echinoderms during multi-species mass spawnings. *Mar Ecol Prog Ser* 361, 161-168.
- Himmelman, J.H., Lavergne, Y., Axelsen, F., Cardinal, A., Bourget, E., 1983. Sea urchins in the Saint Lawrence Estuary: their abundance, size-structure, and suitability for commercial exploitation. *Can J Fish Aquat Sci* 40, 474-486.
- Himmelman, J.H., Steele, D.H., 1971. Foods and predators of the green sea urchin *Strongylocentrotus droebachiensis* in Newfoundland waters. *Mar Biol* 9, 315-322.
- Hobbs, N.T., 2003. Challenges and opportunities in integrating ecological knowledge across scales. *Forest Ecol Manag* 181, 223-238.
- Hurrell, J.W., 1995. Decadal Trends in the North Atlantic Oscillation: Regional Temperatures and Precipitation. *Science* 269, 676-679.
- Johnson, C.R., Mann, K.H., 1988. Diversity, patterns of adaptation, and stability of Nova Scotian kelp beds. *Ecol Monogr* 58, 129-154.
- Johnson, L.E., MacGregor, K.A., Narvaez, C.A., Suskiewicz, T.S., 2019. Subtidal rocky shores of the north-west Atlantic Ocean: The complex ecology of a simple ecosystem, in: Williams, G.A., Bohn, K., Firth, L.B., Hawkins, S.J. (Eds.), *Interactions in the*

- Marine Benthos: Global Patterns and Processes. Cambridge University Press, Cambridge, pp. 90-127.
- Keats, D., South, G., Steele, D., 1985. Algal biomass and diversity in the upper subtidal at a pack-ice disturbed site in eastern Newfoundland. *Mar Ecol Prog Ser*, 151-158.
- Keddy, P.A., 1982. Quantifying within-lake gradients of wave energy - Interrelationships of wave energy, substrate particle-size and shoreline plants in axe lake, Ontario. *Aquat Bot* 14, 41-58.
- Konar, B., 2000. Seasonal inhibitory effects of marine plants on sea urchins: structuring communities the algal way. *Oecologia* 125, 208-217.
- Konar, B., Estes, J.A., 2003. The stability of boundary regions between kelp beds and deforested areas. *Ecology* 84, 174-185.
- Krause-Jensen, D., Marbà, N., Olesen, B., Sejr, M.K., Christensen, P.B., Rodrigues, J., Renaud, P.E., Balsby, T.J., Rysgaard, S., 2012. Seasonal sea ice cover as principal driver of spatial and temporal variation in depth extension and annual production of kelp in Greenland. *Global Change Biol* 18, 2981-2994.
- Krumhansl, K.A., Okamoto, D.K., Rassweiler, A., Novak, M., Bolton, J.J., Cavanaugh, K.C., Connell, S.D., Johnson, C.R., Konar, B., Ling, S.D., Micheli, F., Norderhaug, K.M., Pérez-Matus, A., Sousa-Pinto, I., Reed, D.C., Salomon, A.K., Shears, N.T., Wernberg, T., Anderson, R.J., Barrett, N.S., Buschmann, A.H., Carr, M.H., Caselle, J.E., Derrien-Courtet, S., Edgar, G.J., Edwards, M., Estes, J.A., Goodwin, C., Kenner, M.C., Kushner, D.J., Moy, F.E., Nunn, J., Steneck, R.S., Vásquez, J., Watson, J., Witman, J.D., Byrnes, J.E.K., 2016. Global patterns of kelp forest change over the past half-century. *Proc Natl Acad Sci USA* 113, 13785-13790.
- Krumhansl, K.A., Scheibling, R.E., 2011. Detrital production in Nova Scotian kelp beds: patterns and processes. *Mar Ecol Prog Ser* 421, 67-82.
- Landis, J.R., Koch, G.G., 1977. The measurement of observer agreement for categorical data. *biometrics*, 159-174.
- Lauzon-Guay, J.S., Scheibling, R.E., 2007a. Behaviour of sea urchin *Strongylocentrotus droebachiensis* grazing fronts: food-mediated aggregation and density-dependent facilitation. *Mar Ecol Prog Ser* 329, 191-204.
- Lauzon-Guay, J.S., Scheibling, R.E., 2007b. Seasonal variation in movement, aggregation and destructive grazing of the green sea urchin (*Strongylocentrotus droebachiensis*) in relation to wave action and sea temperature. *Mar Biol* 151, 2109-2118.
- Lauzon-Guay, J.S., Scheibling, R.E., Barbeau, M.A., 2009. Modelling phase shifts in a rocky subtidal ecosystem. *Mar Ecol Prog Ser* 375, 25-39.

- Leach, K., Montgomery, W.I., Reid, N., 2016. Modelling the influence of biotic factors on species distribution patterns. *Ecol Model* 337, 96-106.
- Lecours, V., Devillers, R., Schneider, D.C., Lucieer, V.L., Brown, C.J., Edinger, E.N., 2015. Spatial scale and geographic context in benthic habitat mapping: review and future directions. *Mar Ecol Prog Ser* 535, 259-284.
- Leecaster, M.K., Weisberg, S.B., 2001. Effect of sampling frequency on shoreline microbiology assessments. *Mar Pollut Bull* 42, 1150-1154.
- Leroux, S.J., 2019. On the prevalence of uninformative parameters in statistical models applying model selection in applied ecology. *Plos One* 14, e0206711.
- Levin, S.A., 1992. The problem of pattern and scale in ecology: the Robert H. MacArthur award lecture. *Ecology* 73, 1943-1967.
- Lillesand, T., Kiefer, R.W., Chipman, J., 2014. Remote sensing and image interpretation. John Wiley & Sons.
- Ling, S., Scheibling, R., Rassweiler, A., Johnson, C., Shears, N., Connell, S., Salomon, A., Norderhaug, K., Pérez-Matus, A., Hernández, J., 2015. Global regime shift dynamics of catastrophic sea urchin overgrazing. *Phil Trans R Soc B* 370, 20130269.
- Magurran, A.E., Baillie, S.R., Buckland, S.T., Dick, J.M., Elston, D.A., Scott, E.M., Smith, R.I., Somerfield, P.J., Watt, A.D., 2010. Long-term datasets in biodiversity research and monitoring: assessing change in ecological communities through time. *Trends Ecol Evol* 25, 574-582.
- McGarigal, K., Cushman, S.A., Ene, E., 2012. FRAGSTATS v4: Spatial pattern analysis program for categorical and continuous maps, Computer software program produced by the authors at the University of Massachusetts, Amherst. Available at the following web site: <http://www.umass.edu/landeco/research/fragstats/fragstats.html>.
- Meier, E.S., Kienast, F., Pearman, P.B., Svenning, J.C., Thuiller, W., Araújo, M.B., Guisan, A., Zimmermann, N.E., 2010. Biotic and abiotic variables show little redundancy in explaining tree species distributions. *Ecography* 33, 1038-1048.
- Miller-Rushing, A.J., Inouye, D.W., Primack, R.B., 2008. How well do first flowering dates measure plant responses to climate change? The effects of population size and sampling frequency. *J Ecol* 96, 1289-1296.
- Moffett, K.B., Nardin, W., Silvestri, S., Wang, C., Temmerman, S., 2015. Multiple stable states and catastrophic shifts in coastal wetlands: Progress, challenges, and opportunities in validating theory using remote sensing and other methods. *Remote Sens* 7, 10184-10226.

- Munda, I.M., Lüning, K., 1977. Growth performance of *Alaria esculenta* off Helgoland. Helgoland Wiss Meer 29, 311.
- Narvaez Diaz, C., 2018. Green urchin demography in a subarctic ecosystem: patterns and processes, PhD thesis, Université Laval.
- NOAA, 2018. Climate Prediction Center of the National Oceanic and Atmospheric Administration. U.S. Department of Commerce, USA. <http://www.cpc.ncep.noaa.gov/products/precip/CWlink/pna/nao.shtml>.
- Norton, T., 1992. Dispersal by macroalgae. Br Phycol J 27, 293-301.
- Pedersen, M.F., Nejrup, L.B., Fredriksen, S., Christie, H., Norderhaug, K.M., 2012. Effects of wave exposure on population structure, demography, biomass and productivity of the kelp *Laminaria hyperborea*. Mar Ecol Prog Ser 451, 45-60.
- Petraitis, P.S., Latham, R.E., 1999. The importance of scale in testing the origins of alternative community states. Ecology 80, 429-442.
- R Development Core Team, 2018. R: A language and environment for statistical computing. R Foundation for Statistical Computing, Vienna, Austria. URL <https://www.R-project.org/>.
- Reed, D.C., Laur, D.R., Ebeling, A.W., 1988. Variation in algal dispersal and recruitment: the importance of episodic events. Ecol Monogr 58, 321-335.
- Reed, D.C., Rassweiler, A., Carr, M.H., Cavanaugh, K.C., Malone, D.P., Siegel, D.A., 2011. Wave disturbance overwhelms top-down and bottom-up control of primary production in California kelp forests. Ecology 92, 2108-2116.
- Reed, D.C., Rassweiler, A.R., Miller, R.J., Page, H.M., Holbrook, S.J., 2015. The value of a broad temporal and spatial perspective in understanding dynamics of kelp forest ecosystems. Mar Freshwater Res 67, 14-24.
- Rinde, E., Christie, H., Fagerli, C.W., Bekkby, T., Gundersen, H., Norderhaug, K.M., Hjermann, D.Ø., 2014. The influence of physical factors on kelp and sea urchin distribution in previously and still grazed areas in the NE Atlantic. Plos One 9, e100222.
- Saunders, M., Metaxas, A., 2008. High recruitment of the introduced bryozoan *Membranipora membranacea* is associated with kelp bed defoliation in Nova Scotia, Canada. Mar Ecol Prog Ser 369, 139-151.
- Scheibling, R., 1997. The role of predation in regulating sea urchin populations in eastern Canada. Oceanog Lit Rev 2, 135.

- Scheibling, R.E., Gagnon, P., 2009. Temperature-mediated outbreak dynamics of the invasive bryozoan *Membranipora membranacea* in Nova Scotian kelp beds. *Mar Ecol Prog Ser* 390, 1-13.
- Scheibling, R.E., Hennigar, A.W., Balch, T., 1999. Destructive grazing, epiphytism, and disease: the dynamics of sea urchin-kelp interactions in Nova Scotia. *Can J Fish Aquat Sci* 56, 2300-2314.
- Schneider, D.C., 2001. The rise of the concept of scale in ecology: The concept of scale is evolving from verbal expression to quantitative expression. *AIBS Bulletin* 51, 545-553.
- Schneider, D.C., 2009. *Quantitative ecology: measurement, models and scaling*. Academic Press, Amsterdam and Boston (Massachusetts).
- Simenstad, C.A., Estes, J.A., Kenyon, K.W., 1978. Aleuts, sea otters, and alternate stable-state communities. *Science* 200, 403-411.
- Sivertsen, K., 1997. Geographic and environmental factors affecting the distribution of kelp beds and barren grounds and changes in biota associated with kelp reduction at sites along the Norwegian coast. *Can J Fish Aquat Sci* 54, 2872-2887.
- Sjøtun, K., Christie, H., Helge Fosså, J., 2006. The combined effect of canopy shading and sea urchin grazing on recruitment in kelp forest (*Laminaria hyperborea*). *Mar Biol Res* 2, 24-32.
- St-Pierre, A.P., Gagnon, P., 2020. Kelp-bed dynamics across scales: Enhancing mapping capability with remote sensing and GIS. *J Exp Mar Biol Ecol* 522, 151246.
- Steneck, R.S., Graham, M.H., Bourque, B.J., Corbett, D., Erlandson, J.M., Estes, J.A., Tegner, M.J., 2002. Kelp forest ecosystems: biodiversity, stability, resilience and future. *Environ Conserv* 29, 436-459.
- Steneck, R.S., Leland, A., McNaught, D.C., Vavrinec, J., 2013. Ecosystem flips, locks, and feedbacks: The lasting effects of fisheries on Maine's kelp forest ecosystem. *Bull Mar Sci* 89, 31-55.
- Thrush, S.F., Hewitt, J.E., Dayton, P.K., Coco, G., Lohrer, A.M., Norkko, A., Norkko, J., Chiantore, M., 2009. Forecasting the limits of resilience: integrating empirical research with theory. *P Roy Soc B: Biol Sci* 276, 3209-3217.
- Turner, M.G., Gardner, R.H., O'Neill, R.V., 2001. *Landscape ecology in theory and practice: patterns and process*. (Vol. 401) Springer, New York.
- Turner, M.G., O'Neill, R.V., Gardner, R.H., Milne, B.T., 1989. Effects of changing spatial scale on the analysis of landscape pattern. *Landsc Ecol* 3, 153-162.

- U.S. Army Corps of Engineers, 1984. Shore Protection Manual. Coastal Engineering Research Center, Fort Belvoir, Va.
- Uuemaa, E., Mander, Ü., Marja, R., 2013. Trends in the use of landscape spatial metrics as landscape indicators: A review. *Ecol Indic* 28, 100-106.
- Velimirov, B., Griffiths, C., 1979. Wave-induced kelp movement and its importance for community structure. *Bot Mar* 22, 169-172.
- Wedding, L.M., Lepczyk, C.A., Pittman, S.J., Friedlander, A.M., Jorgensen, S., 2011. Quantifying seascape structure: extending terrestrial spatial pattern metrics to the marine realm. *Mar Ecol Prog Ser* 427, 219-232.
- Welham, S.J., Gezan, S.A., Clark, S., Mead, A., 2015. *Statistical methods in biology: Design and analysis of experiments and regression*. Chapman and Hall/CRC.
- Wheatley, M., Johnson, C., 2009. Factors limiting our understanding of ecological scale. *Ecol Complex* 6, 150-159.

CHAPTER VI

Summary and general conclusions

6.1. SUMMARY

As foundation species, kelp have long been known to increase biodiversity and productivity patterns in shallow rocky reef systems (Dayton, 1985; Estes et al., 2004; Mann, 1973; Steneck et al., 2002). Following the loss of kelp habitats, drastic changes in species distribution, community structure, and ecosystem functioning have been documented in many regions (Filbee-Dexter and Scheibling, 2014; Ling, 2008; Steneck et al., 2002) highlighting the importance of understanding the drivers of kelp distribution patterns to predict and mitigate these changes. In eastern Canada, kelp beds are frequent features of subtidal seascape, being present on shallow rocky reefs along the shores of the Gulf of St. Lawrence, the Maritimes provinces, and Newfoundland. Yet, studies of kelp systems have been somewhat limited geographically, mainly being conducted on the Atlantic coast of Nova Scotia (Filbee-Dexter and Scheibling, 2012; Johnson and Mann, 1988; Lauzon-Guay and Scheibling, 2007; Scheibling et al., 1999) with few studies in the Mingan Archipelago (northern Gulf of St-Lawrence; Gagnon et al., 2004; Gagnon et al., 2005; Himmelman, 1991) and Newfoundland (Caines and Gagnon, 2012; Frey and Gagnon, 2015; Keats, 1991). However, kelp distribution patterns and their driving mechanisms may differ among regions due to differences in kelp species dominance (e.g., kelp beds in Nova Scotia are dominated by *Saccharina latissima* while this species is absent in eastern Newfoundland; Merzouk and Johnson, 2011) and environmental characteristics (e.g., summer water temperature in Nova Scotia is several degrees warmer than in the other two regions; Merzouk and Johnson, 2011). Investigations conducted in poorly studied regions can provide an insight into the local mechanisms driving kelp distribution patterns and, when compared to results obtained in other regions, allow for a more comprehensive

understanding of the generalities and regional specificities in kelp dynamics across eastern Canada.

Another important gap in our knowledge of kelp distribution patterns and their drivers stems from technical limitations; due to the cost-intensive and time-consuming scuba-based methods generally employed for kelp monitoring, most studies have been restricted to small spatial (few 100s m²) and temporal (<5 years) extents, and the dynamics occurring at broader spatiotemporal scales remains largely unexplored. Despite the usefulness of scuba-based studies for the understanding of small-scale patterns in kelp-urchin dynamics and kelp distribution, extrapolation of their findings to broader scales raises concern because ecological processes are generally scale dependent (Lecours et al., 2015; Levin, 1992; Schneider, 2001). Hence, approaches specifically designed to investigate kelp distribution at broad or multiple spatiotemporal scales are needed to increase understanding of the scale-dependent processes modulating the stability and resilience of kelp systems.

The main objective of this research project was to investigate the factors controlling kelp distribution and the stability of kelp-urchin systems in southeastern Newfoundland and the Gulf of St. Lawrence to deepen our understanding of kelp-urchin dynamics in eastern Canada. Specifically, this thesis aimed to 1) identify the threshold urchin density required to maintain the destructive grazing on kelp bed at small spatial scales (m²) at one site in southeastern Newfoundland [Chapter II], 2) quantify broad-scale (km²) kelp distribution patterns in the Mingan Archipelago (northern Gulf of St. Lawrence) by measuring spatial pattern metrics and identify environmental drivers of kelp presence [Chapter IV], and 3) examine temporal variations in broad-scale (km²) kelp bed distribution patterns in the Mingan Archipelago and investigate correlations between these distribution

patterns and oceanographic or atmospheric conditions [Chapter V]. In order to fulfill the last two objectives, a framework for the detection of shallow submerged kelp beds from remotely acquired (aerial or satellite) imagery had to be developed and tested (Chapter III).

6.1.1. Urchin density and kelp bed destruction in southeastern Newfoundland

Chapter II examined the relationships between urchin density, environmental factors (namely temperature and flow acceleration, a proxy for wave action), and kelp bed destruction in southeastern Newfoundland, aiming to identify the threshold urchin density required to maintain kelp bed destruction. Enclosures were built at the interface between kelp bed and urchin barren, which were stocked with urchin densities representing between 25% and 125% of the natural urchin front density in the study area and monitored over two summers. Results highlighted an increase in kelp bed retreat (a measure of kelp bed destruction) over time during summer, but no effect of urchin density, temperature, or flow acceleration. The density of urchins at the front within the enclosures was influenced by the interaction between Julian date, year, and the urchin density treatment applied. Observations in an adjacent un-manipulated control site over a 14-month period indicated that kelp bed retreat increased with increasing temperature and that urchin density in the barren zone (~2 m from the kelp bed) decreased with increasing temperature while it increased with increasing wave action. These results suggest that the threshold urchin front density necessary to maintain kelp bed destruction at the study site in summer is at or below the lowest density treatment applied (25% of the natural urchin front density at the study site, i.e., 88 urchins·m⁻²), and that increasing urchin densities above this threshold does not increase the rate of kelp bed destruction.

6.1.2. Framework for broad-scale (km²) kelp bed detection

Chapter III tested the suitability of conventional image classification methods for mapping kelp distribution from remotely acquired imagery. It aimed to compare simple and robust methods to help guide scientists that are not familiar with remote sensing techniques in the choice of suitable approaches to map completely submerged shallow kelp beds. Three classification methods were compared: 1) a software-led unsupervised classification which groups pixels based on similarity in their spectral signature; 2) a software-led supervised classification in which pixels are assigned to categories based on similarity in the spectral signature of the pixel and that of reference data from each category; and 3) a visual classification carried out by a trained observer. These three classification methods were applied to digital aerial (acquired on board a helicopter) and satellite (SPOT 7) imagery of ~250 ha of shallow (<7 m) seabed in the Mingan Archipelago (northern Gulf of St. Lawrence, Canada). The results clearly demonstrated that simple image classification techniques can accurately detect fully submerged kelp beds. Indeed, high levels of accuracy were obtained with the visual classification of aerial imagery (overall accuracy of 90%) and the supervised classification of satellite imagery (overall accuracy of 89%), which were the top two methods. Hence, this study serves as a framework for future application of these methods in completely submerged kelp bed systems, which will allow kelp ecologists to move beyond the spatially and temporally restrictive limits of traditional scuba-based sampling methods to explore kelp distribution dynamics over broader spatial and temporal domains.

6.1.3. Patterns of spatial distribution of kelp beds in the Mingan Archipelago

Chapter IV aimed to quantify kelp distribution patterns over a broad spatial extent (km^2) in the northern Gulf of St. Lawrence by using spatial pattern metrics and to examine correlations between kelp presence and physical and biotic parameters. In this chapter, the best method for kelp detection from aerial imagery identified in the previous chapter (i.e., visual classification) was applied to map kelp presence from aerial imagery obtained in 2016 around five islands in the Mingan Archipelago. The spatial characteristics of kelp beds were examined by computing spatial pattern metrics quantifying the proportional abundance, shape, area, and clustering of kelp beds. These metrics showed substantial variation in kelp cover (46% to 87%) among islands, as well as considerable variations in kelp patch size (225 to $891,225 \text{ m}^2$) within and among islands. The majority of kelp patches were of relatively small size (over 80% of patches measuring $<1350 \text{ m}^2$), but the few larger kelp patches present in the study area, generally in shallow water near the coastline, enclosed most (98%) of the kelp-covered seabed. Overall, these spatial pattern metrics showed that kelp distribution is not uniform among islands and suggested that the spatial extent over which observations are conducted strongly influences the patterns detected. Moreover, this chapter investigated the relative influence of depth, bottom slope, exposure to waves, and urchin density on kelp presence by applying model selection techniques. Results showed that increasing depth, urchin density, and exposure to waves independently led to a decrease in kelp presence, with depth having the strongest effect.

6.1.4. Temporal trends in kelp distribution in the Mingan Archipelago

Chapter V investigated the spatial configuration and persistence of kelp beds in the

Mingan Archipelago over broad spatial (km²) and temporal (decades) extents. Specifically, changes in kelp distribution over time were monitored using aerial imagery of the study area acquired every five to 11 years between 1983 and 2016, by applying the visual classification method for kelp detection described in Chapter III. Spatial pattern metrics were computed to quantify the spatial characteristics of kelp beds, including kelp coverage, number of kelp patches, mean patch area, and largest patch index, and used to investigate the relationship between these metrics and changes in oceanographic and atmospheric conditions. Results showed that kelp cover increased from 1999 to 2016, and that high storm frequency, cold temperatures, and long-lasting ice cover led to a decrease in kelp coverage and smaller, numerous kelp patches. Two indices were developed to quantify the stability of kelp beds (Kelp Stability Index, or KSI) and the variation in cover type (Cover Type Variability Index, or CTVI) across the study area. Modelling techniques were used to examine the effect of depth, bottom slope, and exposure to waves on these indices. Results indicated that kelp beds persisting through time (high KSI) are more present at shallow depths, as the latter generally experiencing fewer changes in cover type over time compared to deeper areas. Overall, 45% of the study area presented a stable cover type through time (i.e., cover type changing once or less) and only 8% of it exhibiting a highly variable cover (i.e., cover type changing 4 or 5 times over the study period).

6.2. IMPORTANCE OF THE STUDY

The present study provides novel information pertaining to the dynamics between kelp and urchins in regions where studies have been limited to date, and at spatiotemporal

scales largely overlooked in studies of completely submerged kelp systems. Chapter II presents the first manipulative experiment conducted in southeastern Newfoundland aiming to understand how urchin density affects kelp bed destruction and urchin aggregation. It demonstrated that the local threshold urchin density causing kelp bed destruction through grazing during summer is at or below 25% of the natural urchin front density at the study site. Although kelp beds are able to recover during winter and expand over roughly the area grazed by urchins during summer, this study suggests that urchin densities within the study area are too high to allow the expansion of kelp beds farther into the barren and thus maintain this system locked in an urchin-dominated state, preventing a large-scale shift to a kelp-dominated state.

Chapter III proved the usefulness of remote sensing and GIS-based methods to detect kelp beds in shallow, completely submerged areas. Using the framework presented in this chapter, kelp ecologists will be better able to develop broad-scale monitoring programs in systems with characteristics (i.e., depth and turbidity profiles) similar to the Mingan Archipelago. This operational improvement increases our ability to explore kelp distribution patterns at broad spatiotemporal scales and to investigate how stable states are established and maintained in kelp-urchin systems. Chapter IV clearly demonstrated the usefulness of the methods described in Chapter III for the investigation of the spatial patterns in kelp distribution over a broad (km^2) spatial scale and established that the spatial extent over which observations are conducted strongly influences the distribution patterns detected. As the first investigation of kelp distribution patterns using spatial pattern metrics, this study determined that the shape, size, and density of kelp patches vary spatially within a few km^2 . This study also identified depth, exposure to waves, and urchin density as factors

regulating the presence of kelp beds over broad spatial scales, thus providing novel information for the understanding of scale-dependent processes regulating submerged kelp bed distribution. Chapter V is the most spatially and temporally broad analysis of the drivers modulating kelp distribution patterns and kelp bed stability in the Gulf of St. Lawrence to date. As such, it increases knowledge of the environmental parameters driving the spatial distribution of kelp patches and the stability of kelp beds over time. Importantly, this study observed a gradual increase in kelp coverage from 1999 to 2016 in the Mingan Archipelago and a lack of large-scale shifts in kelp distribution during the study period; these two characteristics distinguish the Mingan Archipelago from more southern regions of the Northwest Atlantic, as an example of a temporally-stable, non-cyclical kelp-urchin system. In addition, results from this chapter provide a baseline with which to compare kelp distribution in the Mingan Archipelago in the future and assess the trajectory of this system over time.

Overall, this research project offers a novel broad-scale perspective of the variability in distribution patterns of completely submerged kelp and of the long-term stability of kelp-urchin systems. It increases knowledge of scale dependency in the drivers of kelp distribution patterns while exploring these drivers in regions poorly studied to date. This research project speaks to the importance of exploring multiple scales to understand the dynamics of species distribution, which will allow for the better prediction and mitigation of change in kelp-urchin systems.

6.3. FUTURE DIRECTIONS

By applying a combination of traditional (Chapter II) and novel (Chapters III, IV, and V) techniques for the study of submerged kelp beds, this research project provided new information on the dynamics of kelp systems in two regions of eastern Canada where few studies have been conducted to date. However, it also highlighted areas which deserve further attention, some of which are outlined below.

Chapter II determined that the threshold urchin density required to maintain significant grazing upon a kelp bed at the study site was either equal to the lowest density tested (i.e., 88 urchins·m⁻²), or may be lower. Further studies are needed to investigate if severe declines in urchin density below this threshold would trigger a kelp bed expansion into the urchin barren of a sufficient magnitude to produce a shift from urchin- to kelp-dominated states. Such investigation would require the use of large-scale disturbance plots. Further testing is also needed to determine if these results are representative of the southeastern Newfoundland region as a whole and to disentangle the effects of urchin grazing from those of high late-summer temperature on kelp bed degradation.

In Chapter III, we purposely chose to compare classification methods that were simple to execute with the aim of building a framework that would be accessible to non-specialist map users (*sensu* Andréfouët, 2008) such as kelp ecologists who need access to reliable maps but may not be familiar with cutting-edge advances in remote sensing and GIS technologies. Investigation of more technically complex methods such as object-based classification (Wang et al., 2004) could be of interest to more advanced users, as these methods have the potential to increase the precision and speed of the classification. Also, visual classification techniques, although highly efficient for the detection of submerged

kelp beds on aerial imagery, have the disadvantage of yielding only presence/absence data and hence could not be used to estimate kelp biomass. Further testing would be needed to establish an effective classification method to estimate kelp biomass and to identify more numerous benthic classes, which would require a more meticulous examination of per-pixel reflectance, thorough calibration and careful image pre-processing. Investigation of the gain in accuracy obtained when using imagery with more numerous and/or narrow spectral bands may help researchers aiming to classify more complex benthic systems (e.g., with more habitat classes, or classes that are more difficult to distinguish than in the present study).

Chapters IV and V used spatial pattern metrics to quantify the configuration of completely submerged kelp beds, which is an approach that has not yet been applied to kelp bed systems elsewhere. As such, it highlighted several future directions of research, like the need to investigate if the patterns observed in the Mingan Archipelago are representative of other areas of eastern Canada and to determine if the observed patterns are driven by variations in abiotic or biotic conditions directly affecting kelp dispersal and growth or indirectly affecting kelp by influencing the behaviour of urchins. Monitoring of urchin population density at broad spatial scales (km²) across the Mingan Archipelago over several years, in conjunction with the monitoring of kelp distribution patterns and environmental parameters, would help disentangle the direct and indirect drivers of kelp distribution patterns. Also, Chapter V determined that kelp distribution patterns were correlated with the North Atlantic Oscillation index (NAO index) and ice cover, but further studies are needed to establish a causal link and the mechanisms through which these environmental conditions affect kelp survival, dispersal, and patch configuration.

While the present study mainly focused on quantifying kelp distribution patterns and their drivers, another interesting research avenue would be to investigate the consequences of the spatial patterns observed on kelp communities. For example, assessing the impacts of kelp patch size and patch density on the biodiversity of kelp-associated species would be informative of the effects of spatial configuration on community structure. Fragmentation and patch structure influence herbivory in seagrass (Gera et al., 2013; Pagès et al., 2014) and could have a similar effect on kelp-urchin dynamics. Determining to what extent kelp patch size and density influence the temporal stability of kelp beds would also provide critical information on the resilience of these systems, for example by investigating if large kelp patches occur in a same geographical location for longer periods (i.e., years) than small patches or by quantifying the contribution of shallow persistent kelp patches to recruitment in nearby kelp-devoid areas.

Finally, the present study confirmed that, when considered over broad spatial (km²) and temporal (decades) extents, the Mingan Archipelago constitutes a resilient, non-cyclical kelp-urchin system locked in an urchin-dominated state. Further studies evaluating the effects of natural and anthropogenic disturbances on kelp bed distribution patterns in this area will be needed to better understand the limits of this resilience and identify the threshold for phase shifts between states in this region. Such knowledge will be useful to predict possible changes in this system, for example as a result of changing ocean climate, and inform management practices.

6.4. REFERENCES

- Andréfouët, S., 2008. Coral reef habitat mapping using remote sensing: a user vs producer perspective. Implications for research, management and capacity building. *J Spat Sci* 53, 113-129.
- Caines, S., Gagnon, P., 2012. Population dynamics of the invasive bryozoan *Membranipora membranacea* along a 450-km latitudinal range in the subarctic northwestern Atlantic. *Mar Biol* 159, 1817-1832.
- Dayton, P.K., 1985. Ecology of kelp communities. *Annu Rev Ecol Syst* 16, 215-245.
- Estes, J., Danner, E., Doak, D., Konar, B., Springer, A., Steinberg, P., Tinker, M., Williams, T., 2004. Complex trophic interactions in kelp forest ecosystems. *Bull Mar Sci* 74, 621-638.
- Filbee-Dexter, K., Scheibling, R.E., 2012. Hurricane-mediated defoliation of kelp beds and pulsed delivery of kelp detritus to offshore sedimentary habitats. *Mar Ecol Prog Ser* 455, 51-64.
- Filbee-Dexter, K., Scheibling, R.E., 2014. Sea urchin barrens as alternative stable states of collapsed kelp ecosystems. *Mar Ecol Prog Ser* 495, 1-25.
- Frey, D.L., Gagnon, P., 2015. Thermal and hydrodynamic environments mediate individual and aggregative feeding of a functionally important omnivore in reef communities. *Plos One* 10, e0118583.
- Gagnon, P., Himmelman, J.H., Johnson, L.E., 2004. Temporal variation in community interfaces: kelp-bed boundary dynamics adjacent to persistent urchin barrens. *Mar Biol* 144, 1191-1203.
- Gagnon, P., Johnson, L.E., Himmelman, J.H., 2005. Kelp patch dynamics in the face of intense herbivory: Stability of *Agarum clathratum* (Phaeophyta) stands and associated flora on urchin barrens. *J Phycol* 41, 498-505.
- Gera, A., Pagès, J.F., Romero, J., Alcoverro, T., 2013. Combined effects of fragmentation and herbivory on *Posidonia oceanica* seagrass ecosystems. *J Ecol* 101, 1053-1061.
- Himmelman, J.H., 1991. Diving observations of subtidal communities in the northern Gulf of St. Lawrence. *Can Special Pub Fish Aquat Sci* 113, 319-332.
- Johnson, C.R., Mann, K.H., 1988. Diversity, patterns of adaptation, and stability of Nova Scotian kelp beds. *Ecol Monogr* 58, 129-154.
- Keats, D.W., 1991. Refugial *Laminaria* abundance and reduction in urchin grazing in communities in the north-west Atlantic. *J Mar Biol Assoc Uk* 71, 867-876.

- Lauzon-Guay, J.-S., Scheibling, R.E., 2007. Seasonal variation in movement, aggregation and destructive grazing of the green sea urchin (*Strongylocentrotus droebachiensis*) in relation to wave action and sea temperature. *Mar Biol* 151, 2109-2118.
- Lecours, V., Devillers, R., Schneider, D.C., Lucieer, V.L., Brown, C.J., Edinger, E.N., 2015. Spatial scale and geographic context in benthic habitat mapping: review and future directions. *Mar Ecol Prog Ser* 535, 259-284.
- Levin, S.A., 1992. The problem of pattern and scale in ecology: the Robert H. MacArthur award lecture. *Ecology* 73, 1943-1967.
- Ling, S., 2008. Range expansion of a habitat-modifying species leads to loss of taxonomic diversity: a new and impoverished reef state. *Oecologia* 156, 883-894.
- Mann, K., 1973. Seaweeds: their productivity and strategy for growth. *Science* 182, 975-981.
- Merzouk, A., Johnson, L.E., 2011. Kelp distribution in the northwest Atlantic Ocean under a changing climate. *J Exp Mar Biol Ecol* 400, 90-98.
- Pagès, J.F., Gera, A., Romero, J., Alcoverro, T., 2014. Matrix composition and patch edges influence plant–herbivore interactions in marine landscapes. *Funct Ecol* 28, 1440-1448.
- Scheibling, R.E., Hennigar, A.W., Balch, T., 1999. Destructive grazing, epiphytism, and disease: the dynamics of sea urchin-kelp interactions in Nova Scotia. *Can J Fish Aquat Sci* 56, 2300-2314.
- Schneider, D.C., 2001. The rise of the concept of scale in ecology: The concept of scale is evolving from verbal expression to quantitative expression. *AIBS Bulletin* 51, 545-553.
- Steneck, R.S., Graham, M.H., Bourque, B.J., Corbett, D., Erlandson, J.M., Estes, J.A., Tegner, M.J., 2002. Kelp forest ecosystems: biodiversity, stability, resilience and future. *Environ Conserv* 29, 436-459.
- Wang, L., Sousa, W.P., Gong, P., 2004. Integration of object-based and pixel-based classification for mapping mangroves with IKONOS imagery. *Int J Remote Sens* 25, 5655-5668.

APPENDICES

APPENDIX 2.A: Further details regarding field equipment: fences used to create urchin enclosures and modified underwater swell kinetic instrument (URSKI)

The figures below show equipment built specifically to be used in the field in the present study. In this field experiment, urchin densities were manipulated within enclosures placed at the interface between kelp bed and urchin barren (see section 2.3.2 for details). Enclosures were delimited by 50-cm high fences, which are depicted and described in Figure A.1. During the experiment, the wave environment was quantified using a modified underwater relative swell kinetics instrument (URSKI; Figurski et al., 2011), which is depicted and described in Figure A.2.



Figure A.1. Photographs of the fences used to create urchin enclosures (photos by Anne P. St-Pierre). **Panel A** shows a section of fence laid on the ground upon assembly of the fence components. All fences were 50 cm high and built from aquaculture netting (Polyethylene netting 1.8 mm by 50 mm, mesh aperture of 2.5cm), heavy metal chains (link diameter 9.5 mm) sewn along the bottom of the netting, and small plastic floats (approximately 12 cm by 6 cm, oval shaped) attached every metre along the top of the netting. **Panels B and C** show the fences after installation in the field, when they were secured to the seafloor with eyebolts. The heavy chain weighed down the fence to ensure it remained on the seafloor and conformed to the topography of the latter, while the floats held the fence upright in the water column and allowed it to gently sway with wave surge.

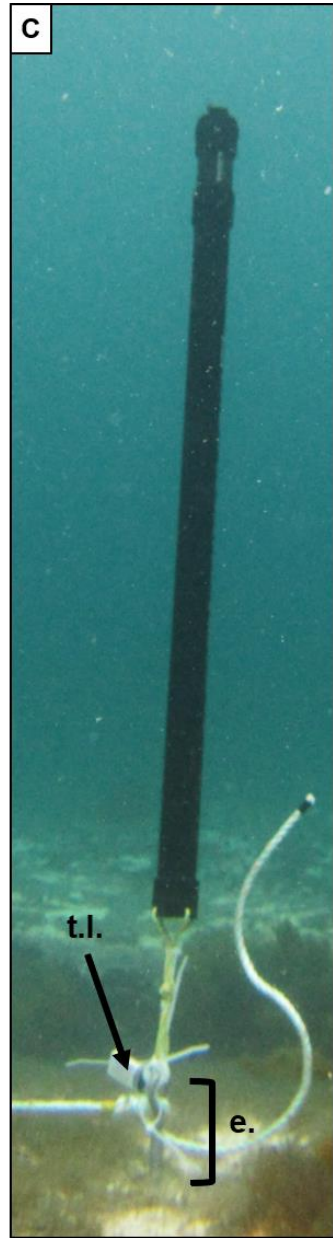
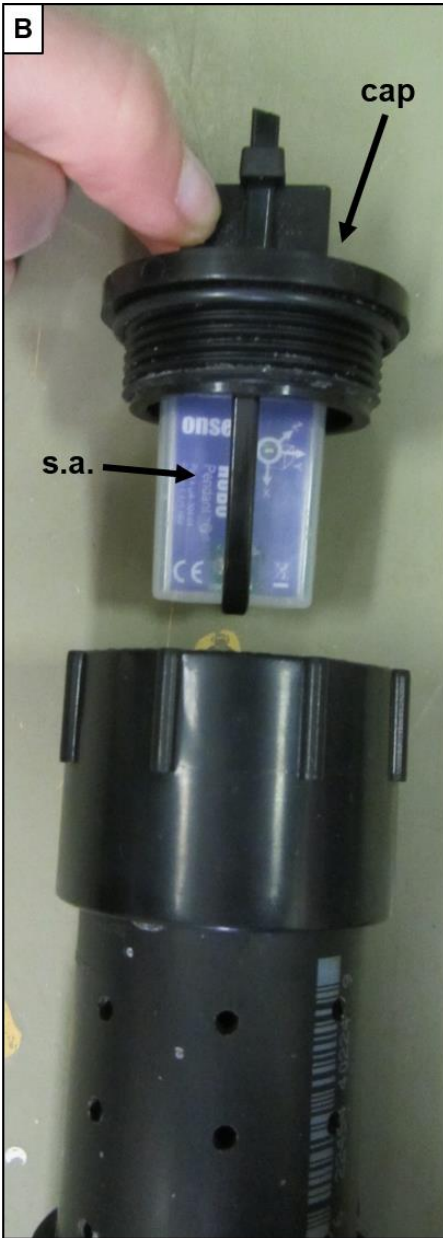
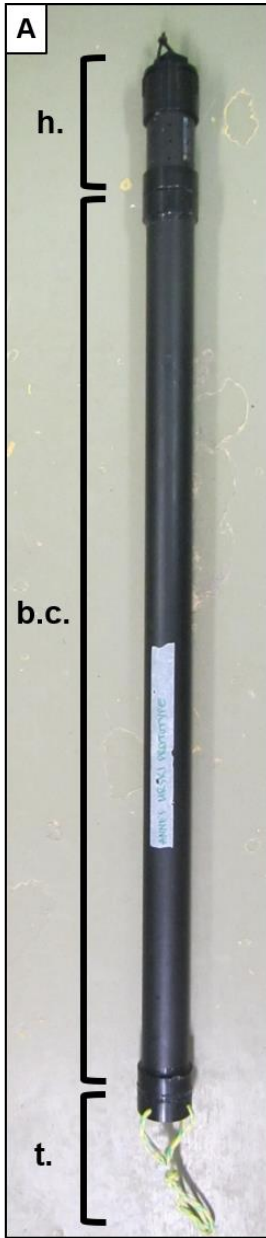


Figure A.2. Modified underwater relative swell kinetics instrument (URSKI; see section 2.3.4). **Panel A** shows the instrument upon fabrication, which consists of a cylindrical housing (h.) which holds the accelerometer, a slightly buoyant cylinder (b.c.) which maintains the instrument upright in the water column, and a tether (t.) affixed to the bottom of the buoyant cylinder which was used to secure the instrument to an eyebolt drilled in the seabed. **Panel B** shows a close-up view of the housing, where the removable screw-in cap of the device is being held out of the housing to show the submersible accelerometer (s.a.) attached inside. The housing and cap were designed to facilitate retrieval and replacement of the accelerometer underwater by simply manipulating the cap without needing to bring the entire instrument to the surface. **Panel C** shows the instrument after installation in the field, secured to an eyebolt (e.) drilled into the seabed. A temperature logger (t.l.) was attached to the same eyebolt and is also visible on this photograph.

**APPENDIX 2.B: Outcome of statistical analyses (see Material and Methods –
Statistical analysis for a detailed description of each analysis)**

Table 2.B.1. Summary of three-way ANCOVA (applied to raw data) examining the effect of Treatment (Natural, High, Medium, Low, and Very low densities, and Control corridor), Julian date (continuous variable), and Year (2015 or 2016) on the rate of kelp bed retreat ($\text{m}\cdot\text{mo}^{-1}$) in the experimental sites during summer. The factor Site was included in the analyses to account for variability inherent to this random factor, but not shown in the table as statistics pertaining to this factor are irrelevant for the present study.

Source of variation	<i>df</i>	χ^2	<i>p</i>
Treatment	5	5.919	0.314
Julian date	1	8.208	0.004
Year	1	3.474	0.062
Treatment x Julian date	5	6.751	0.240
Treatment x Year	5	3.721	0.590
Julian date x Year	1	3.663	0.056
Treatment x Julian date x Year	5	3.926	0.560

df = degrees of freedom; *p* = p value

Table 2.B.2. Summary of two-way ANCOVA (applied to raw data) examining the effect of Julian date (continuous variable) and Year (2015 or 2016) on the rate of kelp bed retreat ($\text{m}\cdot\text{mo}^{-1}$) in the control site year-round. The factor Corridor was included in the analyses to account for variability inherent to this random factor, but not shown in the table as statistics pertaining to this factor are irrelevant for the present study.

Source of variation	<i>df</i>	χ^2	<i>p</i>
Julian date	1	0.211	0.646
Year	1	1.815	0.178
Julian date x Year	1	1.933	0.164

df = degrees of freedom; *p* = p value

Table 2.B.3. Summary of two-way ANOVA (applied to raw data) examining the effect of Temperature (continuous) and Flow acceleration (continuous) on the rate of kelp bed retreat ($\text{m}\cdot\text{mo}^{-1}$) in the experimental sites during summer. The factor Site was included in the analyses to account for variability inherent to this random factor, but not shown in the table as statistics pertaining to this factor are irrelevant for the present study.

Source of variation	<i>df</i>	χ^2	<i>p</i>
Temperature	1	0.038	0.845
Flow acceleration	1	0.139	0.709
Temperature x Flow acceleration	1	0.038	0.845

df = degrees of freedom; *p* = p value

Table 2.B.4. Summary of two-way ANOVA (applied to raw data) examining the effect of Temperature (continuous) and Flow acceleration (continuous) on the rate of kelp bed retreat ($\text{m}\cdot\text{mo}^{-1}$) at the control site year-round. The factor Corridor was included in the analyses to account for variability inherent to this random factor, but not shown in the table as statistics pertaining to this factor are irrelevant for the present study.

Source of variation	<i>df</i>	χ^2	<i>p</i>
Temperature	1	6.805	0.009
Flow acceleration	1	1.126	0.289
Temperature x Flow acceleration	1	0.836	0.361

df = degrees of freedom; *p* = p value

Table 2.B.5. Summary of three-way ANCOVA (applied to raw data) examining the effect of Treatment (Natural, High, Medium, Low, and Very low densities, and Control corridor), Julian date (continuous variable), and Year (2015 or 2016) on the density of urchins (urchins·m⁻²) at the front within the experimental sites during summer. The factor Site was included in the analyses to account for variability inherent to this random factor, but not shown in the table as statistics pertaining to this factor are irrelevant for the present study.

Source of variation	<i>df</i>	χ^2	<i>p</i>
Treatment	5	38.745	<0.001
Julian date	1	21.668	<0.001
Year	1	11.691	0.001
Treatment x Julian date	5	29.500	<0.001
Treatment x Year	5	23.825	<0.001
Julian date x Year	1	7.128	0.008
Treatment x Julian date x Year	5	18.081	0.003

df = degrees of freedom; *p* = p value

Table 2.B.6. Summary of two-way ANCOVA (applied to raw data) examining the effect of Julian date (continuous variable) and Year (2015 or 2016) on the density of urchins at the front in the control site year-round. The factor Corridor was included in the analyses to account for variability inherent to this random factor, but not shown in the table as statistics pertaining to this factor are irrelevant for the present study.

Source of variation	<i>df</i>	χ^2	<i>p</i>
Julian date	1	2.597	0.107
Year	1	1.205	0.272
Julian date x Year	1	0.004	0.949

df = degrees of freedom; *p* = p value

Table 2.B.7. Summary of two-way ANOVA (applied to raw data) examining the effect of Temperature (continuous) and Flow acceleration (continuous) on the density of urchins (urchins·m⁻²) at the front in the experimental sites during summer. The factor Site was included in the analyses to account for variability inherent to this random factor, but not shown in the table as statistics pertaining to this factor are irrelevant for the present study.

Source of variation	<i>df</i>	χ^2	<i>p</i>
Temperature	1	0.312	0.574
Flow acceleration	1	0.321	0.571
Temperature x Flow acceleration	1	0.715	0.398

df = degrees of freedom; *p* = p value

Table 2.B.8. Summary of two-way ANOVA (applied to raw data) examining the effect of Temperature (continuous) and Flow acceleration (continuous) on the density of urchins (urchins·m⁻²) at the front at the control site. The factor Corridor was included in the analyses to account for variability inherent to this random factor, but not shown in the table as statistics pertaining to this factor are irrelevant for the present study.

Source of variation	<i>df</i>	χ^2	<i>p</i>
Temperature	1	0.199	0.656
Flow acceleration	1	0.859	0.354
Temperature x Flow acceleration	1	2.913	0.088

df = degrees of freedom; *p* = p value

Table 2.B.9. Summary of three-way ANCOVA (applied to raw data) examining the effect of Treatment (Natural, High, Medium, Low, and Very low densities, and Control corridor), Julian date (continuous variable), and Year (2015 or 2016) on the density of urchins (urchins·m⁻²) in the barren area in the experimental sites. The factor Site was included in the analyses to account for variability inherent to this random factor, but not shown in the table as statistics pertaining to this factor are irrelevant for the present study.

Source of variation	<i>df</i>	χ^2	<i>p</i>
Treatment	5	3.351	0.646
Julian date	1	0.967	0.325
Year	1	4.066	0.044
Treatment x Julian date	5	3.436	0.633
Treatment x Year	5	3.861	0.570
Julian date x Year	1	3.843	0.048
Treatment x Julian date x Year	5	3.598	0.609

df = degrees of freedom; *p* = p value

Table 2.B.10. Summary of two-way ANCOVA (applied to raw data) examining the effect of Julian date (continuous variable) and Year (2015 or 2016) on the density of urchins in the barren in the control site. The factor Corridor was included in the analyses to account for variability inherent to this random factor, but not shown in the table as the statistics pertaining to this factor are irrelevant for the present study.

Source of variation	<i>df</i>	χ^2	<i>p</i>
Julian date	1	22.715	<0.001
Year	1	24.261	<0.001
Julian date x Year	1	32.039	<0.001

df = degrees of freedom; *p* = p value

Table 2.B.11. Summary of two-way ANOVA (applied to raw data) examining the effect of Temperature (continuous) and Flow acceleration (continuous) on the density of urchins (urchins·m⁻²) in the barren in the experimental sites in summer. The factor Site was included in the analyses to account for variability inherent to this random factor, but not shown in the table as statistics pertaining to this factor are irrelevant for the present study.

Source of variation	<i>df</i>	χ^2	<i>p</i>
Temperature	1	5.993	0.014
Flow acceleration	1	2.163	0.141
Temperature x Flow acceleration	1	2.575	0.109

df = degrees of freedom; *p* = p value

Table 2.B.12. Summary of two-way ANOVA (applied to raw data) examining the effect of Temperature (continuous) and Flow acceleration (continuous) on the density of urchins (urchins·m⁻²) in the barren at the control site. The factor Corridor was included in the analyses to account for variability inherent to this random factor, but not shown in the table as statistics pertaining to this factor are irrelevant for the present study.

Source of variation	<i>df</i>	χ^2	<i>p</i>
Temperature	1	0.103	0.748
Flow acceleration	1	8.370	0.004
Temperature x Flow acceleration	1	4.405	0.036

df = degrees of freedom; *p* = p value

APPENDIX 3.A: Glossary of common terms in remote sensing and GIS used in the present study.

Term	Definition	Source
Color composite image	A color image made by assigning a red, green, and blue colors to each of the separate monotone bands of a multispectral image and then superimposing them.	1
Georectification or georeferencing	The process of referencing features in an image or grid to a geographic coordinate system using ground control points by shifting, rotating, scaling, skewing or projecting the image. This process removes the effects of tilt or relief from a map or image.	1
Ground control point (GCP)	A point on the ground whose location has been determined by a horizontal coordinate system or a vertical datum. Usually a location in the field at which data has been collected for analysis or quality control.	1
Kriging	An interpolation technique in which the surrounding measured values are weighted to derive a predicted value for an unmeasured location. Weights are based on the distance between the measured points, the prediction locations, and the overall spatial arrangement among the measured points.	4
Nearest neighbour resampling	A technique for resampling raster data in which the value of each cell in an output grid is calculated using the value of the nearest cell in an input grid. Nearest neighbour assignment (or resampling) does not change any of the values of cells from the input layer.	1
Orthorectification	The process of correcting the geometry of an image so that it appears as though each pixel were acquired from directly overhead. Orthorectification uses elevation data to correct terrain distortion in aerial or satellite imagery.	4
Pan-sharpening or resolution merging	Shorthand for “panchromatic sharpening”; Process of sharpening a low-resolution, multiband image by merging it with a high-resolution monochrome image.	1
Raster	A spatial data model, which defines space as an array of equally sized cells arranged in rows and columns, and composed of single or multiple bands. Each cell	1

	contains an attribute value and location coordinates. Unlike a vector structure, which stores coordinates explicitly, raster coordinates are contained in the ordering of the matrix. Groups of cells that share the same value represent the same type of geographic feature.	
Signature file	File that contains multivariate statistics for each class or cluster of interest (mean for each class, number of cells in the class, and variance-covariance matrix for the class) used in supervised classifications (e.g., Maximum Likelihood Classification [MLC]).	3
Spectral band	One layer of a multispectral image that represents data values for a specific range of reflected light or heat, such as ultraviolet, blue, green, red, infrared, or radar, or other values derived by manipulating the original image bands. A standard color display of a multispectral image shows three bands, one each for red, green, and blue.	1
Spectral resolution	The range of wavelengths that an imaging system can detect which ultimately affects the number of unique spectral signatures in the imagery.	1
Thematic map	A map of the spatial distribution of various classes of a theme in a geographical context such as land use and land cover, forest type, and hydrogeomorphology. Scale and level of details in a thematic map depend on its intended application.	2

Adapted from:

¹ Kennedy, H., 2001. The ESRI Press dictionary of GIS terminology. ESRI Press.

² Sahu, K.C., 2007. Textbook of remote sensing and geographical information systems. Atlantic Publishers & Dist.

³ ESRI. ArcGIS Desktop 9.3 Help. Access on February 26 2018;
<http://webhelp.esri.com/arcgisdesktop/9.3>

⁴ ESRI. Online technical support, GIS Dictionary. Accessed on February 26 2019:
<https://support.esri.com/en/other-resources/gis-dictionary>

APPENDIX 3.B: Contingency tables for each combination of classification technique and image source.

In each table below, columns show the reference data obtained from ground truthing (i.e., test dataset). Sums at the bottom of each column show the total number of locations truly belonging to kelp or non-kelp classes (based on reference data). Rows present the outcome of the classification applied to the remotely sensed imagery (“Classified data”). Sums at the end of each row show the total number of locations attributed to each class based on classification. Matrix diagonal (bolded values) shows the number of correctly classified locations for each class. All non-diagonal elements in the matrix are locations that have been misclassified. For example, with the unsupervised classification of satellite imagery (Table 3.B.1), 23 non-kelp locations were misclassified as kelp, while 17 kelp locations were wrongly classified as non-kelp.

For more information on contingency tables, refer to Lillesand et al. (2014) and Green et al. (2000). For details of the accuracy metrics used in the present study, refer to section 3.3.5 and see Landis and Koch (1977) and Lillesand et al. (2014).

Table 3.B.1. Contingency table for the unsupervised classification of satellite imagery.

		Reference data		Sum
		Kelp	Non-kelp	
Classified data	Kelp	73	23	96
	Non-kelp	17	18	35
	Sum	90	41	131

Table 3.B.2. Contingency table for the supervised classification of satellite imagery.

		Reference data		Sum
		Kelp	Non-kelp	
Classified data	Kelp	77	3	80
	Non-kelp	13	38	51
	Sum	90	41	131

Table 3.B.3. Contingency table for the visual classification of satellite imagery.

		Reference data		Sum
		Kelp	Non-kelp	
Classified data	Kelp	83	19	102
	Non-kelp	7	22	29
	Sum	90	41	131

Table 3.B.4. Contingency table for the unsupervised classification of aerial imagery.

		Reference data		Sum
		Kelp	Non-kelp	
Classified data	Kelp	61	15	76
	Non-kelp	29	25	54
Sum		90	40	130

Table 3.B.5. Contingency table for the supervised classification of aerial imagery.

		Reference data		Sum
		Kelp	Non-kelp	
Classified data	Kelp	72	7	79
	Non-kelp	18	33	51
Sum		90	40	130

Table 3.B.6. Contingency table for the visual classification of aerial imagery.

		Reference data		Sum
		Kelp	Non-kelp	
Classified data	Kelp	86	10	96
	Non-kelp	4	30	34
Sum		90	40	130

References cited in Appendix 3.B:

- Green, E., Mumby, P., Edwards, A., Clark, C., 2000. Remote Sensing: Handbook for Tropical Coastal Management. United Nations Educational, Scientific and Cultural Organization (UNESCO).
- Landis, J.R., Koch, G.G., 1977. The measurement of observer agreement for categorical data. *biometrics*, 159-174.
- Lillesand, T., Kiefer, R.W., Chipman, J., 2014. Remote sensing and image interpretation. John Wiley & Sons.

APPENDIX 5.A: Assessment of the transferability of observer training in visual classification

Image classification was conducted visually by an observer trained to distinguish kelp and non-kelp benthic classes based on their shade and the contrast between kelp and non-kelp features. The observer's training was conducted by comparing the visual characteristics of kelp and non-kelp areas from color imagery collected in July 2016 and ground truth data (underwater imagery from a drop camera system, acquired at 199 locations throughout the study area of 4 islands, i.e., Île à Firmin, Île du Havre, Île aux Goélands, and Petite île au Marteau) collected within the following three weeks. Further details regarding observer training are available in St-Pierre and Gagnon (2020). All classifications were completed by the same observer to ensure consistency. Classification accuracy was evaluated using contingency tables to calculate the overall accuracy, kappa coefficient, producer's accuracy, and user's accuracy of each classification. See Landis and Koch (1977) and Lillesand et al. (2014) for further discussion of these accuracy statistics.

Section 1. Comparison of accuracy between the classification of color and black-and-white imagery acquired in 2016 at four islands in the Mingan Archipelago

To determine if the training acquired by the observer for the identification of kelp and non-kelp areas on color imagery yielded similar results when applied to color and black-and-white imagery, the observer classified the black-and-white imagery and an accuracy assessment was performed (see below). The color imagery acquired in 2016 was

converted into black-and-white imagery by using the Grayscale function in ArcMap 10.3.1 (Esri, 2015), thus providing imagery in both color types for the exact same extent.

Accuracy assessment of color imagery

The outcome of the accuracy assessment for color imagery presented in the contingency table below (Table 5.A.1) yielded an overall accuracy of 90.0% (with a 95% confidence interval of 5.5%), and a Kappa coefficient of 0.76. Producer’s and user’s accuracy (with 95% confidence interval) are presented in the table below (Table 5.A.2).

Table 5.A.1. Contingency table from the accuracy assessment of the visual classification of color imagery from Île à Firmin, Île du Havre, Île aux Goélands, and Petite île au Marteau.

	Class	Reference data		Sum
		Kelp	Non-kelp	
Classified data	Kelp	86	10	96
	Non-kelp	4	30	34
	Sum	90	40	130

Table 5.A.2. Producer’s and user’s accuracy calculated from the visual classification of color imagery from Île Niapiskau, Île à Firmin, Île du Havre, Île aux Goélands, and Petite île au Marteau.

	Producer’s accuracy (%)	User’s accuracy (%)
Kelp cover	96.6 ± 4.3	89.6 ± 6.6
Non-kelp cover	75.6 ± 14.4	91.2 ± 11.0

Accuracy assessment of black-and-white imagery

The outcome of the accuracy assessment for black-and-white imagery presented in the contingency table below (Table 5.A.3) yielded an overall accuracy of 88.5% (with a 95% confidence interval of 5.9%), and a Kappa coefficient of 0.74. Producer’s and user’s accuracy (with 95% confidence interval) are presented in the table below (Table 5.A.4).

Table 5.A.3. Contingency table from the accuracy assessment of the visual classification of black-and-white imagery from Île Niapiskau, Île à Firmin, Île du Havre, Île aux Goélands, and Petite île au Marteau.

		Reference data		Sum
		Kelp	Non-kelp	
Classified data	Kelp	79	8	87
	Non-kelp	7	36	43
Sum		86	44	130

Table 5.A.4. Producer’s and user’s accuracy calculated from the visual classification of black-and-white imagery from Île à Firmin, Île du Havre, Île aux Goélands, and Petite île au Marteau.

	Producer’s accuracy (%)	User’s accuracy (%)
Kelp cover	91.8 ± 6.4	90.8 ± 6.6
Non-kelp cover	81.8 ± 12.5	83.7 ± 12.2

Conclusion

High overall accuracy and Kappa coefficient were obtained for the classification of both color and black-and-white imagery. Since the accuracy assessment is reasonably good and that the outcome of the classification on both image type is similar, it is concluded that visual characteristics of kelp beds on color or black-and-white aerial imagery from the same archipelago is equivalent.

Section 2. Accuracy assessment of the visual classification applied to black and white imagery acquired in 2016 at Île Niapiskau and Île du Fantôme

To determine if the training acquired by the observer for the identification of kelp and non-kelp areas was spatially transferable, the visual classification technique was applied to black and white imagery from two islands (Île Niapiskau and Île du Fantôme) in the Mingan Archipelago acquired in July 2016. Ground truth data (underwater imagery) collected in the study area of these two islands was also available, since 65 locations had been surveyed with a drop camera system in the three weeks following image acquisition in 2016. However, this ground truth data was not used in observer training; rather, it was only used to assess the accuracy of the classification. Accuracy assessment of classified imagery from these two islands is presented below.

Accuracy assessment

The outcome of the accuracy assessment presented in the contingency table (Table 5.A.5) yielded an overall accuracy of 84.6% (with a 95% confidence interval of 9.5%), and a Kappa coefficient of 0.69. Producer's and user's accuracy (with 95% confidence interval) are presented in the table below (Table 5.A.6).

Table 5.A.5. Contingency table for the visual classification of imagery from Île Niapiskau and Île du Fantôme.

	Class	Reference data		Sum
		Kelp	Non-kelp	
Classified data	Kelp	25	6	31
	Non-kelp	4	30	34
	Sum	29	36	65

Table 5.A.6. Producer's and user's accuracy calculated from the visual classification of imagery from Île Niapiskau and Île du Fantôme.

	Producer's accuracy (%)	User's accuracy (%)
Kelp cover	86.2 ± 14.3	80.7 ± 15.5
Non-kelp cover	83.3 ± 13.6	88.2 ± 12.3

Conclusion

High overall accuracy and Kappa coefficient were obtained for the classification of imagery from Île Niapiskau and Île du Fantôme. Thus, it is concluded that the knowledge

of a trained observer who learned to distinguish the visual characteristics of kelp beds by observing and classifying aerial imagery from the same archipelago can be transferred spatially for the classification of areas within the Mingan Archipelago which were not used during training.

Section 3. Accuracy assessment of the visual classification of black-and-white imagery acquired in 2004 at four islands in the Mingan Archipelago

To determine if the training acquired by the observer for the identification of kelp and non-kelp areas was temporally transferable, the classification technique was applied to imagery acquired in 2004 at Île à Firmin, Île du Havre, Île aux Goélands, and Petite île au Marteau. Ground truth data (underwater imagery) collected in the study area of these four islands was also available, since 30 locations had been surveyed with a drop camera system in the week following image acquisition in 2004. However, this ground truth data was not used in observer training; rather, it was only used to assess the accuracy of the classification. Accuracy assessment of classified imagery from these two islands is presented below.

Accuracy assessment

The outcome of the accuracy assessment presented in the contingency table (Table 5.A.7) yielded an overall accuracy of 72.7% (with a 95% confidence interval of 16.7%), and a Kappa coefficient of 0.43. Producer's and user's accuracy (with 95% confidence interval) are presented in the table below (Table 5.A.8).

Table 5.A.7. Contingency table for the visual classification of imagery collected in 2004 at Île à Firmin, Île du Havre, Île aux Goélands, and Petite île au Marteau.

		Reference data		Sum
		Kelp	Non-kelp	
Classified data	Kelp	16	7	23
	Non-kelp	2	8	10
Sum		18	15	33

Table 5.A.8. Producer's and user's accuracy calculated from the visual classification of imagery collected in 2004 at Île à Firmin, Île du Havre, Île aux Goélands, and Petite île au Marteau.

	Producer's accuracy (%)	User's accuracy (%)
Kelp cover	88.9 ± 17.3	69.6 ± 21.0
Non-kelp cover	53.3 ± 28.6	80.0 ± 29.8

Conclusion

The overall accuracy and Kappa coefficient obtained for the classification of imagery from imagery acquired in 2004 were reasonably high. Thus, it is concluded that the knowledge of a trained observer who learned to distinguish the visual characteristics of kelp beds by observing and classifying aerial imagery from the same archipelago in different years can be transferred for the classification of imagery acquired at different time periods, with reasonable confidence in the classification outcome.

References cited in Appendix 5.A:

Esri, 2015. ArcGIS Desktop; Release 10.3.1, Redland, CA.

Landis, J.R., Koch, G.G., 1977. The measurement of observer agreement for categorical data. *biometrics*, 159-174.

Lillesand, T., Kiefer, R.W., Chipman, J., 2014. Remote sensing and image interpretation. John Wiley & Sons.

St-Pierre, A.P., Gagnon, P., 2020. Kelp-bed dynamics across scales: Enhancing mapping capability with remote sensing and GIS. *J Exp Mar Biol Ecol* 522, 151246.

APPENDIX 5.B: Spatial pattern metrics of the non-kelp benthic class and their correlation with oceanographic and atmospheric parameters

The seven spatial pattern metrics presented in section 5.3.3 were calculated for the non-kelp benthic class. Non-kelp coverage showed an opposite trend to kelp coverage, with a minimum observed in 2016 (37.66%) and maximum in 1983 (55.81%; Table 5.B.1). Largest patch indices for non-kelp benthic class varied between 10.90 (2016) and 14.21% (1988; Table 5.B.1). Mean non-kelp patch area showed marked variations among years, with lowest value of $5902 \pm 2099 \text{ m}^2$ in 2016 and highest of $14878 \pm 4886 \text{ m}^2$ in 1988 (Table 5.B.1). For any given year, the number of non-kelp patches was always higher than the number of kelp patches (Table 5.B.1). While the minimum patch size for both benthic classes was always 225 m^2 (i.e., the area around a single grid intersect), mean patch size was generally higher for the kelp than non-kelp benthic class (all years except 1983; Table 5.B.1). Maximum patch size was higher in the non-kelp than kelp benthic class between 1983 and 1999, but higher in the kelp benthic class in 2004 and 2009 (Table 5.B.1). Shape indices, mean nearest neighbour distances, and clumpiness indices calculated for the non-kelp benthic class showed little variation among years (Table 5.B.1).

Assessment of the correlations between spatial pattern metrics calculated for the non-kelp benthic class and oceanographic or atmospheric parameters from the same year as image acquisition indicated nine correlations as statistically significant (Table 5.B.2, Figure 5.B.1). Non-kelp percent coverage was positively correlated with the NAO indices calculated for the spring (April to July; Pearson's $r = 0.868$, Table 5. B.2, Figure 5.B.1). Largest patch indices for non-kelp was positively correlated with the duration of the ice-

covered season (Pearson's $r = 0.979$, Table 5.B.2, Figure 5.B.1). Number of non-kelp patches was negatively correlated with the average sea surface temperature in July (Pearson's $r = -0.811$, Table 5.B.2, Figure 5.B.1). Shape indices for the non-kelp benthic class was positively correlated with both the date of last ice occurrence (Pearson's $r = 0.828$, Table 5.B.2, Figure 5.B.1) and the duration of the ice-covered season (Pearson's $r = 0.861$, Table 5.B.2, Figure 5.B.1). Clumpiness indices for non-kelp patches was negatively correlated with the date of last ice occurrence (Pearson's $r = -0.893$, Table 5.B.2, Figure 5.B.1). Mean nearest neighbour distance for the non-kelp benthic class was negatively correlated with the anomaly in ice volume (Pearson's $r = -0.857$, Table 5.B.2), the maximum ice volume (Pearson's $r = -0.930$, Table 5.B.2), and the date of last ice occurrence (Pearson's $r = -0.811$, Table 5.B.2), but these correlations are not further discussed due to the low and stable values of nearest neighbour distances suggesting that variations in mean nearest neighbour distance are likely of little biological significance.

Assessment of the correlation between spatial pattern metrics calculated for the non-kelp benthic class and oceanographic or atmospheric parameters from the year prior to image acquisition indicated eight correlations as statistically significant (Table 5.B.3, Figure 5.B.2). Non-kelp percent coverage was negatively correlated with average August sea surface temperature calculated in the year prior to image acquisition (Pearson's $r = -0.921$, Table 5.B.3, Figure 5.B.2). Largest patch indices for non-kelp was negatively correlated with the sum of standardized anomalies in sea surface temperature calculated on the year prior to image acquisition (Pearson's $r = -0.825$, Table 5.B.3, Figure 5.B.2). Shape indices for the non-kelp benthic class was negatively correlated with the average August

sea surface temperature (Pearson's $r = -0.924$, Table 5.B.3, Figure 5.B.2), the date of last ice occurrence (Pearson's $r = -0.849$, Table 5.B.3, Figure 5.B.2) and the NAO indices for spring (April to July; Pearson's $r = -0.897$, Table 5.B.3, Figure 5.B.2), all calculated for the year prior to image acquisition. Mean nearest neighbour distance for the non-kelp benthic class was negatively correlated with the average June sea surface temperature (Pearson's $r = -0.854$, Table 5.B.3) and positively correlated with average August sea surface temperature (Pearson's $r = 0.976$, Table 5.B.3) and the NAO indices for spring (April to July; Pearson's $r = 0.897$, Table 5.B.3), all calculated for the year prior to image acquisition. However, correlations with mean nearest neighbour distances are not further discussed due to the low and stable values of nearest neighbour distances calculated suggesting that variations in mean nearest neighbour distance are likely of little biological significance.

Table 5.B.1. Outcome of the spatial pattern metrics calculated for the non-kelp benthic class on imagery from each of the six years studied. Mean values are presented with standard error (\pm SE).

Year	Percent cover (%)	Largest patch index (%)	Patch area (m ²)			Number of patches	Shape index	Mean nearest neighbour distance (m ²)	Clumpiness index
			Min.	Mean (\pm SE)	Max.				
1983	55.81	13.74	225	14,878 \pm 4886	318,600	87	1.39 \pm 0.07	41.12 \pm 1.91	0.67
1988	47.82	14.21	225	7922 \pm 2818	329,625	140	1.46 \pm 0.07	37.50 \pm 1.08	0.55
1999	51.61	13.47	225	12,469 \pm 4528	312,300	96	1.39 \pm 0.08	38.05 \pm 1.19	0.65
2004	47.67	11.49	225	10,051 \pm 3352	266,400	110	1.36 \pm 0.07	40.39 \pm 1.75	0.66
2009	40.57	12.96	225	6580 \pm 2468	300,600	143	1.33 \pm 0.04	40.91 \pm 1.54	0.66
2016	37.66	10.9	225	5902 \pm 2099	252,900	148	1.28 \pm 0.04	43.66 \pm 1.69	0.67

Table 5.B.2. Pearson correlation coefficients for correlations between environmental parameters (measured during the year of collection) and spatial pattern metrics calculated for the non-kelp benthic class, where bolded values indicate statistical significance (p-value < 0.05). See Table 5.1 for details regarding each environmental parameter.

Spatial pattern metric*	Average temperature				Ice conditions						NAO index		
	May	June	July	May to July average	Sum of standardized anomalies	Anomaly in ice volume	Maximum ice volume	Date of first ice occurrence	Date of last ice occurrence	Duration of ice-covered season	Yearly	Spring	Winter
PC	-0.626	0.520	0.509	0.346	-0.045	0.293	0.391	-0.726	0.218	0.608	0.487	0.868	0.036
LPI	-0.465	0.382	-0.216	0.044	-0.173	0.629	0.685	-0.910	0.773	0.979	-0.059	0.345	-0.247
MPA	-0.564	0.681	0.738	0.595	0.184	0.048	0.210	-0.629	-0.083	0.397	0.594	0.789	0.168
NP	0.534	-0.615	-0.811	-0.576	-0.281	-0.040	-0.215	0.476	0.182	-0.263	-0.532	-0.802	-0.101
SI	-0.483	-0.028	-0.239	-0.331	-0.453	0.761	0.712	-0.663	0.828	0.861	-0.039	0.641	-0.322
MNND	0.275	0.170	0.319	0.387	0.140	-0.857	-0.930	0.445	-0.811	-0.737	0.401	-0.484	0.511
CI	0.009	0.460	0.750	0.669	0.616	-0.636	-0.533	0.340	-0.893	-0.641	0.308	-0.136	0.221

* PC: Percent cover, LPI: Largest patch index, MPA: Mean patch area, NP: Number of patches, SI: Shape index, MNND: Mean nearest neighbour distance, CI: Clumpiness index.

Table 5.B.3. Pearson correlation coefficients for correlations between environmental parameters (measured during the year prior to collection) and spatial pattern metrics calculated for the non-kelp benthic class, where bolded values indicate statistical significance (p -value < 0.05). See Table 5.1 for details regarding each environmental parameter.

Spatial pattern metric*	Average temperature						Number of weeks above 10 C	Ice conditions					NAO index			
	May	June	July	August	September	May to July average		Sum of standardized anomalies	Anomaly in ice volume	Maximum ice volume	Date of first ice occurrence	Date of last ice occurrence	Duration of ice-covered season	Yearly	Spring	Winter
PC	0.011	0.235	-0.498	-0.921	-0.673	-0.252	-0.128	-0.765	-0.195	-0.456	-0.284	0.563	0.472	0.257	-0.680	-0.576
LPI	0.395	0.476	-0.068	-0.809	-0.507	0.191	-0.410	-0.825	-0.586	-0.161	-0.606	0.054	0.315	0.093	-0.687	-0.248
MPA	0.059	0.089	-0.603	-0.718	-0.469	-0.333	0.212	-0.635	-0.211	-0.680	0.025	0.499	0.266	0.061	-0.464	-0.672
NP	-0.081	-0.124	0.512	0.574	0.443	0.263	-0.265	0.472	0.128	0.685	-0.092	-0.514	-0.259	0.016	0.452	0.766
SI	0.022	0.547	0.012	-0.924	-0.809	0.135	-0.572	-0.722	-0.172	0.187	-0.849	0.390	0.684	0.487	-0.897	-0.183
MNND	-0.332	-0.854	-0.383	0.976	0.633	-0.533	0.393	0.421	0.310	-0.149	0.767	-0.128	-0.507	-0.170	0.897	0.365
CI	0.103	-0.491	-0.281	0.697	0.473	-0.249	0.591	0.439	0.135	-0.597	0.853	-0.020	-0.452	-0.564	0.560	-0.360

* PC: Percent cover, LPI: Largest patch index, MPA: Mean patch area, NP: Number of patches, SI: Shape index, MNND: Mean nearest neighbour distance, CI: Clumpiness index.

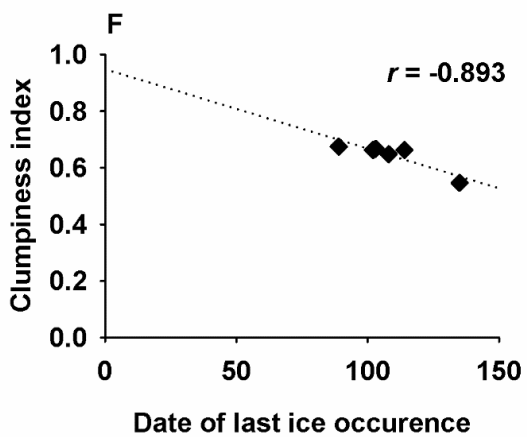
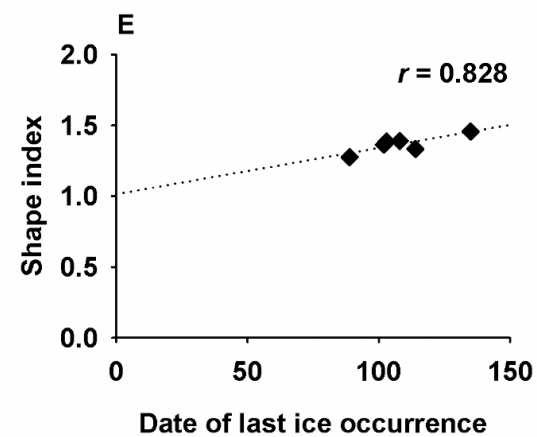
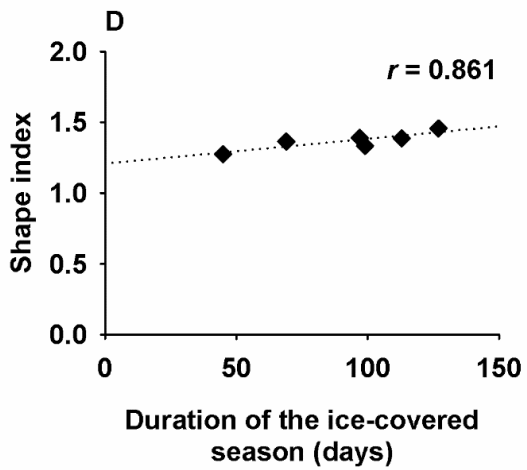
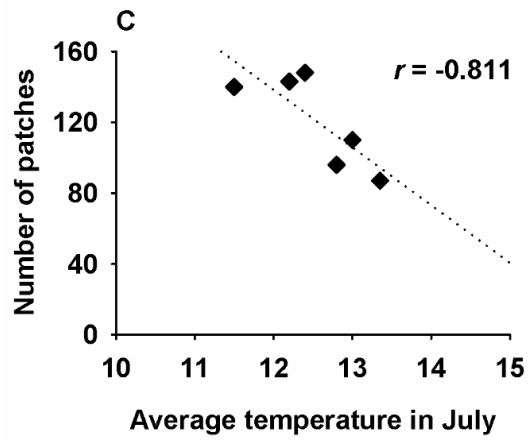
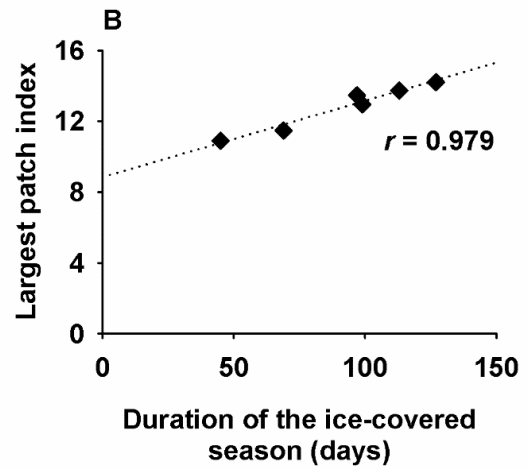
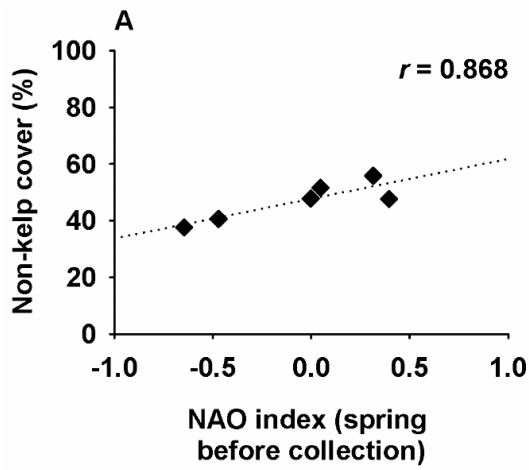


Figure 5.B.1. Relationships between spatial pattern metrics calculated for the non-kelp benthic class and environmental parameters measured in the same years as the collections occurred. Only statistically significant correlations are shown ($p < 0.05$, see Table B.2). Pearson correlation coefficient (r) is indicated for each correlation. NAO index refers to the North Atlantic Oscillation Index (see Section 5.3.3).

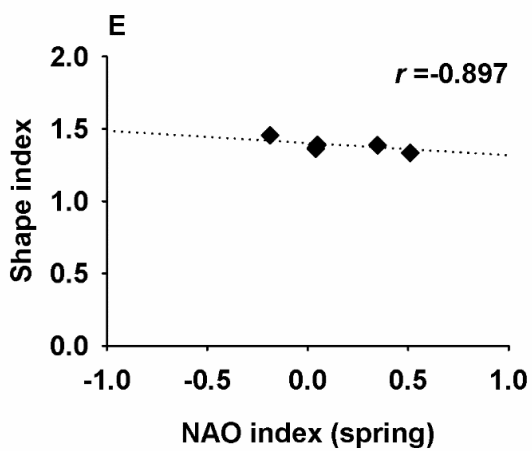
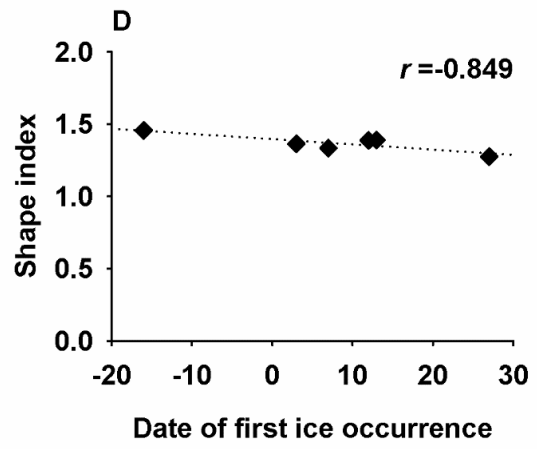
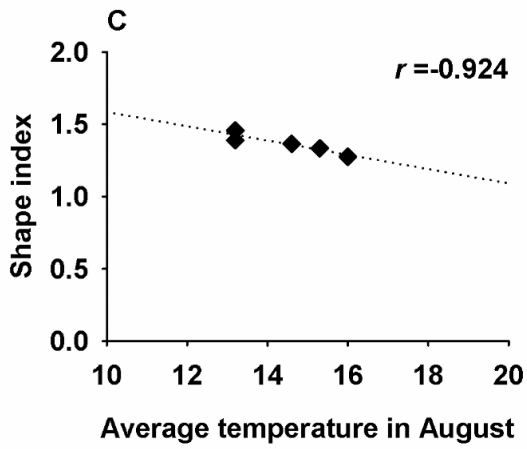
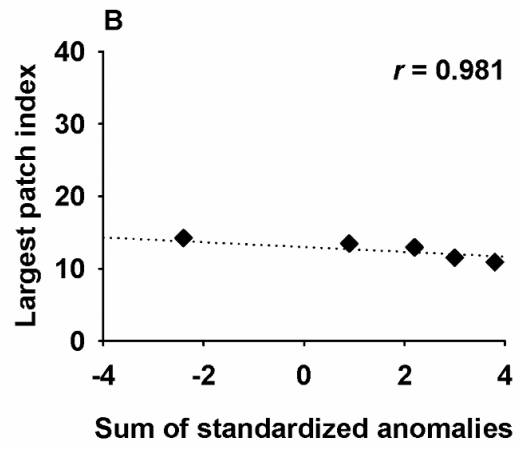
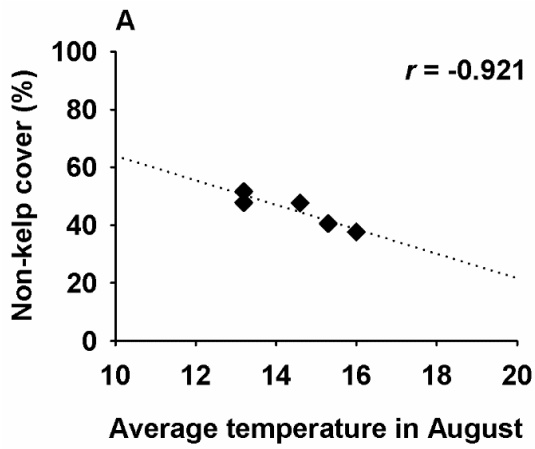


Figure 5.B.2. Relationships between spatial pattern metrics calculated for the non-kelp benthic class and environmental parameters measured in the year prior to each collection occurring. Only statistically significant correlations are shown ($p < 0.05$, see Table B.3). Pearson correlation coefficient (r) is indicated for each correlation. NAO index refers to the North Atlantic Oscillation Index (see Section 5.3.3).

APPENDIX 5.C: Correlations between environmental parameters and spatial pattern metrics calculated for the kelp benthic cover class

Table 5.C.1. Pearson correlation coefficients for correlations between environmental parameters (measured during the year of collection) and spatial pattern metrics calculated for the kelp benthic class, where bolded values indicate statistical significance (p -value<0.05). See Table 5.1 for details regarding each environmental parameter.

Spatial pattern metric*	Average temperature				Ice conditions						NAO index		
	May	June	July	May to July average	Sum of standardized anomalies	Anomaly in ice volume	Maximum ice volume	Date of first ice occurrence	Date of last ice occurrence	Duration of ice-covered season	Yearly	Spring	Winter
PC	0.626	-0.520	-0.509	-0.346	0.045	-0.293	-0.391	0.726	-0.218	-0.608	-0.487	-0.868	-0.036
LPI	0.298	-0.091	-0.017	0.052	0.180	-0.500	-0.631	0.628	-0.551	-0.689	-0.139	-0.700	0.025
MPA	0.687	-0.153	0.081	0.210	0.603	-0.632	-0.476	0.757	-0.724	-0.866	-0.234	-0.712	0.225
NP	-0.350	-0.183	-0.520	-0.504	-0.809	0.566	0.345	-0.566	0.840	0.761	0.050	0.342	-0.140
SI	0.288	0.113	0.309	0.340	0.878	0.036	0.460	0.145	-0.243	-0.173	-0.351	0.035	-0.110
MNND	0.223	0.130	0.761	0.483	0.616	-0.586	-0.373	0.509	-0.882	-0.744	0.300	0.126	0.329
CI	-0.283	0.589	0.818	0.672	0.461	-0.496	-0.483	0.145	-0.771	-0.440	0.415	0.052	0.113

* PC: Percent cover, LPI: Largest patch index, MPA: Mean patch area, NP: Number of patches, SI: Shape index, MNND: Mean nearest neighbour distance, CI: Clumpiness index.

Table 5.C.2. Pearson correlation coefficients for correlations between environmental parameters (measured during the year prior to collection) and spatial pattern metrics calculated for the kelp benthic class, where bolded values indicate statistical significance (p -value<0.05). See Table 5.1 for details regarding each environmental parameter.

Spatial pattern metric*	Average temperature					May to July average	Number of weeks above 10 C	Sum of standardized anomalies	Ice conditions					NAO index		
	May	June	July	August	September				Anomaly in ice volume	Maximum ice volume	Date of first ice occurrence	Date of last ice occurrence	Duration of ice-covered season	Yearly	Spring	Winter
PC	-0.011	-0.235	0.498	0.921	0.673	0.252	0.128	0.765	0.195	0.456	0.284	-0.563	-0.472	-0.257	0.680	0.576
LPI	-0.031	-0.582	0.144	0.981	0.646	-0.050	0.177	0.698	0.311	0.111	0.557	-0.313	-0.465	-0.395	0.775	0.325
MPA	0.162	-0.224	0.270	0.813	0.877	0.170	0.743	0.854	0.022	-0.150	0.799	-0.590	-0.768	-0.603	0.816	0.109
NP	-0.296	0.170	-0.092	-0.592	-0.667	-0.115	-0.750	-0.707	0.007	0.508	-0.869	0.332	0.635	0.733	-0.589	0.359
SI	0.664	0.651	0.371	-0.320	0.273	0.588	0.697	0.329	-0.474	-0.568	0.369	-0.379	-0.398	-0.681	-0.103	-0.729
MNND	-0.075	-0.177	-0.187	0.328	0.336	-0.179	0.722	0.500	0.209	-0.500	0.755	0.072	-0.330	-0.325	0.368	-0.424
CI	0.060	-0.556	-0.403	0.672	0.236	-0.352	0.392	0.235	0.204	-0.592	0.692	0.202	-0.229	-0.455	0.383	-0.425

* PC: Percent cover, LPI: Largest patch index, MPA: Mean patch area, NP: Number of patches, SI: Shape index, MNND: Mean nearest neighbour distance, CI: Clumpiness index.

APPENDIX 5.D: Maps of the distribution of kelp and non-kelp benthic classes in the Mingan Archipelago

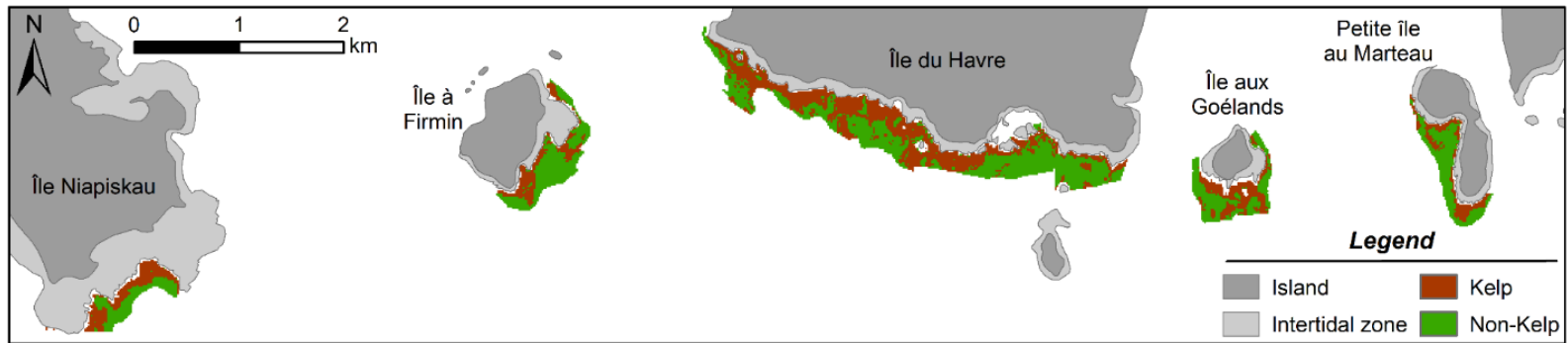


Figure 5.D.1. Distribution of kelp and non-kelp benthic classes based on visual classification of aerial imagery acquired in 1983.

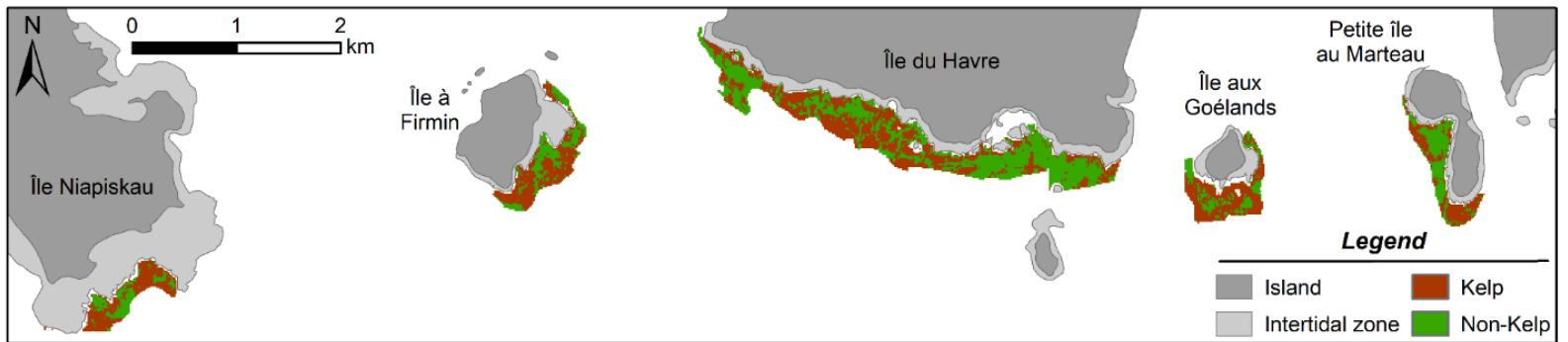


Figure 5.D.2. Distribution of kelp and non-kelp benthic classes based on visual classification of aerial imagery acquired in 1988.

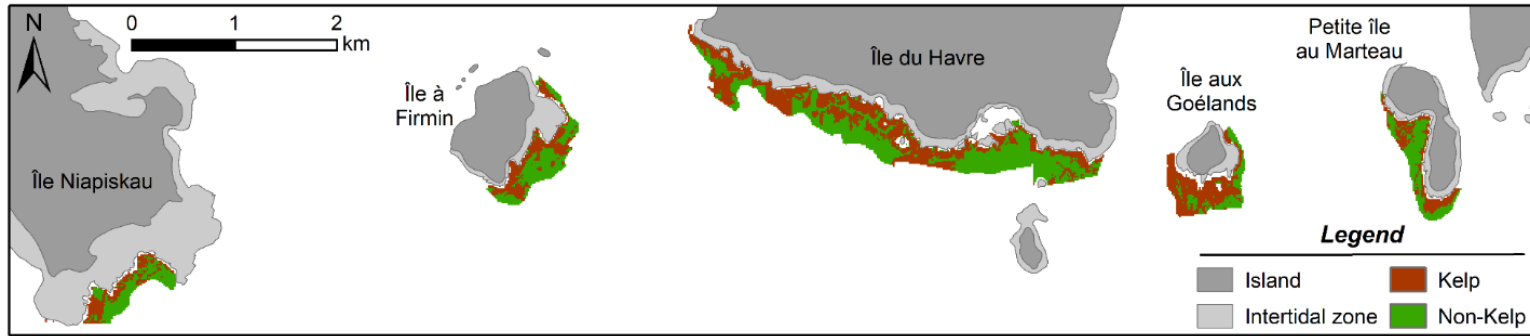


Figure 5.D.3. Distribution of kelp and non-kelp benthic classes based on visual classification of aerial imagery acquired in 1999.

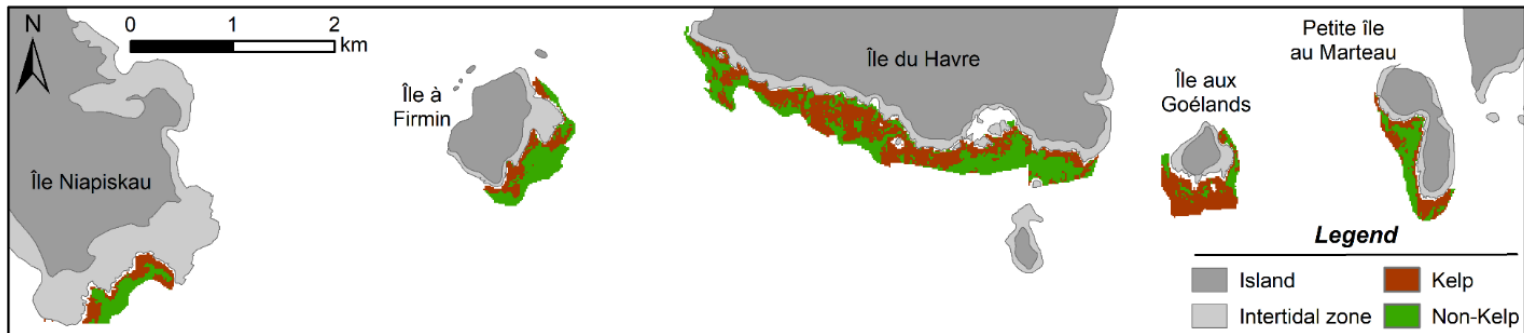


Figure 5.D.4. Distribution of kelp and non-kelp benthic classes based on visual classification of aerial imagery acquired in 2004.

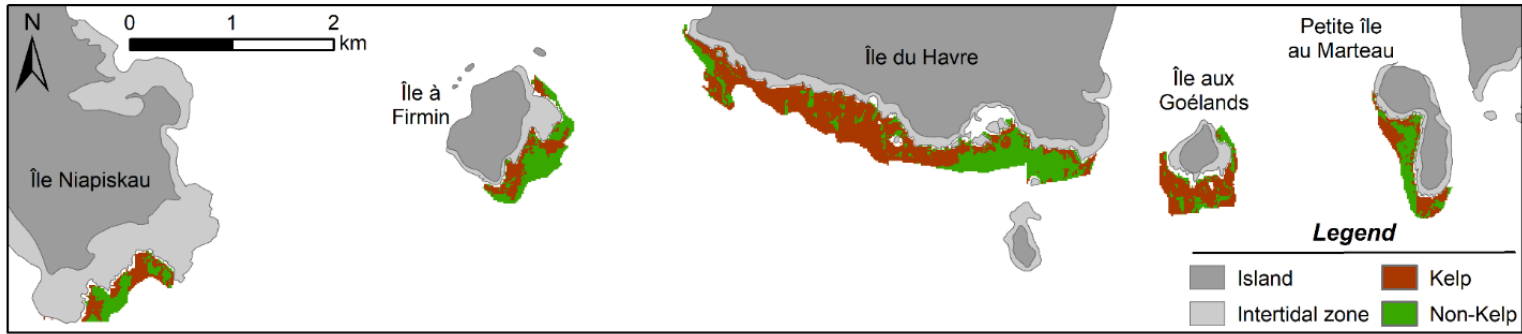


Figure 5.D.5. Distribution of kelp and non-kelp benthic classes based on visual classification of aerial imagery acquired in 2009.

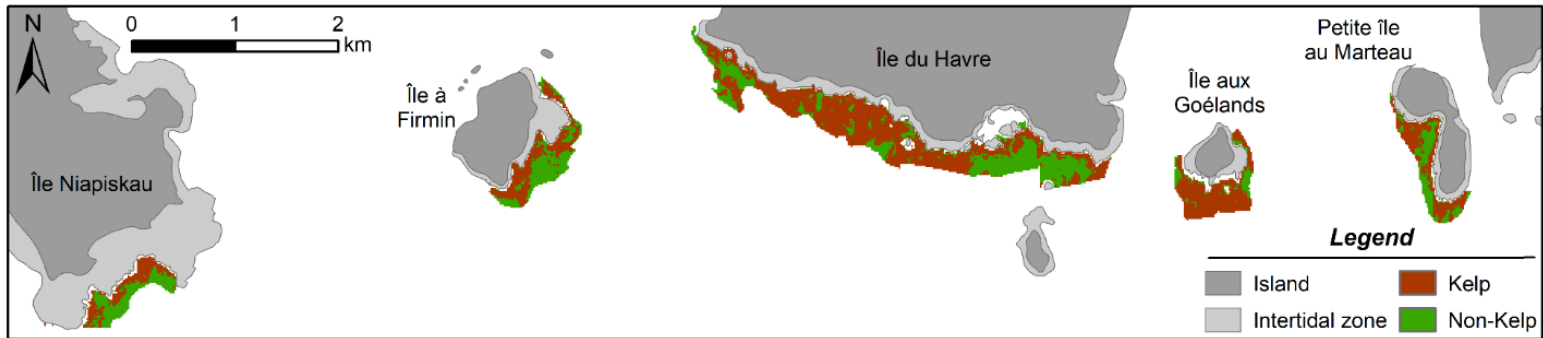


Figure 5.D.6. Distribution of kelp and non-kelp benthic classes based on visual classification of aerial imagery acquired in 2016.

